STUDY OF COMBUSTION, PERFORMANCE AND EMISSIONS OF A DIESEL ENGINE FUELED WITH A TERNARY FUEL (DIESEL-BIODIESEL-ETHANOL) IN BLENDED AND FUMIGATION MODES

MEISAM AHMADIGHADIKOLAEI

PhD

The Hong Kong Polytechnic University

2019

The Hong Kong Polytechnic University

Department of Mechanical Engineering

STUDY OF COMBUSTION, PERFORMANCE AND EMISSIONS OF A DIESEL ENGINE FUELED WITH A TERNARY FUEL (DIESEL-BIODIESEL-ETHANOL) IN BLENDED AND FUMIGATION MODES

MEISAM AHMADIGHADIKOLAEI

A thesis submitted in partial fulfilment of the requirements for the degree of Doctor of Philosophy

August 2018

CERTIFICATE OF ORIGINALITY

I hereby declare that this thesis is my own work and that, to the best of my knowledge and belief, it reproduces no material previously published or written, nor material that has been accepted for the award of any other degree or diploma, except where due acknowledgement has been made in the text.

---------- (Signed)

MEISAM AHMADIGHADIKOLAEI

ABSTRACT

The use of renewable alternative fuels is a potential method to reduce emissions from diesel engines, in order to reduce air pollution and protect human health. Among all the alternative fuels, biofuel, including biodiesel and alcohols and their blend with diesel (especially diesel-biodiesel-ethanol blend (DBE)) is a great option as an alternative to diesel fuel for diesel engines. The effects of using DBE, diesel/biodiesel or diesel/ethanol on the combustion, performance and emissions of diesel engines in either the blended mode or the fumigation mode have been widely reported in the literature. However, there is not enough information about the differences between the effects of the blended mode and the fumigation mode on the performance, combustion and emissions and almost no information on the physicochemical properties of particulate matter (PM) of a diesel engine. Also, only alcohol fuels were utilized in the fumigation mode and the use of a mixture of biodiesel and alcohol as a fumigated fuel for comparison with the blended mode cannot be found. Therefore, this study aims at covering the above knowledge gaps through an experimental study to investigate the effects of different fueling modes of operation, including diesel, blended and fumigation modes, on the engine combustion, performance and emissions of a diesel engine fueled with a ternary fuel (DBE) under various engine speeds and loads. In addition, the present study introduced a combined fumigation and blended mode (F+B) of fueling to investigate its impact in comparison with the fumigation and blended modes.

This study also includes an investigation on the effects of using different alcohols to form the ternary fuel. The alcohols considered include methanol, ethanol, propanol, butanol and pentanol. Each of the alcohol was mixed with diesel and biodiesel to form a ternary fuel with the same oxygen concentration and very close carbon, hydrogen and lower heating value for comparing their effects on the combustion, performance and emissions of the diesel engine. The results indicated that DBE is the most suitable ternary fuel for further investigation.

The experiments were conducted on four fueling modes. In the diesel mode, pure diesel was injected into the engine cylinder. In the blended mode, 80% diesel, 5% biodiesel and 15% ethanol (D80B5E15), by volume, were mixed, and injected into the engine cylinder. In the fumigation mode, a mixture of biodiesel and ethanol (BE) was injected into the intake manifold; while diesel fuel was used as the main fuel. In the F+B mode, half of the BE mixture was injected into the intake manifold and another half of it was blended to

form DBE and used as the main fuel. The experiments were conducted at a constant overall fuel composition of D80B5E15 for the three fueling modes to provide the same fuel composition for comparing their effects. The experiments were divided into three groups. The first and second groups were conducted to investigate the effects of using different fueling modes on the combustion, performance and emissions at five engine loads with a constant engine speed (1800 rpm) and five speeds with a constant load (142.5 Nm), respectively. The third group was conducted to study the physicochemical properties of PM sampled in the different fueling modes with four operating conditions.

According to the average results, it is found that the blended mode has higher peak heat release rate, ignition delay, BTE, nitrogen monoxide (NO), nitrogen oxides (NO_X), coefficient of variation (COV) in Max($dP/d\theta$), but lower duration of combustion, COV_{IMEP}, BSFC, carbon dioxide (CO_2), carbon monoxide (CO), hydrocarbon (HC), nitrogen dioxide (NO_2), PM mass, total number concentration and geometric mean diameter, and similar peak in-cylinder pressure and exhaust gas temperature in comparison with those of the fumigation mode. In regard to the physicochemical properties of the PM, the blended mode has higher organic carbon (OC)/total carbon (TC), high-volatile substance (VS)/total-VS and low-VS/total-VS ratios and faster oxidization reactivity, but lower non-VS/total-VS ratio, TC, OC, elemental carbon (EC), EC/TC ratio, water-soluble organic carbon, polycyclic aromatic hydrocarbons, benzo[a]pyrene equivalent, n-alkanes, inorganic ions, metals and elements, primary particle size, fringe length, tortuosity and fringe separation distance compared to those of the fumigation mode. In addition, it is observed that the values of all the parameters in the F+B mode are between those of the fumigation mode and the blended mode, showing that the F+B mode has the effects between those of the fumigation and blended modes.

It can be found from the results that the use of DBE has different effects on the engine combustion, performance and emissions by using the blended mode or the fumigation mode. It is because, in the blended mode, the lower cetane number and higher heat of evaporation of ethanol cause late combustion and affect other combustion, performance and emission parameters. In the fumigation mode, the combustion of diesel fuel in a homogeneous BE/air mixture inside the engine cylinder also affect combustion parameters, performance and emissions in a different manner than those in the blended mode. These relationships are investigated in this study by relating the performance and emissions to the combustion parameters in each fueling mode.

PUBLICATIONS ARISING FROM THE THESIS

Peer-reviewed Journal Articles:

Meisam Ahmadi Ghadikolaei*, Chun Shun Cheung, Ka-Fu Yung. Study of combustion, performance and emissions of a diesel engine fueled with ternary fuel in blended and fumigation modes. *Fuel* 2019; 235: 288-300.

Meisam Ahmadi Ghadikolaei*, Chun Shun Cheung, Ka-Fu Yung. Study of combustion, performance and emissions of diesel engine fueled with diesel/biodiesel/ alcohol blends having the same oxygen concentration. *Energy* 2018; 157: 258-269.

Meisam Ahmadi Ghadikolaei*, Chun Shun Cheung, Ka-Fu Yung. Comparison between blended mode and fumigation mode on combustion, performance and emissions of a diesel engine fueled with ternary fuel (diesel-biodiesel-ethanol) based on engine speed. *Journal of the Energy Institute* 2018; doi: 10.1016/j.joei.2018.10.010.

Conference Papers:

Meisam Ahmadi Ghadikolaei*, Ka-Fu Yung, Chun Shun Cheung. Chemical properties of PM of a diesel engine fueled with diesel/biodiesel/ethanol in blended and fumigation modes. The 14th International Conference on Combustion and Energy Utilization (ICCEU), November 7-9, 2018, Sendai, Japan.

Meisam Ahmadi Ghadikolaei*, Chun Shun Cheung, Ka-Fu Yung. Effect of different fueling modes on performance and emissions of a diesel engine fueled with diesel-biodiesel-ethanol under different engine speeds and loads. The Advanced Maritime Engineering Conference (AMEC) 2018, Concurrently with 8th Pan Asian Association of Maritime Engineering Societies (PAAMES), October 9-12, 2018, Busan, Korea.

Meisam Ahmadi Ghadikolaei*, Chun Shun Cheung, Ka-Fu Yung. Study of performance and emissions of diesel engine fueled with blends of diesel, biodiesel and alcohols (ethanol, methanol and n-butanol), based on a constant fuel oxygen content. The 13th International Conference on Combustion and Energy Utilization (ICCEU), October 2-5, 2016, Taipei, Taiwan.

* Corresponding author.

ACKNOWLEDGEMENT

First of all I would like to thank Almighty "**Allah**" the lord of the Alamin and the creator of creators, who gave me potential and courage to accomplish this thesis.

I owe my great gratitude to my chief supervisor, **Prof. Chun Shun Cheung,** with whose guidance and constant encouragement I accomplished this study with success. His moral support and masterly guidance were a constant inspiration for me throughout my study. I would also like to express my sincerest gratitude to my co-supervisor, **Dr. Ka-Fu Yung,** for providing insight suggestions in my research.

I wish to express my special thanks to my **parents** and **wife** for their constant encouragement, material support, patience and understanding that were readily forthcoming throughout my study. However, their contribution is immensely unique.

I would like to be grateful to The Hong Kong Polytechnic University for the financial support (account No.: RUAT). It gives me immense pleasure to express my deep sense of gratitude and sincere thanks to the technical staff of the Department of Mechanical Engineering, **Mr. Kwong Shing Tsang**, Department of Applied Biology and Chemical Technology, **Mr. Chi Man Ho** and Department of Civil and Environmental Engineering, **Dr. W.F. Tam** and the people in-charge in the Electron Microscopy Centre, **Dr. Wei Lu** and Materials Research Centre, **Dr. Hon Fai Wong** and teachers and project laboratory's staff of the Mechanical Engineering Department whose valuable suggestions, advice and guidelines proved as a torch bearer and touch stone for my thesis. I would also like to thank **Prof. Sai Hang Ho** and his group mates for their kind assistance and support in doing part of the analyses.

Words are short to express sincere thanks to all my comrades whose insistent comments and suggestions always proved fruitful to my study. The confederation of my friends and colleagues include **Dr. Mohammad Hossein Tahmasebi, Mr. Long Wei**, **Dr. Pak Chung Lau**, **Dr. Shakeel Ahmad**, **Dr. Chun Guan**, **Dr. Ke Yang** and **Dr. Tsz-Lung Kwong.**

MEISAM AHMADI GHADIKOLAEI

TABLE OF CONTENTS

LIST OF FIGURES

LIST OF TABLES

NOMENCLATURE AND ABBREVIATIONS

NOMENCLATURE

$\dot{m}_d$	Diesel fuel mass consumption rate (kg/s for BTE and g/h for BSFC calculations)
$\dot{m}_{DBE}$	Blended fuel mass consumption rate (kg/s for BTE and g/h for BSFC calculations)
$\dot{m}_f$	Fumigated fuel mass consumption rate (kg/s for BTE and g/h for BSFC calculations)
$\overline{X_i}$	Sample observation
$X_1, \ldots, X_N$	Independent variables
X_m	Mean of measurements
λ	Lambda (air/fuel equivalence ratio)
v	Degrees of freedom
$\omega_1, \ldots, \omega_N$	Uncertainties of independent variables
ω_r	Random error
ω_R	Uncertainty of the result
ω_s	Systematic error
$[CO_2]_b$	CO_2 concentration of the exhaust gas in the background (%)
$[CO_2]_d$	CO_2 concentration of the exhaust gas after dilution (%)
$[CO_2]_e$	CO_2 concentration of the exhaust gas before dilution (%)
°CA	Crank angle degree
$^{\bullet}OH$	Hydroxyl radical
A	Frequency factor (s^{-1})
D_S	Fringe separation distance (nm)
E	Activation energy (kJ/mol)
HO_2	Peroxyl radicals
keV	Kiloelectron-volts
L_a	Fringe length (nm)
LHV	Lower heating value (kJ/kg)

LHV_d	Lower heating value (kJ/kg) for diesel
LHV_{DBE}	Lower heating value (kJ/kg) for blended fuel
LHV_f	Lower heating value (kJ/kg) for fumigated fuel
mol	Mole
N	Number of samples or number of particles
n	Reaction order
P_b	Brake power (kW)
pC	Pico coulomb
R	Molar gas constant (8.314 J/mol.K)
R^2	Correlation coefficient
T_f	Tortuosity (non-dimensional ratio)

ABBREVIATIONS

AB	Animal biodiesel
ALM	Accurate lambda meter
ASTM	American Society for Testing and Materials
B	Biodiesel or Blended mode
BaP	Benzo[a]pyrene
BBu	Biodiesel-butanol
BE	Biodiesel-ethanol
BM	Biodiesel-methanol
BMEP	Brake mean effective pressures
BO	Biodiesel-octanol
BPe	Biodiesel-pentanol
BPr	Biodiesel-propanol
BSCO	Brake specific carbon monoxide
$BSCO_2$	Brake specific carbon dioxide
BSFC	Brake specific fuel consumption

BSHC	Brake specific hydrocarbon
BSNO	Brake specific nitrogen monoxide
$BSNO_2$	Brake specific nitrogen dioxide
$BSNO_X$	Brake specific nitrogen oxides
BSPM	Brake specific particulate matter
BTDC	Before top dead center
BTE	Brake thermal efficiency
CI	Compression ignition
CO	Carbon monoxide
CO_2	Carbon dioxide
COV	Coefficient of variation
$COV_{(Max(dP/d\theta))}$	Coefficient of variation in maximum cylinder pressure
COV_{IMEP}	Coefficient of variation in indicated mean effective pressure
CPC	Condensation particle counter
D	Diesel fuel or Diesel mode
DAcBuE	Diesel-acetone-butanol-ethanol
DB	Diesel-biodiesel
DBBu	Diesel-biodiesel-butanol
DBBuPr	Diesel-biodiesel-butanol-propanol
DBE	Diesel-biodiesel-ethanol
DBM	Diesel-biodiesel-methanol
DBPe	Diesel-biodiesel-pentanol
DBPr	Diesel-biodiesel-propanol
DBu	Diesel-butanol
DCP	Diffusion combustion phase
DE	Diesel-ethanol
DEh	Diesel-ethylhexanol
DF	Dual-fuel
DI	Direct injection

DM	Diesel-methanol
DMA	Differential mobility analyzer
DNA	Deoxyribonucleic acid
DO	Diesel-octanol
DOC	Duration of combustion
D_P	Diameter of particle
DPe	Diesel-pentanol
DPr	Diesel-propanol
DR	Dilution ratio
DS	Dry soot
DSC	Differential scanning calorimeter
E	Ethanol
EC	Elemental carbon
EC1	Elemental carbon determined in 98% helium/2% oxygen atmosphere at 580 °C
EC2	Elemental carbon determined in 98% helium/2% oxygen atmosphere at 740 °C
EC3	Elemental carbon determined in 98% helium/2% oxygen atmosphere at 840 °C
ECU	Electronic control unit
EGT	Exhaust gas temperature
EOC	End of combustion
EUSAAR	European supersites for atmospheric aerosol research
F/A	Fuel/air ratio
F+B	Fumigation+blended mode
FAME	Methyl ester of fatty acids
FC	Fuel consumption
F	Fumigation mode
GC/MS	Gas chromatograph/Mass spectrometer
GMD	Geometric mean diameter
HC	Hydrocarbons

HCLD	Heated chemiluminescent analyzer
HFID	Heated flame ionization detector
HRR	Heat release rate
HRTEM	High-resolution transmission electronic microscope
H-VS	High-volatile substance
IC	Inorganic carbon or Ion chromatograph
ID	Ignition delay
IMEP	Indicated mean effective pressure
IMPROVE	Interagency monitoring of protected visual environments
IS	Indicated specific
ISO	International Organization for Standardization
ITE	Indicated thermal efficiency (%)
KHP	Potassium hydrogen phthalate
LPG	Liquefied petroleum gas
LSD	Low-sulfur diesel
L-VS	Low-volatile substance
MDL	Minimum detection limits
MO	Mahua oil
NDIR	Non-dispersive infrared analyzer
NO	Nitrogen monoxide
NO_2	Nitrogen dioxide
non-VS	Non-volatile substances
NO_X	Nitrogen oxides
NPOC	Non-purgeable organic carbon
OC	Organic carbon
OC1	Organic carbon determined in a 100% helium atmosphere at 140 °C
OC2	Organic carbon determined in a 100% helium atmosphere at 280 °C
OC3	Organic carbon determined in a 100% helium atmosphere at 480 °C
OC4	Organic carbon determined in a 100% helium atmosphere at 580 °C

PAH	Polycyclic aromatic hydrocarbon
PCP	Premixed combustion phase
PM	Particulate matter
POC	Pyrolyzed carbon
POHR10	Positions of 10% heat release
POHR50	Positions of 50% heat release
POHR95	Positions of 95% heat release
Pr	Pressure
ROI	Region of interest
rpm	Revolution per minute
RSD	Relative standard deviation
RSO	Rubber seed oil
RSOME	Rubber seed oil methyl ester
SAED	Selected-area electron diffraction
SD	Standard deviation
SEM	Scanning electron microscope
SMPS	Scanning mobility particle sizer
SOC	Start of combustion
SOF	Soluble organic fraction
SOI	Start of injection
STEM	Scanning transmission electron microscope
STN	Speciation trends network
TC	Total carbon
TD-GC/MS	Thermal desorption-gas chromatography/mass spectrometry
TEF	Toxic equivalent factor
TEM	Transmission electron microscope
TEOM	Tapered element oscillating microbalance
TGA	Thermogravimetric analyzer
THC	Total hydrocarbons

TNC	Total number concentration
TOC	Total organic carbon
TOR	Thermal optical reflection
U	Total uncertainty
ULSD	Ultra-low-sulfur diesel
U.S.EPA	United States Environmental Protection Agency
VB	Vegetable biodiesel
VOC	Volatile organic compound
VOF	Volatile organic fraction
VS	Volatile substance
WSIC	Water-soluble inorganic carbon
WSOC	Water-soluble organic carbon
WSTC	Water-soluble total carbon
XRD	X-ray diffraction

CHAPTER 1 INTRODUCTION

1.1 Background

According to 2018 Outlook for Energy [1] and BP Energy Outlook 2018 Edition [2], the world's population (about 7.5 billion, today) is expected to reach approximately 9 billion people by 2040. The huge increase in population will drive the global energy demand up by about 25% from 2016 to 2040. Global transportation-related energy demand is also projected to increase by about 30% in the same period of time; while about 60% of this growth is in liquid fuels [1,3]. Petroleum oil will remain an essential energy source for the transportation sector, despite there will be increasing penetration of alternative fuels, particularly natural gas and liquefied petroleum gas (LPG), and electrical vehicles by 2040 [1-3]. To reduce the threats of engine emissions to the environment and human health, some countries, especially those in Europe, are planning to ban the sale of new vehicles powered by gasoline or diesel engines starting in 2030. However, such motions are aimed at private cars. For commercial vehicles, like the heavy-duty vehicles, diesel engines will remain be the main choice in the foreseeable future. It is expected that diesel fuel demand will grow by about 30% to meet marine and trucking demands from 2016 to 2040. However, the use of diesel oil in transportation sectors leads to increase in air pollution, global warming and human health issues.

In recent years, air pollution is a major concern due to its serious toxicological influence on human health and the environment [4]. In detail, air pollution has long-term impacts on human health such as causing inflammations, respiratory infections, cancer and cardiovascular dysfunctions [5-10]. Various sources such as cigarettes (as a small unit), natural sources like volcanic activities and emissions from industrial activities and automobiles have impacts on the formation of air pollution [11,12]. While in the automobile sector, the diesel engines have a huge effect on the formation of air pollutants, especially NO_X and PM. Thus, the search for environmentally-friendly, economical and sustainable technologies or alternative energy sources for operating diesel engines will remain the major challenges in the future [3,13]. Over the last few decades, several techniques have been applied to overcome these challenges, which include improvement in engine technology, use of emission catalysts and development of alternative fuels. The literature reveals that the use of renewable alternative fuels, in lieu of the non-renewable fossil fuels, is one of the most attractive, suitable and promising

methods to reduce emissions from the transportation sectors [14-16].

Among all the renewable alternative fuels, biodiesel and alcohols (especially ethanol) and their blend with diesel have been widely investigated for use in diesel engines [17-20]. Biodiesel can be blended easily with diesel. The most common method to use biodiesel in a diesel engine is to use it in the blended form with diesel. On the other hand, among the alcohols, methanol and ethanol are immiscible with diesel; while higher molecular weight alcohols are miscible with diesel. Therefore, various techniques have been applied for the application of alcohols in diesel engine. Common techniques to use alcohols in diesel engines include the following:

1. Alcohol-diesel blend: in this method, the alcohol and diesel fuels are premixed uniformly, if they are miscible, and then injected by a high-pressure pump via the fuel injector into the engine cylinder directly.
2. Alcohol fumigation: in this method, the alcohol fuel is introduced into the intake air upstream of the manifold by using low-pressure fuel injectors. However, the amount of injected alcohol should be controlled to prevent flame quenching and misfire at low engine loads and the incipience of engine knock at high engine loads.
3. Alcohol-diesel emulsification: in this method, if the two fuels are immiscible, an emulsifier or co-solvent is used to mix the alcohol with diesel fuel for preventing their separation.
4. Dual injection system: in this method, a separate high-pressure fuel injection system and a related major design change of the cylinder head are required for the injection of the two fuels into the cylinder, using separate fuel injectors [21,22].

However, among the above four methods, the alcohol-diesel blended and alcohol fumigation modes are the most commonly used methods in diesel engines [16,21,23,24].

1.2 Overview and motivation

In recent years, the concept of fuel design has been developed in which different fuels are mixed to obtain the desired fuel properties for application in diesel engines. Since biodiesel-diesel blends and ethanol-diesel blends have their own advantages and disadvantages, they have been blended together to form a ternary fuel, the diesel-biodiesel-ethanol (DBE) blend, with more desired properties. DBE has been focused for potential use in diesel engines due to its similar fuel properties with pure diesel. It can

fulfill the cetane number, viscosity and lubricity requirements for standard diesel fuel [25] and it is stabile even below 0 °C [26]. On the other hand, in addition to the blended mode, ethanol can be applied to a diesel engine in the fumigation mode by injecting it into the air intake to form a uniform air/fuel mixture inside the engine cylinder. As summarized in the review papers [21,27-29], each fueling mode, the blended or the fumigation mode, has its own advantages and disadvantages. For instance, the application of biodiesel and alcohols in the blended mode leads to increase in BTE and decrease in HC and CO emissions, but increase in NO_X emissions in most cases. On the other hand, the application of the alcohols in the fumigation mode has reverse effects of the blended mode, leading to decrease in NO_X, but reduction in BTE and increase in HC and CO emissions in most cases. However, most of the former studies on the application of biofuels, mostly biodiesel and ethanol, to diesel engines were conducted either in the blended mode or in the fumigation mode, separately. Only a few studies [30-33] were conducted to compare the effect of these two modes, using the same fuel, on the same diesel engine and under the same operating conditions. Moreover, in the reviewed studies, only pure alcohol, mainly methanol or ethanol, was utilized as the fumigated fuel.

According to the literature review, there is lack of investigation conducted to understand the differences between the effects of the blended mode and the fumigation mode of operation on the performance, combustion and emissions of a diesel engine, especially on the physicochemical properties of the PM. Also, only alcohol fuels were utilized in the fumigation mode and the use of a mixture of biodiesel and alcohol as a fumigated fuel cannot be found for comparison with the blended mode. Moreover, there are very few studies about the effect of a fumigated fuel, containing a mixture of biodiesel and alcohol, on the combustion, performance and emissions (but no investigation on the physicochemical properties of PM) of diesel engines compared to pure diesel fuel [34,35]. Since DBE is a viable blend for use in diesel engines and it is a widely investigated blended fuel [15,16,27], there is an interest to apply it in the fumigation mode, using a mixture of biodiesel and ethanol as the fumigated fuel, for comparison with the use of DBE blend, on the combustion, performance and emissions of a diesel engine with the same fuel composition and operating conditions.

Epidemiological and toxicological studies show that the PM emission is of major concern because exposures to it might have pulmonary and cardiovascular morbidity and mortality consequences due to its physicochemical properties [36-40]. Since diesel

engines can produce reactive PM which is harmful for environmental chemistry, climate and public health [41]; therefore, information about the physicochemical properties of PM from diesel engines is required in order to find the appropriate methods to reduce PM emissions. However, very few studies have been conducted to investigate the physicochemical properties of PM from diesel engines operating in the blended mode and/or in the fumigation mode; while there is almost no study comparing the physicochemical properties of PM from blended mode operation with that form fumigation mode operation. Therefore, the present research aims at covering the above knowledge gaps by conducting experiments to compare the impact of blended mode, using DBE as the fuel, with fumigation mode, using BE (mixture of biodiesel and ethanol) as the fumigated fuel and diesel as the main fuel to form DBE, on the engine combustion, performance, emissions and especially on the physicochemical properties of PM. In addition, since the blended mode and fumigation mode have their own advantages and disadvantages; therefore, the combined operation in blended and fumigation modes may be useful to achieve the advantages of both modes, simultaneously. This type of fueling system is introduced in this study as a fumigation+blended (F+B) mode.

1.3 Objective and scope

The present experimental study aims to investigate the effects of using DBE in different fueling modes (blended, F+B and fumigation modes) on the engine combustion, performance and emissions. In addition, this study investigates the physicochemical properties of PM emitted from the engine using DBE in different fueling modes. In the blended mode, 80% diesel, 5% biodiesel and 15% ethanol (D80B5E15), by volume %, were mixed. In the fumigation mode, a mixture of biodiesel and ethanol (BE) was injected into the intake manifold and diesel fuel was used as the main fuel. In the F+B mode, half of the mixture of BE was injected into the intake manifold as the fumigated fuel and another half of the BE mixture was blended with diesel to form the DBE and used as the main fuel. The experiments were conducted at different engine speeds and loads at a constant mixture composition of D80B5E15 for the blended, F+B and fumigation modes of operation to provide the same fuel composition and operating conditions for comparing the effects of each fueling mode.

In particular, the objectives of the present experimental research involve:

1. To investigate the effects of alternative fuels (a ternary blend, DBE) in the blended and fumigation modes on the engine combustion, performance and emissions of a diesel engine under different engine loads and engine speeds.
2. To investigate the effects of a combined fumigation and blended (F+B) mode on the engine combustion, performance and emissions of a diesel engine.
3. To investigate in particular the physical (particle number, size, mass, morphology, micro-structure and nano-structure) and chemical (elemental carbon, organic carbon, water-soluble organic carbon, particle volatility, oxidation reactivity, particle-phase polycyclic aromatic hydrocarbons, particle-phase n-alkanes, metals, elements and inorganic ions) properties of PM emitted from the engine using the ternary fuels in different modes of operation.
4. To investigate the combustion mechanisms (in relation to the different modes of combustion) affecting the performance and emissions of the engine.

1.4 Outline

The background, overview, motivation, objective and scope of the present study are presented in this Chapter. Chapter 2 is an overview of the literature to show the methods, operating conditions and finding of former investigations which are related to this study. Chapter 3 presents the experimental setup and procedures for conducting the tests and analyzing the results. Chapter 4 compares the effects of using ethanol, as the alcohol for blending with diesel and biodiesel, with the effects of using other alcohols, namely methanol, propanol, n-butanol and n-pentanol, on the combustion, performance and emissions of a diesel engine. The results and discussions on the effects of the different fueling modes (diesel, DBE blended, DBE fumigation, DBE F+B) are presented in four separate chapters as: Chapter 5 on the engine combustion and performance; Chapter 6 on the gaseous emissions; Chapter 7 on the physical properties of PM; and Chapter 8 on the chemical properties of PM. The conclusions and suggestions for future study are presented in Chapter 9.

CHAPTER 2 LITERATURE REVIEW

This chapter reviews former studies conducted to investigate the effect of using DBE, in the blended or fumigation mode, on diesel engines. For studies conducted in the blended mode, firstly, properties of DBE, secondly, influence of DBE blends on the combustion, performance and emissions, and finally, influence on the physicochemical properties of PM are presented. However, for studies conducted in the fumigation mode, since there is lack of related studies involving the use of BE as the fumigated fuel, the effects of using pure alcohols, in particularly those involving the use of ethanol, as the fumigated fuel on the combustion, performance and emissions, and physicochemical properties of PM are reviewed. At the end of this chapter, the knowledge gaps to be filled up by this study are identified.

2.1 Blended mode

2.1.1 Properties of ternary blend

In recent years, biodiesel and ethanol have gained much attention for the potential use as alternative fuels for diesel engines. This attention is due to their advantages such as wide availability, easy handling, reasonable price and easy operating. Also both of them are renewable and can be produced domestically in many countries. In addition, reduction in emissions such as CO, unburned hydrocarbon and PM by use of biodiesel and ethanol in diesel engines [21,27,28] is another important advantage of these two fuels.

Biodiesel, which is mainly Methyl Ester of Fatty Acids (FAME), can be produced from vegetable oils (both edible and non-edible), animal fat and waste cooking oil [42]. Biodiesel can be used in diesel engines as a single fuel or as a diesel-biodiesel blend; while no or little engine modifications [42,43] are required. However, ethanol cannot be used as a single fuel in diesel engines and it should be blended with diesel with an emulsifier (known as diesohol or e-diesel) or other. Ethanol has both positive and negative effects on the properties of the blended fuel. On the one hand, it can improve the cold flow properties such as cloud point, pour point and freezing point [44,45] and filter plugging point and filterability [44]. On the other hand, it leads to decrease in density, calorific value, kinematic viscosity [45] and flash point [46,47] and increase in corrosive behavior [48] of the blended fuel.

Despite of the advantages of ethanol, there are some technical barriers and problems in the direct use of ethanol in diesel engines due to the limited solubility of ethanol in diesel [49-51]. Therefore, different additives (emulsifiers) have been added to the diesel-ethanol blend to form stable diesohol. However, the additives can only improve the solubility, but they cannot affect certain important properties of the blended fuel. For instance, the low flash point of diesohol cannot be improved with the additives [52].

The use of biodiesel as a fuel additive in diesohol has positive influence like increase in solubility of ethanol in diesel over a wide range of temperature and improvement in the physicochemical properties of diesohol [16,26]. The fuel formed by the combination of diesel, biodiesel and ethanol is referred to as DBE. DBE has good stability even under under sub-zero temperature [16,53] and it has equal or superior physicochemical properties compared to fossil diesel fuel [16,53,54], diesel-biodiesel or diesohol [16,55]. The water tolerance and stability of DBE is also better than diesohol and biodiesel-diesel [56]. Different percentages of ethanol, biodiesel and diesel have been tested in ternary blend, for example use of ethanol up to 40% with 10% biodiesel and 50% diesel [57]. According to the two review papers of Shahir et al. [16,27], it can be concluded that the physicochemical properties of DBE are almost similar to the diesel fuel and it is suitable for use in diesel engines.

2.1.2 Effect of blended mode on engine combustion, performance and regulated emissions

Among all the alternative fuels, biodiesel, lower and higher alcohols or their blends with diesel fuel (in binary, ternary or quaternary blends) have been utilized in various studies to investigate their effects on the combustion, performance and emissions characteristics of different diesel engines. In addition to DBE, these include blends of diesel-biodiesel (DB) [15,58-75], diesel-ethanol (DE) [76-78], biodiesel-ethanol (BE) [76,79,80], diesel-methanol (DM) [77,78,81,82], biodiesel-methanol (BM) [80,83,84], diesel-biodiesel-methanol (DBM) [65,71,85-87], biodiesel-butanol (BBu) [79,88-91], diesel-butanol (DBu) [77,91-96], diesel-biodiesel-butanol (DBBu) [66,69,73,91,97-104], diesel-pentanol (DPe) [92-94,96,105], biodiesel-pentabol (BPe) [90,106], diesel-biodiesel-pentanol (DBPe) [63,68,73,107,108], diesel-propanol (DPr) [109-112], biodiesel-propanol (BPr) [113], diesel-biodiesel-propanol (DBPr) [73,114-116], diesel-octanol (DO) [117-119], biodiesel-octanol (BO) [106,120], diesel-ethylhexanol (DEh) [121] diesel-biodiesel-

butanol-propanol (DBBuPr) [122] and diesel-acetone-butanol-ethanol (DAcBuE) [123]. Various investigations conducted with DBE on diesel engines are reviewed in this section.

According to literature, studies about the effect of DBE on the performance and emissions of diesel engines can be traced back to about 1995. Ali et al. [124] performed experiments to optimize the blend of diesel, methyl tallowate and ethanol with concentrations of 80:13:7, 70:19.5:10.5 and 60:26:14 (by volume %) respectively, to find a suitable blended fuel to reduce engine emissions. It was found that the blended fuel with concentration of 80:13:7 had the lowest emissions and it had no significant effect on the engine power output. Shi et al. [56] investigated the effects of DB12E3 and DB16E4 (by volume %) on the engine performance and emissions of a diesel engine under various engine speeds and loads. It was recorded that the use of DBE caused reduction in PM and CO, but increase in BSFC, NO_X and HC compared to the diesel fuel. Also, Shi et al. [125] found that the application of DB20E5 (by volume %) had lower PM, but higher NO_X compared to the diesel fuel. In another study, Barabás et al. [126] observed that DBE caused decrease in BTE, PM, HC and CO and increase in BSFC, CO_2 and NO_X in comparison with the diesel fuel. In addition, various studies about the use of DBE in diesel engines, which are summarized in some review papers [15,17,27], which show that investigations on the combustion, performance and emissions of diesel engines fueled with DBE blends remain active in recent years.

Oliveira et al. [127] evaluated the combustion, performance and emissions of a four-cylinder stationary diesel engine under a fixed engine speed of 1800 rpm with different engine loads, varying from 0 kW to 37.5 kW, fueled D93B7 (as a reference fuel), D88B7E5, D83B7E10 and D78B7E15 (by mass %). According to their results, the increase in ethanol concentration in the blends led to reduction in duration of combustion, CO_2 and NO_X and increase in ID and fuel consumption compared to those of D93B7. The in-cylinder peak pressure and the heat release rate were decreased at low engine loads, but increased at medium and high engine loads with the increase in ethanol concentration in comparison with D93B7. The CO and HC emissions were increased at low and medium loads, but dropped at high engine loads with the rise in ethanol content compared to D93B7.

Tse et al. [128,129] analyzed the performance, emissions and soot properties of a four-cylinder DI diesel engine at a fixed engine speed of 1800 rpm with five engine loads fueled with diesel, biodiesel, DB and DBE. For the blended fuels, the biodiesel concentration was fixed at 15% (by volume %); while ethanol had various concentrations of 0, 5, 10 and 20%. Their results revealed that the increase in ethanol concentration in the DBE caused decrease in duration of combustion, BSNO_X, BSPM mass, TNC and increase in BSFC, BTE (slight rise), in-cylinder pressure, peak heat release rate and ID. It was also reported that the increase in ethanol in the DBE led to decrease in diffusion combustion duration and hence lower mass of fuel burned in the diffusion mode, resulting in lower PM emissions.

Shinde et al. [130] investigated the influence of DBE on the performance and emissions of a single-cylinder, variable compression ratio diesel engine under a fixed engine speed and six engine loads with three compression ratios of 16,17 and 18. Three blended fuels, D90B5E5, D80B10E10 and D80B5E15, were used. It was found in general that all the tested blends had higher BTE, but lower smoke at almost all the tested engine loads and compression ratios compared to the diesel fuel. However, the DBE blends had a reduction effect on CO_2 only at higher engine loads (75 and 100% loads).

Paul et al. [131] investigated the effect of DBE on the combustion, performance, exergy and emission characteristics of a single-cylinder diesel engine under a constant speed of 1500 rpm and six engine loads. Five fuels were tested as D100, D45B50E5, D40B50E10, D35B50E15 and D30B50E20. It was found the D35B50E15 blend was the best blended fuel in regard to the combustion, performance, exergy and emission characteristics. Because this blended fuel had the lowest BSFC, HC and CO and the highest BTE, exergetic efficiency, maximum in-cylinder pressure and heat release rate among all the tested fuels. This blended fuel also had lower NO_X emissions compared to the diesel fuel.

Aydın and Öğüt [132] explored the impact of DBE fuel on the performance and emissions of a single-cylinder diesel at a constant engine load with various engine speeds. Four blended fuels (D95B2.5E2.5, D90B5E5, D92.5B2.5E5 and D92.5B5E2.5, based on volume %) were analyzed to compare their effects on the performance and emissions (including CO_2, CO, HC, O_2, NO_X and SO_2) in comparison with pure diesel fuel. The results showed that the D92.5B5E2.5 was the optimum in regard to the emissions; while pure diesel had the highest engine performance.

Jamrozik et al. [133] investigated the influence of using DBE on the combustion, performance, and emissions characteristics on a single-cylinder DI diesel engine under a constant engine speed and three engine loads of 70, 85 and 100% of the maximum load. Ethanol up to 50% (volume %) was added to diesel-biodiesel blends. It was recorded that in general the increase in ethanol in the blends caused increase in fuel consumption, BTE, ID, $BSNO_X$, $BSCO_2$, in-cylinder temperatures and IMEP and decrease in duration of combustion and BSCO. It was found that with up to 30% of ethanol in the blended fuel, BSHC and COV_{IMEP} of the blended fuels were almost similar to the diesel fuel; while further increase in ethanol concentration up to 50% caused increase in BSHC and COV_{IMEP} compared to the diesel fuel.

Tan et al. [134] investigated the influence of DBE emulsions on the single-cylinder DI diesel engine under nine engine speeds. The experiments were conducted on five fuels including pure diesel, DB20, DB15E5, DB10E10 and DB5E15 (by volume %). The diesel content was fixed at 80% for all the blended fuels. According to the results, the use of DB and DBE fuels caused reduction in engine power, torque, exhaust gas temperature, BTE, volumetric efficiency, CO and CO_2, but increase in BSFC, under almost all engine speeds compared to the diesel fuel. However, the DB fuel had higher NO_X at all speeds; while the DBE fuels had lower NO_X at most of the tested speeds in comparison with the diesel fuel.

Hu et al. [135] investigated the volatile organic compound (VOCs) emissions of a single-cylinder diesel engine under five operating conditions fueled with diesel and DBE (10% ethanol and 30% biodiesel, volume %). In that study, benzene, ethylbenzene, toluene, n-butyl acetate, styrene, m-xylene, p-xylene, o-xylene, n-undecane were analyzed with Gas chromatograph/ Mass spectrometer (GC/MS). It was found that benzene and toluene were the major VOCs for both fuels. In addition, it was observed that in general DBE fuel had lower VOCs compared to the diesel fuel.

Emiroğlu et al. [136] studied the combustion, performance and emissions of a single-cylinder diesel engine fueled with diesel, biodiesel and alcohols (methanol, ethanol and butanol) at a constant engine speed of 1500 rpm with four brake mean effective pressures (BMEP) of 0.09, 0.18, 0.27 and 0.36 MPa. Five fuels including pure diesel, D80B20, D70B20M10, D70B20E10 and D70B20Bu10 were utilized. According to the results for the engine combustion, it was observed that ignition delays, maximum cylinder pressures,

maximum pressure rises and maximum heat release rates of the alcohols were higher than those of pure diesel for all the engine loads. In regard to the engine performance, the increase in the BSFCs and similar BTEs were for alcohol blends compared to the diesel fuel. For emissions, alcohol fuels had lower CO and smoke, but higher NO_X and HC in comparison with the diesel fuel.

Noorollahi et al. [137] investigated the influence of DBE on the performance and emissions of a single-cylinder DI diesel engine at four engine speeds under full engine load. In addition, the fuel properties of DBE were analyzed. Four fuels including D100, D97B2E1, D94B4E2 and D91B6E3 were tested. It was concluded that D91B6E3 had the best efficiency, performance, and emission among the all the tested fuels. However, the amount of ethanol used in the blended fuels was very low in that investigation.

Guedes et al. [138] investigated the effects of DBE on the combustion and performance of a four-cylinder diesel engine (Euro III) under three engine speeds and two loads with different fuel injection timings for the fuel. The biodiesel percentages in blends were 7 and 15%, the ethanol percentages were 0, 5, 10, 15 and 20% by volume and the diesel percentage varied to achieve the desired blend percentages; while 1% additive was added to each blend to ensure the blend's stability. It was found that the increase in ethanol in the blended fuel caused increase in fuel consumption and ignition delay at various injection timings. In addition, the best fuel injection optimizations were observed for the advance in fuel injection by 1°CA for each 5% ethanol increment from B15E5 to B15E15 due to ethanol's combustion postponing characteristic properties.

Prakash et al. [139] attempted to find an optimum ternary fuel blend with castor oil-diesel-bioethanol suitable for small diesel engines in regard to the combustion, performance and emissions. Experiments were conducted on a single-cylinder diesel engine at constant engine speed of 1500 rpm with four engine loads. Five fuels including pure diesel, neat castor oil (biodiesel), D30B60E10, D30B50E20 and D30B40E30 were tested. For engine combustion, it was found that castor oil and all blended fuels had lower maximum rate of pressure rise, but longer ignition delay and combustion duration compared to the diesel fuel. In regard to engine performance, castor oil and all blended fuels caused increase in BSFC and decrease in BTE. In addition, castor oil and all blended fuels had a reduction effect only for NO emissions, but CO, HC and smoke of these fuels were higher than diesel fuel. The lowest NO and BTE and the highest BSFC,

CO, HC and smoke among all the tested fuels were recorded for the neat castor oil. According to the results, the D30B40E30 was selected as the optimum blended fuel.

Madiwale et al. [45] analyzed the fuel properties and engine performance of a single-cylinder diesel engine fueled with diesel, ethanol and biodiesel (from different feedstocks including Jatropha, Soybean, Palm, and Cotton seed) at a fixed speed of 1500 rpm with five engine loads. Two types of blends were prepared as diesel-biodiesel blends without ethanol (20, 40, 60 and 80% of biodiesel, by volume %) and diesel-biodiesel blends with 5% ethanol. It was recorded that the use of ethanol as an additive into the DB blends caused decrease in the density, calorific value and kinematic viscosity, improvements in the cold flow properties such as cloud point and pour point and increase in the BSFC and BTE compared to DB.

Turkcan [140] investigated the injection, combustion, performance and emission parameters of a four-cylinder, common rail DI diesel engine under a constant engine speed of 2000 rpm with four engine loads fueled with diesel, biodiesel and ethanol. Two types of biodiesel were tested as animal biodiesel (AB) and vegetable biodiesel (VB). The experiments were conducted at five fuels namely pure diesel, D55AB20E25, D45AB20E35, D55VB20E25 and D45VB20E35, by mass percentage. In general, all the DBE fuels led to reduction in maximum pressure rise rate, in-cylinder pressure, smoke and HC and increase in ID, BSFC and NO_X in comparison with pure diesel fuel. It was also found that the blended fuels caused reduction in BTE at low engine load, but increase at medium and high loads.

Mahmudul et al. [141] investigated the combustion characteristics of a single-cylinder diesel engine at 1200 rpm with one engine load fueled with diesel, D95B5, D80B20, D75B5E20 and D75B5Bu20 by volume %. It was obtained that all the blended fuels had slight increase in in-cylinder pressures compared to diesel. The ethanol blend had the lowest ID among all tested fuels. Also it had slightly higher energy release and faster mass burned fraction compared to diesel.

It can be concluded, despite of many studies had been conducted in the last two decades to investigate the effects of DBE on the combustion, performance and regulated emissions of diesel engines, there are continued investigations in recent years to understand the effects of different blending ratios and different biodiesel on the performance, as well as the combustion and emissions characteristics of diesel engines.

2.1.3 Effect of blended mode on physicochemical properties of PM

According to the literature review, only a few studies have been performed to explore the effects of DBE on the physicochemical properties of PM. However, many studies have been conducted to investigate the physicochemical properties of PM using diesel, biodiesel or diesel-biodiesel blends [142-144].

Chen et al. [145] performed some experiments to investigate the impact of DE and DBE on the combustion and PM emissions of a four-cylinder diesel engine using six fuels including pure diesel, DE10, DE30, DB5E10, DB10E20 and DB10E30. It was found that the increase in ethanol in the DBE fuels caused decrease in the PM mass, smoke and dry soot (DS) compared to the diesel fuel. However, the sulfates of all the fuels were almost similar to each other. The soluble organic compounds (SOF) were lower for DBE than diesel fuel; while the lowest SOF value was recorded for 20% ethanol in DBE. It was reported that about 80% of PM emitted from DB10E30 was SOF and about 10% was DS; while the diesel had the lowest SOF, but highest DS percentages among all the tested fuels.

Tse et al. [128,146] examined the performance, emissions and soot properties of a four-cylinder DI diesel engine under a constant engine of 1800 rpm with five engine loads (BMEPs of 0.09, 0.17, 0.35, 0.58 and 0.70 MPa), fueled with diesel, biodiesel, DB and DBE. For the blended fuels, the biodiesel concentration was fixed at 15% (by volume %); while ethanol had various concentrations of 0, 5, 10 and 20%. For the soot properties, it was found that the biodiesel and all the blended fuels had higher BSVOF compared to the diesel fuel; while the pure biodiesel had the highest value among all the fuels. However, the increase in ethanol in the blends caused a slight reduction in BSVOF (DBE20 had lower BSVOF than DBE5). It was also found that the increase in ethanol in DBE caused increase in mass fraction of VOF in PM at both low and high loads compared to the diesel fuel. In addition, the biodiesel has the highest mass fraction of VOF in PM among all the tested fuels. For DBE20, about 50% of PM was VOF at low load and about 20% of PM was VOF at high load. For the diesel, about 30% of PM was VOF at low load and about 10% of PM was VOF at high load.

They extended their investigations to the morphology and oxidation reactivity of the PM using High-resolution transmission electronic microscope (HRTEM) and thermogravimetric analyzer (TGA), respectively. Their results revealed that increase in

ethanol in the blended fuel caused increase in amorphous nano-structure characterized by smaller particles and agglomerates. In addition, it was found that agglomerates from different fuels (diesel, biodiesel and DBE) at different loads were observed to be composed of fine primary particles to form a mixture of chain-like structures and clusters of spherules (Fig. 2.1and Fig. 2.2). The increase in fuel oxygen content led to reduction in size of primary particle, agglomerates, fringe separation and fringe-length, but increase in tortuosity in comparison with the diesel fuel.

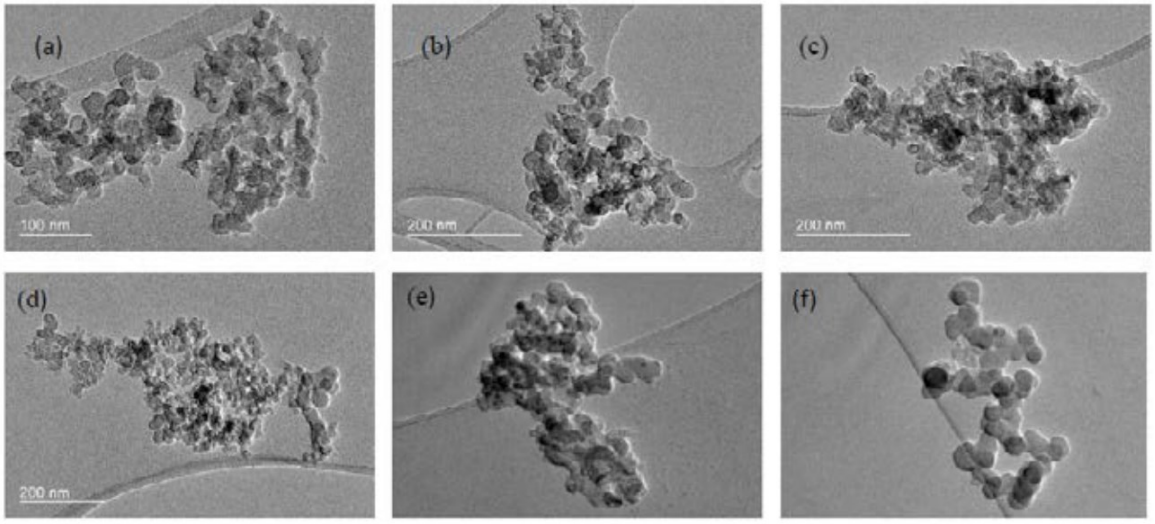

Fig. 2.1 TEM images of soot particles from (a) ULSD, (b) biodiesel, (c) DBE0, (d) DBE5, (e) DBE10 and (f) DBE20 at engine load of 0.17 MPa [128].

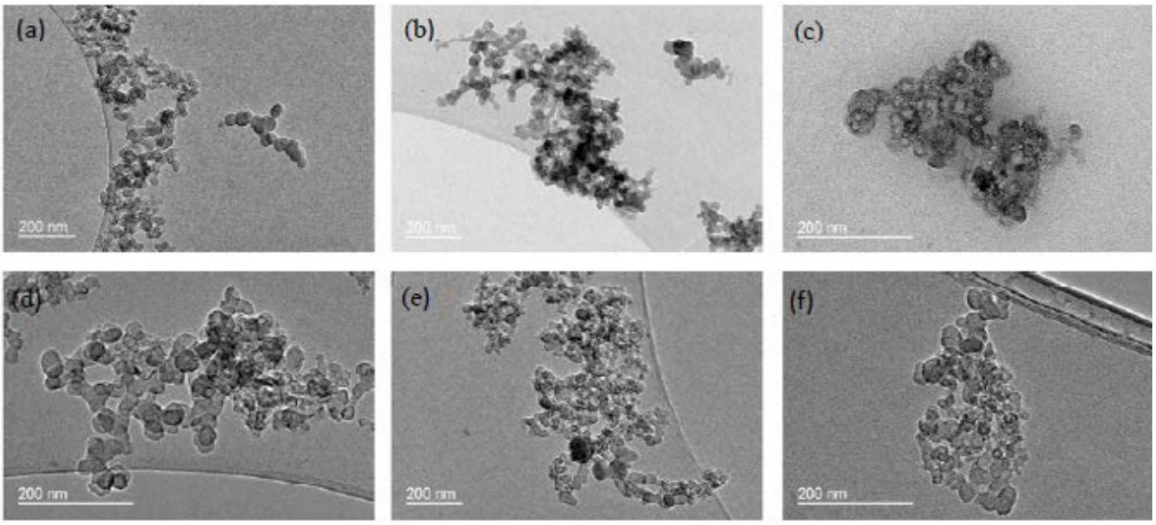

Fig. 2.2 TEM images of soot particles from (a) ULSD, (b) biodiesel, (c) DBE0, (d) DBE5, (e) DBE10 and (f) DBE20 at engine load of 0.58 MPa [128].

The TGA results indicated that the increase in fuel oxygen content caused reduction in ignition temperature (Fig. 2.3), activation energy and frequency factor and increase the oxidization reactivity (Fig. 2.4) compared to those of diesel fuel.

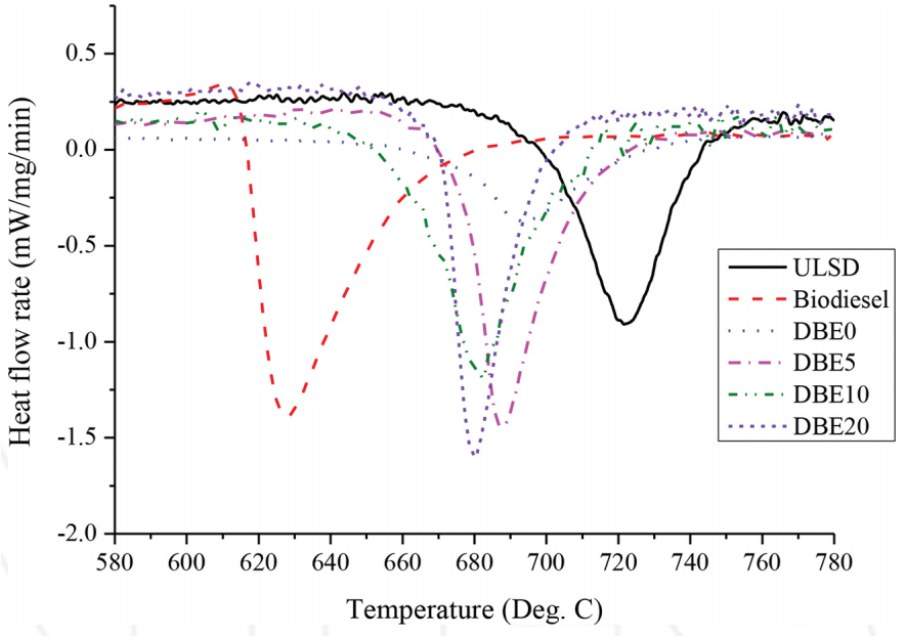

Fig. 2.3 Heat flow rate (derivative of DSC signal) curves for different fuels at a high engine load (0.58 MPa) [146].

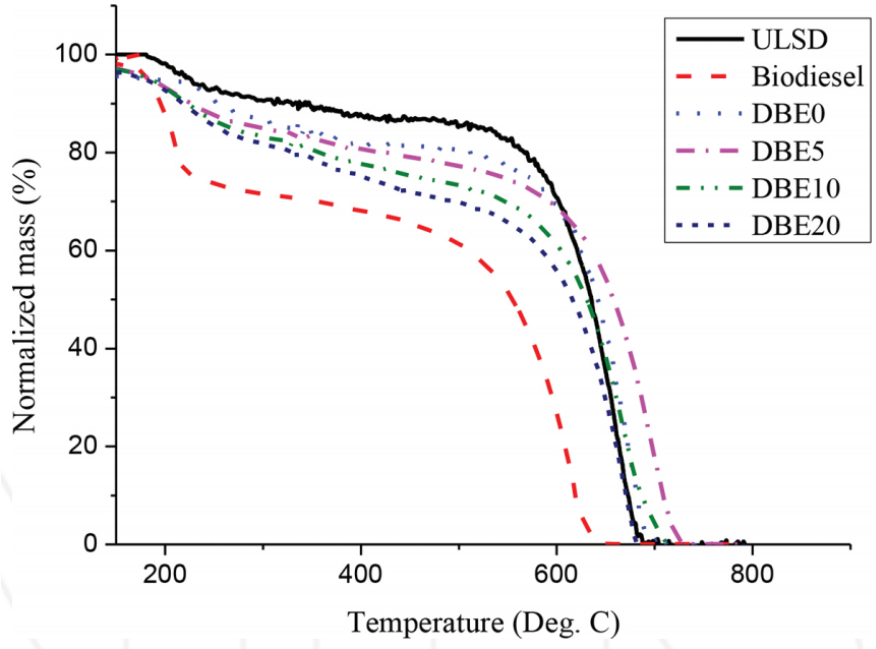

Fig. 2.4 Particulate mass reduction curve for different fuels at high engine load (0.58 MPa) [146].

Guan et al. [147] investigated the particle-phase compounds of PM emitted from a four-cylinder diesel engine. Experiments were operated at a fixed speed of 1800 rpm with two engine loads (25 and 75% of full torque) and fueled diesel, DB20, DB50, DBE5 and DBE10 (by volume %); while 10% biodiesel was added to each DBE blend as a co-solvent. It was recorded that both DB and DBE fuels had lower soot formation at both loads; while the DBE had better physicochemical aspects in soot compared to the DB. Also all the blended fuels had almost lower n-alkanes (C10-C30). Polycyclic aromatic hydrocarbons (PAHs) of both blends also reduced with use of DB and DBE blends; while DBE had higher effect on PAHs reduction than DB. The total particle-phase nitro-PAHs emissions of both DB and DBE were lower than pure diesel; while DBE10 had the lowest value. However, the use of DB and DBE caused increase in the total particle-phase oxy-PAHs emission in comparison with the diesel fuel.

According to the above studies, it can be concluded that most of the investigations are related to the engine combustion, performance and regulated emissions and only a few studies have been performed to explore the effect of DBE on the physicochemical properties of PM.

2.2 Fumigation mode

2.2.1 Effect of fumigation mode on engine combustion, performance and regulated emissions

According to the literature, various studies have been conducted to explore the effects of fumigated alcohols on the combustion, performance and emissions of diesel engines. Besides ethanol, the fumigated alcohols used include methanol [148-169], butanol [148,170-176] and propanol [148]. In addition, some studies utilized biodiesel (e.g. pine oil [177,178]) as a fumigated fuel. Due to lack of investigation on DBE using a mixture of biodiesel and ethanol as the fumigated fuel, the literature review presented in this section is mostly related to investigations conducted using fumigated ethanol. In those studies, fumigated fuel was injected into the intake manifold; while diesel fuel was injected into the engine cylinder directly.

The application of fumigated ethanol for diesel engines can be found in about 1980s [179]. Broukhiyan and Lestz [180] investigated the effects of fumigated ethanol, with up to 50% of the total fuel energy, on the engine performance and emissions of a light-duty

diesel engine under twelve operating conditions. It was found that fumigated ethanol caused decrease in PM and NO_X compared to the diesel fuel; while engine knock was recorded using higher ethanol percentage. In another study, Heisey and Lestz [181] tested the fumigated ethanol and methanol, with up to 55% of the total fuel energy, and found that the fumigated alcohols caused reduction in PM and NO_X and increase in ID and BTE compared to baseline diesel operation. Hayes et al. [182] also examined the impact of fumigated ethanol on the combustion and emissions of a turbocharged DI diesel engine under a constant engine speed of 2400 rpm with three loads. It was recorded that the fumigated ethanol had lower NO_X, but higher rate of pressure rise, peak pressure, HC and CO than those of baseline diesel operation.

Chauhan et al. [183] found that ethanol in fumigation mode improved engine performance and caused reduction in exhaust temperature NO_X, CO_2 and CO, but a penalty of increase in HC in comparison with baseline diesel operation. Pannirselvam et al. [184] explored the influence of fumigated ethanol on the performance and emissions of a diesel engine under various fumigated ethanol percentages and operating conditions. Their results showed that the fumigation mode had lower BTE and NO_X and higher HC and CO emissions compared to baseline diesel operation.

More recently, Morsy [185] investigated the impact of fumigated ethanol on the performance and emissions of a single-cylinder diesel engine under a constant engine load with six engine speeds. It was found the use of fumigated ethanol caused reduction in exhaust gas temperature and increase in BSFC, CO, HC and thermal and exergy efficiencies compared to baseline diesel operation.

Lee and Kim [34] investigated the impact of using wood pyrolysis oil+ethanol mixture as a fumigated fuel on the combustion, performance and emissions of a single-cylinder DI diesel engine under a constant engine speed of 1000 rpm with various engine loads. Three mixtures for fumigated fuel (20, 30 and 40% of wood pyrolysis oil mixed with ethanol, by mass %) were tested and the pure diesel was used as a pilot fuel. It was found that the use of fumigation mode caused reduction in in-cylinder pressure, HRR, indicated fuel conversion efficiency, COV_{IMEP}, $ISNO_X$ and smoke opacity, but increase in ISHC, ISCO and particle number concentration compared to baseline diesel operation. Similar results were also reported by Lee et al. [35] for fuel conversion efficiency, $ISNO_X$, ISHC and ISCO using wood pyrolysis oil+ethanol mixture as a fumigated fuel.

Bharathiraja et al. [186] explored the performance and emissions of a single-cylinder diesel engine using fumigation mode under a fixed engine speed and various engine loads. Ethanol and methanol were introduced into the intake manifold to achieve fumigation ratios of 10, 20 and 30% based on energy. It was reported that both fumigated fuels caused reduction in NO_X, CO_2 and smoke and increase in BSFC, CO and HC compared to baseline diesel operation. For BTE, the fumigated fuels had lower BTE at low load, but slightly higher BTE at medium and high loads. It was concluded that the ethanol had better performance and lower emissions compared to methanol.

Kumar et al. [187] investigated the effect of fumigated high octane fuels (ethanol, methanol and eucalyptus oil) on the combustion, performance and emissions of a single-cylinder diesel engine at a fixed engine speed of 1500 rpm with two engine loads. In single-fuel mode, two fuels including pure diesel and pure Mahua oil (MO) were used. In dual-fuel (DF) mode, the ethanol, methanol or eucalyptus oil was injected into the intake manifold via a carburetor and MO was used as a pilot fuel. The amount of fumigated fuels was tested up to the maximum possible limit. For engine combustion, it was found that fumigated fuels had longer ID than pure diesel and MO for both load and different fumigated fuel percentages; while the methanol the longest ID. However, the values of peak in-cylinder pressure, maximum HRR and duration of combustion were varied with different types and percentages of fumigated fuels and engine loads. In regard to engine performance, the fumigated fuels had higher BTE than pure MO at 100% load, but almost lower at 40% load. Compared to pure diesel, the fumigated fuels had almost lower BTE at both loads (except eucalyptus oil at high load). The fumigated eucalyptus oil had the maximum BTE among the fumigated fuels. In the respect of emissions, all fumigated fuels caused decrease in NO_X and increase in HC and CO at both tested loads compared to pure diesel and MO. However, fumigated fuel had lower smoke opacities only compared to pure MO for both loads. At low engine load, all the fumigated fuel and even pure MO had huge increase in smoke opacities in comparison with diesel.

Geo et al. [188] analyzed the effects of fumigated ethanol on the combustion, performance and emissions of a single-cylinder diesel engine at a fixed speed of 1500 rpm with four engine loads. The fumigated ethanol fractions were varied and three types of fuels including diesel, rubber seed oil (RSO) and rubber seed oil methyl ester (RSOME) were employed as pilot fuels. The results showed that the increase in ethanol led to reduction in duration of combustion, brake specific energy consumption (BSEC),

exhaust gas temperature and smoke; however, increase in peak in-cylinder pressure, maximum rate of pressure rise, ID, BTE, NO_X, HC and CO compared to baseline diesel, RSO and RSOME fuels.

Lee et al. [189] investigated the effect of ethanol in fumigation mode on the combustion, performance and emissions of a heavy-duty single-cylinder diesel engine conducted at constant engine speed of 1000 rpm with different engine loads. The fumigated fuel ratio (ethanol-diesel ratio) was controlled according to the input energy from 0 to about 50% of input energy. It was observed that the increase in ethanol caused reduction in indicated thermal efficiency (ITE), exhaust loss, $ISNO_X$, ISPM, mean size of the PM emissions and increase in ID, combustion loss, heat transfer loss, ISCO and ISHC in comparison with the diesel fuel. Also, the increase in ethanol led to reduction in total particle number (TNC), but increase in the number of nucleation mode particles compared to baseline diesel operation. However, the effect of using fumigated ethanol on the in-cylinder pressure, heat release rate and duration of combustion varied for different engine loads.

Pedrozo and Zhao [190] investigated the impact of fumigated ethanol on the combustion, performance and emissions of a single-cylinder diesel engine. The tests were conducted at different ethanol fractions, exhaust gas recirculation (EGR) ratios, effective compression ratios (ECR) and global fuel/air equivalence ratios at a constant engine speed (1200 rpm) and high load (IMEP of 1.8 MPa). It was observed that the increase in fumigated ethanol fraction led to reduction in maximum in-cylinder pressure, maximum HRR, ID (auto ignition was recorded), duration of combustion, combustion efficiency and $ISNO_X$ and increase in net indicated efficiency, COV_{IMEP}, ISCO, ISHC and ISsoot under almost all the tested EGRs compared to baseline diesel operation. It was reported that the use of Miller cycle and charge air cooling could reduce the in-cylinder gas temperature and control the auto ignition caused by fumigated ethanol.

The above studies show that the fumigation mode is still an attractive method in application to diesel engines. There are still active investigations conducted to find a suitable fumigated fuel and fumigated percentage to achieve the desired engine emissions and engine performance. However, most of the former studies are related of the fumigated ethanol and there are very few experiments about the use of a mixture of biodiesel and ethanol (BE) as the fumigated fuel. In addition, most of experiments were conducted under various engine loads at a constant engine speed, resulting in little

information about the effects of engine speed on the engine combustion, performance and emissions. Therefore, there is a knowledge gap about the effects of using BE as the fumigated fuel on the engine combustion, performance and emissions, which needs to be filled.

2.2.2 Effect of fumigation mode on physicochemical properties of PM

According to the literature, there are very few studies about the influence of the fumigation mode on physicochemical properties of PM of a diesel engine. For instance, Ruiz et al. [191] investigated the diesel PM oxidation reactivity and nano-structure and morphological characteristics of a dual-fuel combustion engine using ethanol or n-butanol as the fumigated fuel, with fumigation ratios of 10 and 15% based on the energy of baseline diesel operation. The results showed that the use of ethanol or n-butanol as fumigated fuel caused increase in PM, THC and VOF compared to baseline diesel operation; while ethanol had the maximum values. In addition, according to TGA results, the soot produced by the fumigation mode (for both ethanol and n-butanol) was more reactive to oxidation and exhibited higher active surface area in comparison with soot obtained under pure diesel operation; while ethanol had the highest values. However, the results obtained from TEM, X-ray diffraction spectroscopy (XRD) and Raman spectroscopy showed that the fumigation mode had almost no effect on the soot nano-structure or PM morphology at both engine loads compared to soot obtained under pure diesel operation. The measured soot nano-structure or morphology include interplanar distance between carbon layers, stacking thickness, fringes length (analyzed by XRD), Raman peaks intensity ratio (analyzed by Raman spectroscopy), aggregate images, mean primary particle diameter and fractal dimension of aggregates (analyzed by TEM).

Gargiulo et al. [192] investigated the combustion, performance, emissions and physicochemical properties of soot from a single-cylinder dual-fuel engine using ethanol as a port injected fuel. The tests were performed using various ethanol percentages at constant speed of 2000 rpm with two engine loads (medium and high loads). In regard to PM, it was found that the increase in fumigated ethanol led to decrease in BSPM mass and PM total number concentration. However, the TEM results showed that increase in fumigated ethanol had no effect on the average size of primary particles and a negligible effect on the soot nano-structural properties. The TGA analyses also revealed that the use of fumigated ethanol had faster oxidation reactivity than pure diesel, and the soot mass

losses for fumigated ethanol occurred at lower temperature compared to diesel.

It can be concluded from the above studies that investigation on the effects of fumigation fuel on the physicochemical properties of PM from diesel engine remains a knowledge gap in the literature, especially in the use of BE as the fumigated fuel. Therefore, more experiments are needed to fill this gap.

2.3 Comparison between blended and fumigation modes on engine combustion, performance and emissions

Several studies have been conducted to compare the effects between the blended and fumigation modes on the diesel engine combustion, performance and emissions. Mariasiu et al. [33] studied the performance and emissions of a single cylinder diesel engine using DB5 (95% diesel+ 5% biodiesel by volume %), blended mode (DBE15) and fumigation mode (DB+ ultrasonic fumigation of bioethanol) under a constant speed of 1800 rpm and four engine load. It was found that the fumigation mode had lower BSFC (-7.45%), NO_X (-3.8%) and THC (-1.63%), and higher CO (11.1%) emissions compared to the blended mode.

Abu-Qudais et al. [30] compared the effects of ethanol fumigation and ethanol-diesel blend on the performance and emissions of a single cylinder diesel engine at different engine speeds. In that study, 20% of ethanol was mixed with diesel and 20% of ethanol (ethanol percentage as a fraction of the diesel energy input at full rack setting) was used in the fumigation mode. The results revealed that both modes had better performance and emissions compared to baseline diesel operation; however, the fumigation mode showed higher BTE and lower CO, HC and soot emissions, in comparison with the blended mode.

Cheng et al. [31] compared the influences of 10% blended methanol (by volume %) or 10% fumigation methanol with waste cooking oil biodiesel on the performance and emissions of a diesel engine at a constant engine speed of 1800 rpm with five engine loads. It was observed that both modes of operation led to decrease in CO_2, NO_X and particulate mass emissions and reduction in mean particle diameter in comparison with baseline diesel operation; while the blended mode led to the lowest GMD and total number concentration among all the tested fuels and modes of operation. Compared to the diesel fuel operation, CO and HC emissions were similar in the blended mode, but

were higher in the fumigation mode. In addition NO_2 emission in the fumigation mode was higher than that of the blended mode and diesel mode. In regard to BTE, a higher BTE was found at low engine load for the blended mode compared to the fumigation mode; while a higher BTE was observed at medium and high engine loads for the fumigation mode.

In addition, Şahin et al. [32] compared the impact of n-butanol/diesel blends and n-butanol fumigation on the performance and emissions of a turbocharged diesel engine, using 2%, 4%, and 6% by volume of n-butanol, under different engine loads and engine speeds. It was found that both modes (blended and fumigation) led to reduction in smoke compared to the diesel fuel; while the reduction was higher in the fumigation mode. NO_X emission of fumigation mode was lower than that of diesel fuel; however, NO_X emission of the blended mode was higher than that of diesel fuel. HC emissions of both modes were higher than that of diesel fuel; being higher in the fumigation mode that in the blended mode. Similarly, CO_2 emissions were increased for the two modes compared to that of diesel fuel; however, CO_2 emissions were lower in the fumigation mode than in the blended mode. In regard to BSFC, n-butanol fumigation caused increase in BSFC at all test conditions; while the blended mode led to reduction in BSFC for 2% and 4% n-butanol blends (except 6% n-butanol blend which caused increase in BSFC). Also, the HRR diagrams of the blended modes were similar to those of diesel fuel; however, the HRR diagrams of fumigation mode had a double peak structure. The first peak, which was small, occurred earlier than that of diesel fuel and the second peak, which was also the main peak, took place later.

It can be observed that only a few studies have been conducted to investigate the differences between the blended mode and the fumigation mode on the engine combustion, performance and emissions; while almost no information is available in regard to the difference between the two modes on the physicochemical properties of PM. In addition, only pure alcohols were used as fumigated fuels and BE cannot be found as a fumigated fuel for comparison with blended mode (DBE). Thus, there are needs of more experimental studies to fill these gaps.

2.4 Summary

According to the above literature review, it can be concluded that despite of different studies had been conducted using blended and fumigation ethanol, the following knowledge gaps still exist.

- There is lack of investigation that compare the blended mode with fumigation mode using DBE fuels on the engine combustion, performance and emissions;
- There is lack of investigation on the effects of a combination of fumigation and blended modes (F+B mode) on the engine combustion, performance, emissions and physicochemical properties of PM;
- There is lack of study about the physicochemical properties of PM for DBE blended and fumigation mode of operation;
- There is lack of study on the use BE as the fumigated fuel;

This study will address the above issues.

CHAPTER 3 EXPERIMENTAL SETUP AND PROCEDURES

The present chapter describes the experimental setup and procedures for investigating the engine performance, combustion and emissions under different fueling modes. The measurement and analysis of combustion and performance parameters, the regulated emissions and the methodologies for analysis of the physicochemical properties of the PM samples are also explained.

3.1 Test engine rig

The test engine was a 4-cylinder, direct injection (DI), naturally aspirated, water-cooled diesel engine. The engine speed and torque were controlled by use of an eddy-current dynamometer and Ono Sokki heavy diesel engine test system. The schematic diagram of the experimental setup and the specifications of the test engine are shown in Fig. 3.1 and Table 3-1, respectively. In addition, schematic diagrams for different fueling modes investigated in the present study, including diesel, blended, fumigation and combined fumigation+blended are also presented in Fig. 3.1.

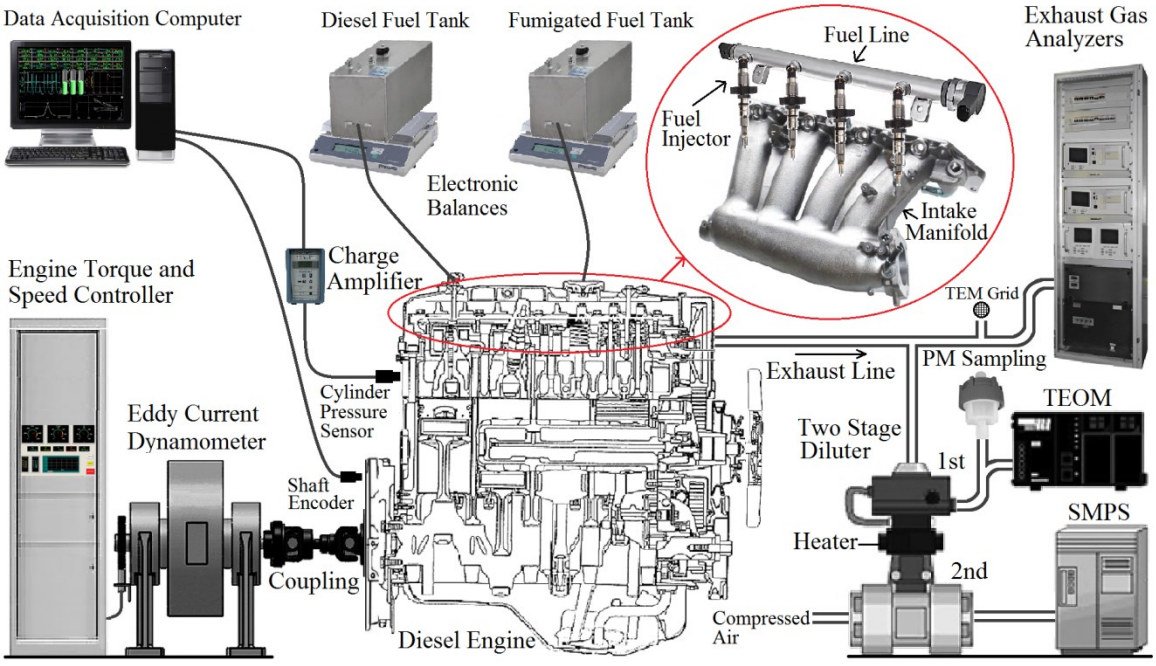

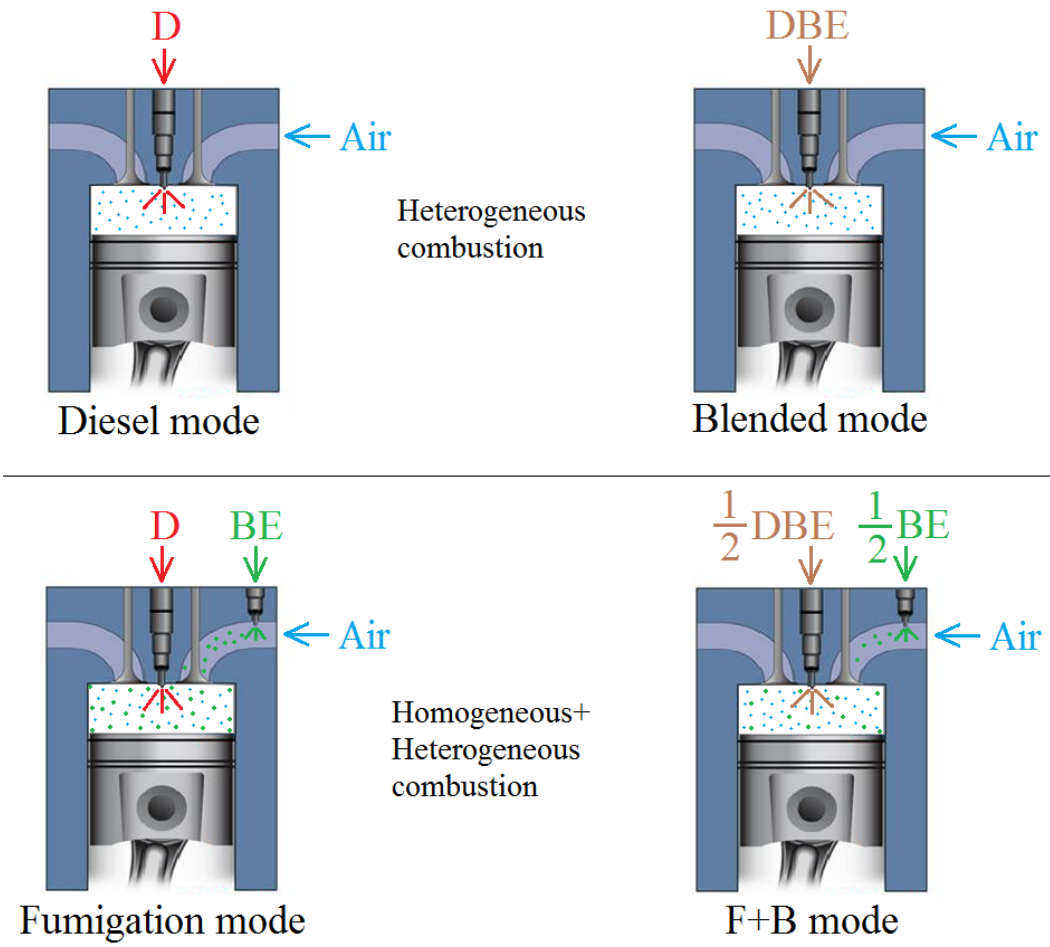

Fig. 3.1 Schematic diagrams of the experimental setup (up) and fueling modes (down) investigated in the present study.

Table 3-1 Specifications of test engine

Model	**Isuzu 4HF1**
Engine type	In-line 4-cylinder DI
Combustion chamber shape	Omega
Maximum power	88 kW/ 3200 rpm
Maximum torque	285 Nm/ 1800 rpm
Bore × stroke	112 mm × 110 mm
Displacement	4334/cc
Compression ratio	19.0: 1
Fuel injection timing	8° BTDC
Injection pump type	Bosch in-line type
Injection nozzle	Hole type (with 5 orifices)

3.2 Test procedures

In this study, the experiments for engine combustion, performance and emissions can be separated into three groups. The first group concerns with the effects of using different fueling modes (diesel, blended, F+B and fumigation modes) on the engine combustion, performance and emissions at different engine loads. In this case, the experiments were conducted under a constant engine speed of 1800 rpm with five engine loads of 57, 99.8, 142.5, 185.3 and 228 Nm corresponding to 20, 35, 50, 65 and 80% of the full engine torque, respectively. The second group is related to the effects of using different fueling modes on the engine combustion, performance and emissions at different engine speeds. In this case, the tests were performed at a constant engine torque of 142.5 Nm (50% of the full engine torque) with five engine speeds of 1400, 1600, 1800, 2000 and 2200 rpm. The third group is aimed to study the physicochemical properties of PM. In this case, the tests were performed at a low engine speed of 1400 rpm and at a high engine speed of 2200 rpm, and at each engine speed, tests were performed at 20% and 80% loads. The operating conditions covered in the present study are summarized in Table 3-2.

At each operating condition, the engine was allowed to run for around one hour until the exhaust gas temperature, the cooling water temperature, the lubricating oil temperature as well as the CO_2 concentration reached steady-state conditions and data was measured subsequently. The steady state experiments were repeated three times for the first and second groups of tests and two times for the third group for ensuring that the data was repeatable within the experimental uncertainties of the measurements. The experimental results were compared with the two-tailed student's T-test to verify if they are significantly different from each other at 95% significance level.

Table 3-2 Operating conditions for the present study

Group of test	Purpose	Engine speed (rpm)	Engine load (Nm)	No. of operating conditions
1	Combustion, performance and emissions	1800	57, 99.8, 142.5, 185.3 and 228	5
2	Combustion, performance and emissions	1400, 1600, 1800, 2000 and 2200	142.5	5
3	Physicochemical properties of PM	1400 and 2200	57 and 228	4

3.3 Fuel properties and fueling modes

The main fuels involved in this study include diesel with fuel sulfur content of less than 10 ppm by weight (Euro V), waste cooking oil biodiesel in compliance with EN14214 standard and ethanol with a high purity of 99.9% (sugarcane feedstock). The properties of diesel and biodiesel used in this study meet all the limitations from the American standard (ASTM) and European standard (ISO), respectively. The properties of the fuels are shown in Table 3-3. The biodiesel was produced from waste cooking oils collected from restaurants in Hong Kong by a local company (Dynamic Progress Company). The composition of the biodiesel is shown in Table 3-4. The biodiesel composition was determined by a Hewlett-Packard 7890 SERIES II Gas chromatograph with Flame ionization detector (FID). The detector and injection systems were conducted at a constant temperature (280 °C). While a heating program from 100 °C to 220 °C with a constant rate of 3 °C/ min for 15 minutes was utilized for the Durabond-Wax capillary column (30 m × 0.25 mm × 0.25 μm). The retention time of each fatty acid methyl ester peak from the amount of their respective standards showed the fatty acid profile and hence determined the composition of biodiesel.

Table 3-3 Properties of the tested fuels [128]

Parameters [a]	**Diesel (Euro V)**	**Biodiesel (waste cooking oil)**	**Ethanol (sugarcane feedstock)**
Cetane number	52	51	6
Lower heating value (MJ/kg)	42.5	37.5	28.4
Density (kg/m^3) at 20 °C	840	871	786
Viscosity (mPa.S) at 40 °C	2.4	4.6	1.2
Heat of evaporation (kJ/kg)	250-290	300	840
Carbon content (% mass)	86.6	77.1	52.2
Hydrogen content (% mass)	13.4	12.1	13
Oxygen content (% mass)	0	10.8	34.8
Sulfur content (ppm)	<10	<10	0
Flash point (°C)	78	210	15
Stoichiometric air–fuel ratio [b]	14.56	12.59	9.00

a: according to the ASTM standard for diesel, and ISO standard for biodiesel and ethanol obtained from [128] and fuel suppliers; b: calculated according to [193].

Table 3-4 Composition of fatty acids in waste cooking oil biodiesel

	Fatty acid methyl esters		**Composition, by weight (%)**
c10:0	Methyl caprate	Capric acid	0.1
c12:0	Methyl laurate	Lauric acid	0.2
c14:0	Methyl myristate	Myristic acid	0.7
c16:0	Methyl palmitate	Palmitic acid	17.3
c16:1	Methyl palmitoleate	Palmitoleic acid	1.3
c18:0	Methyl stearate	Stearic acid	3.6
c18:1	Methyl oleate	Oleic acid	48.7
c18:2	Methyl linoleate	Linoleic acid	23.7
c18:3	Methyl linolenate	Linolenic acid	4.4

The four fueling modes adopted in this study (Fig. 3.1) are diesel alone, blended, fumigation and fumigation+blended (F+B) modes. The first mode involves using pure diesel to obtain the baseline results. The pure diesel fuel was directly injected into the engine cylinder and the ignition was initiated by hot compressed air which is a type of heterogeneous combustion. The second mode is the blended mode, in which the ternary blend contains 80% diesel, 5% biodiesel and 15% ethanol (D80B5E15) by volume was tested. The type of combustion in blended mode is the same as that in the diesel mode, i.e., heterogeneous combustion. The third mode is the fumigation mode. In this mode, a mixture comprising 25% biodiesel and 75% ethanol (BE) was injected into the intake manifold with fuel injectors, one for each cylinder, with an injection pressure of 0.35 MPa; while diesel fuel was injected directly into the cylinders, with a desired overall fuel consumption comprising 80% diesel and 20% BE (5% biodiesel and 15% ethanol), to match with the composition of the fuel used in the blended mode. During the intake and compression strokes, the BE is mixed with air to form a homogeneous mixture and then the main fuel is injected into the cylinder, resulting initiation of combustion by the hot compressed air/BE mixture (homogeneous+heterogeneous combustion), which is different from that of the diesel or blended mode (heterogeneous combustion). As ethanol is a corrosive fuel, a Teflon fuel line (PTFE) which is suitable for ethanol up to 85% (E85) was utilized to deliver the BE fuel in the intake manifold. An electronic control unit (ECU) was used to adjust and control the fueling rate of BE; while the amount of diesel fuel was adjusted automatically through the Ono Sokki heavy diesel engine test system. Two electronic balances with readability and precision of 0.1g were used to measure the mass consumption rates of diesel and BE. To achieve the 20% of fumigated

fuel, firstly the engine was run by diesel only at the desired engine load, then the fumigated fuel (BE) was injected into the intake manifold; while the mass of diesel fuel would be reduced automatically by the Ono Sokki heavy diesel engine test system to maintain the desired engine load and the consumed masses of diesel and fumigated fuel were recorded with the two electronic balances. If the consumed volume of the fumigated fuel was less than 20% of the total volume (diesel+fumigated fuel), the amount of injected BE fuel was increased by adjusting the ECU. In contrast, if the consumed volume of the fumigated fuel was more than 20% of the total volume, the rate of injected BE fuel was decreased by adjusting the ECU. After several trials on the measurements of diesel and BE mass flow rates, the desired fuel content (D80B5E15) for each engine load could be achieved. The fourth mode is the F+B mode. In this case, half of the BE mixture was injected into the intake manifold; while another half of the BE mixture was blended with diesel to form the DBE mixture comprising 90% diesel, 2.5% biodiesel and 7.5% ethanol for direct injection into the diesel engine. Therefore, the final fuel content in the F+B mode is also D80B5E15. The type of combustion in the F+B mode is a homogeneous+heterogeneous combustion which is the same as that of the fumigation mode; while the amount of the homogeneous mixture (BE injected) for the F+B mode is half of the fumigation mode. The constant fuel percentage (D80B5E15) is the key point for comparison of different fueling modes.

According to the literature [15,17,27], alternative fuels in various percentages even up to 50% (10% biodiesel with 40% ethanol or 40% biodiesel with 10% ethanol) have been mixed with diesel fuel. On the other hand, some studies have reported (based on experiments) that there is a limitation to use the certain amount of biodiesel and ethanol mixing with diesel fuel in those diesel engines which have no engine modification. For instance, 20% biodiesel or 25-30% biodiesel+ethanol [16] can be mixed with diesel fuel in diesel engine without need for major engine modification. However, in this study, since the fumigation mode which might has an effect on the engine operating was tested; therefore there was a limitation of using biodiesel and ethanol. Thus, some tests were conducted to find a suitable biodiesel+ethanol percentage which had not much effect on the engine operating, and finally 20% of biodiesel+ethanol was selected for this study. In regard to the selection 5% biodiesel, two criteria were considered. Firstly, there is a need of using the highest biodiesel content to make the DBE blended fuel stable (for the blended mode). Secondly, there is a need of using the lowest biodiesel content in the

fumigation mode; because a low pressure fuel injector (0.35 MPa) cannot be worked properly with use of higher biodiesel content due to its higher viscosity and density. Thus, the 5% biodiesel was selected which had a sufficient effect in stabilizing the DBE blend (in blended mode) and also it could be easily injected with low injection pressure (in fumigation mode).

Fuel samples were observed for four months to understand the stability of the blended fuels. No phase separation was observed for the DBE for blended mode and BE for fumigation mode up to four months. However, the DBE for F+B mode had a phase separation after about two months due to the low percentage of biodiesel in the blended fuel.

3.4 Combustion and performance analyses

The combustion characteristics of a diesel engine are normally reflected by the variation in in-cylinder pressure and heat release rate. The influence of different fueling modes on the combustion characteristics can be investigated by comparing the heat release rates to obtain information in regard to ignition delay (ID), in-cylinder gas temperature, start of combustion (SOC), duration of combustion (DOC), rate of pressure rise and rate of heat release rise. Start of combustion (SOC) is defined as the zero crossing of heat release (which means the beginning of rapid pressure rise or the beginning of heat release) in the unit of crank-angle degree (°CA). Ignition delay is the interval between the start of fuel injection (8 °CA BTDC) and the SOC. End of combustion (EOC) is the point at 95% of heat release. Duration of combustion is defined as the interval between the SOC and the EOC. Premixed combustion phase (PCP) is calculated based on the heat release in the interval between the SOC and the end of rapid decrease of heat release rate. Diffusion combustion phase is the heat release in the interval between the end of PCP and the EOC.

In addition, some other parameters of engine combustion and performance were analyzed and calculated, which include brake thermal efficiency (BTE), brake specific fuel consumption (BSFC), coefficient of variations (COV) of IMEP and maximum pressure, exhaust gas temperature, mass fraction burnt and air/fuel ratio.

For engine combustion analyses, the in-cylinder pressure was measured using a piezoelectric pressure sensor (type 6056A, Kistler Co., Inc.) and a charge amplifier (type 5011B, Kistler Co., Inc.) was employed to amplify the recorded in-cylinder pressure

signals. The crank-angle signal was measured by a crank-angle encoder (type CA-RIE-360/720, DEWETRON GmbH) with resolution of 0.5 °CA. First Law of Thermodynamics was employed to convert the measured pressure data to HRR data using the commercial software DEWESoft^{TM} (DEWETRON GmbH).

To calculate the BSFC and BTE for engine performance analyses, the fuel consumptions were recorded for five minutes gravimetrically. Two electronic balances (Shimadzu Balance, Model BX-32KH) with readability and precision of 0.1g were utilized to measure the fuel consumptions, one for diesel fuel (for diesel mode) or the blended fuel (for blended mode) and the other for the fumigated fuel (for fumigation mode). The exhaust gas temperature was measured by use of a K-type thermocouple.

The brake thermal efficiency (BTE) is the efficiency that chemical energy of a fuel is turned into useful work, calculated as shown below for each mode of operation:

$$BTE_{Diesel} = \frac{P_b}{(\dot{m}_d \times LHV_d)} \quad 3.1$$

$$BTE_{Blend} = \frac{P_b}{(\dot{m}_{DBE} \times LHV_{DBE})} \quad 3.2$$

$$BTE_{Fumigation} = \frac{P_b}{(\dot{m}_d \times LHV_d) + (\dot{m}_f \times LHV_f)} \quad 3.3$$

$$BTE_{F+B} = \frac{P_b}{(\dot{m}_{DBE} \times LHV_{DBE}) + (\dot{m}_f \times LHV_f)} \quad 3.4$$

While the brake specific fuel consumption (BSFC) is the ratio of fuel mass consumption rate to the brake power, calculated as shown below for each mode of operation:

$$BSFC_{Diesel} = \frac{\dot{m}_d}{P_b} \quad 3.5$$

$$\mathrm{BSFC_{Blend}} = \frac{\dot{\mathrm{m}}_{\mathrm{DBE}}}{\mathrm{P_b}} \quad 3.6$$

$$BSFC_{Fumigation} = \frac{\dot{m}_d + \dot{m}_f}{P_b} \quad 3.7$$

$$BSFC_{F+B} = \frac{\dot{m}_{DBE} + \dot{m}_f}{P_b} \quad 3.8$$

Where BTE is the brake thermal efficiency (%), BSFC is the brake specific fuel consumption (g/kWh), P_b is the brake power (kW), $\dot{m}_d$, $\dot{m}_{DBE}$ and $\dot{m}_f$ are the fuel mass consumption rates (kg/s for BTE and g/h for BSFC calculations) for diesel, blended and fumigated fuels, respectively. LHV_d, LHV_{DBE} and LHV_f are the lower heating values (kJ/kg) for diesel, blended and fumigated fuels, respectively.

3.5 Gaseous emissions measurement

The gaseous emissions measured in the present study include carbon monoxide (CO), nitrogen oxides (NO_X) and total hydrocarbons (THC). In addition, concentrations of carbon dioxide (CO_2) and oxygen were measured for reference. CO and CO_2 were measured with Non-dispersive infrared analyzers (300 NDIR, CAI Inc.). NO_X was recorded through a Heated chemiluminescent analyzer (600 HCLD, CAI Inc.); while its components, NO_2 and NO, could be evaluated separately. HC was measured with a Heated flame ionization detector (300 HFID, CAI Inc.). O_2 was recorded with an Accurate lambda meter-gauge (ALM-Gauge, Ecotrons Inc.) which consists a Bosch LSU 4.9 wideband oxygen sensor and a Bosch driver chip CJ125. All the analyzers were calibrated before the start of measurements with zero and span gases. All the regulated gaseous emissions were directly sampled from the engine exhaust line, where NO_X and HC were sampled through a heated line which was maintained at 190°C. All gaseous emissions were recorded over a period of five minutes to obtain the average values. The measured volumetric concentrations, expressed in % or ppm, are converted into brake specific concentrations, expressed in g/kWh, following the procedures in [194].

3.6 Particulate matter (PM) sampling and measurement

For particulate measurement, the exhaust gas was diluted with a two-stage mini-diluter (Dekati Ltd, Finland). The first stage was heated at about 160 °C (the final PM temperature was 47±5 °C) with an electrical heater; while the second stage was not heated. The sampled gas was taken from the exhaust manifold through an insulated and heated sampling line to prevent the condensation of volatile substances and deposition of solid particles on the interior pipe wall. The actual dilution ratio (DR) in this study was calculated according to the measured CO_2 concentrations in the raw exhaust, background and diluted exhaust as presented in the following equation.

$$DR = \frac{[CO_2]_e - [CO_2]_b}{[CO_2]_d - [CO_2]_b} \qquad 3.9$$

Where $[CO_2]_e$, $[CO_2]_b$ and $[CO_2]_d$ are the CO_2 concentrations of the exhaust gas before dilution, in the background and after dilution, respectively. In the present study, depending on the engine operating conditions, the first-stage DR varied from 5.48 to 8.3 and the second-stage DR varied from 44.9 to 67.9.

3.6.1 PM mass, particle number concentration and size distribution

For measuring PM mass concentration, the first-stage diluted exhaust gas was delivered to a Tapered element oscillating microbalance (TEOM 1105, Rupprecht & Patashnick Co., Inc.), and for measuring the particle size distribution and number concentration, the second-stage one was connected to a Scanning mobility particle sizer (SMPS model 3494, TSI Inc.) (Fig. 3.1). The SMPS consists of a Differential mobility analyzer (DMA model 3071 A, TSI Inc.) and a Condensation particle counter (CPC model 3022, TSI Inc.). The particle number concentration and size distribution was measured from 15 nm to 750 nm. PM mass concentration was measured for five minutes continuously; while particle number concentration and size distribution was measured four times at each operating condition and the averages of the results are presented.

3.6.2 Particulate matter sampling for chemical analysis

Particulate samples are required for analysis of the chemical properties of the particulate matter. The PM samples were taken from the first diluter (first-stage diluted exhaust gas). For getting the samples required for off-line PM measurement, two types of filter including 47 mm diameter quartz fiber filter and Teflon filter were utilized. The quartz fiber filter (type QM-H, Whatman^{TM}, Sweden) was made from 100% pure quartz and could be used up to 900 °C. The quartz fiber filter was utilized to collect the PM for analyses of the OC-EC, water-soluble organic carbon, PAHs, n-alkanes, particle volatility, oxidation reactivity and inorganic ions. The Teflon filter (Membrane filter, PTFE supported, Whatman^{TM}, Germany) with pore size of 0.2 μm was employed to collect the PM for the metal and elements analysis.

The PM sampling durations varied from 3 to 20 min, depending on the engine operating conditions, to obtain enough PM mass (more than 1 mg) for PM analyses, for each fueling mode. The filters with deposited PM were stored one day in a desiccator cabinet, maintained at temperature of 22±2 °C and humidity of 50±5%, to remove water content from the filters and permit the collected PM mass to reach equilibrium for weighing (similar method to [195]). The PM mass was calculated as the difference in mass of the filter after PM sampling with that of the same filter before PM sampling (the blank filter), as measured with a micro balance (Sartorius MC5, capacity of 5.1 g with readability of 1 μg). To increase the accuracy in PM mass measurement, each filter (before and after PM sampling) was weighed five times and the average result was utilized. The collected

samples were stored in a desiccator cabinet for less than 3 days until they were delivered for the extraction or analysis for all the off-line PM measurements. To obtain the chemical properties (e.g. ions, metals or etc.) of PM from exhaust (without filter or solvent), chemical properties of three blank filters for each analysis were subtracted from the total chemical properties of PM, filter and solvent. Therefore, only the amount of chemical properties of PM from exhaust without contaminants (chemical properties) from filters or solvents (for extraction) are presented in this study.

3.7 Physical properties of PM

PM emission is a major concern because exposure to it has various effects in pulmonary and cardiovascular morbidity and mortality due to its different physicochemical properties [36-40]. Therefore, there are needs of more studies to investigate the physicochemical properties of PM emitted from the engine using different fueling modes. In regard to the investigation of physical properties of PM emissions, the micro-structure and nano-structure are analyzed in the present study.

3.7.1 Micro-structure and nano-structure of PM

For the morphology and the nano-structure analyses of the PM, two equipment including Field emission-scanning transmission electron microscope (known as STEM, Jeol JEM-2100F) and Field emission-scanning electron microscope (known as SEM, Tescan MAIA3) were employed. The magnification and resolution of each equipment are presented in Table 3-5.

Table 3-5 Magnification and resolution of STEM and SEM

Equipment	**Maximum magnification**	**Resolution**
Field emission-scanning transmission electron microscope (STEM)	up to 910,000X	0.23 nm
Field emission-scanning electron microscope (SEM)	up to 500,000X	1 nm at 15 kiloelectron-volts (keV) and 1.4 nm at 1 keV in the beam deceleration mode

The literature shows that the samples for micro-structure and nano-structure analyses have been collected directly or indirectly from the PM sources. In direct PM sampling, the TEM grid is directly exposed to the PM sources (e.g. exhaust from engines, burners

or etc.) using collectors like probes based on aerodynamic quenching, N_2 dilution, and thermophoresis [196-202]. The collectors have been located in different positions to collect the samples, such as inside the engine cylinder (in-flame soot sampling) [203-205], in the engine exhaust pipe [204,206,207] or after a diluter [208,209]. However, in-flame soot sampling has some disadvantages, such as difficulty in inserting the probe into the engine cylinder, and the soot particles may not be formed completely due to the short time duration between the combustion and TEM sampling. On the other hand, long sampling time and adding air in a diluter during the dilution process will affect the particle structures.

In in-direct PM sampling, firstly the particles are collected using filters and then extracted by solvents to form a solution, and finally some droplets are put on the TEM grids and after drying, the samples are ready for analysis [210-214]. However, this method has the disadvantage in affecting the physicochemical properties of the particles due to suspending the particles in a liquid medium [215,216] and also changing the shape and structure of the agglomerated particles.

For the present study due to the disadvantages of in-flame, diluted or filter sampling methods as mentioned above, the required PM sample for STEM and SEM analyses was directly collected from the exhaust pipe on a TEM grid using a solenoid valve in combination with a time controller (accuracy of operating time was ±1%) as shown in Fig. 3.2. The 3 mm copper grid with 400 meshes supported by holey-carbon film was utilized. The hot particles from exhaust gas can stick on the TEM grid due to the thermophoretic effect [207]. The solenoid valve is suitable for application of hot gas (steam) and sustainable with solid particulate contaminants. The orifice size of the solenoid valve is 3 mm, the maximum working temperature is 180 °C and the maximum working pressure is 2 MPa. The sampling time varied from 50 ms to 10 s, according to the operating conditions: 50ms for 2200rpm-228Nm, 700ms for 1400rpm-228Nm, 5s for 2200rpm-57Nm and 10s for 1400rpm-57Nm. The sampling time was selected after doing some pretests with STEM to find the time required for deposition of sufficient particles on the TEM grids for analysis. Since the sampling time was short (50ms to 10s), the hot exhaust gas from the exhaust pipe had no effect on the working efficiency of the solenoid valve. Since the use of gold film may change the shape and the location of the particles and clusters and also the copper grid has high conductivity; therefore, no gold film was used for SEM analyses.

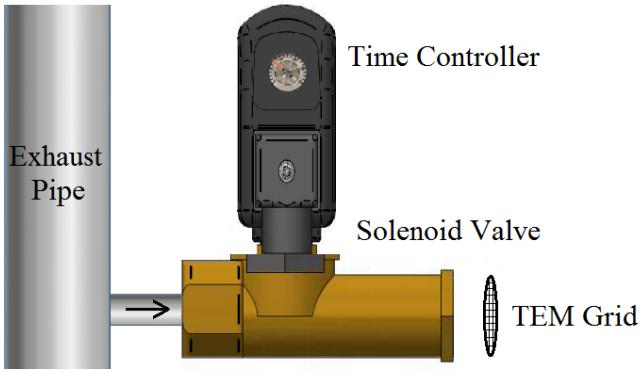

Fig. 3.2 TEM sampling setup.

For analyzing the micro-structure (including primary particle size and aggregate particle size) and nano-structure (including fringe length, separation distance and tortuosity) of PM from STEM and SEM images, a commercial image processing software (Image-Pro Plus 6.0, Media Cybernetics) was employed. To increase the accuracy of the results, about 200 spherical particles with clear boundaries were randomly selected to investigate the primary particle size for each operating condition. In regard to nano-structure of PM, about 10 regions of interest (ROI) without underlying carbon films were chosen from the STEM images to analyze the fringe length, separation distance and tortuosity of PM for each fueling mode.

According to the results summarized in [217], various fringe parameters have been identified including fringe length, tortuosity (curvature, elongation or aspect ratio), fringe separation (interplanar spacing), parallel stacking number and orientation (structural ordering) to reflect the nano-structure of a particle. However, the fringe length, tortuosity and fringe separation distance are most closely related to the physico-chemical properties of the PM [218]. Therefore, they are selected to analyze in the present study. The term fringe length is a measure of the physical extent of the atomic carbon layer planes which can be obtained from the high resolution TEM image (STEM image). The fringe length also shows the dimension of the basal plane diameter. The term tortuosity is a measure of the curvature of the fringes and shows the extent of odd numbered (5-membered and 7-membered) carbon rings with the substance. The tortuosity is also a measure of disorder within the substance. The tortuosity of a fringe is calculated as a ratio of fringe length to distance between two endpoints. The term fringe separation reflects the mean distance between the adjacent carbon layer planes [217]. The fringe length, tortuosity and fringe separation distance are presented in Fig. 3.3.

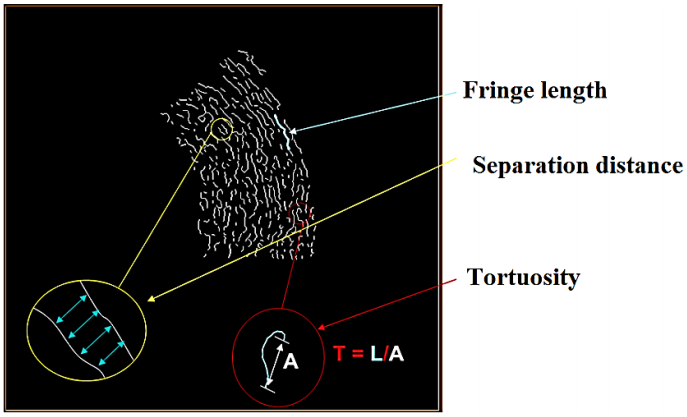

Fig. 3.3 Schematic of fringe length, tortuosity and separation distance [219].

Before analyzing the fringe length, tortuosity and fringe separation distance, the STEM images have to be pre-process flowing the pre-processing procedures described in [217]. The flow chart of the image processing program for STEM images is shown in Appendix A. The pre-processing procedures in one STEM image, as an example for this study, are presented in Fig. 3.4 to Fig. 3.7.

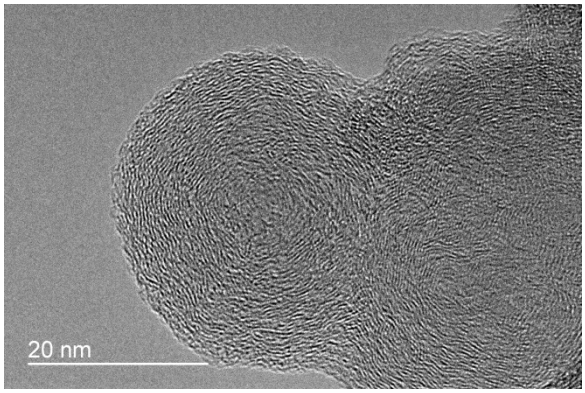

Fig. 3.4 Original STEM image.

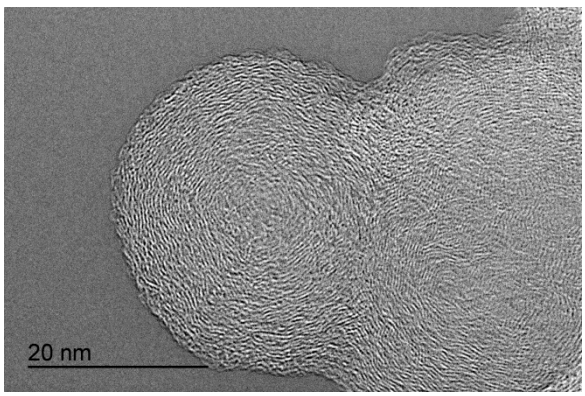

Fig. 3.5 STEM image after applying negative transformation.

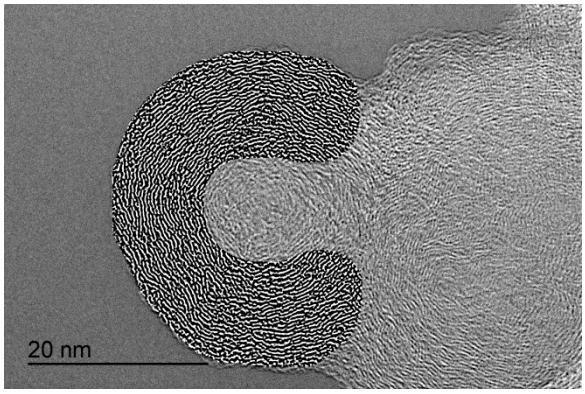

Fig. 3.6 STEM image after applying contrast enhancement, Gaussian lowpass filter and top-hat transformation.

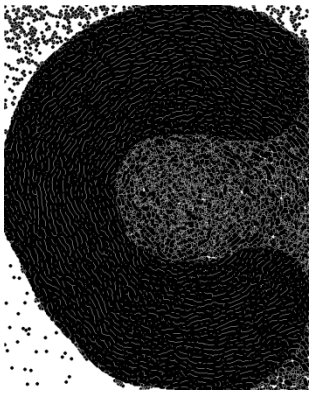

Fig. 3.7 STEM image after applying threshold, morphological opening and closing and Skeletonization.

3.8 Chemical properties of PM

It is well known that to reduce the amount of PM emissions or make them less detrimental to human health and the environment, it is necessary to determine their chemical properties. Since the diesel engine is a source of PM to the atmosphere, there are needs of more investigations on the chemical properties of PM emitted by diesel engines. In this study, the chemical properties of PM emitted by the diesel engine under various fueling modes, including organic carbon, elemental carbon, volatile and non-volatile substances, oxidation reactivity, water soluble organic carbon, inorganic ions, metals, elements, PAHs and n-alkanes, are analyzed.

3.8.1 Carbonaceous components analysis

Carbonaceous component (total carbon, TC) is abundant material of PM emitted from a diesel engine. TC consists of organic carbon (OC) and elemental carbon (EC) which are harmful for the environment and human health. OC, due to consisting of some semi-volatile hydrocarbons, is a suspected human carcinogen component [220]. On the other hand, EC has an effect on the air pollution, global carbon cycles and it can absorb the solar radiation resulting in energy redistribution and climate change [221-223]. Therefore, some methods are needed to reduce the OC and EC emission from diesel engines. In this study, the use of DBE in the blended and fumigation modes is tested to investigate its effect on the amount of EC and OC compared to the diesel mode.

According to the available methods reported in the literature the thermal/optical methods are the accepted and the most widely used methods for OC/EC analysis [224,225]. In the last three decades, these approaches have been introduced for various protocols, including the IMPROVE (Interagency Monitoring of Protected Visual Environments) [226-229], NIOSH (National Institute of Occupational Safety and Health) [226,230], EUSAAR (European Supersites for Atmospheric Aerosol Research) [231] and STN (Speciation Trends Network, a modification of NIOSH) [232] protocols. The separation between OC and EC in these protocols is based on the different volatility properties of OC and EC at different analyzing temperatures. The EC compared to OC, is a low-volatility component which is not liberated in an inert atmosphere under temperatures < 350°C [233].

In the present study, the OC and EC were analyzed according to IMPROVE-A (Interagency Monitoring of Protected Visual Environments) TOR (thermal optical reflection) protocol using DRI Model 2001 Thermal/optical carbon analyzer (Atmoslytic Inc., Calabasas, CA 91302, USA). According to the nominal IMPROVE-A TOR protocol [227], eight carbon fractions can be defined including OC fractions (OC1, OC2, OC3, OC4 and POC) and EC fractions (EC1, EC2 and EC3). The OC is determined as four OCs plus a Pyrolyzed carbon (POC), including OC1 (140 °C) + OC2 (280 °C) + OC3 (480 °C) + OC4 (580 °C) + POC in a 100% helium (He) atmosphere. The Pyrolyzed carbon, namely POC, is the carbon which is evolved from the time that the carrier gas flow is changed from helium to helium/oxygen at 580°C to the time that the laser-measured filter reflectance reaches its initial value. The EC consists three ECs minus the POC (EC=EC1+EC2+EC3-POC). The EC1, EC2, and EC3 are determined in 98%

helium/ 2% oxygen atmosphere at 580 °C, 740 °C and 840 °C, respectively. The total carbon is determined as the summation of OC and EC (TC=OC+EC) [227]. The DRI carbon analyzer can detect the OC and EC according to the preferential oxidation of OC and EC compounds (using helium and oxygen atmosphere) at different temperatures in the carbon range of 0.05 to 750 µg carbon/cm^2.

Before conducting the OC/EC analyses, the analyzer was calibrated with four standards including 5% nominal methane (CH_4) in He, 5% nominal CO_2 in He, Potassium hydrogen phthalate (KHP) and sucrose. The calibration slopes were historically differed by less than 5% based on these four compounds. The CH_4 was used as the internal standard which was injected at the end of each analysis. To obtain the amount of carbon in µg, the integrated peak area of each measurement was divided by the calibration peak area and then multiplied by an instrument-specific calibration factor (Internal Standard Calibration Method). According to the DRI carbon analyzer catalogue, the minimum detection limits (MDL) of the analyzer (analyses of 693 individual blanked quartz-fiber filters) defined as three times the standard deviation of measured results for OC, EC and total carbon (TC) are presented in Table 3-6 were used to collect the particles from the first-stage diluter for analyzing of carbonaceous components including EC and OC; while they were prebaked at 800 °C for 3 hours to remove or minimize the carbon contamination of the filters. For carbon analysis, a small part of filter (area of 0.526 cm^2) was punched and then directly inserted into the DRI carbon analyzer. In addition, the analyzer precision is about 5% for the homogeneous deposits containing >10 µg/filter of TC.

Quartz filters were used to collect the particles from the first-stage diluter for analyzing the carbonaceous components including EC and OC; while they were prebaked at 800 °C for 3 hours to remove or minimize the carbon contamination of the filters before they were used for collecting the PM samples. For carbon analysis, a small part of the filter (area of 0.526 cm^2) was punched and then directly inserted into the DRI carbon analyzer.

Table 3-6 Minimum detection limit (MDL) of the DRI carbon analyzer

Component	**Minimum detection limit (µg/cm^2)**
Total organic carbon	0.82
High-temperature organic carbon	0.81
Total elemental carbon	0.19
High-temperature elemental carbons	0.12
Total carbon	0.93

3.8.2 Water-soluble organic carbon

The organic carbon in the PM can be divided into water-soluble organic carbon (WSOC) and water-insoluble organic carbon [234,235]. According to the literature, the water-soluble materials from PM which are toxic when respired [236-238] have impacts on the pro-inflammatory response resulting in cardiovascular diseases and promoting pulmonary [236], DNA damage [237], environment climate changing by altering cloud droplet formation and cloud properties [239]. Therefore, various studies have been conducted to investigate the WSOC and water-soluble components from PM of engines [92,235,240-243] and atmospheric aerosol [234,244-248]. The present study also aims to explore the effect of different fueling modes on the WSOC of PM emitted from the diesel engine.

The water-soluble organic carbon (WSOC) was analyzed using a Total organic carbon analyzer (TOC-L_{CSN}, Shimadzu, Japan) with a Non-dispersive infrared detector (NDIR) after catalytic conversion of the OC to CO_2 at 680 ºC. The specifications of the total organic carbon analyzer are presented in Appendix B. The analyzer can detect the total carbon (TC) and inorganic carbon (IC). The sample is burned in the analyzer combustion tube at 680 ºC and the TC components in the sample are converted to carbon dioxide (CO_2) which can be detected by NDIR. The IC measured by the analyzer consists of the carbon contained in carbonates and in carbon dioxide dissolved in water. The IC was eliminated, automatically by the analyzer, prior to analysis by acidification using 1.5% hydrochloric acid (HCl) to obtain a pH of less than 3 in which all carbonates are converted to CO_2. The CO_2 and dissolved CO_2 in the sample are volatilized by bubbling (sparging) air or nitrogen gas that does not contain CO_2 through the sample. Then the IC in the sample is converted to CO_2 which can be detected by the NDIR. The total organic carbon (TOC) is the difference between amounts of TC and IC. In regard to calibration, 50 ppm TC and 50 ppm IC standard solutions were inserted to the analyzer as stock solutions and then the analyzer would dilute the standards automatically to 40, 20 and 10 ppm for both TC (calibration curve with R^2=0.9999) and IC (calibration curve with R^2=0.9998) calibrations.

In regard to the analysis of WSOC, PM collected by quartz fiber filter was extracted using 25 ml of Milli-Q water (Millipore^{TM}) by an ultrasonic extractor for 2 hours. The temperature of ultrasonic water was kept about 20 °C by adding ice to prevent the evaporation of volatile components during the extraction. The solution was filtrated to

remove the big solid particles by using PTFE syringe filter with pore size 0.45μm (Allpure^{TM}). All the apparatuses were washed with Milli-Q water before extraction to minimize the contaminants in the apparatuses.

3.8.3 Particle volatility and oxidation reactivity

Diesel particles contain soot, adsorbed hydrocarbons and other substances. The soot is non-volatile; while the adsorbed hydrocarbons are volatile. The volatility of the particulate matter affects its oxidation properties which is an important parameter in the design of after-treatment system for PM oxidation. In this study, the volatile and non-volatile fractions of the particles were analyzed using a Thermogravimetric analyzer/ Differential scanning calorimeter (TGA/DSC3+, Mettler Toledo). Parts of the PM collected on the quartz fiber filter (about 12 mg of PM and filter for all the conditions) were put into an Alumina (Al_2O_3) crucible with capacity of 70 μL and then inserted to the TGA/DSC3+ for analysis. The two-stage heating program, including the de-volatilization stage and the oxidation stage, is presented in Table 3-7. For the de-volatilization process (steps 1 to 4), the sample was heated only in nitrogen atmosphere in order to remove the volatile substances (the oven temperature was up to 400 ºC). While for the oxidation process (steps 5 to 8), the sample was oxidized in an air atmosphere and the oven temperature reached up to 850 ºC. The nitrogen and air flow rates were maintained at 50 mL/min.

Table 3-7 Two-stage heating program for TGA

Stage	Program
I	**De-volatilization**
1	Initial atmosphere: nitrogen
2	Isothermal for 10 min
3	Ramp 3°C/min to 45°C
4	Ramp 10°C/min to 400°C
II	**Oxidation**
5	Changing atmosphere: air
6	Ramp 10°C/min to 850°C
7	Isothermal for 10 min
8	Cooling to room temperature

Results obtained from the TGA/DSC analysis can be used to calculate the oxidation kinetics of soot particles, based on the modified Arrhenius expression [249-251] shown below:

$$-\frac{dm}{dt} = Ae^{-E/RT}\, m^n \qquad 3.10$$

When the time step is set small enough in the oxidation process, it can be assumed that the TGA curve is composed of very small linear segments of ΔT; therefore:

$$-\frac{\Delta m}{\Delta t} = Ae^{-E/RT}\, m^n \qquad 3.11$$

The logarithmic form of the equation above is:

$$ln\left(-\frac{\Delta m}{\Delta t} m^{-n}\right) = ln\, A - \frac{E}{R}\left(\frac{1}{T}\right) \qquad 3.12$$

where m is instantaneous mass (mg) of the soot sample during the soot oxidation process, t is the time (s) during the soot oxidation process, A is the frequency factor (s^{-1}), E is the activation energy (kJ/mol), R is the molar gas constant (8.314 J/mol.K), T is the instantaneous heating temperature (TGA furnace temperature) (K) and n is the reaction order. Since air is used for the second stage of TGA program in the temperature range of 400°C to 850°C; therefore, the oxidation kinetics of soot particles can be calculated from the results obtained in the second stage of TGA program. The reaction order can be assumed to be 1 [249,250]. The activation energy and frequency factor can be obtained from the slope and intercept of the parametric plot of $ln\left(-\frac{\Delta m}{\Delta t} m^{-n}\right)$ versus $\left(\frac{1}{T}\right)$.

3.8.4 Polycyclic aromatic hydrocarbons (PAHs) and n-alkanes

Nowadays, there is increasing concern about the amount of organic compounds (e.g. PAHs and n-alkanes) in the environment, because some of the PAH compounds are highly mutagenic or carcinogenic; while benzo[a]pyrene (B[a]P) has been identified as being highly carcinogenic [252-256]. The effects of different fueling modes on the PAHs and n-alkanes emitted from the diesel engine are investigated in this study. The PAHs and n-alkanes were determined using in-injection port Thermal desorption-gas chromatography/mass spectrometry (TD-GC/MS) method and analyzed by an Agilent 6890 GC/5975 MS detector (Santa Clara, CA, USA). In the TD-GC/MS method, only a small part of the quartz filter (0.52 cm^2) was directly inserted into the analyzer. In this study, the service of Hong Kong Premium Services and Research Co. was employed to conduct the PAHs and n-alkanes analysis. The collected samples were sent to the

company for analysis. Detailed PAHs and n-alkanes analysis procedure is available in [257]. This method has some advantages compare to the solvent extraction method, like decrease in time, labor and operating cost by avoiding sample pre-treatment, avoiding the contamination from solvent impurities (due to no extraction usage) and requiring less filter material for analysis [257-259]. To minimize the evaporation of semi-volatile components, the samples were kept at around 4°C until the analysis time. The analyses were repeated three times to increase the accuracy and the average results are presented.

3.8.5 Inorganic ions

Engines can produce ions due to the combustion of fuels and lubricating oil. Therefore, various studies have been conducted to determine the amount of ions emitted from engines and investigate the effect of using different fuels (like biofuels) on the ion concentrations [260-264]. The present study also aims to explore the amount of inorganic ions in the PM, but under various fueling modes using DBE. The inorganic ions investigated in this study include sodium (Na^+), potassium (K^+), ammonium (NH_4^+) and nitrate (NO_3^-).

Sodium (Na^+), potassium (K^+) and ammonium (NH_4^+) ions were determined by an Ion chromatograph (IC) (761 SD Compact IC, Metrohm Ltd., Switzerland). The analyzer was operated at the measured conductivity of about 800 μS/cm, measured pressure of 7.4 MPa and pump flow rate of 0.90 ml/min. The used column was METROSEP C 4 150/4.0 (6.1010.420) with size of 4.0 ×150 mm and 1.7 millimolar (mM) nitric acid and 0.7 mM dipicolinic acid were used as eluents. Four calibration standard points (0.25, 0.5, 1 and 2 ppm) were utilized to get the calibration curves. The calibration correlation coefficients (R^2) are recorded as 0.9998 for sodium, 0.9989 for potassium and 0.9999 for ammonium.

The nitrate (NO_3^-) was analyzed by a Scanning spectrophotometer (UV-2101PC, Shimadzu). The specifications of the scanning spectrophotometer are presented in Appendix C. The wavelength of 220 nm detected the nitrate and organic matters; while the wavelength of 275 showed the organic matters. Thus the nitrate was calculated as the difference between the two readings. Five calibration standard points (0.5, 1, 2, 4 and 10 ppm) were prepared and a calibration curve with R^2=0.9990 was obtained. The PM extraction procedure for inorganic ions analysis was the same as that for WSOC.

3.8.6 Metals and elements analysis

It is well known the trace amount of heavy metals and trace elements are existed normally in the drinking water and foods. But, some of heavy metals and trace elements are essential for the body; while some of them are harmful and toxic (e.g. Pb, Zn, As, Ni, Ti, Cu, Cd and V) [265,266]. Thus, many investigations can be found in regard to the amount of metals and elements in the atmosphere and tunnel aerosols [248,267-276] or PM emitted from motor vehicles [143,277-280]. However, there is no information about the effects of different fueling modes on the concentrations of metals and elements emitted from a diesel engine using DBE. Therefore, the present study aims to fill in this knowledge gap.

For metal and elements analysis, an Inductively coupled plasma optical emission spectrometer (Agilent 700 Series ICP-OES) was employed. The operation conditions for ICP-OES are presented in Appendix D. Sixteen metals were selected for metal analysis. Four calibration standard points (0.5, 1, 5, 10 and 20 ppm) were prepared and the calibration correlation coefficients (R^2) were found for Al (0.9997), Ca (0.9960), Cd (0.9991), Co (1.0000), Cr (0.9996), Cu (0.9997), Fe (0.9993), K (0.9996), Mg (0.9990), Mn (0.9994), Na (0.9988), Ni (0.9999), Pb (0.9999), S (1.0000), Ti (0.9997) and Zn (0.9987). The relative standard deviations (RSD) for calibration curves of all metals (based on average) were about 1.6%. The Indium (In) was used as an internal standard. To prepare the standard solutions, firstly the required standard for each metal was poured into the volumetric flask, and secondly a blank solution (1% nitric acid (HNO_3) + 99% Milli-Q water) was added to the volumetric flask up to 25 ml.

The PM collected by Teflon filters was digested as listed in the following procedures.

- Putting the Teflon filter into the centrifuge vial;
- Adding of 10 ml acid (25% HNO_3+75% HCl);
- Putting the vial on the hot plate (95 °C) for 3 hours;
- Cooling to room temperature for 24 hours for complete digestion;
- Pouring the cooled solution after filtration (using PTFE syringe filter with pore size of 0.45μm (Allpure^{TM})) into the volumetric flask.
- Adding Milli-Q water into the flask up to the marked line to get 25 ml solution.

It is noticeable that the acid (25% HNO_3+75% HCl) was selected after various trials (such as pure HNO_3, pure HCl and 50% HNO_3+50% HCl), because it has the highest efficiency to digest the PM for metal analysis. All the apparatus were cleaned by a mixture of acid and Milli-Q water before using. The petri slides were soaked for half an hour by 10% HNO_3, 10% HCl and 80% Milli-Q water (by volume) and then rinsed by Milli-Q water. Centrifuge vials were washed three times with the same mixture for petri slides; while volumetric flasks were soaked for 24 hours and then rinsed with Milli-Q water. For Teflon filter cleaning, three acid concentrations (pure HNO_3, pure HCl and 50% HNO_3+50% HCl) were tested; while pure HNO_3 had the highest effect on removing the metals from the blank filters. Therefore, the blank filters were soaked for 1 hour in HNO_3 and then dried in a clean area (fume hood). In order to minimize the contaminating effect of metal apparatus on metal analysis, metal apparatuses were not used (for instance use of plastic forceps instead of metal forceps).

3.9 Experimental errors and uncertainties

The total (overall) uncertainty in this study was calculated by the root-sum-square combination of fixed and random errors contributions, according to Moffat [281] and the uncertainties at 95% confidence level for the combustion, performance and emissions parameters are presented as error bars in the Figures and also in Table 3-8. For the chemical properties of PM, the standard errors at 95% confidence level are presented as error bars in the Figures. The detailed procedure to calculate the error and uncertainty is presented in Appendix E.

Table 3-8 Type of used equipment with range and accuracy

Parameters	**Type of equipment**	**Range**	**Accuracy**	**Uncertainty % (at 95%)**
NO or NO_X	600 HCLD Analyzer	0-3000 ppm (NO or NO_X)	±0.5%	±1.00
HC	300 HFID Analyzer	0-30000 ppm of carbon	±1%	±1.98
CO_2	300 NDIR Analyzer	0-20%	±1%	±1.96
CO	300 NDIR Analyzer	0-25000 ppm	±1%	±1.97
PM mass	TEOM 1105	$0.1 mg/m^3$ to several g/m^3	$\pm 0.1 mg/m^3$	±1.91
TNC and GMD	SMPS model 3494	5-1000 nm	$\pm \frac{\sqrt{N}}{N}$	±2.07 TNC ±0.87 GMD
Rotational speed	FC 3000 Engine Automatic Measure	0-8000 rpm	±1% Accuracy and ±5 rpm for	

	and Control System		Control	
Torque	FC 3000 Engine Automatic Measure and Control System	0-600 Nm	±0.3% Accuracy and ±0.2% for Control	-
Fuel mass consumption	BX32KH Digital Balance	0-32 kg	±0.2 gram	-
Time	Alba Stopwatch	0- up to 23 h 59 min 59 s 99/100sec	± 20s per month	-
Converting of pressure signal to voltage	Charge Amplifier, Kistler Co., Type 5011B	±10 - ±999000 pC	±0.5%	-
In-cylinder pressure	Piezoelectric Pressure Sensor, Kistler Co., Type 6056A	0-250 bar	≤ ±0.3%	-
Crank-angle signal acquisition	CA-RIE-360/720 Encoder, (DEWETRON GmbH)	0-6000 rpm	±2.5%	-
BSFC				±2.15
BTE				±2.16
ID or DOC				±1.95
Peak pressure				±1.16
Peak HRR				±1.98
$COV_{(Max(dP/d\theta))}$				±1.21
COV_{IMEP}				±1.23
EGT				±0.78

CHAPTER 4 EFFECT OF ETHANOL IN COMPARISON WITH OTHER ALCOHOLS IN FORMING THE TERNARY FUEL

Different alcohols can be mixed with biodiesel and diesel to form the ternary fuel. This chapter reports a study on the combustion, performance and emissions of the diesel engine fueled with diesel/biodiesel/alcohol blends having the same oxygen concentration. The test was conducted with seven fuels including pure diesel, DB, DBM, DBE, DBPr, DBBu and DBPe, which (except the diesel fuel), have almost the same LHV and hydrogen and carbon concentrations; while the oxygen content of each blended fuel was exactly the same. The effect of ethanol, as compared to the other alcohols, can be identified. The results, as presented in this chapter, have been published in [282,283].

4.1 Experimental setup and procedure

The experiments were conducted at a constant engine speed of 1800 rpm with five engine loads of 10, 30, 50, 70 and 90% of the full engine torque, corresponding to 28.5, 85.5, 142.5, 199.5 and 256.5 Nm. Seven fuels were used, which include diesel (D), waste cooking oil biodiesel (B), lower alcohols (methanol (M) and ethanol (E)) and higher alcohols (2-propanol (Pr), n-butanol (Bu) and n-pentanol (Pe)), were blended with various blending mass percentages to obtain six blended fuels with constant fuel oxygen, almost constant carbon and hydrogen contents and almost constant lower heating values. The six blended fuels are designated as DB (D53.7 B46.3), DBM (D82.74 B9.26 M8), DBE (D79.25 B9.26 E11.49), DBPr (D75.71 B9.26 Pr15.03), DBBu (D72.22 B9.26 Bu18.52) and DBPe (D68.76 B9.26 Pe21.98). In each blended fuel, the fuel oxygen content was maintained at 5.0%. When an alcohol was added, the biodiesel was kept at 9.26% to provide 1% oxygen; while the content of diesel fuel was reduced and the alcohol contributed 4% of the oxygen. Since methanol has the highest oxygen content, hence DBM contains only 8% methanol, comparing with 21.98% of pentanol for DBPe. It can be seen from Table 4-1 that the carbon contents vary from 81.7% to 82.2%, the hydrogen contents differ from 12.8% to 13.3% and the lower heating values change from 40.2 MJ/kg to 40.3 MJ/kg for the blended fuels. Fuel samples were prepared and observed for three weeks to understand the stability of the six blended fuels. For all the blended fuels, no phase separation was observed during the experiments. Except DBM, the other blended fuels were stable for three weeks. For the DBM sample, phase

separation occurred after approximately 10 hours. The use of surfactants (emulsifiers), co-solvents [87] or higher percentage of biodiesel can solve the miscibility problem of methanol in DBM fuel. Since all the alcohol blended fuels (irrespective of DBM) were stable with 9.26% of biodiesel (using low percentage of biodiesel to better sensing of alcohols' effects on the parameters) without using any chemical surfactants, the methanol suffered a phase separation in DBM fuel; while the chemical surfactants (or higher percentage of biodiesel) could not be utilized for DBM fuel due to fixing of the same condition compared to the other blended fuels. Therefore, since no phase separation occurred during the experiments for the DBM case, the results pertaining to DBM are included in this study for comparison.

All the alcohols used in this study had high purities of over 99.8%. Information of the diesel fuel and biodiesel has been given in Chapter 3. The properties of the tested fuels are presented in Table 4-1. The engine operation, experimental error analysis and measurement methods follow those described in Chapter 3. The steady state experiments were repeated two times for ensuring that the data was repeatable within the experimental uncertainties of the measurements.

Table 4-1 Properties of the tested fuels

Properties	Cetane No.	LHV (MJ/kg)	Density (kg/m3) at 20 °C	Viscosity (mPa S) at 40 °C	Heat of evaporation (kJ/kg)	Boiling point (°C)	Flash point (°C)	C (% mass)	H (% mass)	O (% mass)	Sulfur (ppm)
Diesel [129][a]	52	42.5	840	2.4	270	180-360	78	86.6	13.4	0	<10
Biodiesel [129][a]	51	37.5	871	4.6	300	-	210	77.1	12.1	10.8	<10
Methanol 168][a]	5	19.58	791.3	0.58	1162.64	64.7	12	37.48	12.58	50	0
Ethanol [129][a]	8	26.83	789.4	1.13	918.42	78.3	17	52.14	13	34.8	0
Propanol [284]	12	30.63	803.7[b]	1.74	727.88	97.1	11.7	59.96	13.42	26.62	-
Butanol [284]	17	33.09	809.7[b]	2.22	581.4	117.5	35	64.82	13.6	21.6	-
Pentanol [284]	18.2	34.65	814.8[b]	2.89	308.05	137.9	49	68.13	13.72	18.15	-
DB (D53.7 B46.3)		40.2	854.4					82.2	12.8	5.0	<10
DBM (D82.74 B9.26 M8)		40.2	839.0					81.8	13.2	5.0	<9.2
DBE (D79.25 B9.26 E11.49)		40.2	837.1					81.8	13.2	5.0	<8.9
DBPr (D75.71 B9.26 Pr15.03)		40.3	837.4					81.7	13.3	5.0	<8.5
DBBu (D72.22 B9.26 Bu18.52)		40.3	837.3					81.7	13.3	5.0	<8.1
DBPe (D68.76 B9.26 Pe21.98)		40.3	837.3					81.7	13.3	5.0	<7.8

a= from the same laboratory; b= at 15°C.

4.2 Engine combustion

The following parameters were selected to analyze the effect of alternative fuels on the engine combustion characteristics and performance: in-cylinder pressure, heat release rate (HRR), ignition delay (ID), duration of combustion (DOC), coefficient of variation (COV) of indicative mean effective pressure (IMEP), COV of maximum cylinder pressure derivative (Max ($dP/d\theta$)), brake specific fuel consumption (BSFC) and brake thermal efficiency (BTE).

Typical curves of in-cylinder pressure and HRR are shown in Fig. 4.1 for low (28.5 Nm), medium (142.5 Nm) and high (256.5 Nm) engine loads. Fig. 4.2 (a and b) reveal the peak in-cylinder pressure and peak HRR, respectively. The similar in-cylinder pressure and heat release rate curves of the blended fuels with diesel (Fig. 4.1) indicates that alternative fuels have undergone similar combustion process, including a premixed combustion phase followed by a diffusion combustion phase.

Fig. 4.1 and Fig. 4.2 (a) illustrate that the in-cylinder pressure increases, with the peak value occurring further away from the top dead center, with increasing engine load for all the tested fuels which is due to more fuel consumption at higher loads [86]. Similar behavior was observed in [87,128,129,285] with diesel, DB, DBE and DBM. However, for HRR, Fig. 4.1 and Fig. 4.2 (b) show that the peak HRR increases with increasing load only from 28.5 Nm to 142.5 Nm (except for D and DBPe at 199.5 Nm) and then it decreases at the high load (256.5Nm) for all the tested fuels. Similar trend in the peak HRR (increase in peak HRR at low and medium loads and decrease at high engine load) was also reported in the literature [128,129,286] for diesel, biodiesel and DBE. At the very high engine load of 199.5 Nm or 228 Nm, the combustion temperature is high and the fuel/air ratio is also much richer than that at the lower engine loads; however, there is not enough time for mixing of fuel and air, resulting in incomplete combustion and decrease in the peak HRR. In addition, the ID (Fig. 4.3 (a)) is shorter at very high engine load, thus less fuel is accumulated during the delay time to burn in the premixed burning phase, resulting in the decrease of peak HRR.

Fig. 4.1 and Fig. 4.2 (a) illustrate that all the blended fuels cause a slight reduction in the peak in-cylinder pressure at the low engine load (except for DB and DBM) and a slight increase at the medium and high loads in comparison with the diesel fuel. However, on the average of five loads, peak in-cylinder pressures of all the blended fuels have only

about 1% increase (almost similar) compared to that of diesel fuel Thus, there is no significant difference between the blended fuels on the peak in-cylinder pressure. The small drop in peak in-cylinder pressure at low load for the blended fuels is due to the lower combustion temperature and the higher ignition delay (compared to other loads and use of diesel) which cause initiation of combustion further away from the top dead center during the expansion stroke [128,129].

For HRR, all the ternary blended fuels lead to an increase in the peak HRR at all loads compared to pure diesel, as shown in Fig. 4.1 and Fig. 4.2 (b). This increase in the peak HRR can be attributed to the better volatility and lower viscosity (hence better fuel atomization) of the alcohols and the longer ignition delay associated with the lower cetane number of the alcohols which cause accumulation of more fuel during the delay time to burn in the premixed burning phase and hence the higher peak HRR [83,287,288]. In contrast, the higher viscosity and lower ignition delay of biodiesel cause decrease in the peak HRR in comparison with the diesel fuel.

On the average of five loads, the higher alcohols have the same trend in the increase of peak HRR, about 22.1% increase for DBPe, DBPr and DBBu, compared to that of pure diesel fuel. However, the lower alcohols cause less increase in the peak HRR, being 14.8% for DBE and 5.9% for DBM. In contrast, biodiesel has a reduction of 3% in the peak HRR. Same behavior (increase in the peak HRR for alcohols and reduction in the peak HRR for biodiesel) was also found in [287] for DBB and DBPe and in [285] for DB. It can be inferred that the magnitude of the peak HRR is almost dependent on the ignition delay of the fuels (as shown in Fig. 4.3 (a)).

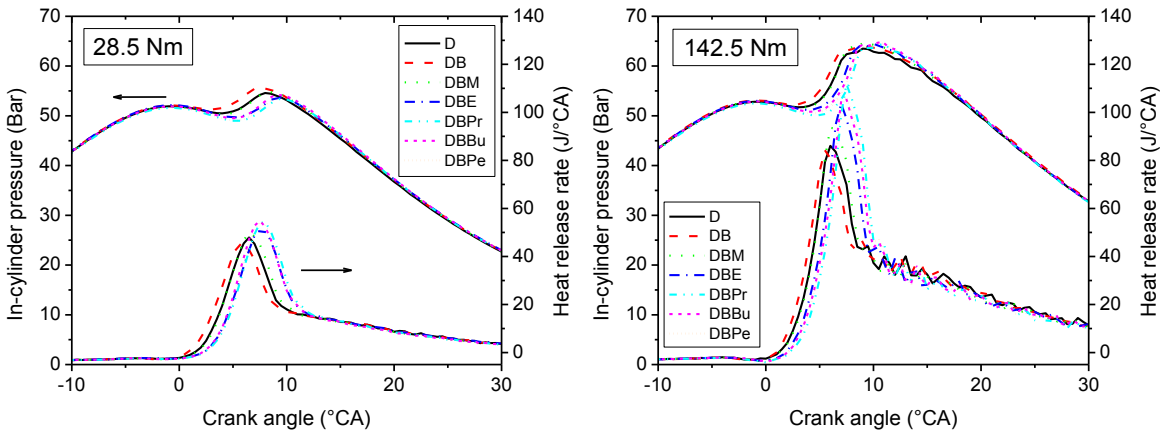

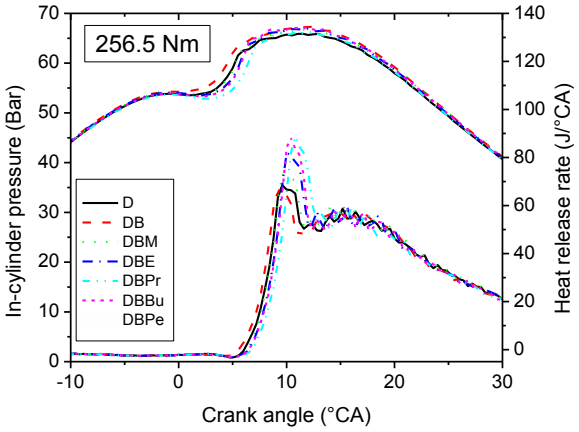

Fig. 4.1 Variations of in-cylinder pressure and heat release rate with low, medium and high loads for different fuels.

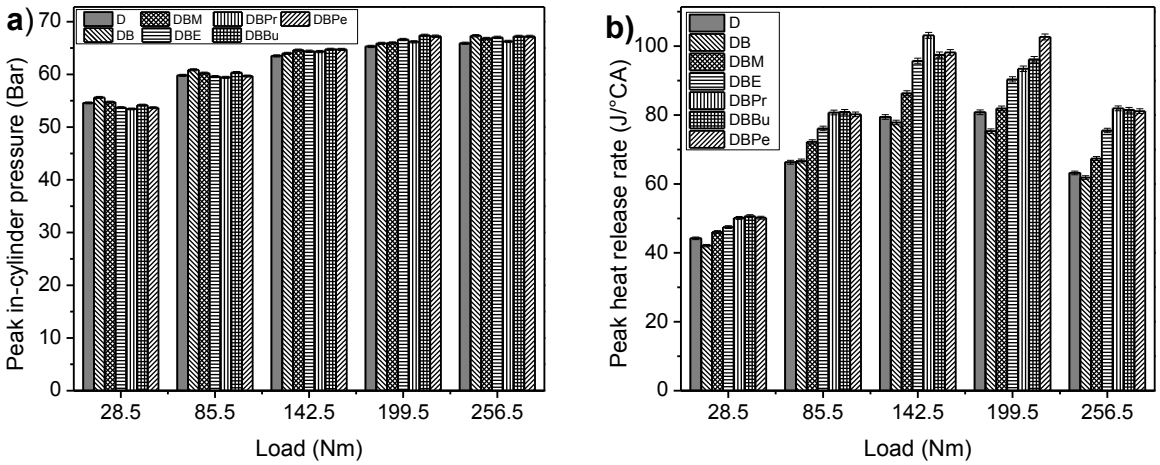

Fig. 4.2 Variations of (a) peak in-cylinder pressure (b) and peak HRR with engine load for different fuels.

Fig. 4.3 (a and b) indicate the variations of ignition delay and duration of combustion of the tested fuels, respectively. It can be seen from Fig. 4.3 (a and b) that the increase in engine load causes decrease in ID and increase in DOC for all the tested fuels. The ID is reduced due to increase in in-cylinder temperature [57] as a consequence of increase in engine load. For DOC, the increase in load leads to longer duration of fuel injection, air/fuel mixture formation [289] and fuel combustion.

Fig. 4.3 (a and b) demonstrate that all the ternary blended fuels cause increase in ID and shorter DOC in comparison with those of diesel fuel. The lower cetane number and

higher latent heat of evaporation of the blended fuels, as a consequence of the alcohols, cause decrease in in-cylinder temperature and increase in ID compared to the diesel fuel [125,290,291]. For DB, the higher bulk modulus and higher viscosity of biodiesel cause earlier start of injection (hence combustion) and reduction in ID [292,293]. The shorter DOC with use of alcohols in the blended fuels has various reasons. Firstly, the addition of alcohols into the blended fuels leads to achieve higher HRR in the premixed combustion phase caused by the longer ignition delay [127]. Secondly, faster flame propagation of alcohols can shorten the DOC [294]. Thirdly, oxygen in the alcohols can suppress the pyrolysis process and enhance the oxidation during the combustion resulting in shorter DOC [295].

On the average of five engine loads, the increase in ID is in the order of DBPr (9.7%), DBPe, DBBu and DBE (6.7%) and DBM (1.7%) compared to the diesel fuel; while DB has a reduction of 3.9% in ID. The longest ID of DBPr is due to the slower H-abstraction and inhibition of isomerization in the branched chain alcohols (2-propanol was tested) compared to the straight chain alcohols [296]. For DOC, the average results show that the higher alcohols have similar effect in reduction of DOC (about 2.3% for pentanol, propanol and butanol); while the lower alcohols have less influence in reduction of DOC (1.1% for methanol and ethanol) compared to the diesel fuel. In addition, biodiesel has an identical DOC (only 0.6% increase which is not significant with T-test at 95% level) in comparison with that of diesel fuel. It can be found that the sequence of DOC is almost opposite to the ID of the fuels.

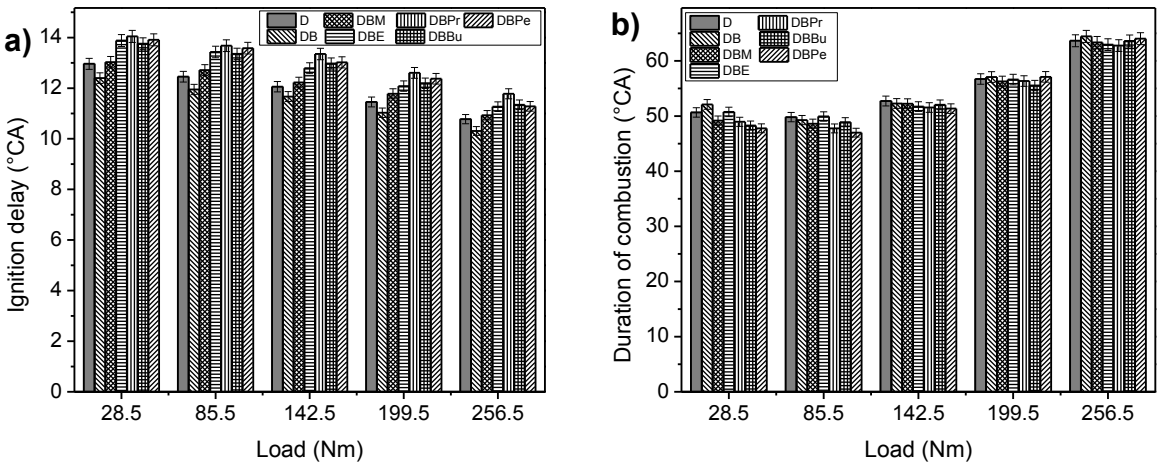

Fig. 4.3 Variations of (a) ignition delay (b) and duration of combustion with engine load for different fuels.

Coefficient of variation in indicated mean effective pressure (COV_{IMEP}) is an important parameter of cyclic variability. COV_{IMEP} is defined as the cyclic variability in indicated work per cycle. This parameter is calculated based on the standard deviation in IMEP divided by the mean IMEP, and is usually expressed in percent; while an excess of 10% in COV_{IMEP} could result in vehicle drivability problems [297]. Fig. 4.4 (a) shows that the COV_{IMEP} (for 500 working cycles) of all the tested fuels varies with engine load; while the maximum and minimum COV_{IMEP} are recorded at the engine loads of 28.5 Nm and 85.5 Nm, respectively for all the tested fuel, except for DBM and DBE. The higher COV_{IMEP} at the lowest load (28.5 Nm) indicates a bigger variation of indicative work done among each cycle due to less stable combustion associated with the lower combustion temperature and incomplete combustion.

The average results in Fig. 4.4 (a) reveal that despite of a slight reduction in COV_{IMEP} by using DBM (only 1.6%), the application of alternative fuels causes increase in COV_{IMEP} in the order of DBBu and DB (9%), DBE (7.8%), DBPe (5.8%) and DBPr (2.7%) compared to that of diesel fuel.

Coefficient of variation in maximum cylinder pressure ($COV_{Max(dP/d\theta)}$) is another indicator of combustion process which shows whether the combustion process of an engine is fast and robust or that is slow and less repeatable [297]. $COV_{Max(dP/d\theta)}$ also can implicitly reflect the level of combustion noise. Fig. 4.4 (b) illustrates that the $COV_{Max(dP/d\theta)}$ (for 500 working cycles) of all the tested fuels (irrespective of DBBu) increases from low load (28.5 Nm) to medium load (142.5 Nm) and then decreases until the highest tested load (256.5 Nm).

Also, it can be clearly seen from Fig. 4.4 (b) that the use of different fuels has various effects on $COV_{Max(dP/d\theta)}$ compared to the diesel fuel. Biodiesel causes a reduction of 3% and methanol has an identical value (only 0.5% reduction) in $COV_{Max(dP/d\theta)}$ in comparison with the diesel fuel; while the other blended alcohols fuels lead to increase in $COV_{Max(dP/d\theta)}$ in the sequence of DBPe (12.8%), DBPr and DBBu (7.5%) and DBE (1.4%).

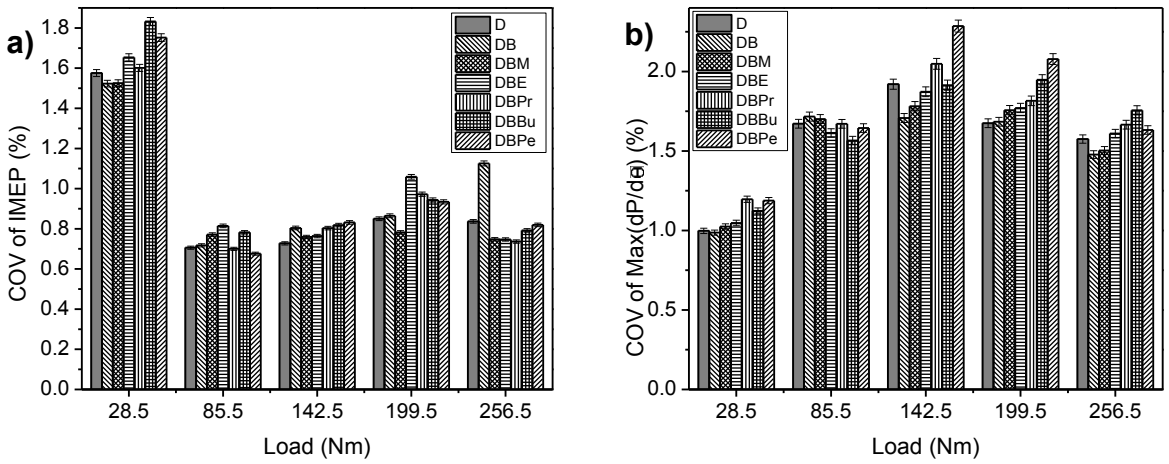

Fig. 4.4 Variations of (a) COV_{IMEP} and (b) $COV_{Max(dP/d\theta)}$ with engine load for different fuels.

Fig. 4.5 indicates the variation of exhaust gas temperature (EGT) with engine load. It is clearly observed that the increase in engine load causes increase in EGT for all the tested fuels. With increase in engine load, more fuel is injected into the cylinder for burning which causes the rise in in-cylinder temperature and thus increase in EGT [73]. The average results in Fig. 4.5 show that all the alternative fuels lead to slight decreases (about 1.5% for all blends) in EGT compared to the diesel fuel. This small reduction in EGT is due to the lower calorific value and higher latent heat of evaporation (cooling effect) of the alcohols and biodiesel which can reduce the combustion temperature [27] and thereby reduce the EGT compared to the diesel fuel. According to Fig. 4.5, the maximum reduction is recorded at the engine load of 256.5 Nm for all the blended fuels which shows that the alternative fuels have a strong influence on the reduction of EGT only at higher engine loads.

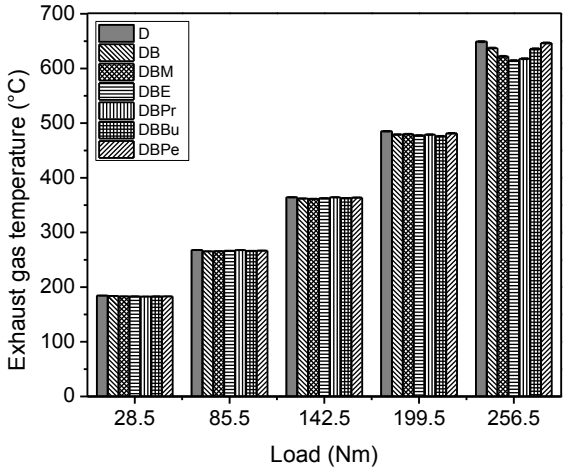

Fig. 4.5 Variation of exhaust gas temperature with engine load for different fuels.

4.3 Engine performance

Variations of BTE and BSFC are presented in Fig. 4.6 (a and b), respectively. It can be seen that the best engine performance occurs at the engine load of 199.5 Nm which has the highest BTE and the lowest BFSC for all the tested fuels. At low engine loads, the combustion temperature is low; therefore, incomplete combustion takes place. On the other hand, at very high loads, the combustion temperature is high and the fuel/air ratio is richer; however, there is not enough time for mixing of fuel and air, resulting in incomplete combustion and decrease in BTE and increase in BSFC.

Fig. 4.6 (b) illustrates that all the blended fuels have higher BSFC (except for DBM at 256.5 Nm) at all the tested loads compared to the diesel fuel. Lower calorific value (due to using alcohols and biodiesel) and lower density (due to use of alcohols) of the blended fuels are the reasons leading to the increase in BSFC compared to the diesel fuel [73,284,298,299]. And in order to maintain the same output power by the blended fuels, more fuel is required. The increases in BSFC on the average of five loads are found as about 6.6% (DBE, DB, DBPr and DBPe), 4% (DBBu) and 2.3% (DBM) compared to that of diesel fuel.

For BTE, the average results of five loads from Fig. 4.6 (a) show that DBM (3.5%) and DBBu (1.5%) have higher BTE and other blended fuels have similar BTE (about 1% reduction which is not significant with T-test) in comparison with the diesel fuel. The higher or similar BTEs (despite of increase in BSFC) of the blended fuels is due to the lower fuel viscosity, improvement in fuel atomization and increase in oxygen contents which improve the combustion process for converting the chemical energy of fuel into the useful engine work and thereby increase the BTE compared to the diesel fuel [128]. It can be inferred from the above results that DBM shows the best performance, because it has the highest BTE among all the tested fuels and the lowest BFSC among all the tested blended fuels. Methanol has the shortest chain and the lowest molecular weight [284] among all the tested alcohols which leads to easier ignition and better combustion and hence resulting in the highest BTE and the lowest BSFC. In addition, the lowest boiling point of methanol among the tested alcohols causes reduction in heat losses and hence resulting in higher BTE.

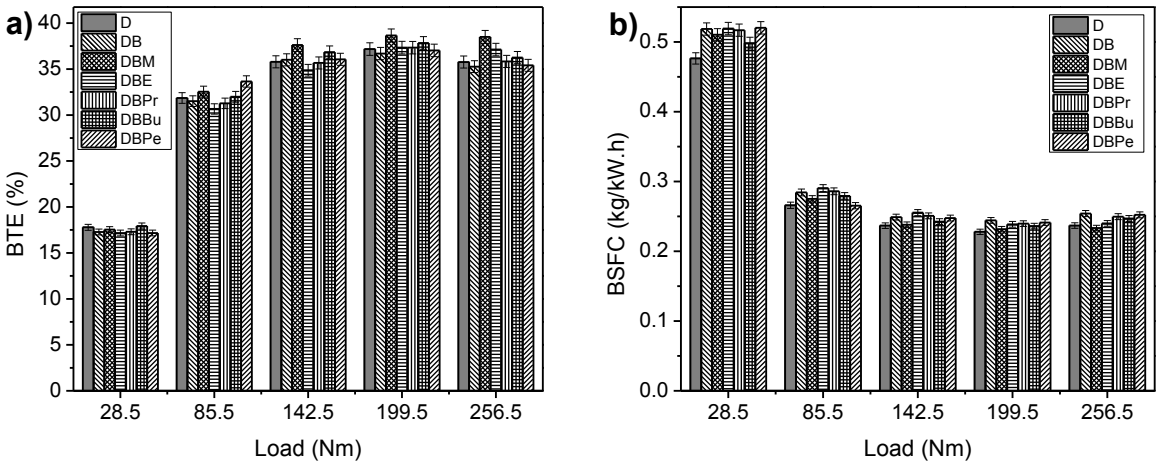

Fig. 4.6 Variations of (a) BTE and (b) BSFC with engine load for different fuels.

4.4 Exhaust gaseous emissions

Fig. 4.7 shows the variation of $BSCO_2$ with engine load. It can be seen from Fig. 4.7 that the variation of $BSCO_2$ is almost similar to that of the BSFC (Fig. 4.6 (b)) at different engine loads. It is also found that the lowest $BSCO_2$ is recorded at the engine load of 199.5 Nm (which also has the lowest BSFC) and the highest $BSCO_2$ is observed at the engine load of 28.5 Nm (which also has the highest BSFC) for all the tested fuels.

Fig. 4.7 also illustrates that all the ternary blended fuels can reduce $BSCO_2$ compared to the diesel fuel. Similar trend in reduction of $BSCO_2$ with ethanol and DBE was reported in [127,128,300] and a slight increase and no significant effect in CO_2 was found in [301] using pure biodiesel (5.63% increase), DB50 (2.77% increase) and DB20 and DB10 (identical) compared to the diesel fuel. The lower carbon-to-hydrogen ratio and the higher oxygen content of the ternary blended fuels cause reduction of $BSCO_2$ in comparison with the diesel fuel [300,302,303]. The percentage reductions in $BSCO_2$ are 8.2% for DBM, 3.2% for DBBu and about 1.8% for DBE, DBPe and DBPr, compared to the diesel fuel, which are similar to the results of BSFC. Moreover, DB has an identical $BSCO_2$ (a slight increase of 1.4% which is not significant with T-test) compared to the diesel fuel. It can be inferred that only DBM is effective on reducing $BSCO_2$, with a magnitude of 8.2%, which is due to its lowest BSFC (Fig. 4.6 (b)) among all the tested fuels. The other blended fuels have almost similar effect on the $BSCO_2$ compared to the diesel fuel.

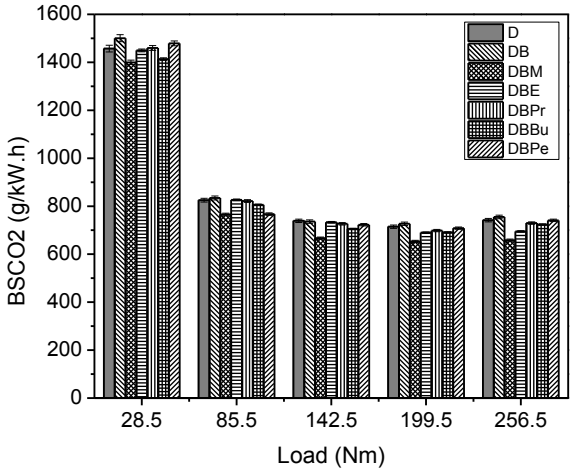

Fig. 4.7 Variation of $BSCO_2$ with engine load for different fuels.

The effects of increase in in-cylinder temperature and complete combustion as a subsequence of increasing engine load (except at 256.5 Nm) on reduction of BSCO emission can be seen in Fig. 4.8. Similar behavior was observed in [127] for DBE. Fig. 4.8 also depicts that all the blended fuels (except DBM at 85.5 Nm) cause BSCO increase at lower loads (28.5 and 85.5 Nm) and decrease at higher loads (199.5 and 256.5 Nm) compared to the diesel fuel. On the average of five loads, the reductions in BSCO are in the order of DBM (23.9%), DB (11.3%), DBPr and DBBu (6.4%), DBPe (3.5%) and DBE (only 0.4%) in comparison with the diesel fuel. Other studies also found reduction in CO for DB and DBBu [69] and for DBPe [68]. At low load the effect of lower combustion temperature (cooling effect due to higher latent heat of evaporation) dominates the effect of oxygen content of the blended fuels (complete combustion), which suppress the CO oxidation process, resulting in the increase in BSCO emission compared to the diesel fuel [57,300]. However, with increasing engine load, the effect of combustion temperature becomes weaker and it can be seen at higher tested loads the BSCO emissions of the blended fuels are lower than that of diesel fuel. It can be found from the above results that DBM has the highest influence on reduction of BSCO (23.9%) which can be attributed to better combustion and performance (lowest COV_{IMEP} and BSFC and highest BTE) of DBM compared to the other blended fuels. After DBM, DB shows high effect on reduction (11.3%) in BSCO which can be attributed to the long duration of combustion (as shown in Fig. 4.3 (b)), and hence longer time is available for oxidation of CO to CO_2.

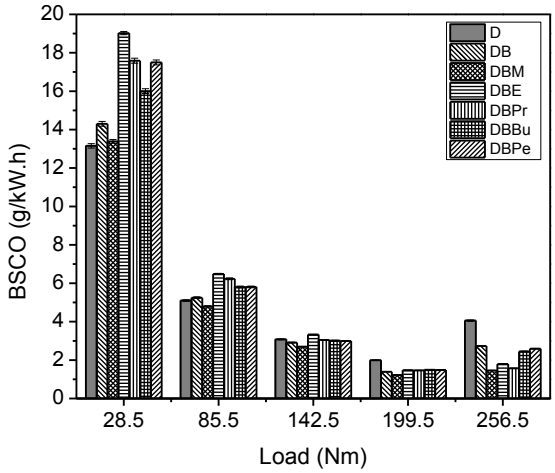

Fig. 4.8 Variation of BSCO with engine load for different fuels.

Fig. 4.9 depicts that the increase in load causes decrease in BSHC for all the tested fuels. At low engine load the combustion temperatures are insufficient to initiate complete combustion resulting in increments of BSHC emissions for all the tested fuels. However, at higher loads the combustion temperatures are high enough to achieve a more complete combustion, leading to decrease in BSHC for all the tested fuels.

Fig. 4.9 also shows that all the blended fuels (irrespective of DBE at 85.5 Nm) can reduce the BSHC from the engine load of 85.5 Nm to the highest engine load of 256.5 Nm. The increase in BSHC at the lowest load with the blended fuels is similar to that in the case of BSCO (Fig. 4.8), which is due to incomplete combustion as a consequence of higher latent heat of evaporations of the alcohols and biodiesel compared to the diesel fuel. However, the effect of higher oxygen content of the blended fuels is a dominant factor at higher engine loads (from 85.5 Nm to 256.5 Nm) which causes more complete combustion and increases the oxidation of unburned hydrocarbons at higher in-cylinder temperatures [105] resulting in lower BSHC compared to the diesel fuel. Some studies also found an increase in THC at lower and even medium loads and a reduction at higher load with the use of alcohol blends (like DBE [127,304], DBBu and DBPe [73] and BPn [305]) compared to the diesel fuel. In addition, other studies found that the use of DE and DBE [125,306,307], DBPe [68] and diesel blended with ethanol or methanol [28] can increase the combustion quality, due to more oxygen content in the fuel, and reduce the THC, in comparison with the diesel fuel. On the average of five engine loads, the reductions in BSHC are in the order of DBM (24.3%), DBPe, DBPr and DB (12.3%) and DBE and DBBu (8.8%) compared to the diesel fuel. It can be concluded from the above

results that, similar to BSFC and BSCO, the effect of using DBM on reduction of BSHC (24.3%) is higher than the other blended fuels which is due to better combustion and performances of DBM (lowest COV_{IMEP} and BSFC and highest BTE). The other blended fuels have almost similar impacts on the reductions of BSHC.

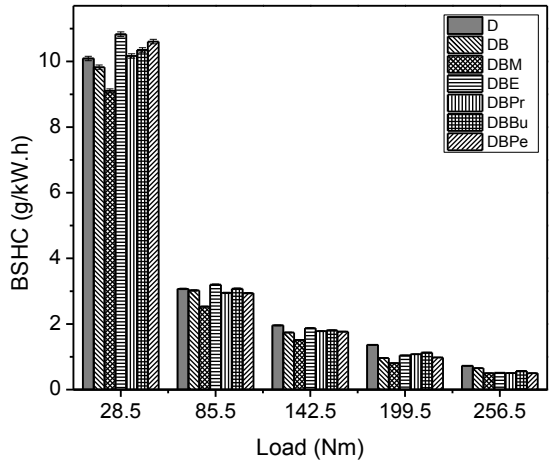

Fig. 4.9 Variation of BSHC with engine load for different fuels.

Fig. 4.10 shows that the $BSNO_X$ approximately decreases with increasing engine load which is in line with the results of other studies with use of diesel and DBE [127,128] and diesel, DBu and DPe [287]. Fig. 4.10 also reveals that all the blended fuels (except DB at all loads and DBPe at 28.5 Nm) cause decrease in $BSNO_X$ at all the tested loads compared to the diesel fuel. On the average of five loads, reductions in $BSNO_X$ are in the order of 19.3% for DBPr, 14.2% for DBM, 11.7% for DBPe, 4.7% for DBE and DBBu; while DB has an increase of 5.8% in $BSNO_X$ in comparison with the diesel fuel. Despite of the huge effect of combustion temperature on formation of NO_X, it can be found from the above results that the combustion duration (residence time) also has an effect on NO_X formation. DBPr has the highest impact on the reduction of $BSNO_X$ (23.3%) among all the tested blended fuels due to its shortest duration of combustion, as shown in Fig. 4.3 (b), for formation of NO_X. On the other hand, DB leads to higher $BSNO_X$ (5.8%) which can be attributed to its longest duration of combustion. In addition, Koivisto et al. [296] reported that the increase in alcohol branch (from 1-Octanol to 3-Octanol or adding two methyl group branches to 3-Octanol to form 3,7-Dimethyl-3-octanol) caused reduction in NO_X emission due to increase in ignition delay and decrease in adiabatic flame temperature. The 2-propanol used in this study has higher branch than the other alcohols,

thus DBPr has the longest ID (Fig. 4.3 (a)) and the lowest NO_X (Fig. 4.10). Reduction in $BSNO_X$ was also reported in some studies using ethanol [127,128], butanol and pentanol [287] and butanol and propanol [284]. In addition, the increase in NO_X using biodiesel was also reported in many studies as shown in the review paper [72].

It can be inferred from the above results that the effects of higher latent heat of evaporation and lower calorific value of alcohol fuels are dominant factors, compared to other parameters (like lower cetane number and higher oxygen content of blends which increase the combustion temperature), which cause reduction in $BSNO_X$ for different loads.

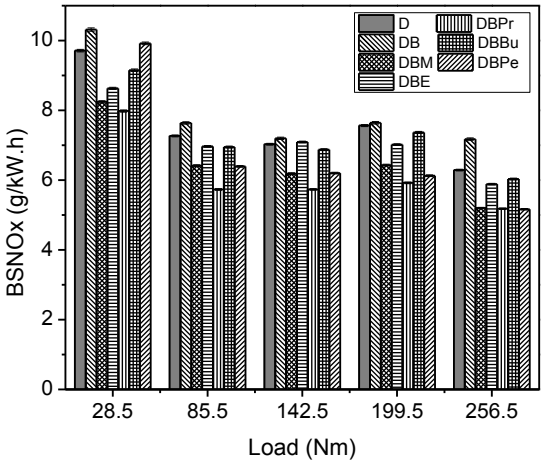

Fig. 4.10 Variation of $BSNO_X$ with engine load for different fuels.

4.5 PM emissions

Fig. 4.11 illustrates that the increase in engine load (except at 28.5 Nm) leads to increase in BSPM for all tested fuels. The small reduction in BSPM from low load (28.5 Nm) to medium load and then a significant increase until the highest load (256.5 Nm) was reported in other studies [128,129] for DBE and diesel. At higher engine loads, the shorter time available for soot oxidation [83] causes increase in soot formation, resulting in the increase of BSPM. Also, the fuel/air mixture is richer and there is lower oxygen concentration for soot oxidation. Moreover, the ignition delay becomes shorter; therefore, more fuel is burned during the diffusion combustion period, resulting in the increase in PM emissions [105].

Fig. 4.11 also shows that the utilization of blended fuels (except DB at the engine loads of 25.8 and 85.5 Nm) has a positive effect on the reduction of BSPM at various loads compared to the diesel fuel. According to the average of five loads, the reductions in BSPM are in the sequence of DBE and DBM (70%), DBBu (61%), DBPr (46.2%), DBPe (32.6%) and DB (only 5.2%) compared to the diesel fuel. This finding is in line with some other studies for DBE [129,308], pentanol [105], butanol and pentanol [92] and DBE and DBM [86]. The reasons for the decrease in BSPM with the oxygenate fuels can be attributed to the following factors. Firstly, there are lower aromatic and sulfur contents (except DB) in the blended fuels [105]. Secondly, higher oxygen content of the blended fuels enhances the soot oxidation, because through the hydroxyl radical ($^{\bullet}OH$) formation, the oxygen component consumes the soot precursors which causes lower soot formation [27]. Thirdly, the carbon to hydrogen mass ratio of all the blended fuels is lower than that of diesel fuel [105].

It is found from the above results that all the alcohol fuels have huge effect on the reduction of BSPM; while DB shows a smaller effect (only 5.2% reduction) on BSPM reduction compared to the other tested fuels. The smaller impact of DB on the reduction of BSPM is due to its shortest ignition delay and hence longer diffusion combustion period, resulting in higher soot formation. In addition, the bonding of two oxygen atoms of biodiesel as R(C=O) OR with one carbon [309,310] causes the decomposition of $CH_3O(CO)^{\bullet}$ radical to form CO_2 (CH_3+CO_2) instead of CO (CO+CH_3O) [311-313]. While for reduction in soot formation, each oxygen atom can remove one carbon atom from the reactive pool (consuming the soot precursors by oxygen atoms); however, for biodiesel, the two oxygen atoms can only remove one carbon atom which is less efficient [309,313] compared to the fuels containing one oxygen atom in their structure like the alcohols. Therefore, biodiesel shows the weakest effect on the reduction (only 5.2%) of BSPM in comparison with the other blended fuels with alcohol (especially DBE and DBM with 70% reduction). On the other hand, the lowest BSPM of the DBE and DBM fuels can be attributed to the shorter chains of methanol and ethanol which lead to easy extraction of oxygen atoms from the decomposition of their molecule structures resulting in higher consumption of soot precursors by these free oxygen radicals compared to the longer-chain alcohols like propanol, butanol and pentanol.

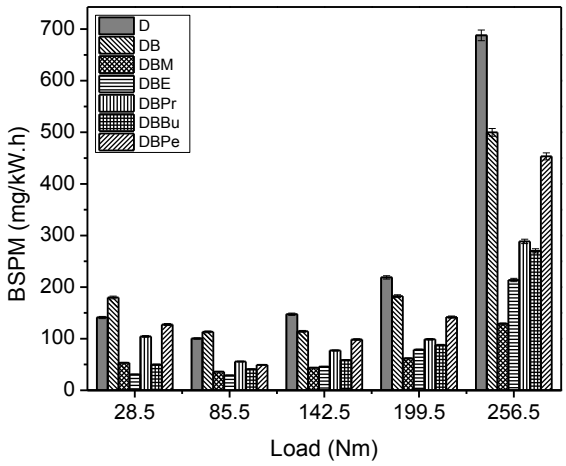

Fig. 4.11 Variation of BSPM with engine load for different fuels.

Fig. 4.12 and Fig. 4.13 depict that the increase in engine load causes an increase in both total number concentration (TNC) and geometrical mean diameter (GMD) of the PM for all the tested fuels. In other studies, the increase in TNC and GMD of diesel and DBE [128], diesel and pentanol [105] and diesel, butanol and pentanol [92] with increasing engine load was also reported. The same factors which cause increase in BSPM will also cause increase in TNC. Moreover, as the number of particles is increase, the particle coagulation rate is also increases and hence larger particles are formed, leading to larger GMD [314].

Fig. 4.12 and Fig. 4.13 also show that all the blended fuels have a positive influence on reduction of TNC (irrespective of DBPr and DBPe at the engine loads of 142.5, 199.5 and 256.5 Nm) and GMD for different loads. On the average of five loads, the reductions in TNC are in the order of DBE (37.3%), DBBu (31.1%), DBM (22%), DB (9%) and DBPe (only 1.1%) compared to the diesel fuel; while DBPr has an identical TNC (only 0.2% increase which is not significant with T-test) with the diesel fuel. For GMD, the average results show that the decreases are in the sequence of DBPr, DBE, DBBu and DBPe (10.3%) and DB and DBM (5.25%) in comparison with the diesel fuel. The decrease in TNC and GMD with use of ethanol, butanol and pentanol was also found in the literature [92,105,128,129]. The same factors which cause reduction in BSPM due to the use of the blended fuels will also cause reduction in TNC and subsequently reduction in GMD. In regard to the effect of ID on PM, Koivisto et al. [296] found that the use of an alcohol caused increase in total particle number and smaller particle size compared to those of hydrocarbon fuels due to longer ignition delay caused by the alcohols. In the

present study, the highest TNC and lowest GMD are also recorded for DBPr which has the longest ignition delay.

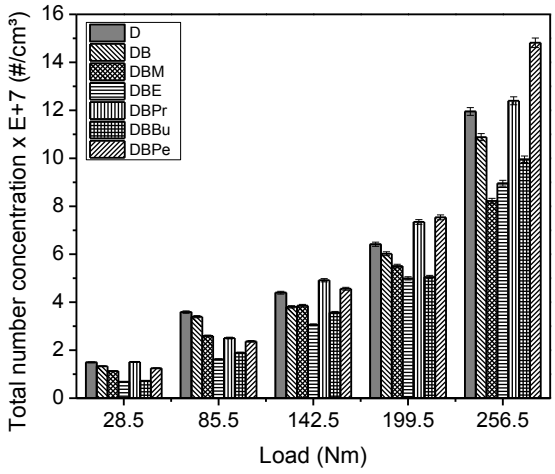

Fig. 4.12 Variation of total number concentration with engine load for different fuels.

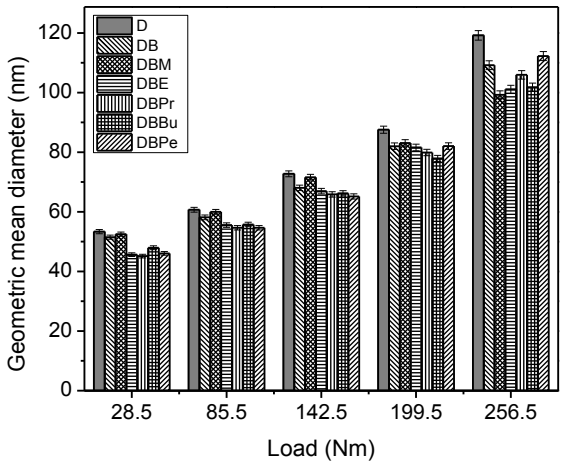

Fig. 4.13 Variation of geometric mean diameter with engine load for different fuels.

4.6 Summary

A summary of the results based on the average of five loads is listed in Table 4-2. Despite all the blended fuels have almost the same C/H/O composition and LHV, there are some differences in the influence of each fuel to the combustion, performance and emissions of the diesel engine. According to the average of five engine loads, it was observed that all the tested blended fuels using alcohols had almost similar trends on the engine

combustion, performance and emissions; while the use of biodiesel blend (DB) had opposite trends in some parameters. In detail, the alcohols blends had higher HRR, ID and COV $_{Max(dP/d\theta)}$ and lower DOC, $BSCO_2$ and $BSNO_X$ in comparison with the diesel fuel; however, biodiesel blend (DB) had lower HRR, ID and COV $_{Max(dP/d\theta)}$, higher $BSNO_X$ and similar DOC and $BSCO_2$ compared to those of diesel fuel. It is noticeable that all the blended fuels with alcohol can reduce both NO_X and particulate emissions, which are major problems with diesel engines. Moreover, they have higher PM reduction effects than the DB fuel.

Among the ternary blended fuels, DBM showed the best engine performance (highest BTE among all the fuels and lowest BSFC among all the blends) and had the lowest emissions of $BSCO_2$, BSCO, BSHC, and BSPM (same with ethanol blend) and COV_{IMEP} compared to all the other tested fuels. However, there is problem with its miscibility to form a stable ternary fuel. On the other hand, DBE achieved the lowest BSPM (same as DBM), TNC and GMD. Ethanol can form a stable ternary fuel and it is widely available, compared to the higher alcohols.

Table 4-2 Effect of used alternative fuels on the engine combustion and performance and emissions based on the average of five engine loads

Parameter	Order (Highest to lowest)
Peak in-cylinder Pr	All the blended fuels (1%) ≈ **Diesel**
Peak HRR	DBPe ≈ DBPr ≈ DBBu (22.1%) > DBE (14.8%) > DBM (5.9%) > **Diesel >** DB (-3%)
ID	DBPr (9.7%) > DBPe ≈ DBBu ≈ DBE (6.7%) > DBM (1.7%) > **Diesel** > DB (-3.9%)
DOC	DB (0.6%) ≈ **Diesel** ≈ DBE ≈ DBM (-1.1%) > DBBu ≈ DBPr ≈ DBPe (-2.3%)
COV_{IMEP}	DBBu ≈ DB (9%) > DBE (7.8%) > DBPe (5.8%) > DBPr (2.7%) > **Diesel** > DBM (-1.6%)
COV $_{Max(dP/d\theta)}$	DBPe (12.8%) > DBPr ≈ DBBu (7.5%) > DBE (1.4%) > **Diesel** ≈ DBM (-0.5%) > DB (-3%)
EGT	**Diesel** > All the blended fuels (-1.5%)
BSFC	DBE ≈ DB ≈ DBPr ≈ DBPe (6.6%) > DBBu (4%) > DBM (2.3%) > **Diesel**
BTE	DBM (3.5%) > DBBu (1.5%) > **Diesel** ≈ rest blended fuels (-1%)
$BSCO_2$	DB (1.4%) ≈ **Diesel** > DBE ≈ DBPe ≈ DBPr (-1.8%) > DBBu (-3.2%) > DBM (-8.2%)
BSCO	**Diesel** ≈ DBE (-0.4%) > DBPe (-3.5%) > DBBu ≈ DBPr (-6.4%) > DB (-11.3%) > DBM (-23.9%)
BSHC	**Diesel** > DBBu ≈ DBE (-8.8%) > DB ≈ DBPr ≈ DBPe (-12.3%) > DBM (-24.3%)
$BSNO_X$	DB (5.8%) > **Diesel** > DBBu ≈ DBE (-4.7%) > DBPe (-11.7%) > DBM (-14.2%) > DBPr (-19.3%)
BSPM	**Diesel** > DB (-5.2%) > DBPe (-32.6%) > DBPr (-46.2%) > DBBu (-61%) > DBM ≈ DBE (-70%)
TNC	DBPr(0.2%) ≈ **Diesel** > DBPe(-1.1%) > DB(-9%) > DBM(-22%) > DBBu(-31.1%) > DBE(-37.3%)
GMD	**Diesel** > DBM ≈ DB (-5.25%) > DBPe ≈ DBBu ≈ DBE ≈ DBPr (-10.3%)

CHAPTER 5 COMBUSTION AND PERFORMANCE OF DIESEL ENGINE WITH DIFFERENT FUELING MODES

The results and discussion in regard to the combustion and performance of a diesel engine operated with the four fueling modes under various engine loads and speeds are presented in this chapter. The results pertaining to the engine load have been published in [315].

5.1 Engine combustion

The combustion characteristics in the present study were obtained on the average of 500 consecutive cycles to minimize the influence of cycle-to-cycle variations based on the in-cylinder pressure and heat release rate (HRR). The combustion parameters investigated are similar to those mentioned in Chapters 3 and 4.

5.1.1 In-cylinder pressure and heat release rate

5.1.1.1 Based on engine load

Fig. 5.1 illustrates the typical curves of in-cylinder pressure and HRR at 1800 rpm with low (57 Nm), medium (142.5 Nm) and high (228 Nm) engine loads for diesel, blended, F+B and fumigation modes. The peak in-cylinder pressure and peak HRR curves are also shown in Fig. 5.2 (a) and (b), respectively. Fig. 5.1 and Fig. 5.2 (a) reveal that the in-cylinder pressure increases, and occurs further away from the top dead center, with increase in engine load for all the tested fueling modes which is due to more fuel consumption at higher loads [86]. Similar trend was recorded in the literature using diesel, blended [87,128,129] and fumigation modes [167]. However, Fig. 5.1 and Fig. 5.2 (b) show that the peak HRR increases with rise in load from 57 Nm to 185.3 Nm and then decreases at 228 Nm for all the fueling modes. Similar variation of HRR with engine load was observed in the literature for diesel, blended [128,129,286] and fumigation modes [167]. At the very high engine load of 228 Nm, the combustion temperature is high and the fuel/air ratio is also much richer (Fig. 5.20) than that of the lower engine loads; however, there is not enough time for mixing of fuel and air, resulting in incomplete combustion and decrease in the peak HRR. In addition, the ID (Fig. 5.7 (a)) is shorter at very high engine load, thus less fuel is accumulated during the delay time to burn in the premixed burning phase, resulting in the decrease of peak HRR.

The impact of different fueling modes on the in-cylinder pressure and HRR are shown in Fig. 5.1 and Fig. 5.2 (a). Compared to the diesel fuel operation, the blended, F+B and fumigation modes of operation have peak in-cylinder pressure being lower at low engine load, similar at medium load and higher at high load (especially for the fumigation mode). The small reduction in peak in-cylinder pressure at low engine load is due to the lower combustion temperature and the higher ignition delay (Fig. 5.7 (a)) which lead to SOC occurring further away from the top dead center during the expansion stroke [128,129]. On the other hand, the increase in the peak in-cylinder pressures at the highest load (228 Nm) is due to higher combustion temperatures and lower ignition delay of the F+B and fumigation modes (Fig. 5.7 (a)) compared to the diesel fuel operation. Some other studies also found the peak in-cylinder pressure decreases at low engine load and increases at high engine load using the blended mode [128,129] and fumigation mode [167,316] operations in comparison with baseline fuels. However, the results based on the average of five loads and T-test at 95% level indicate that there is almost no difference among the peak in-cylinder pressures of the blended (-0.2%), F+B (0.9%) and fumigation (1.3%) modes compared to the diesel fuel operation.

For HRR, the blended, F+B and fumigation modes have higher peak HRR at almost all the tested engine loads (except for fumigation mode at the engine load of 57 Nm). The average of five loads from Fig. 5.1 and Fig. 5.2 (b) shows that the blended (20.4%), F+B (6.3%) and fumigation (2.2%) modes of operation cause increase in peak HRR at all loads in comparison with pure diesel. For the blended mode, this increase in peak HRR can be attributed to the better volatility and lower viscosity (contributing to better fuel atomization) of ethanol and the longer ignition delay (due to low cetane number of ethanol) which lead to accumulation of more fuel during the delay time to burn in the premixed burning phase and hence the higher peak HRR [83,287,288,297]. In the fumigation mode, the ignition delay is shorter (Fig. 5.7 (a)), the duration of combustion is longer (Fig. 5.7 (b)), the fuel is not well atomized due to the low fuel injection pressure of 0.35 MPa, and fuel mixing with air is poor compared to the blended mode; therefore, the fumigation mode has less effect on the increase in peak HRR (only 2.2%). In addition, the lean mixture of fumigated fuel and air plus the low combustion temperature at the low load of 57 Nm cause deterioration in the combustion efficiency [31] and even a drop in the peak HRR. The change in peak-HRR in the F+B mode is in between those of the blended and fumigation modes.

Fig. 5.3 shows that the cumulative heat release fractions of all the tested fueling modes have almost similar trend at low, medium and high engine loads. A small difference is recorded for the first 20% of cumulative heat release fraction due to the difference in the ID of the different fueling modes. The fumigation mode has shorter ID, thus earlier increase in the cumulative heat release fraction is recorded compared to the diesel mode. On the other hand, the blended mode has longer ID, so later increase in the cumulative heat release fraction is observed. Despite of the late increase in the first 20% of cumulative heat release fraction, the blended mode reaches 100% cumulative heat release fraction earlier due to its faster burning rate (as shown in Fig. 5.7 (c)).

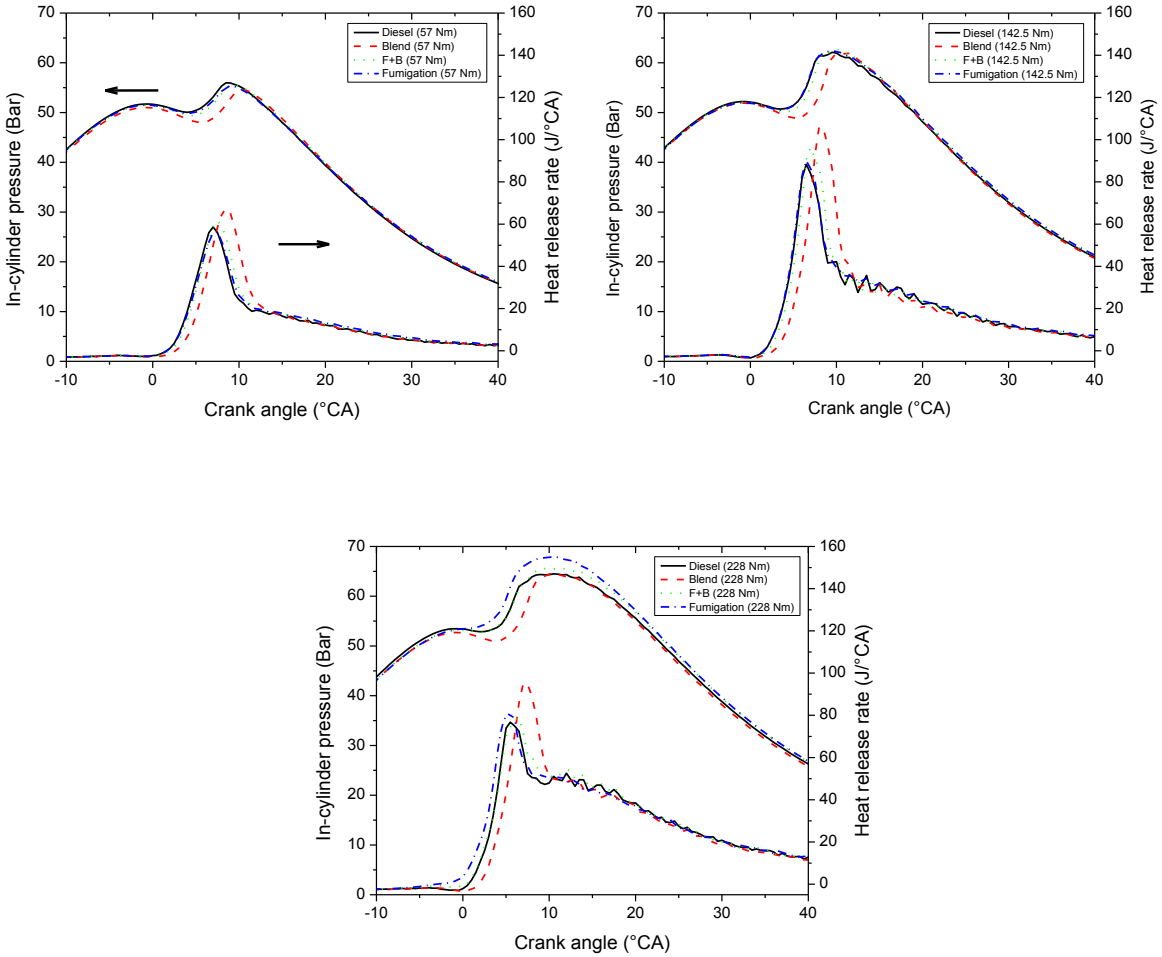

Fig. 5.1 Variations of in-cylinder pressure and HRR with low, medium and high loads.

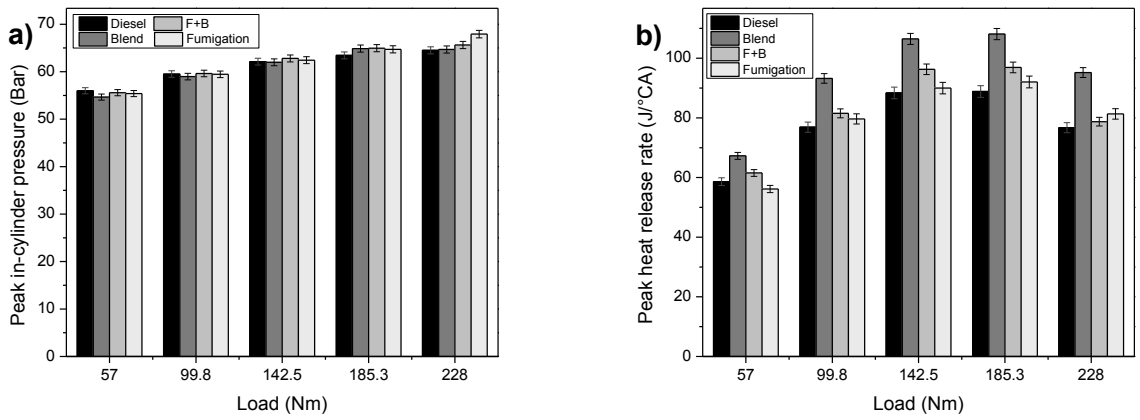

Fig. 5.2 Variations of (a) peak in-cylinder pressure and (b) peak HRR with engine load.

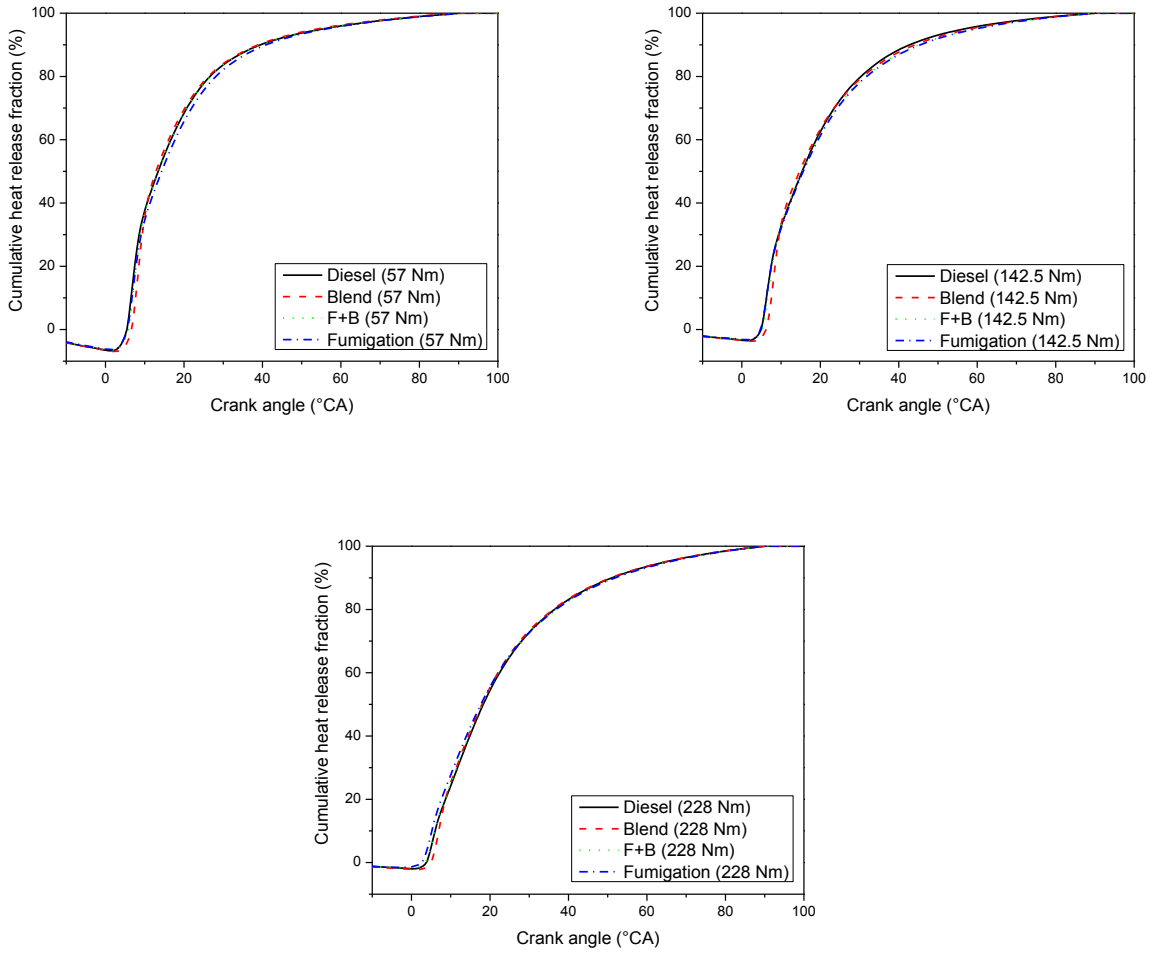

Fig. 5.3 Variation of cumulative heat release fraction with low, medium and high engine loads.

5.1.1.2 Based on engine speed

Typical curves of in-cylinder pressure and HRR are illustrated in Fig. 5.4 for low (1400 rpm), medium (1800 rpm) and high (2200 rpm) engine speeds. Also, Fig. 5.5 (a) and (b) show the peak in-cylinder pressure and peak HRR, respectively. It can be seen from Fig. 5.4 and Fig. 5.5 (a) and (b) that the peak in-cylinder pressure and peak HRR occur further away from the top dead center with increasing engine speed; while the peak in-cylinder pressure decreases and the peak HRR increases (irrespective of the engine speed of 2200 rpm) with increasing engine speed for all the tested fueling modes due to increase in ignition delay [297] (as shown in Fig. 5.8 (a) for ID). Labeckas et al. [317] also reported that the increase in engine speed from 1400 to 2200 rpm caused increase in peak HRR at λ= 5.5 and 3 with the use of DBE in a CI engine. Wei et al. [318] and Song et al. [319] also found an increase in the peak HRR with increasing engine speed in the fumigation mode with methanol as the fumigated fuel.

Also, at low speed, the blended, F+B and fumigation modes cause slight increase in peak in-cylinder pressure. On the other hand, at high speed, the blended mode causes a slight drop; while the F+B and fumigation modes have similar peak in-cylinder pressure, compared to that of the diesel mode. At medium speed, all the four fueling modes have almost similar peak in-cylinder pressures. However, based on the average results of the five speeds, the T-test at 95% confidence level indicates that there are almost no differences among the peak in-cylinder pressures of the blended (only 0.6% rise), F+B (1%) and fumigation (1%) modes with the pure diesel mode.

For the peak HRR, the blended and F+B modes lead to increase in peak HRR at all the tested engine speeds compared to that of the diesel mode. According to the average of five speeds, the blended mode leads to 18.4% increase, the F+B mode causes 7.7% increase; while the fumigation mode has almost equal value (only 0.3%) in the peak HRR in comparison with that of the diesel mode. The increase in HRR based on different engine speeds was also found in the literature when using DBE blend [317] and fumigated methanol [318,319].

Fig. 5.6 also reveals that the cumulative heat release fractions of all tested fueling modes have almost similar trend for low, medium and high engine speeds. A small difference is recorded in the first 20% of cumulative heat release fractions due to the difference in ID of the different fueling modes (similar observation with engine loads in Fig. 5.3).

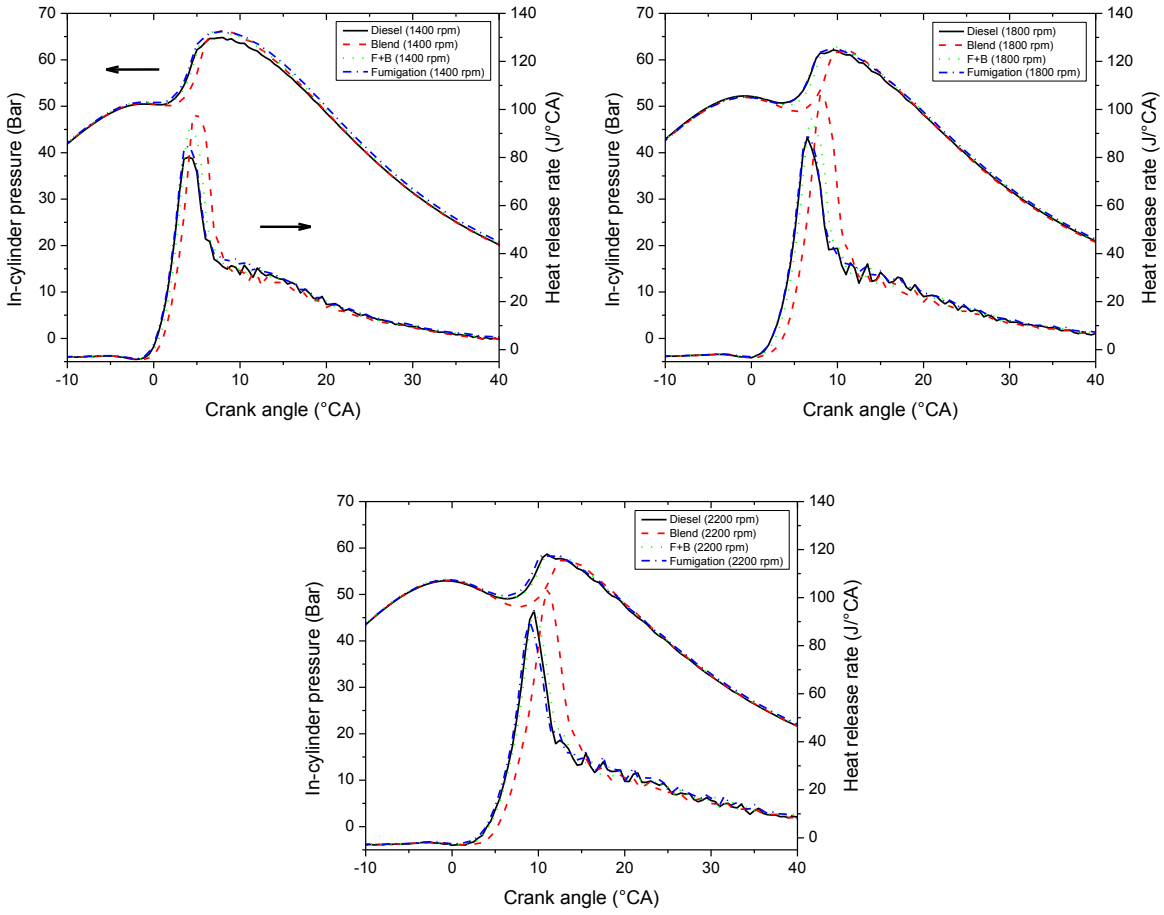

Fig. 5.4 Variations of in-cylinder pressure and HRR with low, medium and high engine speeds.

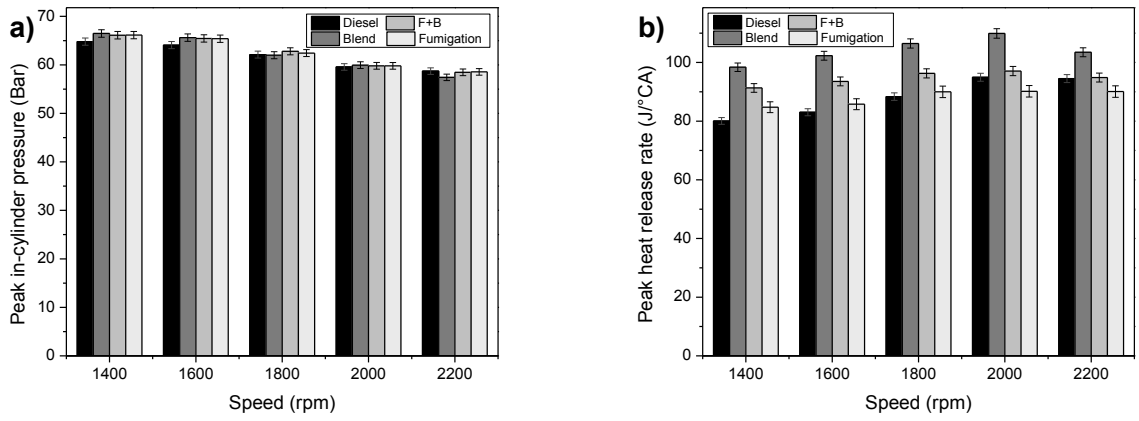

Fig. 5.5 Variations of (a) peak in-cylinder pressure and (b) peak HRR with engine speed.

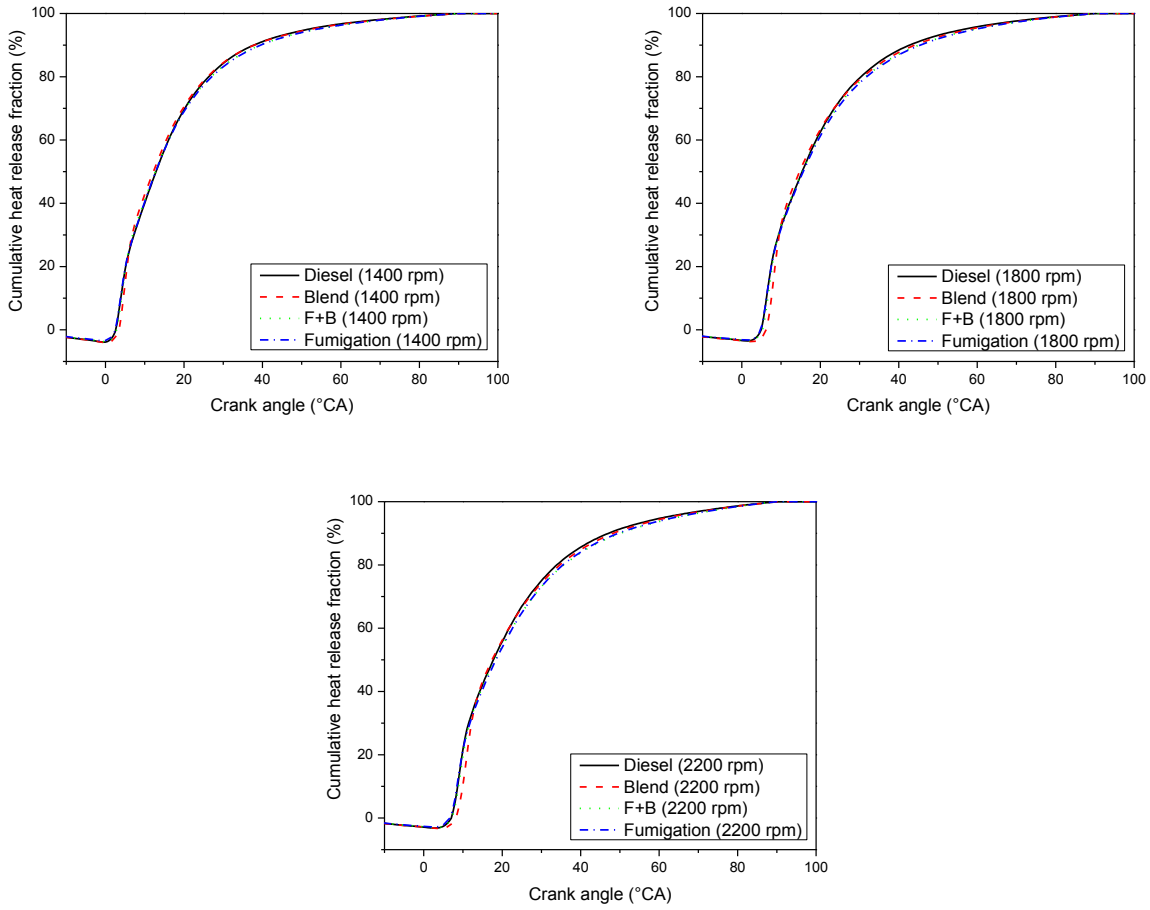

Fig. 5.6 Variation of cumulative heat release fraction with low, medium and high engine speeds.

5.1.2 Ignition delay and duration of combustion

5.1.2.1 Based on engine load

The impacts on the ignition delay (ID) and duration of combustion (DOC) based on different engine loads are presented in Fig. 5.7 (a) and (b), respectively. It can be seen from these Figures that the increase in engine load causes shorter ID and longer DOC for all the tested fueling modes. The ID is reduced due to increase in in-cylinder combustion temperature [57] as a consequence of the increase in engine load. For DOC, the increase in load causes increase in durations of fuel injection, air/fuel mixture formation and combustion, and hence the increase in DOC [289]. Also, Fig. 5.7 (a) demonstrates that ID is longer for the blended mode at all engine loads, in comparison with the pure diesel mode; however, the fumigation mode has shorter ID than the blended mode and could be shorter than that of the pure diesel mode. The longer ID of the blended mode is due the lower cetane number and higher latent heat of evaporation of ethanol which causes

increase in ID and decrease in in-cylinder temperature, respectively, compared to the diesel fuel [125,290].

In the fumigation mode, pure diesel fuel which has high cetane number is injected into the engine cylinder and ignited by the hot compressed air/fumigated fuel mixture; in addition, the combustion mixture is also richer than that in the other fueling modes (Fig. 5.20) due to the highest fuel consumption in the fumigation mode. Thus, the shorter ID in the fumigation mode is due to less influence of cetane number of ethanol and more effect of the combustion in an environment with higher fuel/air ratio. These effects also are applicable for the F+B mode at the engine load of 228 Nm, at which the combustion temperature is high enough resulting in shorter ID. On the other hand, the longer ID of the fumigation mode at the engine load of 57 Nm (low load) is due to the lower in-cylinder temperature as a consequence of higher latent heat of evaporation of ethanol, which dominates over the effect of the higher cetane number of diesel and equivalence ratio. In addition, the very lean fumigated fuel/air mixture (not the overall equivalence ratio as shown in Fig. 5.20) plus low combustion temperature at low engine load (57 Nm) cause increase in ID for the fumigation mode. On the average of five loads, the blended mode causes longer ID (10.1%), the F+B mode has almost similar ID (only slight increase of 1.4% which is not significant with T-test at 95% level); while the fumigation mode has a slight decrease in ID (-1.9%), compared to the pure diesel mode.

For DOC, the average of five loads shows that the blended mode has shorter DOC (-3.1%), the F+B mode has similar DOC (only slight increase of 1% which is not significant with T-test at 95% level) and the fumigation mode has longer DOC (3.4%), compared to the diesel mode. The shorter DOC in the blended mode is due to the following reasons. Firstly, ethanol in the blended fuel causes longer ignition delay and hence increase in heat released in the premixed combustion phase [127]. Therefore, more fuel is burned in the premixed combustion phase (Fig. 5.1, Fig. 5.2 (b) and Fig. 5.9). Secondly, ethanol and biodiesel lead to increase in oxygen content of the blended fuel hence suppress the pyrolysis process and enhance the rate of oxidation during combustion [295]. Jamrozik et al. [133] also found a reduction in DOC and an increase in ID with using with using DBE blends.

However, the shorter ID (Fig. 5.7 (a)) in the fumigation mode causes decrease in fuel burned in the premixed combustion phase and increase in fuel burned in the diffusion

combustion phase (Fig. 5.1, Fig. 5.2 (b) and Fig. 5.9), resulting in longer DOC. In addition, despite of the faster flame propagation speed of ethanol, the fumigated fuel is not well atomized due to the low fuel injection pressure and fuel mixing with air is poor; therefore, it takes more time to burn the fumigated fuel, resulting in longer DOC in the fumigation mode. The highest BSFC of fumigation mode (Fig. 5.18 (b)) has an effect on the increase in DOC (especially in diffusion combustion phase as shown in Fig. 5.9). Also, the fumigated fuel is distributed into the combustion chamber; therefore, the flame propagation is weaker in the lean air/fuel mixture and it takes more time to burn the fumigated fuel inside the engine cylinder. On average of the five loads, the DOC of the F+B mode is almost similar to that of the pure diesel mode (1%) and it is in between those of the blended mode (-3.1%) and the fumigation mode (3.4%).

Fig. 5.7 (c) illustrates the overall combustion progression (including ID, DOC and positions of 10%, 50% and 95% heat release) of the four fueling modes at the engine speed of 1800 rpm with five engine loads. The fuel injection starts at 8 °CA before top dead center. Despite of slight reduction in ID as a consequence of increase in engine load, it can be observed that the increase in load can increase the overall combustion progression for all the tested fueling modes which is due to rise in duration of combustion. It can also be seen that the blended mode has almost similar while the fumigation mode has slightly longer overall combustion progression compared to the diesel mode. Fig. 5.7 (c) also illustrates that the interval of crank angle degrees for achieving 50% of heat release in the blended mode is the shortest among all the tested fueling modes which means the blended mode has a faster combustion to reach 50% of heat release.

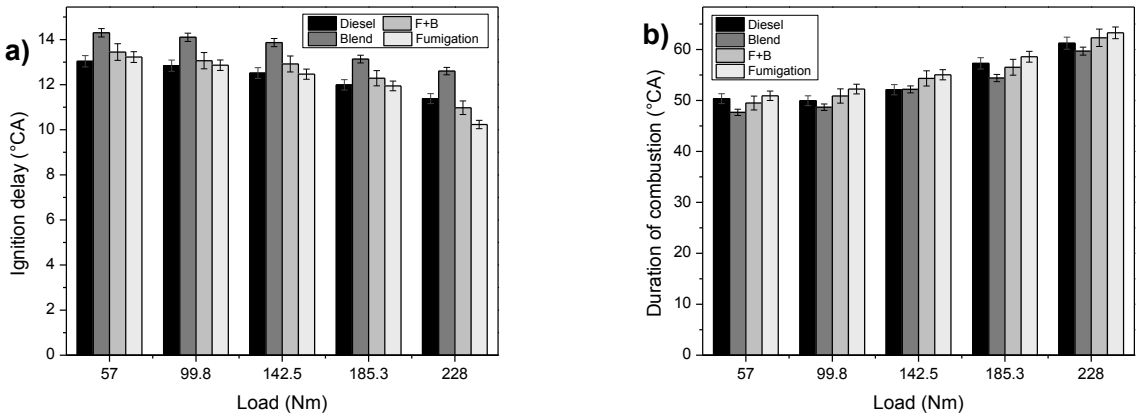

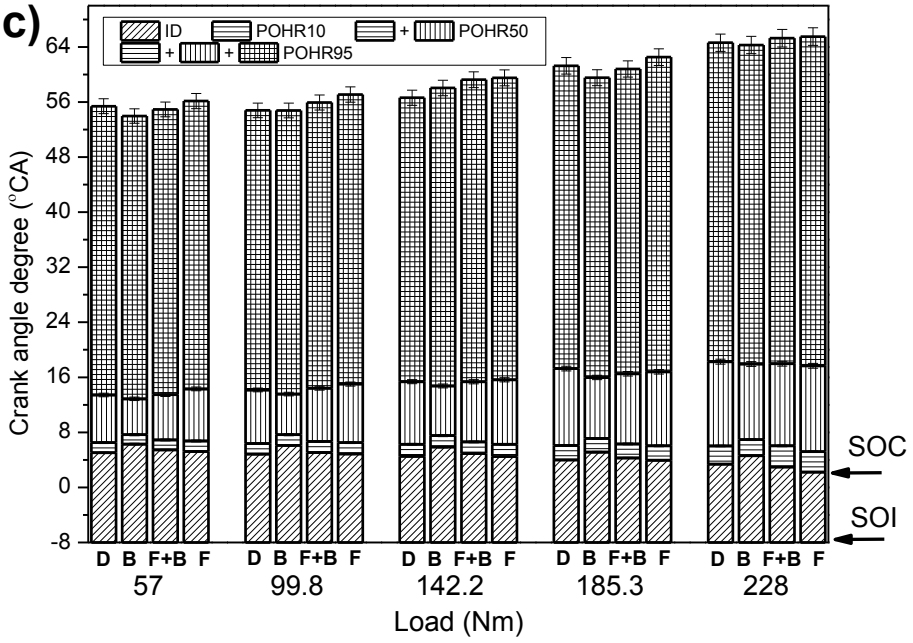

Fig. 5.7 Variations of (a) ignition delay, (b) duration of combustion and (c) and overall combustion progression with engine load.

5.1.2.2 Based on engine speed

Variations of ID and DOC with engine speeds are presented in Fig. 5.8 (a) and (b), respectively. The two Figures illustrate that both ID and DOC of all the tested fueling modes (except a slight reduction in DOC at the engine speed of 2000 rpm) increase with increasing engine speed. In general, the increase in engine speed (at constant load) causes almost linear increase in ID and DOC in terms of °CA, but slight reduction in ID and DOC based on milliseconds [297] which are similar to the results in the present study in which there are increase based on °CA and slight decrease based on millisecond for both ID and DOC. The increase in ID based on °CA is due to more restriction to free gas flow and lower degree of scavenging of the engine cylinder with increase in engine speed [317]; while the increase in DOC is due to increase in duration of fuel injection and air/fuel mixture formation. In addition, the increase in engine speed causes shorter time duration for each crank angle, necessitating longer crank angle to initiate combustion and to complete combustion of the fuel.

Fig. 5.8 (a) depicts that on the average of five engine speeds, the blended mode causes 8.1% increase in ID, the F+B mode causes only 1.7% increase in ID; while the fumigation mode reduce the ID by 1.4% compared to that of the pure diesel mode. Also,

Fig. 5.8 (b) illustrates that compared to pure diesel mode, the fumigation mode and the F+B mode have 5.5% and 5% longer DOC, respectively; while the blended mode has almost equal DOC (0.3% reduction, which is not significant with T-test at 95% confidence level).

It can be observed from Fig. 5.8 (c) that the increase in speed can increase the overall combustion progression for all the tested fueling modes. Fig. 5.8 (c) shows that the interval of crank angle degrees for achieving 50% of heat release of the blended mode is shorter than that of the diesel mode and the fumigation mode which means the blended mode has a faster combustion to reach 50% of heat release (same behavior with different loads in Fig. 5.7 (c)).

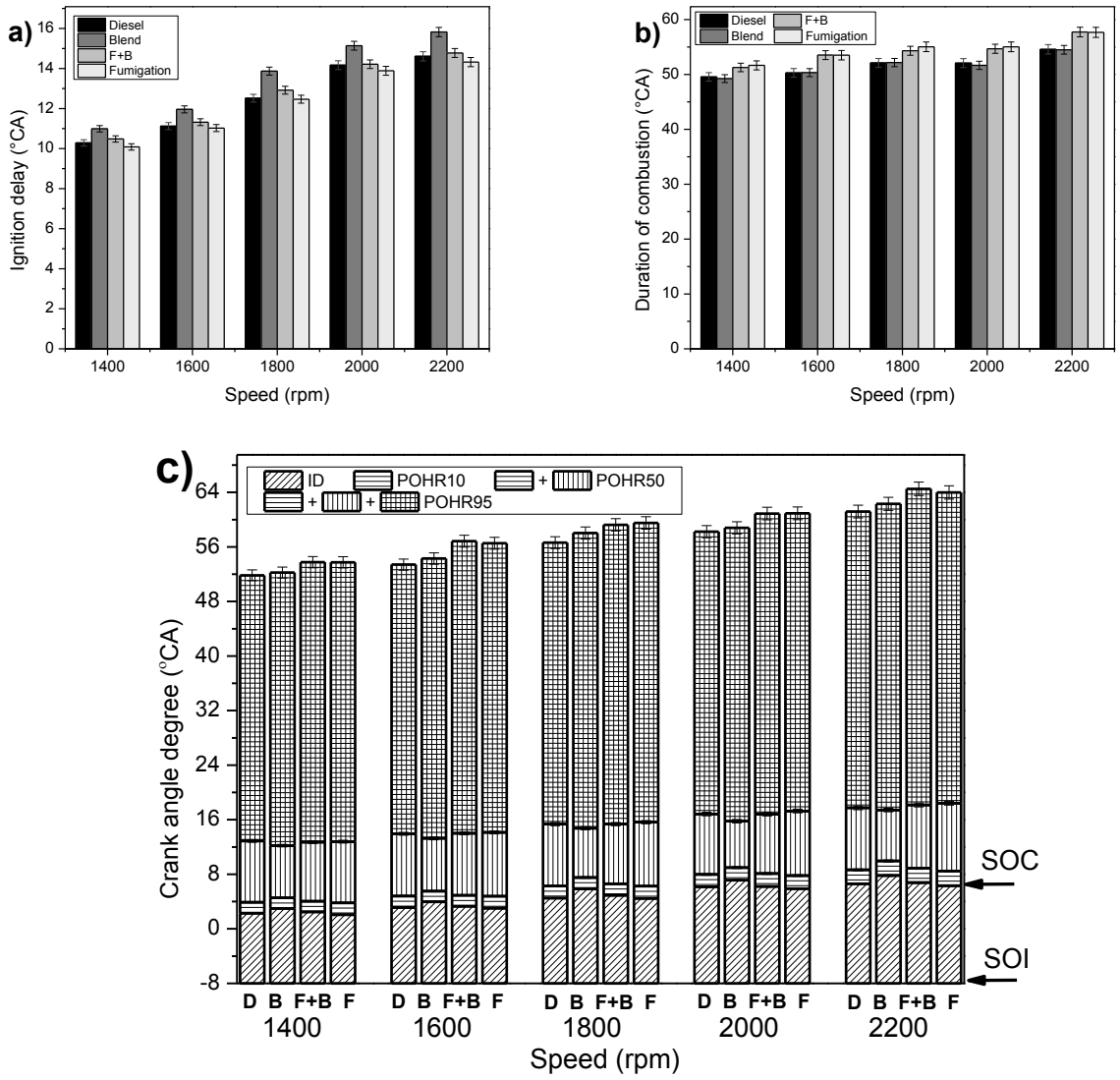

Fig. 5.8 Variations of (a) ignition delay, (b) duration of combustion (c) and overall combustion progression with engine speed.

5.1.3 Premixed and diffusion combustion phases

5.1.3.1 Based on engine load

Fig. 5.9 (a-c) show variations of premixed combustion phase, diffusion combustion phase and overall premixed/diffusion combustion fraction, respectively with engine load for different fueling modes. It can be seen from Fig. 5.9 (a and b) that the increase in engine loads causes increase in premixed combustion phase (but drop at 228Nm similar to peak HRR in Fig. 5.2 (b)) and diffusion combustion phase. Tse et al. [129] also found an increase in total heat release rate and diffusion combustion phase with increase in engine load for diesel and DBE. The same factors which cause the variation of peak HRR with engine loads also cause the change in the premixed combustion phase; while the increase in diffusion combustion phase with increase in engine loads is due to increase in fuel equivalence ratio. Fig. 5.9 (c) also shows that the increase in engine load leads to increase in overall diffusion combustion fraction and hence decrease in overall premixed combustion fraction for all the fueling modes due to increase in fuel equivalence ratio and shorter ID.

Fig. 5.9 (a and b) also illustrate that the blended, F+B and fumigation modes have higher premixed combustion phase (except equal at 57Nm for fumigation), but lower diffusion combustion phase (except increase at low loads and equal at medium load for fumigation) compared to the diesel mode at all the engine loads. The reasons are already mentioned in DOC sections. However, the higher diffusion combustion phase in the fumigation mode at low loads is due to the lower in-cylinder temperature as a consequence of higher latent heat of evaporation of fumigated ethanol, and the very lean fumigated fuel/air mixture (not the overall equivalence ratio as shown in Fig. 5.20). But, these effects are insignificant at higher engine loads due to the higher combustion temperature and more complete combustion. On the average of five engine loads, the increases in premixed combustion phase are 47.2% for blended, 31.0% for F+B and 22.3% for fumigation modes in comparison with the diesel mode. On the other hand, the blended (-19.1%) and F+B (-7.0%) modes have higher diffusion combustion phase, but the fumigation mode (1.7%) has similar diffusion combustion phase compared to the diesel mode.

In addition, it can be seen from Fig. 5.9 (c) that the use of blended, F+B and fumigation modes can reduce the diffusion combustion fraction at all the tested loads (except fumigation at low loads of 57Nm and 99.8Nm) compared to the diesel mode; while the

blended mode has the highest reduction.

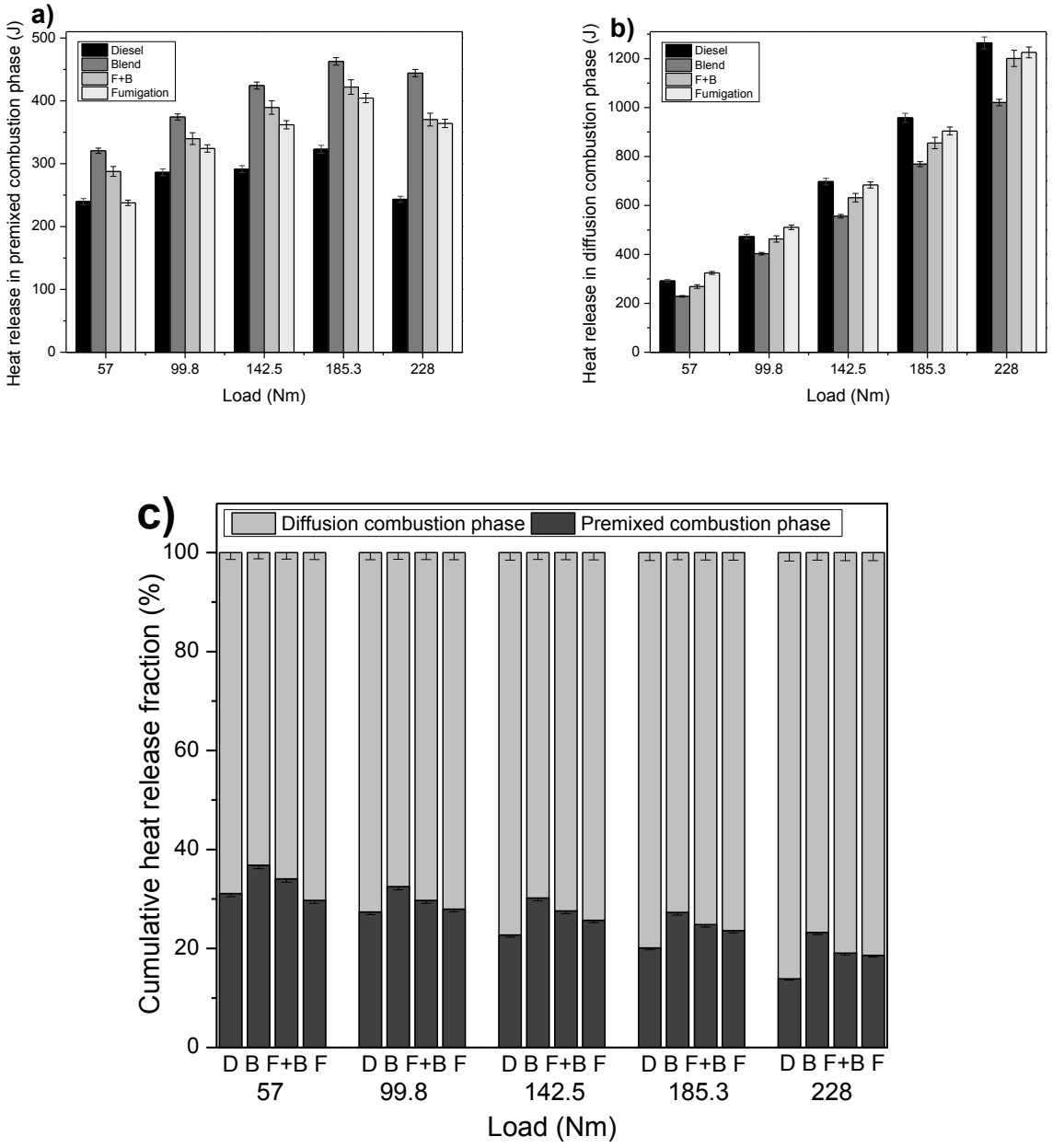

Fig. 5.9 Variations of (a) heat release in premixed combustion phase, (b) heat release in diffusion combustion phase (c) and overall premixed/diffusion combustion fraction with engine load.

5.1.3.2 Based on engine speed

Fig. 5.10 (a-c) show that the increase in engine speed has an effect only on the increase in premixed combustion phase (except at 57Nm for diesel and fumigation modes) and no significant impacts on the diffusion combustion phase and overall premixed/diffusion combustion fraction for all the fueling modes. The increase in premixed combustion

phase with increase in engine speed is due to the longer ID as shown in Fig. 5.8 (a).

In addition, it can be seen from Fig. 5.10, that the blended, F+B and fumigation modes have higher premixed combustion phase, but lower diffusion combustion phase (except increase at low speed and equal at medium speed for fumigation) compared to the diesel mode at all the engine speeds which are similar to the finding based on the five engine loads.

On the average of five engine speeds, the increases in premixed combustion phase are in the order of blended (43.6%), F+B (31.6%) and fumigation (22.2%) modes compared to the diesel mode. The reductions in diffusion combustion phase are -19.5% for blended mode and -8.6% for F+B mode; while fumigation mode (-1.3%) has similar diffusion combustion phase compared to the diesel mode. It can be inferred from the results that the effect of using blended, F+B and fumigation on the premixed and diffusion combustion phases is independent to the engine speed and load. Because, the increase in premixed combustion phase and reduction in diffusion combustion phase by them, based on average of five engine speeds are almost similar to average of five engine loads. In addition, Fig. 5.10 (c) shows that the use of blended, F+B and fumigation modes can reduce the diffusion combustion fraction at all the tested speeds (except fumigation at low speeds of 1400 rpm and 1600 rpm) compared to the diesel mode; while the blended mode has the highest reduction which is similar to the finding based on the five engine loads.

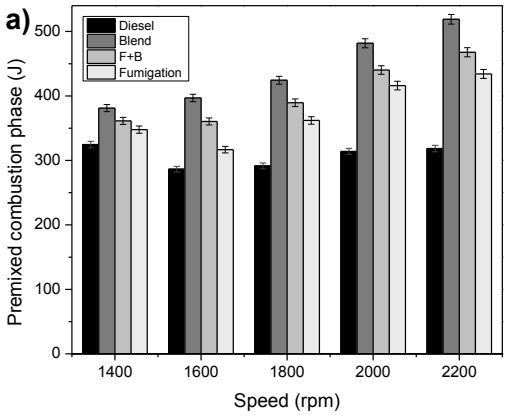

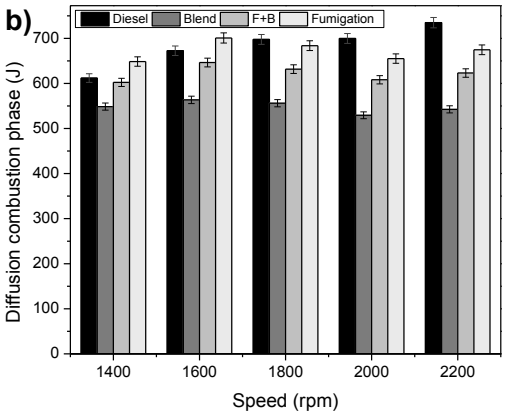

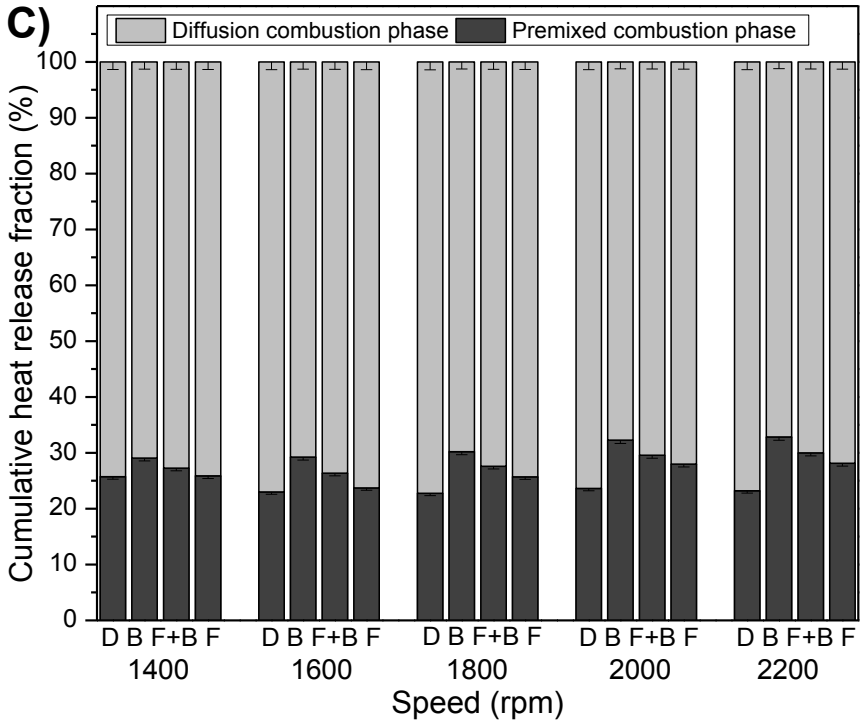

Fig. 5.10 Variations of (a) premixed combustion phase, (b) diffusion combustion phase (c) and overall premixed/diffusion combustion fraction with engine speed.

5.1.4 Coefficient of variation in indicated mean effective pressure at different engine loads and speeds

The coefficient of variation in indicated mean effective pressure (COV_{IMEP}) which can be derived from the pressure data, is an important parameter of cyclic variability. COV_{IMEP} is defined as the cyclic variability in indicated work per cycle; while the vehicle drivability problems occur when the COV_{IMEP} exceeds of 10% [297]. COV_{IMEP} is calculated according to the standard deviation in IMEP divided by the mean IMEP, and is usually expressed in percent unit. Fig. 5.11 and Fig. 5.12 show the COV_{IMEP} (calculated for 500 working cycles) of five tested engine loads and five engine speeds, respectively. It can be seen from Fig. 5.11 that the COV_{IMEP} firstly decreases from the engine load of 57 Nm to 99.8 Nm and then increases up to the engine load of 228 Nm for all the tested fueling modes. Similar trend was recorded in [282] using diesel and DBE blend. For various engine speeds, Fig. 5.12 illustrates that the increase in engine speed causes increase in COV_{IMEP} for the fumigation mode; while other fueling modes have different trends with increase in engine speed.

Fig. 5.11 and Fig. 5.12 also reveal that the COV_{IMEP} of the diesel mode is about 1% and COV_{IMEP} of the fumigation mode is more than 1% which is similar to the finding in [190,320] for diesel and fumigated ethanol. According to the average of five engine loads, the use of DBE in the blended (6.6%), F+B (16.1%) and fumigation (26.3%) modes causes increase in COV_{IMEP} compared to the diesel mode. For the five engine speeds, the average results show the increase in COV_{IMEP} for the blended (8.8%), F+B (26.4%) and fumigation (53.5%) modes. Similar results were found using blended mode [282] and fumigation mode [190,320,321].

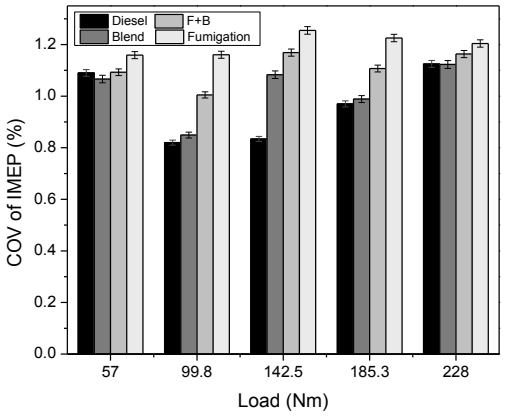

Fig. 5.11 Variation of COV_{IMEP} with engine load.

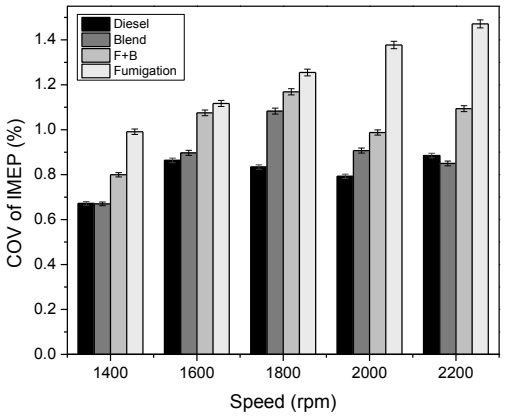

Fig. 5.12 Variation of COV_{IMEP} with engine speed.

5.1.5 Coefficient of variation in maximum cylinder pressure at different engine loads and speeds

Coefficient of variation in maximum cylinder pressure (COV $_{Max(dP/d\theta)}$) is another indicator which shows whether the combustion process of an engine is fast and robust or is slow and less repeatable [297]. COV $_{Max(dP/d\theta)}$ also can implicitly reflect the level of combustion noise. Fig. 5.13 and Fig. 5.14 illustrate the COV $_{Max(dP/d\theta)}$ (for 500 working cycles) under five engine loads and speeds, respectively. It can be found from Fig. 5.13 that the COV $_{Max(dP/d\theta)}$ increases from low load to medium load and then decreases until the highest tested load (228 Nm) for all the tested fueling modes. For different engine speeds, Fig. 5.14 depicts that all fueling modes have the same behavior on increasing in COV $_{Max(dP/d\theta)}$ with increasing engine speed.

In regard to the effect of using DBE on COV $_{Max(dP/d\theta)}$, it can be clearly seen from Fig. 5.13 and Fig. 5.14 that the use of DBE in the blended and F+B modes causes increase in COV $_{Max(dP/d\theta)}$ at all loads or speeds, respectively. However, the fumigation mode has lower COV $_{Max(dP/d\theta)}$ compared to the diesel mode at almost all the tested engine loads and speeds. On the average of five loads, the blended (9.2%) and F+B (3.4%) modes cause increase in COV $_{Max(dP/d\theta)}$, but the fumigation (-2.7%) mode has lower COV $_{Max(dP/d\theta)}$ compared to the diesel mode. Similarly for different engine speeds, the blended (6%) and F+B (4.3%) modes cause increase in COV $_{Max(dP/d\theta)}$, but the fumigation (-2.9%) mode has lower COV $_{Max(dP/d\theta)}$ in comparison with the diesel mode. The results from Fig. 5.13 and Fig. 5.14 show that the fumigation mode has slower combustion than the other fueling modes which is consistent with the findings in Fig. 5.7 (c) and Fig. 5.8 (c).

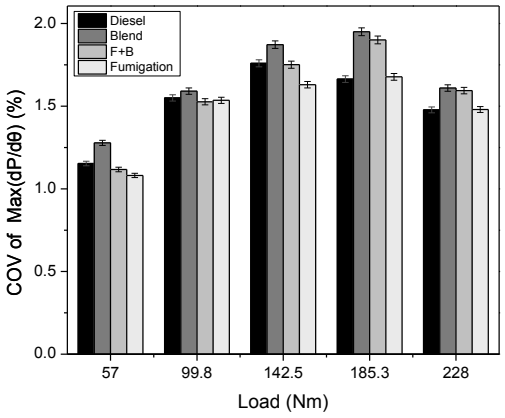

Fig. 5.13 Variation of COV $_{Max(dP/d\theta)}$ with engine load.

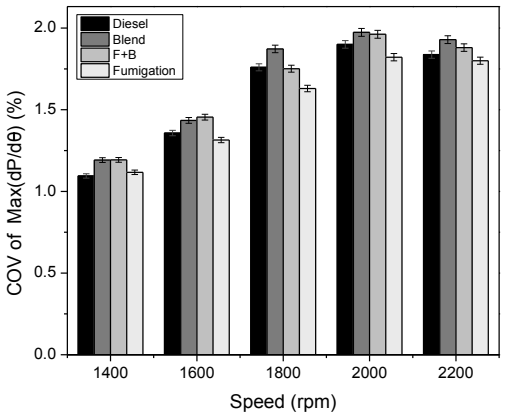

Fig. 5.14 Variation of COV $_{Max(dP/d\theta)}$ with engine speed.

5.1.6 Exhaust gas temperature at different engine loads and speeds

Fig. 5.15 and Fig. 5.16 indicate the variations of exhaust gas temperature with five engine loads and speeds, respectively. It is clearly observed from Fig. 5.15 and Fig. 5.16 that the increase in engine load or speed causes increase in exhaust gas temperature for all the tested fueling modes; while the influence of engine load is higher than that of engine speed. With the increase in engine load, more fuel is injected into the cylinder for burning which leads to increase in in-cylinder temperature and thus increase in exhaust gas temperature. In respect to the influence of using different fueling modes on exhaust gas temperature, the results in Fig. 5.15 and Fig. 5.16 show that the blended, F+B and fumigation modes lead to slight decrease in exhaust gas temperature only at medium and high engine loads compared to the diesel mode. This small reduction in exhaust gas temperature is due to the higher latent heat of evaporation and lower calorific value (cooling effect) of ethanol and biodiesel which can reduce the combustion temperature [27] and thereby reduce the exhaust gas temperature, compared to the diesel mode. However, the average results and the T-test reveal that there are almost no differences (only about 0.5% reduction) among the four fueling modes for different engine loads and speeds.

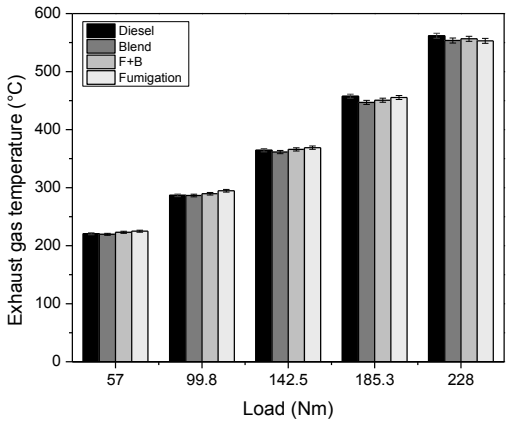

Fig. 5.15 Variation of exhaust gas temperature with engine load.

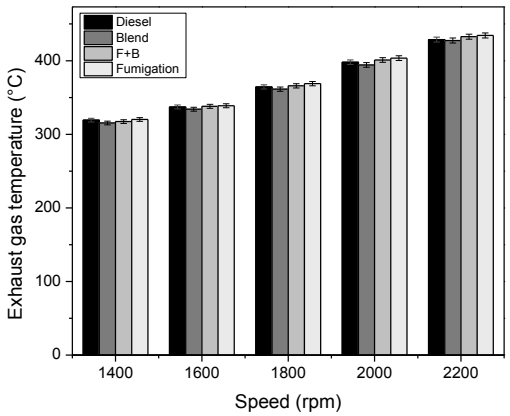

Fig. 5.16 Variation of exhaust gas temperature with engine speed.

5.1.7 Pre-ignition analysis

Since the fumigation fuel might have an effect on the pre-ignition in the engine cylinders due to injection of fumigated fuel into the cylinders before main fuel injection; therefore, a pre-ignition analysis for all the tested loads and speeds was conducted in this study. While only the results of the highest engine load (228Nm) and speed (2200 rpm) are presented in Fig. 5.17 due to the highest combustion temperatures at these conditions which might be favorable for pre-ignition. The pre-ignition analysis in this study is obtained from the peak in-cylinder pressures of 500 working cycles. It is found that fortunately all the tested fueling modes, even the fumigation mode, have no pre-ignition at all the tested loads and speeds (Fig. 5.17 is only shown as an example). Since ethanol

has lower cetane number and higher heat of evaporation which lead to decrease in combustion temperature; therefore, it prevents the early combustion (pre-ignition) in the fumigation mode.

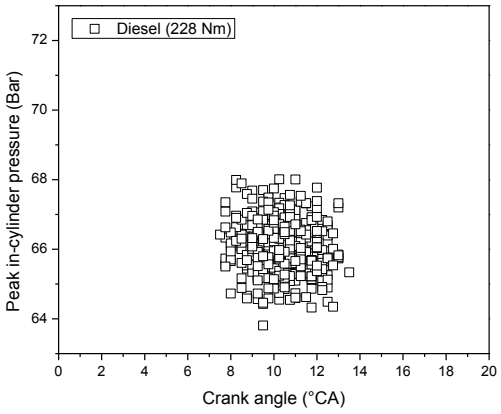

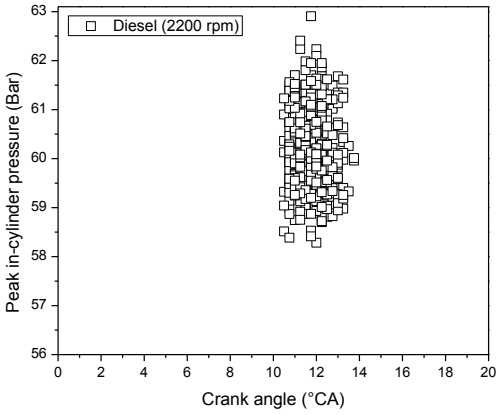

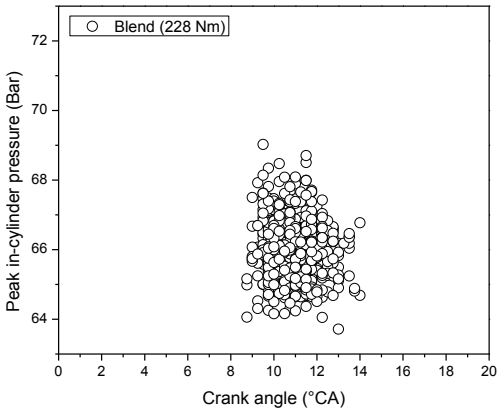

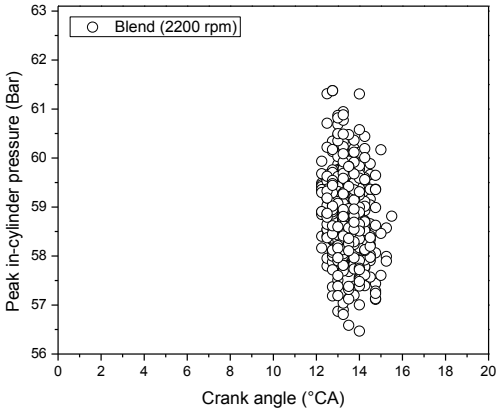

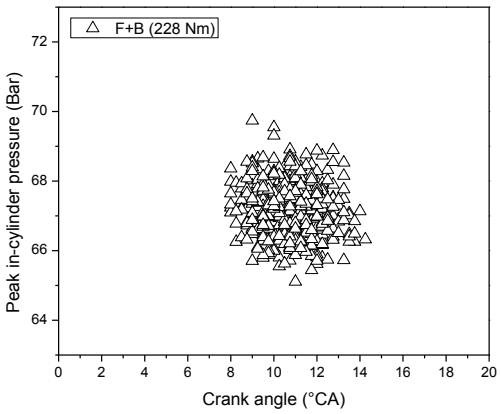

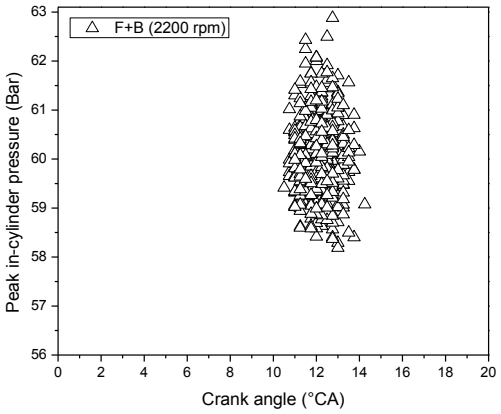

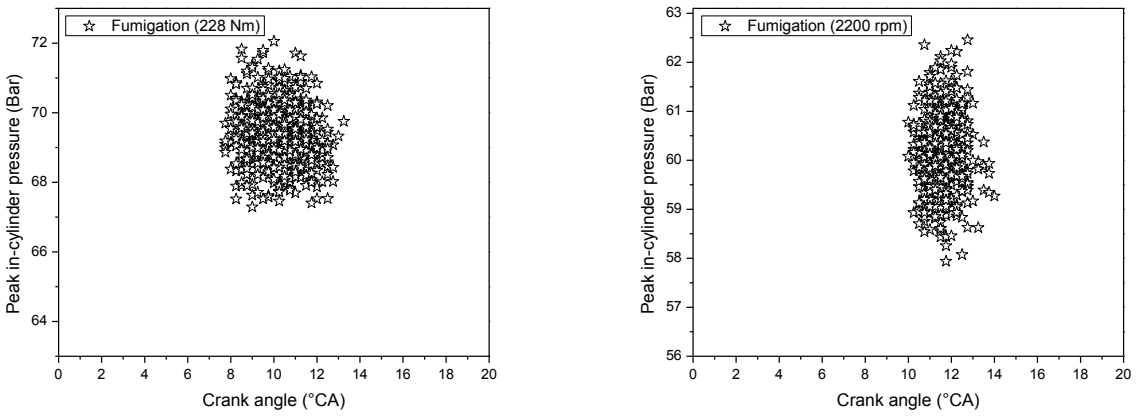

Fig. 5.17 Peak in-cylinder pressure for 500 working cycles for different fueling modes at high engine load (left) and high engine speed (right).

5.2 Engine performance

5.2.1 Brake thermal efficiency and brake specific fuel consumption

5.2.1.1 Based on engine load

The influences of engine load and type of fueling modes on BTE and BSFC are illustrated in Fig. 5.18 (a) and (b), respectively. It can be seen from Fig. 5.18 (a) and (b) that the best engine performance occurs at the engine load of 185.3 Nm engine load which has the highest BTE and the lowest BSFC for all the fueling modes. In contrast, the worst engine performance takes place at the lowest engine load of 57 Nm for all modes due to incomplete combustion as a consequence of the low combustion temperature and low fuel air ratio. On the other hand, at the very high engine load of 228 Nm, the combustion temperature is high and the fuel/air ratio is also much richer (Fig. 5.20); however, there is not enough time for mixing of fuel and air, resulting in incomplete combustion and decrease in heat release (Fig. 5.2 (b)), BTE and increase in BSFC, except the BTE and BSFC for the fumigation mode which are similar to the engine load of 185.3 Nm. The effect of engine load on the BTE (Fig. 5.18 (a)) is similar to that on the HRR (Fig. 5.2 (b)). The BTE increases from the engine load of 57 Nm to 185.3 Nm and then decreases at the engine load of 228 Nm for all the fueling modes, except that for the fumigation mode which has almost the same BTE at both engine loads of 185.3 Nm and 228 Nm.

Fig. 5.18 (a) and (b) also reveal that the blended, F+B and fumigation modes cause lower BTE (except for the blended mode which has similar BTE) and increase in BSFC. On the average of five loads, the decreases in BTE are in the order of fumigation mode (-5.8%) and F+B mode (-3.6%), with equal BTE (only slight increase of 0.6% which is not significant with T-test at 95% level) for the blended mode, compared to the diesel mode. The increases in BSFC are in order of fumigation mode (11.2%), F+B mode (9%) and blended (5%) mode. Lower calorific value (due to using biodiesel and ethanol) and lower density (due to use of ethanol) lead to increase in BSFC, as compared to the diesel fuel [73,284,297,298], because more fuel is required in order to maintain the same output power. In the blended mode, despite of increase in BSFC (5%), the BTE is similar to the diesel mode (0.6%). The lower viscosity of ethanol leads to improvement in fuel atomization and the increase in oxygen content in the fuel improve the combustion process; while the cooling effect of ethanol has adverse effect to the combustion process, thereby leading to equal BTE with that of the pure diesel mode [128]. However, in the fumigation mode, the fuel injected into the intake manifold is not well atomized, due to the low fuel injection pressure, resulting in poor mixing of air and the fumigated fuel, which cause the highest reduction in in-cylinder temperature; therefore, incomplete combustion occurs resulting in lower BTE and increase in BSFC compared to the diesel mode. Şahin et al. [32] also found that the fumigation mode had lower BTE and higher BSFC than the blended mode, using n-butanol. For the F+B mode, the results show that it has the impact of both blended mode and fumigation mode, on the BSFC and BTE. Because, the changes in BSFC (9%) and BTE (-3.6%) of the F+B mode are between those of the blended and fumigation modes.

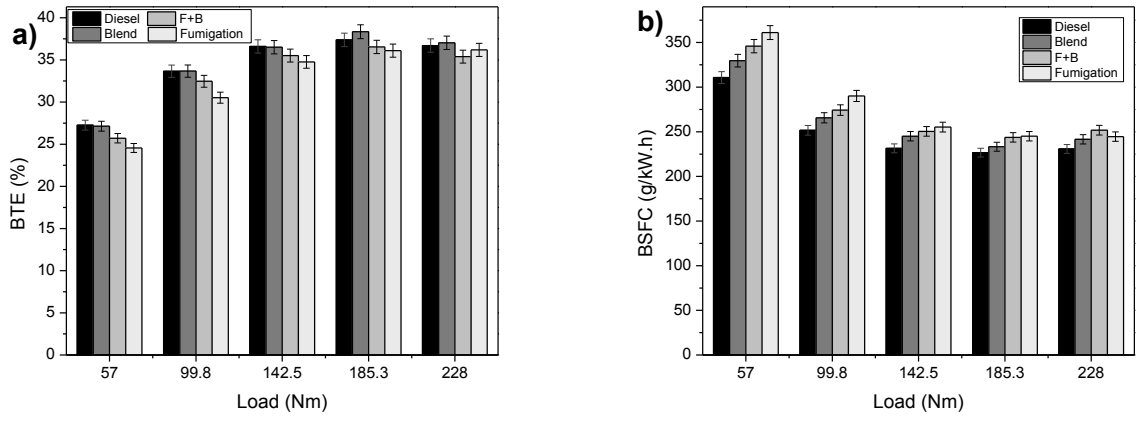

Fig. 5.18 Variations of (a) BTE and (b) BSFC with engine load.

5.2.1.2 Based on engine speed

The variations of BTE and BSFC with engine speed and type of fueling mode are illustrated in Fig. 5.19 (a) and (b), respectively. It can be seen that the increase in engine speed causes reduction in BTE and increase in BSFC for all the tested fueling modes. The decrease in BTE and increase in BSFC with increasing engine speed were also reported for diesel and blended fuels [97,99,101-103,317] in CI engine. Fig. 5.19 (a) also shows that on average of the five engine speeds the fumigation and F+B modes cause 5% and 3.6% reduction in BTE, respectively; while the blended mode has similar (0.05% increase) BTE compared to the pure diesel mode. For BSFC, Fig. 5.19 (b) illustrates that on average of the five engine speeds, the blended, F+B and fumigation modes cause 5.5%, 9.1% and 10.2% increase in BSFC, respectively compared to the pure diesel mode.

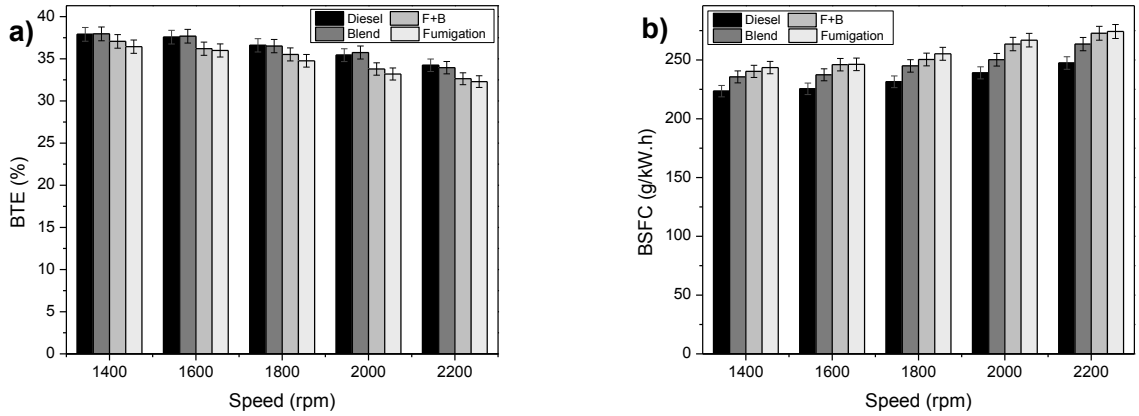

Fig. 5.19 Variations of (a) BTE and (b) BSFC with engine speed.

5.2.2 Equivalence ratio

5.2.2.1 Based on engine load

Variations of equivalence ratio (calculated according to [193]) with engine load and types of fueling mode are presented in Fig. 5.20. The equivalence ratios of all tested modes increase with rise in engine loads due to increase in fuel consumption. On the average of five loads, increases in equivalence ratio using biofuels are observed in the order of fumigation mode (9%), F+B mode (7%) and blended mode (2.5%) compared to pure diesel mode. The higher equivalence ratios of F+B and fumigation modes are due to the lower calorific values of biodiesel and ethanol compared to pure diesel and lower BTE resulting in more fuel being consumed. While the blended mode has only a slight increase

in equivalence ratio (2.5%) due to its better BTE. The equivalence ratio is the highest with the fumigation mode for engine loads of 57 Nm to 185.2 Nm because of incomplete combustion; therefore, more fuel is needed. However, at the engine load of 228, the equivalence ratio of the fumigated mode is slightly lowered, compared to that of the F+B mode, probably due to improvement in combustion of the slightly richer biofuel/air mixture with an increase in engine load. The increase in equivalence ratio using ethanol fumigation was also reported in other works [320,322].

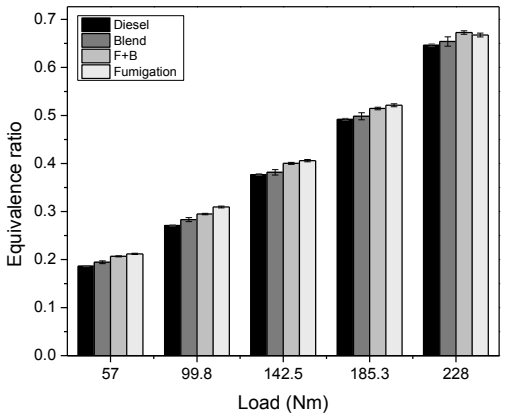

Fig. 5.20 Variation of equivalence ratio with engine load.

5.2.2.2 Based on engine speed

Fig. 5.21 depicts the variation of equivalence ratio with engine speed and type of fueling mode. As shown in Fig. 5.21, the equivalence ratios of all the tested fueling modes increase with increasing engine speed due to increase in the amount of fuel injected into the cylinder. The results based on the average of five speeds show that the fumigation mode has 6.4% increase, the F+B mode has 5.6% increase; while the blended mode has almost equal (0.04% increase) in the equivalence ratio compared to the diesel mode.

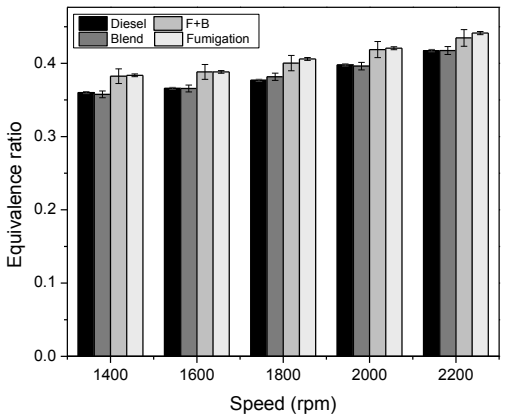

Fig. 5.21 Variation of equivalence ratio with engine speed.

5.3 Summary

The effects of the blended, F+B and fumigation modes on the engine combustion and performance based on the average of five loads and speeds compared to those of the diesel mode are presented in Table 5-1. It can be seen that the impact of using different fueling modes on the all the tested parameters is independent of the different engine loads or speeds, because the trends and percentages of increase or reduction in these parameters on the average of five loads are almost similar to those of the five speeds.

It can also be seen that the blended and fumigation modes have opposite effects in some combustion and performance parameters (ID, DOC, COV $_{Max(dP/d\theta)}$ and BTE) as shown in Table 5-1. For instance, the blended mode causes increase in ID, but the fumigation mode causes decrease in ID, compared to the diesel mode. In addition, the blended mode causes a huge increase in the peak HRR (20.4% for loads and 18.4% for speeds); while the fumigation mode has only a very small effect (2.2% for loads and 0.3% for speeds), compared to the diesel mode. On the other hand, the blended mode has higher BTE and lower BSFC than the fumigation mode. These parameters are the primary factors for the different effects caused by the blended and fumigation modes on the emissions and physicochemical properties of PM. Moreover, since the F+B mode has the combustion and performance parameters in between those of the blended and fumigation modes; therefore, the emissions and physicochemical properties of PM of F+B mode are also expected to be in between those of the blended and fumigation modes.

It is found that despite of using the same overall fuel composition of D80B5E15 for both blended and fumigation modes, different results in the combustion parameters compared to the diesel mode were obtained from the two fueling modes due to differences in the mode of combustion; namely, heterogeneous combustion for the blended mode versus homogeneous+ heterogeneous combustion for the fumigation mode. The blended mode has the same combustion mode with the diesel mode; therefore, the differences in the combustion parameters are only due to the differences in fuel properties (DBE versus diesel). However, in the fumigation mode, the differences in the parameters are due to differences in both fuel properties and combustion mode (heterogeneous combustion versus homogeneous+ heterogeneous combustion).

Table 5-1 Effect of fueling modes on the engine combustion and performance based on the average of five engine loads and speeds

Parameter	Order (Highest to lowest)
Based on five loads	
Peak in-cylinder pressure	Fumigation (1.3%) ≈ F+B (0.9%) ≈ **Diesel** ≈ Blend (-0.2%)
Peak HRR	Blend (20.4%) > F+B (6.3%) > Fumigation (2.2%) > **Diesel**
ID	Blend (10.1%) > F+B (1.4%) ≈ **Diesel** > Fumigation (-1.9%)
DOC	Fumigation (3.4%) > F+B (1%) ≈ **Diesel** > Blend (-3.1%)
Premixed combustion phase	Blend (47.2%) > F+B (31.0%) > Fumigation (22.3%) > **Diesel**
Diffusion combustion phase	Fumigation (1.7%) ≈ **Diesel** > F+B (-7.0%) > Blend (-19.1%)
COV_{IMEP}	Fumigation (26.3%) > F+B (16.1%) > Blend (6.6%) > **Diesel**
$COV_{Max(dP/d\theta)}$	Blend (9.2%) > F+B (3.4%) > **Diesel** > Fumigation (-2.7%)
EGT	**Diesel** ≈ All the tested fueling modes (-0.5%)
BSFC	Fumigation (11.2%) > F+B (9%) > Blend (5%) > **Diesel**
BTE	Blend (0.6%) ≈ **Diesel** > F+B (-3.6%) > Fumigation (-5.8%)
Equivalence ratio	Fumigation (9%) > F+B (7%) > Blend (2.5%) > **Diesel**
Based on five speeds	
Peak in-cylinder pressure	Fumigation (1%) ≈ F+B (1%) ≈ Blend (0.6%) ≈ **Diesel**
Peak HRR	Blend (18.4%) > F+B (7.7%) > Fumigation (0.3%) ≈ **Diesel**
ID	Blend (8.1%) > F+B (1.7%) > **Diesel** > Fumigation (-1.4%)
DOC	Fumigation (5.5%) > F+B (5%) > **Diesel** ≈ Blend (-0.3%)
Premixed combustion phase	Blend (43.6%) > F+B (31.6%) > Fumigation (22.2%) > **Diesel**
Diffusion combustion phase	**Diesel** ≈ Fumigation (-1.3%) > F+B (-8.6%) > Blend (-19.5%)
COV_{IMEP}	Fumigation (53.5%) > F+B (26.4%) > blended (8.8%) > **Diesel**
$COV_{Max(dP/d\theta)}$	Blend (6%) > F+B (4.3%) > **Diesel** > Fumigation (-2.9%)
EGT	**Diesel** ≈ All the tested fueling modes (-0.5%)
BSFC	Fumigation (10.2%) > F+B (9.1%) > Blend (5.5%) > **Diesel**
BTE	Blend (0.05%) ≈ **Diesel** > F+B (-3.6%) > Fumigation (-5%)
Equivalence ratio	Fumigation (6.4%) > F+B (5.6%) > Blend (0.04%) ≈ **Diesel**

CHAPTER 6 REGULATED EMISSIONS OF DIESEL ENGINE WITH DIFFERENT FUELING MODES

The results and discussion in regard to the regulated gaseous emissions of the diesel engine operated with the four fueling modes under various engine loads and speeds are presented in this chapter. The regulated emissions include CO, HC and NOx. The result for CO_2 is also included as a reference. Results pertaining to the engine load have been published in [315].

6.1 Brake specific CO emission

6.1.1 Based on engine load

Fig. 6.1 depicts that BSCO emission decreases with increasing engine load for all the tested modes due to increase in combustion temperature and more complete combustion. The reduction in CO with increase in load was also reported for diesel and blended fuels [127] and for operation in the fumigation mode [322,323] when using ethanol. It can be seen from Fig. 6.1 that the blended, F+B and fumigation modes cause increase in BSCO emission at all the tested engine loads, except at 185.3 and 228 Nm for the blended fuel. In the blended mode, at low load, the lower combustion temperature associated with the cooling effect due to the higher latent heat of evaporation of ethanol is dominating, which suppresses the CO oxidation process, resulting in higher BSCO in comparison with the diesel mode [57,300]. The increment of BSCO is 39.3% using the blended mode at engine load of 57 Nm. However, with increase in engine load, the impact of combustion temperature becomes weaker; while the oxygen content of the fuel becomes more dominating, hence BSCO of the blended fuel is lower than that of the diesel mode at higher loads (185.3 and 228 Nm as shown in Fig. 6.1). The reduction in BSCO is 1.3% at the engine load of 228 Nm using the blended mode.

The BSCO is the highest in the fumigation mode. In the fumigation mode, the effect of incomplete combustion, lower combustion temperature and higher BSFC lead to higher CO emission at all the tested loads. The higher CO emission in the fumigation mode compared to the blended mode was also found in [31]. In addition, an increase in CO was reported for fumigated fuels in [28,150] and diesel-biodiesel-alcohol blends based on engine loads in [75,86] and based on engine speeds in [97,103,324]. On the average of

five loads, the F+B mode causes 87.7% increase in BSCO which is in between those of the blended mode (17%) and the fumigation mode (152.9%), compared to the diesel mode. The lower combustion temperature associated with the cooling effect due to the higher latent heat of evaporation of ethanol dominates the effect of higher oxygen content of the biodiesel and ethanol fuels resulting in incomplete combustion, suppressed CO oxidation and hence increase in BSCO in comparison with the diesel mode [57,300]. Since the fumigation mode has lower BTE and higher fuel/air ratio than the other tested fueling modes, it has the highest BSCO.

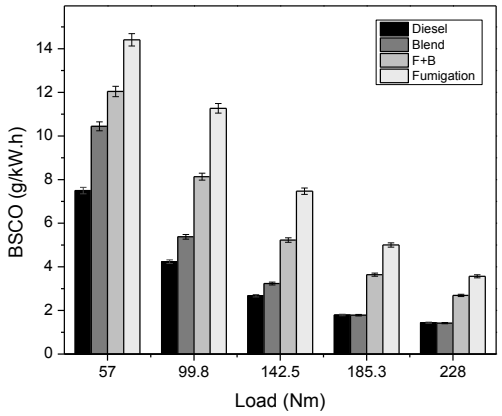

Fig. 6.1 Variation of BSCO with engine load.

6.1.2 Based on engine speed

Fig. 6.2 shows that the increase in engine speed does not have a significant influence on the BSCO because both CO formation and oxidation are both engine load dependent. Same trend (almost constant CO with speed) was also found in [137] using diesel and DBE. Fig. 6.2 also illustrates the increase in BSCO using the blended, F+B and fumigation modes compared to the diesel mode at all the tested engine speeds. On the average of five speeds, the increases in BSCO are in the order of fumigation mode (185.7%), F+B mode (109.9%) and blended mode (19.9%) in comparison with that of the diesel mode.

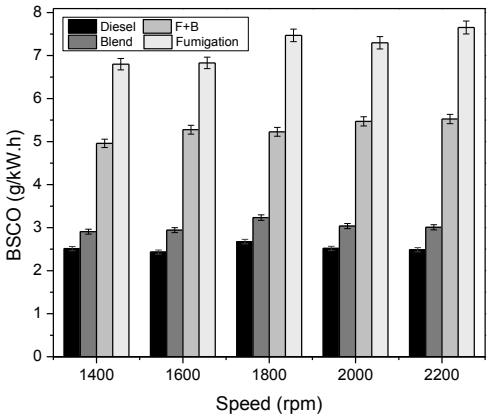

Fig. 6.2 Variation of BSCO with engine speed.

6.2 Brake specific HC emission

6.2.1 Based on engine load

Fig. 6.3 shows the effects of engine load and different fueling mods on BSHC, which are similar to those for BSCO (Fig. 6.1). BSHC emission decreases with increase in engine load and the blended, F+B and fumigation modes of operation cause higher BSHC emission at all the tested engine loads (except at the engine loads 185.3 and 228 Nm for the blended fuel).

For the blended mode, the higher BSHC at the low engine load (similar to BSCO) is due to incomplete combustion as a consequence of the higher latent heat of evaporation of ethanol compared to the diesel; while leads to 22.7% increase in BSHC at the engine load of 57 Nm. But, the higher oxygen content of ethanol and biodiesel in the blended fuel is the more dominating factor at higher engine loads which causes more complete combustion and increase the rate of oxidation of unburned hydrocarbons at higher in-cylinder temperatures [105] resulting in lower BSHC emissions in comparison with the diesel mode. The reduction in BSHC is 14.7% in the blended mode at the engine load of 228 Nm. The higher BSHC at lower and even medium engine loads and a lower BSHC at higher load using DBE blend was observed in other studies [127,304]. For the fumigation mode, some factors have impact on huge increase in BSHC emission. Firstly, the large droplet size of fumigated fuels (due to low injector pressure) causes initiation of incomplete combustion. Secondly, the mixture of fumigated fuels and air causes decrease in combustion temperature (production of quenching flame layers), especially at lower

loads resulting in initiation of incomplete combustion. Thirdly, the fumigation mode has the highest equivalence ratio (Fig. 5.20) and fuel consumption (Fig. 5.18 (b)) resulting in more fuel in combustion. Finally, some fraction of fumigated fuels could easily escape into the low temperature quenching regions close to the combustion chamber walls and crevices (like the region between the piston crown and the cylinder wall) especially during the compression stroke and expansion stroke, which becomes one of the primary sources of unburned hydrocarbon emission [297,319]. The higher HC emission in the fumigation mode compared to that in the blended mode was also reported in the literature [31,32]. The increase in HC emissions using fumigation mode was also reported in review studies [28,150].

According to Fig. 6.3, on the average of five loads, the blended mode (4.6%), F+B mode (86.5%) and fumigation mode (158.2%) have higher BSHC emission compared to that of the pure diesel mode. It is noticeable that, similar to BSCO emission, the value of BSHC emission of the F+B mode is in between that of the blended mode and the fumigation mode.

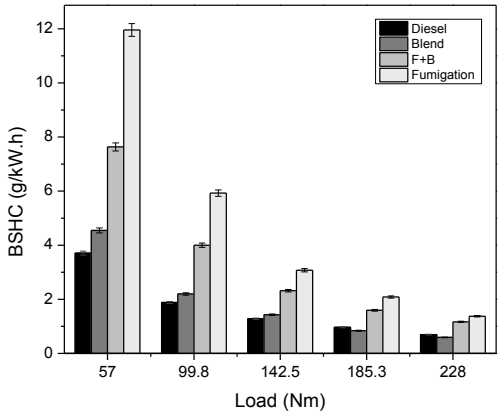

Fig. 6.3 Variation of BSHC with engine load.

6.2.2 Based on engine speed

Fig. 6.4 depicts that the increase in engine speed causes slight decrease in BSHC for all the tested fueling modes as a consequence of increase in combustion temperature and hence more complete combustion. The decrease in HC emission as a result of increase in engine speed was also found in some studies [107,137,325] using diesel and blended fuels.

Fig. 6.4 also shows that the blended, F+B and fumigation modes have higher BSHC compared to the pure diesel mode at all the tested engine speeds. On the average of five speeds, the increases in the BSHC are in the order of fumigation (161.4%), F+B (91.3%) and blended (8.4%) modes in comparison with the pure diesel mode. The higher latent heat of vaporizations of ethanol and biodiesel lead to the decrease in combustion temperature, resulting in incomplete combustion and the increase in THC emissions [288,300] compared to the diesel fuel. Atmanli et al. [101] also found that the blended fuel (diesel-biodiesel-n butanol) had higher BSHC compared to the diesel based on the average of different engine speeds. Aydin and Öğüt [132] also recorded higher HC emission using DBE compared to the diesel at various speeds.

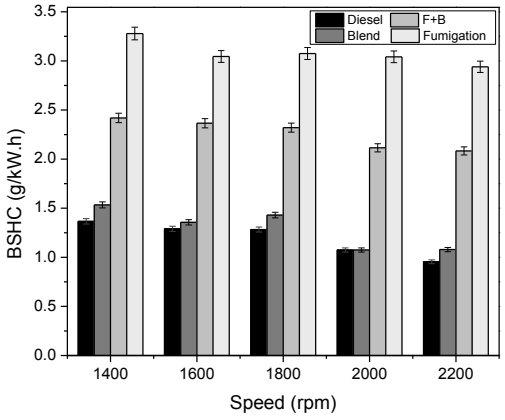

Fig. 6.4 Variation of BSHC with engine speed.

6.3 Brake specific NO_X, NO and NO_2 emissions

6.3.1 Based on engine load

The variations of $BSNO_X$, BSNO and $BSNO_2$ with engine loads for different fueling modes are presented in Fig. 6.5, Fig. 6.6 and Fig. 6.7, respectively. It can be seen from Fig. 6.5 that the $BSNO_X$ approximately decreases with increasing engine load which is in line with results reported other investigations with using diesel and DBE blend [128,289] and with fumigation mode [31]. Fig. 6.5 and Fig. 6.6 also reveal that the blended, F+B and fumigation modes have lower $BSNO_X$ and BSNO at all engine loads compared to the pure diesel mode. According to the average of five loads, the reductions in $BSNO_X$ emissions are in the order of fumigation mode (-8.6%), F+B mode (-5.6%) and blended mode (-3.6%) compared to that of the pure diesel mode; while the reductions in BSNO

are in the order of fumigation mode (-32.8%), F+B mode (-24%) and blended mode (-8.9%). The effects of higher latent heat of evaporation and lower heating value of biodiesel and ethanol are the dominating factors, compared to the other parameters (like lower cetane number and higher oxygen content of biodiesel and ethanol which increase the combustion temperature), which cause reduction in $BSNO_X$ for all the tested fueling modes. The lowest $BSNO_X$ in the fumigation mode is due to the lower combustion temperature as a consequence of incomplete combustion. In the fumigation mode, the fumigated fuel is injected into the cylinder via intake manifold which absorbs the heat inside the combustion chamber, causing a lower temperature environment for combustion; therefore, incomplete combustion takes place resulting in higher CO, HC and lower NO_X emissions. It can be inferred from the above results that the F+B mode benefits the effects of both blended and fumigation modes. Higher effect of the fumigation mode on reduction in NO_X emission compared to the blended mode was reported in the literature [31,32].

However, despite of reduction in $BSNO_X$ in the blended, F+B or fumigation modes of operation, $BSNO_2$ emissions (Fig. 6.7) are increased in the order of the fumigation mode (187.2%), the F+B mode (111.5%) and the blended mode (3.3%) compared to that of the pure diesel mode, based on the average of five engine loads. This finding is in line with [31], which found higher $BSNO_2$ emissions of the blended and fumigation modes higher than that of the baseline fuel and the impact of fumigation mode on increase in $BSNO_2$ was higher than that of blended mode.

It is known that the NO formed in the flame zone can be rapidly converted to NO_2 through the following reaction when the fluid is cooled [297]:

$$NO + HO_2 \rightarrow NO_2 + OH \qquad 6.1$$

The cooler regions are reduced with the increase of engine load, resulting in less conversion of NO into NO_2 [62]; therefore, the NO_2 emission decreases with increasing engine load (Fig. 6.7). The increases in $BSNO_2$ emissions when using the blended, F+B and fumigation modes can be attributed to two reasons. Firstly, in hydrocarbon decomposition processes, ethanol is a well-known chain-carrying agent which can react with OH radicals to reform the peroxyl radicals (HO_2); thus, the ethanol is a source of HO_2 [326] which increases the formation of NO_2. Secondly, the lower combustion temperature due to ethanol can enhance the conversion of NO into NO_2. Therefore, the

$BSNO_2$ emissions of the blended, F+B and fumigation modes are higher than that of the pure diesel mode; while the highest $BSNO_2$ achieved by the fumigation mode is due to the lowest combustion temperature associated with the fumigation mode of operation.

It can be inferred from the above results for different engine loads that the ratios of NO_2/NO_X for the diesel mode and the blended and F+B modes are in the normal range (10%-30% according to [297]). However, in the fumigation mode there is a huge increase in NO_2, resulting in higher ratio of NO_2/NO_X. The ratios of NO_2/NO_X for diesel, blended, F+B and fumigation modes are 11.7%, 16.5%, 28.3% and 34.6%, respectively.

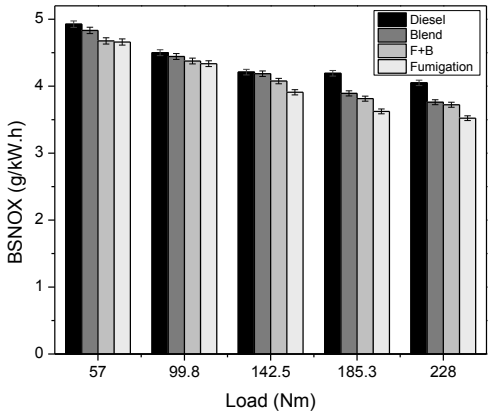

Fig. 6.5 Variation of $BSNO_X$ with engine load.

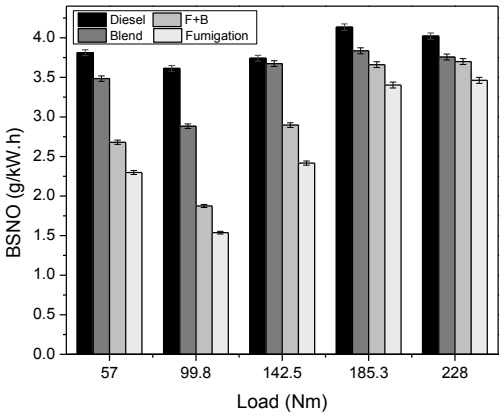

Fig. 6.6 Variation of BSNO with engine load.

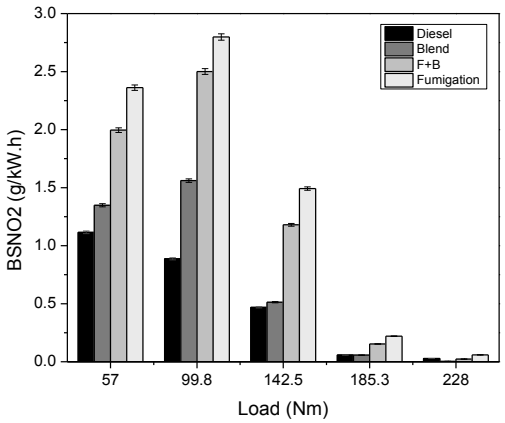

Fig. 6.7 Variation of $BSNO_2$ with engine load.

6.3.2 Based on engine speed

The variations of $BSNO_X$, BSNO and $BSNO_2$ with engine speeds for different fueling modes are presented in Fig. 6.8, Fig. 6.9 and Fig. 6.10, respectively. It can be seen that they all decrease with increasing engine speed due to shorter duration of combustion in terms of millisecond which causes less time available for NO_X formation [72]. Atmanli et al. [102] also found the increase in engine speed causes decrease in $BSNO_X$, BSNO and $BSNO_2$ using diesel and diesel-biodiesel-n butanol blends. Similarly, Labeckas et al. [317] reported a decrease in NO_X at higher engine speed using diesel and DBE blends.

In comparison with the diesel mode, on the average of five speeds, there is an increase in $BSNO_2$ in the fumigation (185.6%), F+B (117%) and blended (9.9%) modes, but reduction in $BSNO_X$ (-7.5% for fumigation, -6% for F+B and -3.2% for blended modes) and BSNO (-30.2% in the fumigation mode, -20.7% in the F+B mode and -4.6% in the blended mode).

Similar increase in NO_2 emission was found in the literature [102,103] using diesel-biodiesel-butanol blends compared to that of pure diesel fuel at different engine speeds. Cheng et al. [31] reported that the use of fumigated methanol and methanol blend had higher NO_2 than using diesel fuel; while the fumigated methanol had a huge increase in NO_2 compared to the blended methanol. In addition, some studies [168,327-329] found that the use of fumigated alcohol fuels caused increase in NO_2 and decrease in NO and NO_X emissions based on engine load. Prakash et al. [139] also found a reduction in NO emission of a diesel engine using DBE blends compared to the diesel fuel.

According to the above results for various engine speeds, the ratios of NO_2/NO_X for diesel fuel and blended and F+B mode are in the normal range (10%-30% according to [297]). But, the fumigation mode has a huge rise in NO_2 resulting in higher ratio of NO_2/NO_X. The ratios of NO_2/NO_X for diesel, blended, F+B and fumigation modes are 11.8%, 13.2%, 25.9% and 34.2%, respectively.

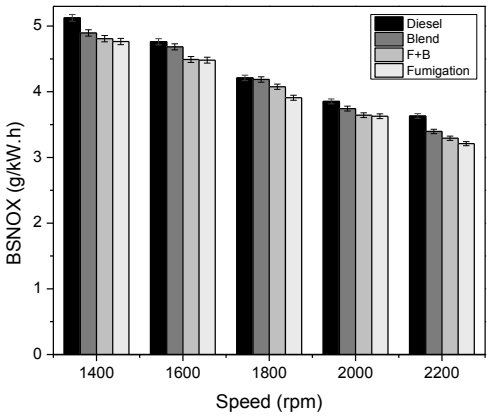

Fig. 6.8 Variation of $BSNO_X$ with engine speed.

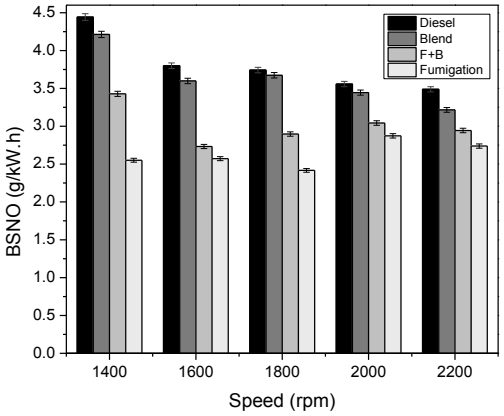

Fig. 6.9 Variation of BSNO with engine speed.

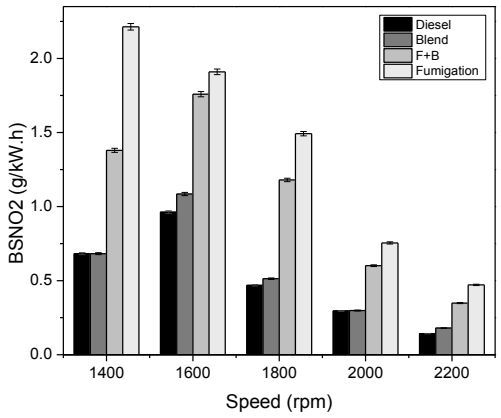

Fig. 6.10 Variation of $BSNO_2$ with engine speed.

6.4 Brake specific CO_2 emission

6.4.1 Based on engine load

Variation of $BSCO_2$ with engine loads for all the tested fueling modes is presented in Fig. 6.11. It can be observed that the variation of $BSCO_2$ is almost similar to that of the BSFC (Fig. 5.18 (b)) at different engine loads. The lowest $BSCO_2$ is found at the engine load of 185.3 Nm (which has the lowest BSFC) and the highest $BSCO_2$ is observed at the engine load of 57 Nm (which has highest BSFC) for all the tested fueling modes. Despite of higher BSFC of the blended, F+B and fumigation modes (as shown in Fig. 5.18 (b)), based on the average of five loads, the $BSCO_2$ of the blended mode is lower (-3.3%) than the pure diesel mode; while the changes in the F+B mode (-0.5%) and in the fumigation mode (0.6%), compared to the pure diesel mode, are statistically insignificant at the 95% confidence level. The reduction in CO_2 emission using the blended mode was reported in the literature [103,127,128,137,300,330]. The reduction in CO_2 emission in the blended mode and similar CO_2 emission in the F+B and fumigation modes is due to the lower C/H ratio and higher oxygen content of biodiesel and ethanol in comparison with the diesel fuel [300,302,303]. However, the blended mode has lower BSFC compared to the F+B and fumigation modes, which causes reduction in carbon available for formation of CO_2, resulting in lower $BSCO_2$. In addition, the lowest $BSCO_2$ in the blended mode is due to improvement in BTE [31] in comparison with the other fueling modes.

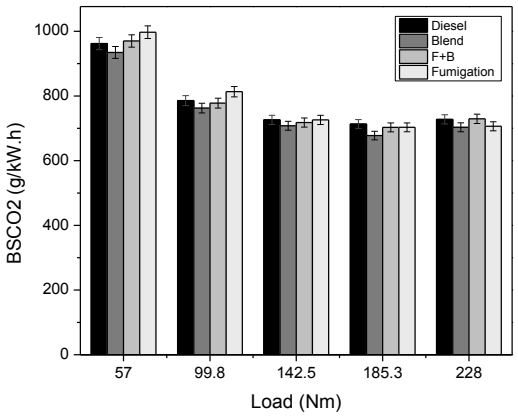

Fig. 6.11 Variation of $BSCO_2$ with engine load.

6.4.2 Based on engine speed

Fig. 6.12 shows that the variation of $BSCO_2$ with engine speed is also similar to that of BSFC (Fig. 5.19 (b)). The increase in $BSCO_2$ with increasing engine speed is due to the increase in fuel consumption which is in line with the results in [137] using diesel and DBE. According to the average of five speeds, despite of increase in BSFC (Fig. 5.19 (b)), the blended mode has lower $BSCO_2$ (-2.7% reduction); while the F+B mode (only -0.4%) and fumigation mode (only 0.2%) have similar $BSCO_2$ compared to that of the pure diesel mode.

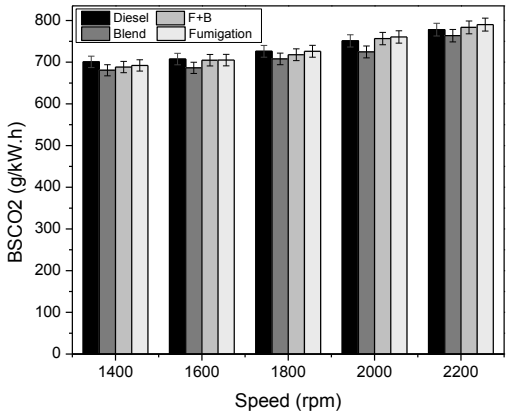

Fig. 6.12 Variation of $BSCO_2$ with engine speed.

6.5 Summary

The influence of different fueling modes on the regulated gaseous emissions based on the average of five loads and speeds compared to those of the diesel mode are presented in Table 6-1. It can be seen that the effects of using different fueling modes on almost all the tested parameters is independent of the different engine loads or speeds, because the trends and percentages of change in those parameters on the average of five loads are almost similar to those parameters on the average of five speeds. In addition, it can be observed that the fumigation mode is more effective in reducing $BSNO_X$ and BSNO than the blended mode. On the other hand, the fumigation mode has higher $BSCO_2$, BSCO and BSHC than the blended mode. Since the fuels used in the blended mode and the fumigation mode have the same composition (D80B5E15), it can be concluded that the gaseous emissions are affected by the mode of operation.

Table 6-1 Effect of fueling modes on the regulated gaseous emissions based on the average of five engine loads and speeds

Parameter	Order (Highest to lowest)
Based on five loads	
BSCO	Fumigation (152.9%) > F+B (87.7%) > Blend (17%) > **Diesel**
BSHC	Fumigation (158.2%) > F+B (86.5%) > Blend (4.6%) > **Diesel**
$BSNO_X$	**Diesel** > Blend (-3.6%) > F+B (-5.6%) > Fumigation (-8.6%)
BSNO	**Diesel** > Blend (-8.9%) > F+B (-24%) > Fumigation (-32.8%)
$BSNO_2$	Fumigation (187.2%) > F+B (111.5%) > Blend (3.3%) > **Diesel**
$BSCO_2$	Fumigation (0.6%) ≈ **Diesel** ≈ F+B (-0.5%) > Blend (-3.3%)
Based on five speeds	
BSCO	Fumigation (185.7%) > F+B (109.9%) > Blend (19.9%) > **Diesel**
BSHC	Fumigation (161.4%) > F+B (91.3%) > Blend (8.4%) > **Diesel**
$BSNO_X$	**Diesel** > Blend (-3.2%) > F+B (-6%) > Fumigation (-7.5%)
BSNO	**Diesel** > Blend (-4.6%) > F+B (-20.7%) > Fumigation (-30.2%)
$BSNO_2$	Fumigation (185.6%) > F+B (117%) > Blend (9.9%) > **Diesel**
$BSCO_2$	Fumigation (0.2%) ≈ **Diesel** ≈ F+B (-0.4%) > Blend (-2.7%)

CHAPTER 7 PARTICULATE EMISSION AND PHYSICAL PROPERTIES OF PM FOR DIFFERENT FUELING MODES

PM emissions including their mass, number, size and morphology have negative influence on the human health with chronic complications and environment [199,207]. The small particles can penetrate deeply into the lung tissue through the respiratory passageways which causes more damaging lung tissue compared to the large particles [199]. However, the large particles which have the majority proportion of PM mass have a strong effect on the global climate by absorbing the solar radiation and reacting with other types of atmospheric constituents. The PM emissions on the mountains may cause melting of the snow and ice due to absorbing the solar radiation, which may create serious problem in the environment. Also, some part of the PM mass are soluble in water (formation of water-soluble organic carbon, WSOC); therefore, they are a threat to the animals and environment of the underwater. Thus, more concerns are needed in regard to reduction of these emissions. Since diesel engines are one of the sources of PM emissions; therefore, this section aims to investigate these emissions emitted from a diesel engine under various operating conditions and fueling modes. The results and discussion in regard to the particulate emissions and physical properties of the PM of a diesel engine operated under the four fueling modes and various operating conditions are presented in this chapter. The parameters investigated include brake specific particulate mass emission, total number concentration, geometric mean diameter, we well as the micro-structure and nano-structure of the particles.

7.1 Brake specific PM mass (BSPM), total number concentration (TNC) and geometric mean diameter (GMD)

7.1.1 BSPM at different engine loads

Fig. 7.1 shows the variation of BSPM with engine load. In all the fueling modes, the BSPM decreases slightly from the engine load of 57 Nm to 99.8 Nm, and then increases up to the highest engine load of 228 Nm. This trend was also reported in the literature using DBE and diesel fuels [128,129]; and using alcohol fumigation with ethanol and methanol) [24,168]. It is because at the lowest engine load combustion is incomplete due to the low combustion temperature; therefore, BSPM is higher than that at the engine load of 99.8 Nm. On the other hand, the subsequent increase in BSPM at higher engine load

can be attributed to the following factors. Firstly, as more fuel is burned, the available time for soot oxidation after the end of the diffusion combustion phase is shorter [331], resulting in the increase in particulate formation as well as the reduction in time for soot oxidation, and thus there is an increase in BSPM. Secondly, the higher F/A ratio results in less oxygen available for soot oxidation. Thirdly, the ignition delay becomes shorter; therefore, more fuel is burned in the diffusion combustion period (Fig. 5.9), resulting in the increase in particulate formation [105]. Finally, as more fuel is injected into the engine, there is less time available for air and fuel mixing. Incomplete combustion due to lack of enough time for fuel and air mixing also causes an increase in BSPM.

Fig. 7.1 also illustrates that the BSPM emissions of the blended and F+B modes are lower than that of the diesel mode at all the tested engine loads. However, the fumigation mode has lower BSPM only at the higher engine loads of 185.3 and 228 Nm which is similar to the findings in diffusion combustion phase (Fig. 5.9 (b)). On the average of five loads, the reductions in BSPM are in the order of blended mode (-47.9%) and F+B mode (-28.4%); while the fumigation mode has similar BSPM (only a slight increase of 1.2% which is not significant with T-test at 95% level) compared to that of the diesel mode. The reduction in PM mass emissions can be found in the literature when using DBE in the blended mode [27,86,129,282,308] and using ethanol and methanol in the fumigation mode [24,28,168,322]. The increase in BSPM in low load (idle) and decrease in BSPM at higher engine load was also reported in [24] using fumigated ethanol compared to diesel.

There are several factors that contribute to the reduction in BSPM when using biofuels. Firstly, the C/H mass ratio of the fuels used in the blended, F+B and fumigation modes is lower than that of diesel fuel, resulting in the decrease in BSPM [105]. Secondly, the lower aromatic and sulfur contents of these fuels also lead to the decrease in BSPM [105], because the aromatics are soot precursors; while sulfur could form sulfate which is also part of the particulate matter. Thirdly, the higher oxygen content of these fuels enhances soot oxidation through the hydroxyl radical (•OH) formation, leading to lower soot formation [27].

However, when operating in the fumigation mode, the following factors lead to the increase in BSPM at low and medium loads. Firstly, the fumigated fuel is uniformly mixed with air inside the engine cylinder. At low and medium engine loads, the equivalence ratio of the uniformly mixed air/fuel mixture is very low, and the combustion

temperature is also low, leading to very poor combustion of the fumigated fuel. Part of the fuel might enter into the engine exhaust and condense during the cooling down process in the PM sampling process, leading to an increase in the PM emission. The increase in unburned fuel emission at low and medium engine loads could also be observed in the high HC emissions in the fumigation mode of operation (Fig. 6.3). Secondly, part of the fumigated fuel could easily escape into the low temperature quenching regions close to the combustion chamber walls and crevices which can produce higher PM emissions, especially during the low and medium loads. Thirdly, the injection pressure for the fumigated fuel was only 0.35 MPa which will cause the formation of larger fuel droplets, and the larger fuel droplets will cause the formation of more particles and larger particles (as shown in TNC and GMD at Fig. 7.3 and Fig. 7.4, respectively) and hence increase in PM emissions. Fourthly, the shorter ID and longer DOC in the fumigation mode (Fig. 5.7 (a) and (b)) lead to increase in the diffusion combustion period (Fig. 5.9 (b)) during which soot is formed. Finally, the fumigation mode has higher BSFC and overall equivalence ratio which cause more fuel available for PM formation and less oxygen available for soot oxidation, respectively. However, at the higher engine loads of 185.3 and 228 Nm, the effect of the above factors is weakened due to more complete combustion, as a consequence of the higher in-cylinder temperature associated with the high engine loads. Therefore, the BSPM of the fumigation mode are lower than those of the diesel mode at the engine loads of 185.3 and 228 Nm. For the F+B mode, the results show that it has a reduction of -28.4% in BSPM, which is located in between those of the other two modes of operation.

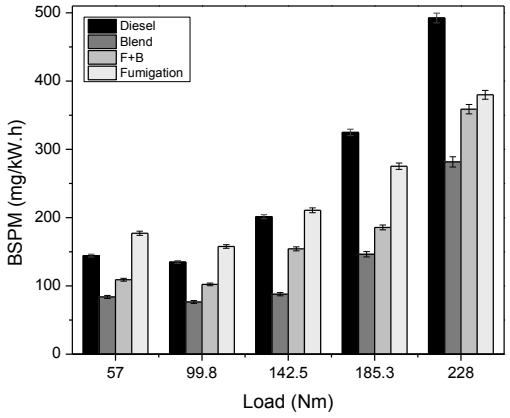

Fig. 7.1 Variation of BSPM with engine load.

7.1.2 BSPM at different engine speeds

The variation of BSPM with engine speed for different fueling modes is presented in Fig. 7.2. It can be observed that it increases with increasing engine speed for all the fueling modes. At higher engine speed, there is a reduction in volumetric efficiency and an increase in the fuel/air ratio, resulting in less oxygen available for soot oxidation and more fuel is involved for soot formation, respectively. In addition, at higher engine speed, there is less time for air and fuel mixing and less time for combustion in each engine cycle, which will cause incomplete combustion and an increase in BSPM. Some studies also found the increase in smoke opacity (soot) using diesel, blended fuels (diesel-biodiesel-alcohols [107,317]) and fumigated methanol [319], and increase in PM emissions [332] with the increase in engine speed.

Fig. 7.2 also illustrates that the blended and F+B modes lead to decrease in BSPM at all the tested engine speeds, but the fumigation mode has higher BSPM at low and medium speeds. On the average of five engine speeds, the blended mode has the lowest BSPM among all the fueling modes. The blended mode causes a reduction in BSPM (-51%) compared to diesel. The F+B mode has lower BSPM (-20.6%) in comparison with the diesel mode; while the fumigation mode has similar BSPM (1.5%) compared to the diesel mode, which are similar to the effects of engine loads shown in Fig. 7.1).

It is found that the fumigation mode has lower PM mass compared to the diesel mode only at the highest engine speed of 2200 rpm due to more dependency of PM mass on the size of particles rather than the number of particles for different engine speeds. It is because most of the particles emitted from all the tested fueling modes are in the small size range (nano and ultra-fine particle as shown in Fig. 7.10) which has light weight. The TNC (Fig. 7.7) of fumigation mode is higher than that of the diesel mode at the engine speed of 2200 rpm; however, the majority of the particles are in the small size range (nano and ultra-fine particle as shown in Fig. 7.10), resulting in smaller GMD (Fig. 7.8) and hence lower PM mass. In addition, the increment ratio of TNC by the fumigation mode compared to the diesel mode at the highest speed (17.6% at 2200 rpm) is lesser than that at the lower speeds (e.g. 52.3% at 1400 rpm); therefore, the effect of smaller particles (hence lighter weight) causes reduction in PM mass at the highest engine speed.

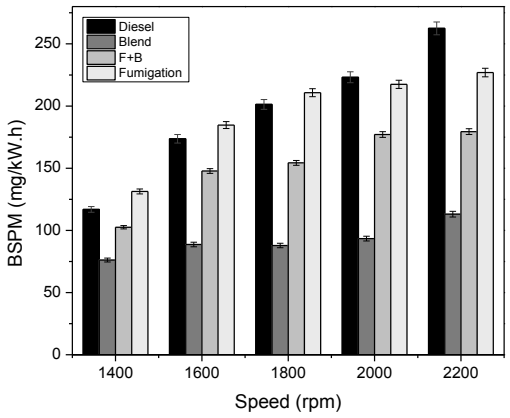

Fig. 7.2 Variation of BSPM with engine speed.

7.1.1. TNC and GMD at different engine loads

Fig. 7.3, Fig. 7.4 and Fig. 7.5 reveal that both TNC and GMD of the particles increase with increasing engine load for all the tested fueling modes which are in line with those reported in the literature when using DBE in the blended mode [128], and using ethanol and methanol in the fumigation mode [167,168,327,328]. The same factors which lead to the increase in PM mass also lead to the increase in TNC. For GMD, at high engine loads, the huge number of particles causes increase in particle coagulation rate, leading to the formation of particles with larger GMD [314].

Fig. 7.3 and Fig. 7.4 also illustrate that the blended and F+B modes have lower TNC (except almost similar TNC at lower and medium loads for the F+B mode) and lower GMD at all the tested loads compared to those of the diesel mode. However, the fumigation mode has lower TNC and GMD only at the higher engine loads of 185.3 and 228 Nm. Zhang et al. [327] also found that the GMD of particles in fumigation operation with methanol was higher at low and medium engine loads and lower at high engine loads compared to the diesel mode. Similarly, the increase in GMD at lower engine load and decrease in GMD at higher engine load using fumigated ethanol was reported in [322]. On the average of five loads, the blended mode has lower TNC (-18.5%), the F+B mode has similar TNC (only -1.2%); while the fumigation mode has higher TNC (27.8%) than the diesel mode. For GMD, the blended mode (-9.3%) and the F+B mode (-4.8%) cause reductions; while the fumigation mode has almost equal GMD (only 1.5% which is not significant with T-test at 95% level), compared to those of the diesel mode. When operating in the blended, F+B and fumigation modes the fuels in use contains ethanol and

biodiesel. The lower aromatic and sulfur contents and the lower C/H mass ratio [105] of the fuels contribute to less particulate formation; while the higher oxygen content of the fuels enhances soot oxidation [27], causing reduction in TNC and GMD compared to those of the diesel mode. The reductions in TNC and GMD can also be found in the literature when using DBE [129,308] and the fumigation mode (ethanol and methanol) [167-169,322,327]. On the other hand, an increase in TNC was reported in [24] using fumigated ethanol at all the tested loads compared to the diesel fuel. In the present study, in the fumigation mode, the reductions in TNC and GMD is found only at higher engine loads because at low and medium loads, the same factors that lead to the increase in PM mass also lead to the increase in TNC (Fig. 7.3) and GMD (Fig. 7.4) compared to the diesel mode. However, at higher engine loads, the combustion is complete as a consequence of higher in-cylinder temperature, resulting in lower TNC and GMD in the fumigation mode, in comparison with those of the diesel mode.

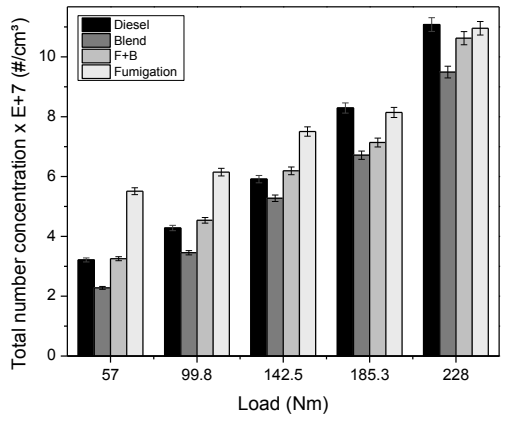

Fig. 7.3 Variation of total particle number concentration with engine load.

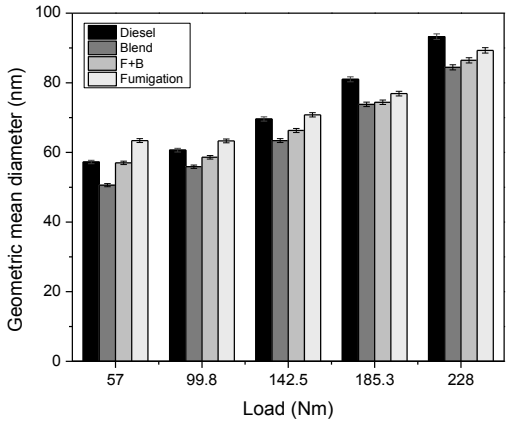

Fig. 7.4 Variation of geometric mean diameter with engine load.

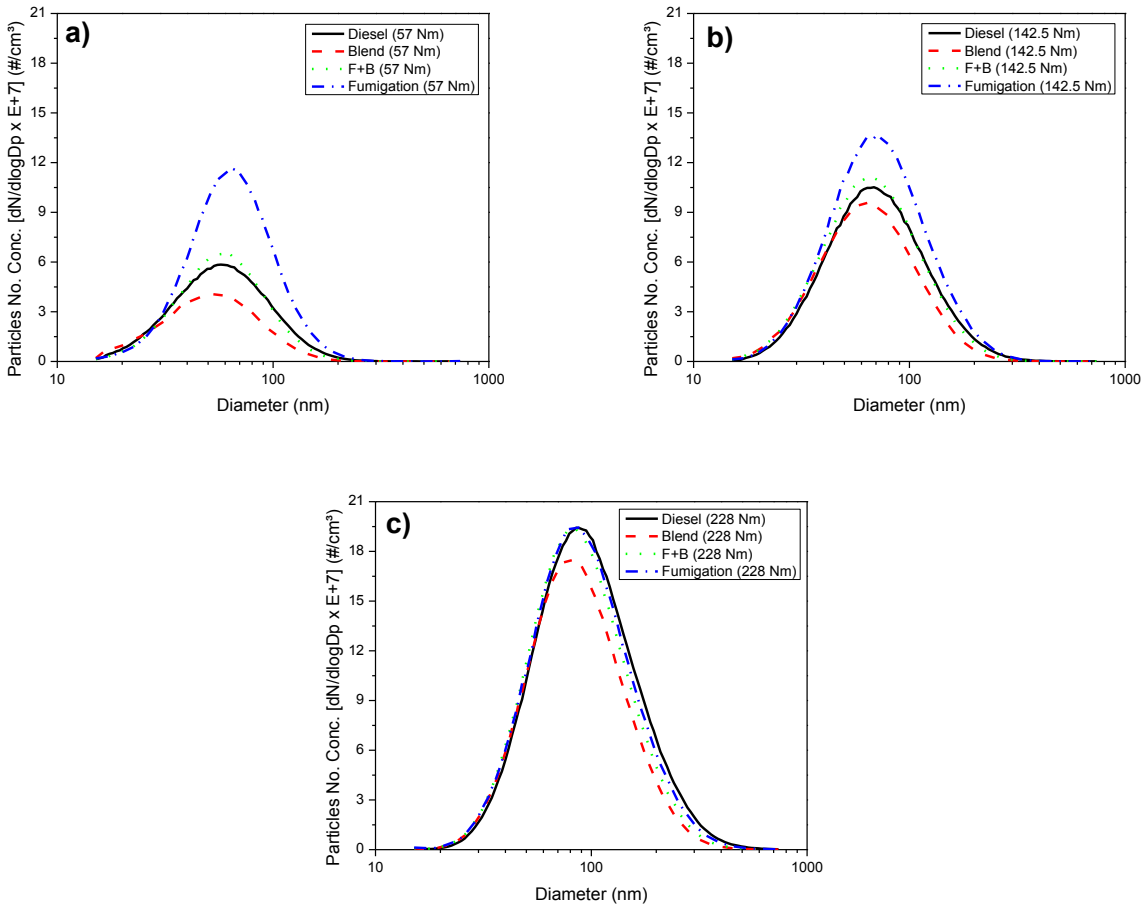

Fig. 7.5 Variation of particle size distribution with (a) low, (b) medium and (c) high engine loads.

Fig. 7.5 shows the particle number-size distributions as measured by the SMPS for particles in the size range of 15 nm to 750 nm under low, medium and high engine loads. The particles emitted from a diesel engine can be classified into nano-particle (particle diameter ≤ 50 nm), ultra-fine particle (50 nm < particle diameter ≤ 100 nm) and fine particle (particle diameter > 100 nm), as suggested by Kittelson in [333,334]. The variation of concentrations of nano-particle, ultra-fine particle and fine particle (up to 750 nm for this study) with engine load for different fueling modes is presented in Fig. 7.6 (a and b). It can be seen from Fig. 7.6 (a), with increase of engine load, there is not much change in the number of nano-particles, a slight increase in the number of ultra-fine particles and a significant increase in fine particles, and the increase in TNC. Thus, the increase in TNC with increase in engine load is mainly due to the increase of fine particles. It is because, with the increase in TNC with engine load, the smaller particles will coagulate into larger particles due to the higher coagulation rate. In addition, Fig. 7.6 (b) shows the increase in engine load has an effect on reducing the fractions of nano-

particles and ultra-fine particles in TNC and the increase in fraction of fine particles in TNC. Fig. 7.6 (b) also reveals that, for all the fueling modes, the particles are mainly less than 100nm in size; while the blended mode has the highest concentration of nano-particle and the lowest concentration of fine particle. On the average of five engine loads (Fig. 7.6 (a)) the blended mode has lower nano-particles (-6.5%), ultra-fine particles (-19.3%) and fine particles (-35.4%) than the diesel mode. The F+B mode has higher nano-particles (5.0%), similar ultra-fine particles (0.5%) and lower fine particles (-15.3%) compared to the diesel mode. But, the fumigation mode causes increase in nano-particles (16.5%), ultra-fine particles (34.5%) and fine particles (31.7%) in comparison with the diesel mode.

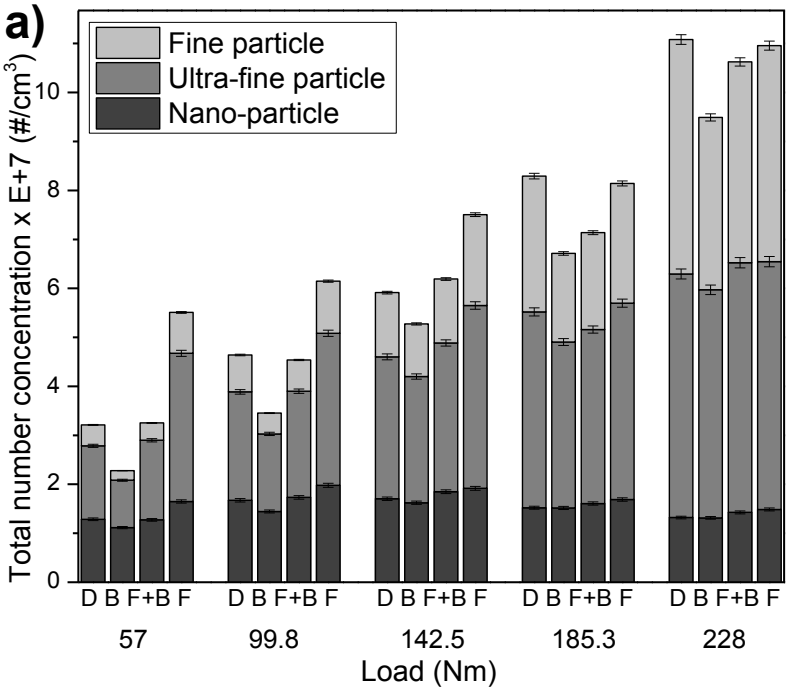

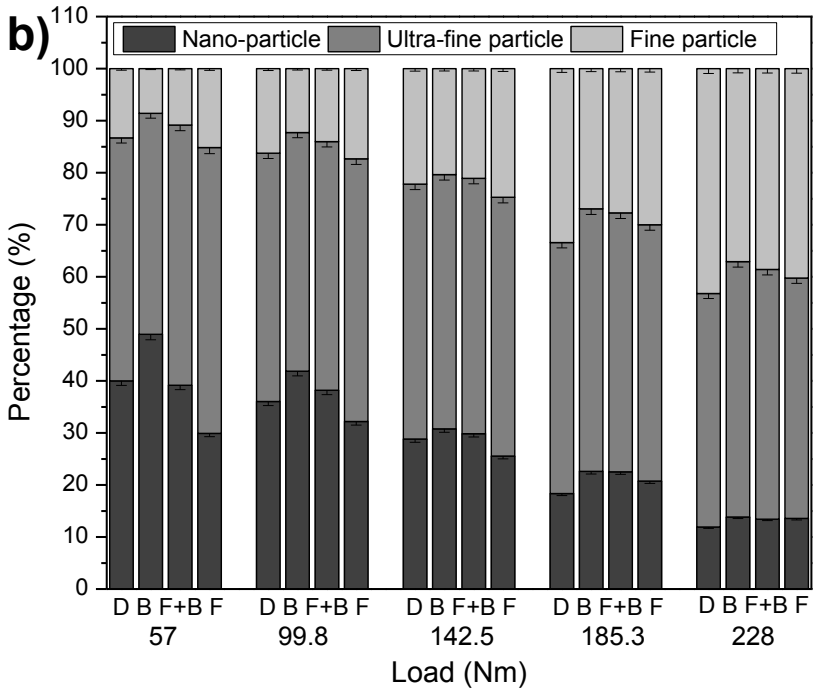

Fig. 7.6 Variations of (a) number and (b) percentage of nano-particle ($D_P \leq 50$ nm), ultra-fine particle ($50 \text{ nm} < D_P \leq 100$ nm) and fine particle ($D_P > 100$ nm) with engine load.

7.1.3 TNC and GMD at different engine speeds

The effect of engine speed on TNC and GMD are shown in Fig. 7.7 and Fig. 7.8, respectively; while Fig. 7.9 shows the particle number-size distributions at low, medium and high engine speeds. It can be observed that the increase in engine speed causes increase in TNC, but has no significant influence on GMD, for almost all the tested fueling modes. With an increase in engine speed, similar factors that lead to the increase in BSPM will also cause the increase in TNC. Di et al. [332] found an increase in TNC and decrease in GMD using diesel-diglyme blend with increasing engine speed. Despite of the increase in TNC, there is little change in GMD because with an increase in engine speed, there is less time available (shorter duration of combustion in term of time) for particle coagulation and agglomeration.

Fig. 7.7 and Fig. 7.8 also illustrate that the blended and F+B modes lead to decrease in TNC and GMD at all the tested engine speeds (except the TNC in the F+B mode at low and medium speeds), but the fumigation mode has higher TNC at all the tested engine speeds and higher GMD at low and medium speeds. On the average of five engine speeds, the blended mode has the lowest TNC and GMD among all the fueling modes. The blended mode causes reduction in TNC (-12.1%) and GMD (-9%) compared to the

diesel mode. The F+B mode has similar TNC (0.7%) and lower GMD (-5.2%) in comparison with those of the diesel mode; while the fumigation mode has higher TNC (31.6%) and similar GMD (0.6%) compared to the diesel mode.

The reduction in TNC and GMD can also be observed in the literature using DBE [129,308] and also using ethanol and methanol in the fumigation mode [167-169,322,327]. However, in the present study, for the fumigation mode, the reduction in GMD is found only at higher engine speeds; the TNC is higher than that in the diesel mode for all tested speeds; and the percentage increase in TNC at the highest speed is lower than that at the lowest speed. Similar result (an increase in TNC) was also reported in [24] using fumigated ethanol compared to the diesel mode.

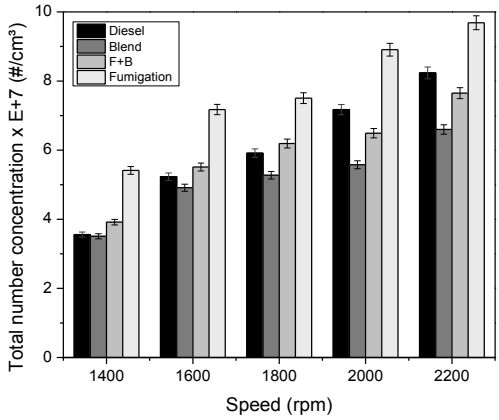

Fig. 7.7 Variation of total particle number concentration with engine speed.

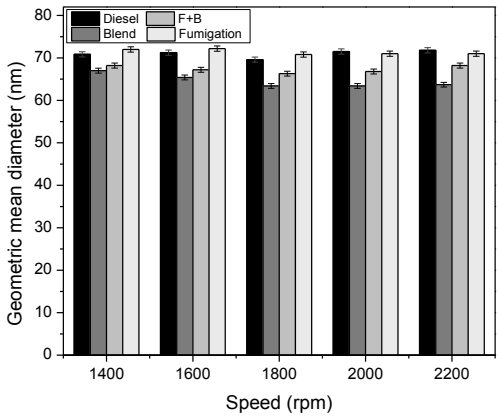

Fig. 7.8 Variation of geometric mean diameter with engine speed.

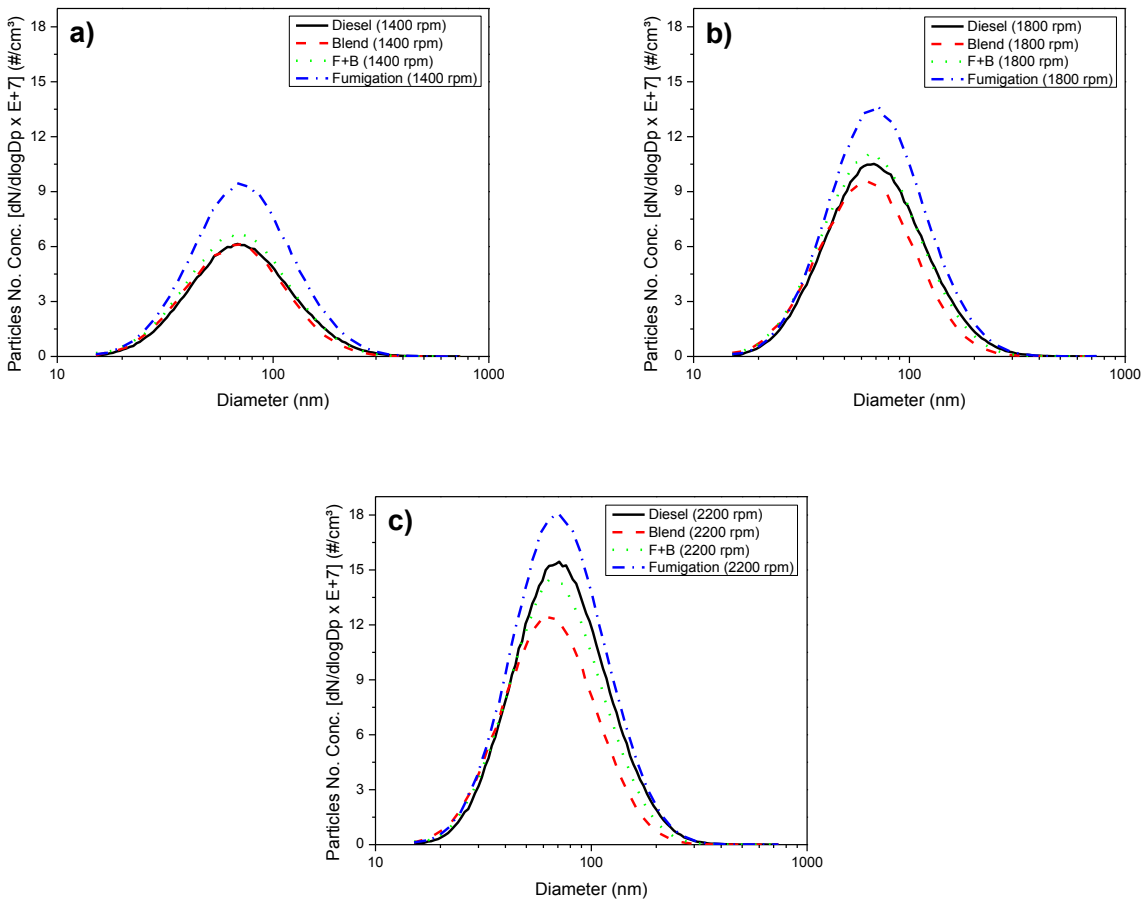

Fig. 7.9 Variation of particle size distribution with (a) low, (b) medium and (c) high engine speeds.

Fig. 7.10 (a) shows that, with the increase in engine speed, there is an increase in the amount of nano-particle, ultra-fine particle and fine particle for all the fueling modes, such that there is little change in the percentage of each group of particles in the TNC. In addition, according to Fig. 7.10 (b), similar to the results of various engine loads, most of the particles are less than 100 nm in diameter, for all the fueling modes. Also, the blended mode has the highest concentration of nano-particles and lowest concentration of fine particles. On the average of five engine speeds (Fig. 7.10 (a)), the blended, F+B and fumigation modes have similar effects with the five engine loads (Fig. 7.6 (a)). In detail, the blended mode causes reduction in nano-particles (-3.4%), ultra-fine particles (-12.1%) and fine particles (-21.8%), compared to the diesel mode; the F+B mode has higher nano-particles (5.1%), similar ultra-fine particles (0.8%) and lower fine particles (-4.4%), in comparison with the diesel mode, but the fumigation mode has higher nano-particles (19.8%), ultra-fine particles (32.5%) and fine particles (44.3%) than the diesel mode.

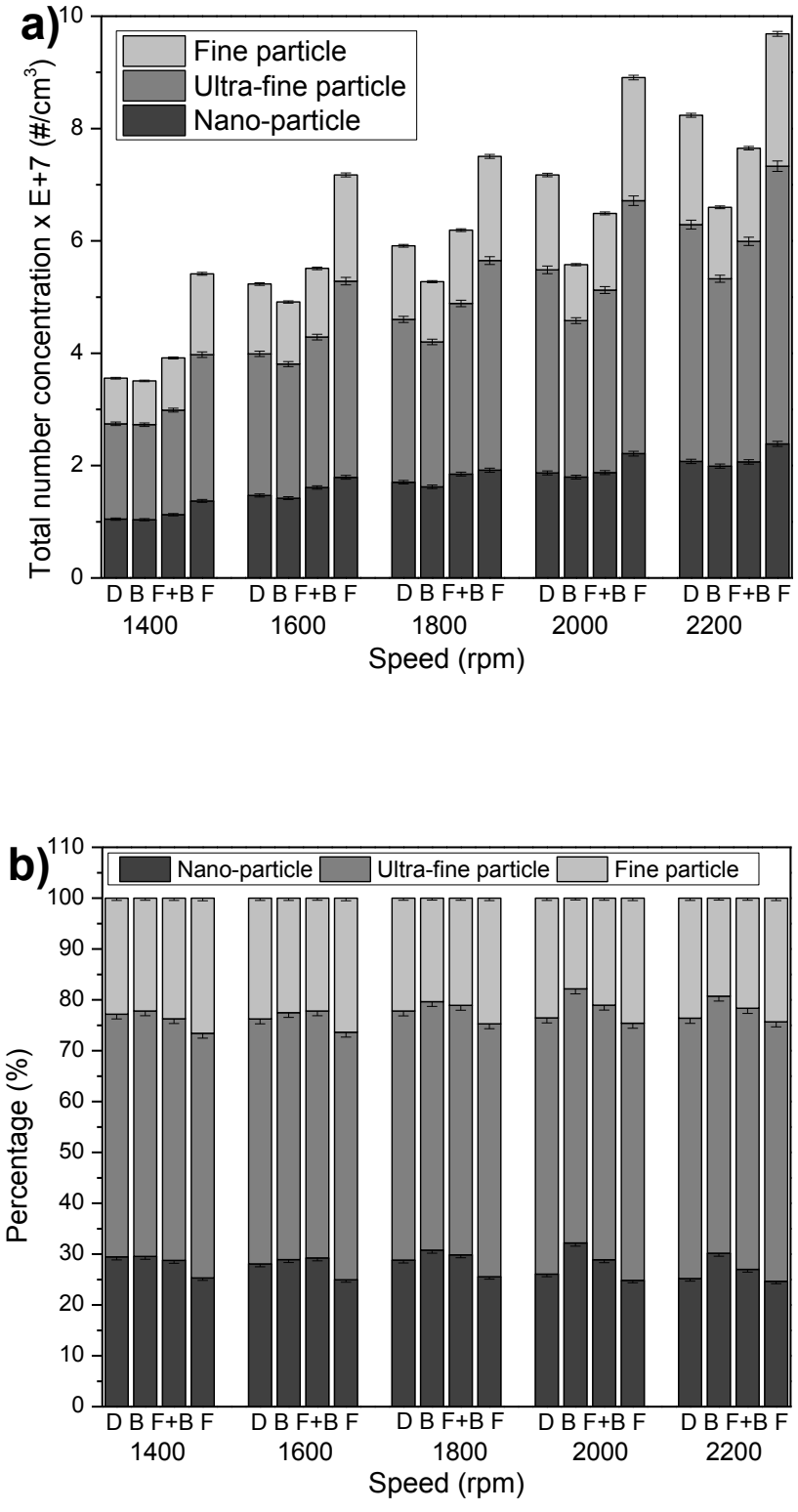

Fig. 7.10 Variations of (a) number and (b) percentage of nano-particle ($D_P \leq 50$ nm), ultra-fine particle ($50 \text{ nm} < D_P \leq 100$ nm) and fine particle ($D_P > 100$ nm) with engine speed.

7.1.4 BSPM, TNC and GMD at four operating conditions

The effects of engine speed and load on the BSPM, TNC and GMD have been explained with five speeds and five loads for various fueling modes of operation in previous sections. Since the analyses on the physicochemical properties of PM in this study are conducted at four operating conditions, indicated as 1400rpm-57Nm, 1400rpm-228Nm, 2200rpm-57Nm and 2200rpm-228Nm; therefore, there is a need to determine the BSPM, TNC and GMD for these conditions which are the basic information for the analyses of physicochemical properties of PM.

Fig. 7.11 (a-c) show the variations of BSPM, TNC and GMD, respectively, with the four operating conditions. Fig. 7.12 illustrates the variation of particle size distribution for the four operating conditions. Similar to above sections, the increase in engine speed or load causes increase in BSPM, TNC and GMD (except no change for GMD with speed). Also, the blended and F+B modes have lower BSPM, TNC and GMD than the diesel mode at the four operating conditions; while the fumigation mode has an effect on reducing BSPM, TNC and GMD at only high engine load (228Nm) for both speeds. On the average of four operating conditions, the blended mode has lower BSPM (-42.5%), TNC (-22.3%) and GMD (-8.8%) and the F+B mode has lower BSPM (-25.3%) and GMD (-3.4%) and similar TNC (-1.8%) compared to the diesel mode; while the fumigation mode has almost similar BSPM (1.9%), and GMD (1.4%), but higher TNC (36.2%) than the diesel mode. These results are similar to those reported in the previous sections for the five engine loads and the five engine speeds.

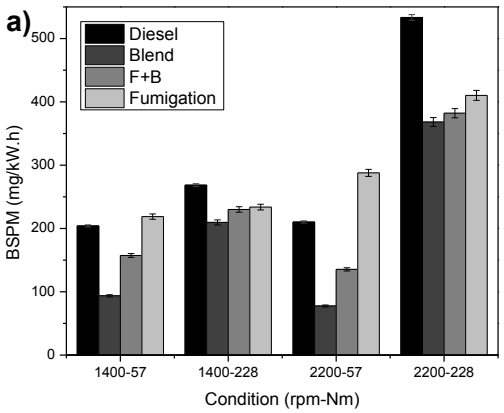

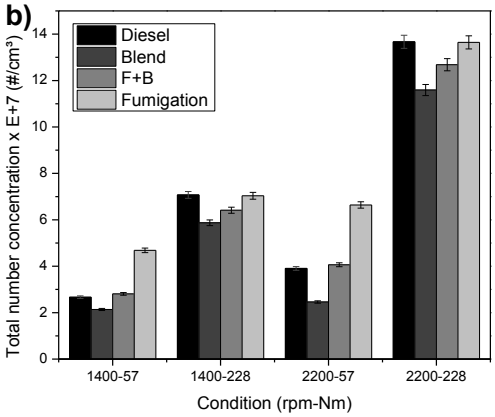

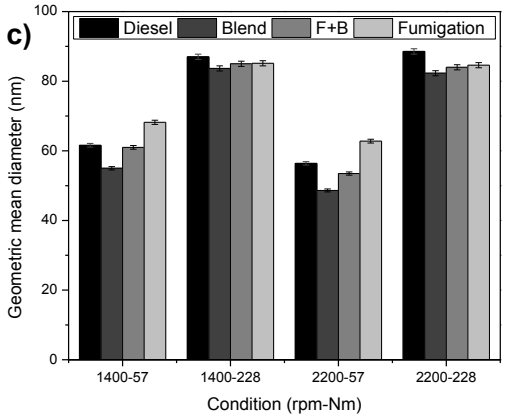

Fig. 7.11 Variations of (a) PM mass, (b) particle number concentration and (c) geometric mean diameter with engine speed and load.

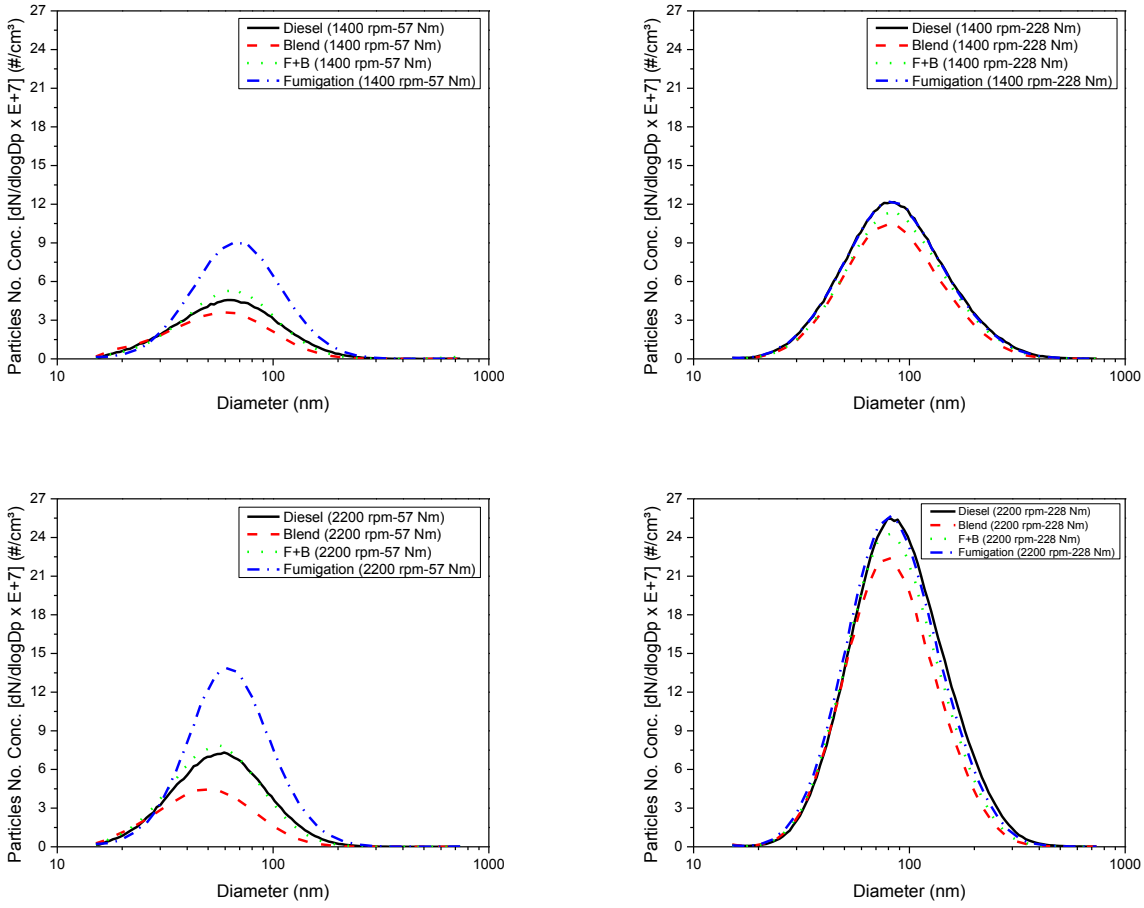

Fig. 7.12 Variation of particle size distribution with engine speed and load.

The measured particles are further classified into nano-particles (diameter of particle, $D_P \leq 50$ nm), ultra-fine particles (50 nm $< D_P \leq 100$ nm) and fine particles ($D_P > 100$ nm). Fig. 7.13 (a) illustrates that the increase in engine load causes not much change in the number of nano-particles, a slight increase in the number of ultra-fine particles and the increase in the number of fine particles; and an increase in TNC. However, in regard to the percentage of each group of particles in the TNC, Fig. 7.13 (b) shows the increase in engine load has an effect on the reduction in the fraction of nano-particles and ultra-fine particles in TNC and the increase in fraction of fine-particles in TNC. Fig. 7.13 (a and b) also show that, with the increase in engine speed, there is an increase in the amount of nano-particles, ultra-fine particles and fine-particles for all the fueling modes, such that there is little change in the percentage of each group of particles in the TNC. Similar to the results of five engine loads and five speeds, the average results for the four operating conditions in Fig. 7.13 (a) show that the blended mode has less nano-particles (-9.1%), ultra-fine particles (-23.2%) and fine-particles (-38.5%), compared to the diesel mode. The F+B mode has more nano-particles (3.1%), similar ultra-fine particles (1.4%) and less fine-particles (-13.5%), compared to the diesel mode. However, the fumigation mode has an effect on increase in nano-particles (19.2%), ultra-fine particles (49.4%) and fine-particles (50.1%), in comparison with the diesel mode.

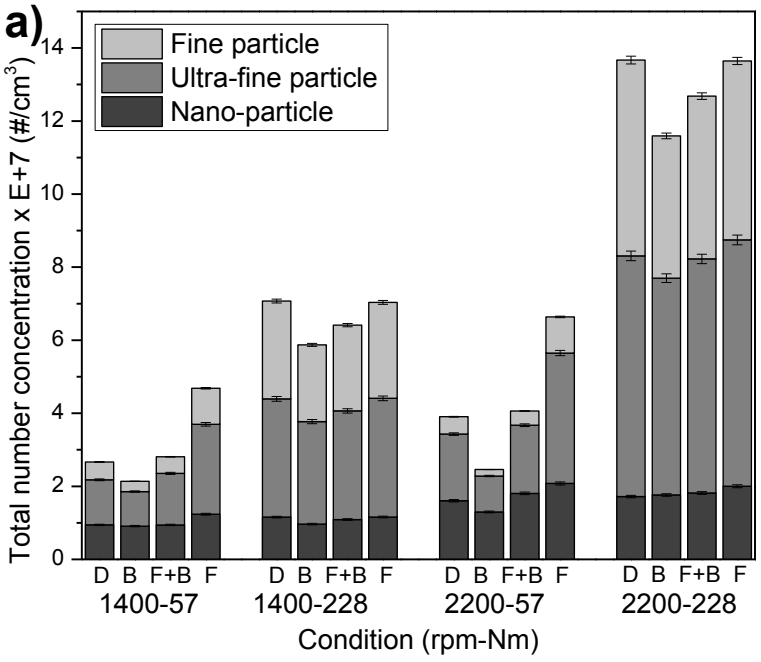

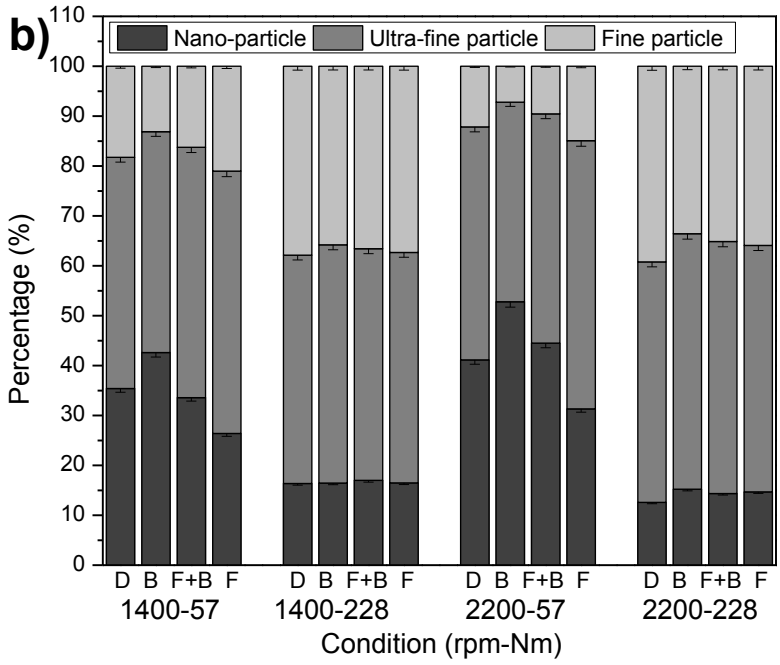

Fig. 7.13 Variations of (a) number and (b) percentage of nano-particle ($D_P \leq 50$ nm), ultra-fine particle ($50 \text{ nm} < D_P \leq 100$ nm) and fine particle ($D_P > 100$ nm) with engine speed and load.

7.2 Micro-structure

In the combustion process, the fuel forms gas phase soot precursors, which subsequently form soot nuclei. The soot nuclei grow to form primary soot particles ("spherulite" shape) with mean diameters of about 30 nm. The primary particles will then coagulate and agglomerate to form agglomerates of difference sizes and shapes (small aggregates as "clusters" or "chains" shapes and large agglomerates in the range of 1-2 μm diameter as "flakes" or "spherules" shapes) [214,215]. Investigations on the primary particle size and the morphology of the aggregate particles under different fueling modes and operating conditions are presented in this section.

7.2.1 Morphology of aggregate particles

In this study, SEM and STEM were used to investigate the morphology of aggregate particles. Fig. 7.14 shows the low magnification images of PM deposited on a TEM grid, analyzed by SEM and STEM at the operating condition of 2200rpm-57Nm; while Fig. 7.15 shows the corresponding results at the operating condition of 2200rpm-228Nm. The low magnification images of PM deposited on a TEM grid can be used to visualize the size, number and shape of particle agglomerates and clusters in regards to the PM

physical properties analysis. In this study, since the PM were collected directly from the exhaust pipe; therefore, the shape of particle agglomerates and clusters for all the fueling modes is in the original configuration compared to the in-direct PM sampling which changes the original shape of particle agglomerates and clusters. In the SEM images, the particles are shown in white color; while in the STEM images, the particles are shown in black color. It can be seen that the size, number and shape of particles and aggregate particles in the SEM images are almost similar to those of the STEM images. This confirms that the analyses of the size, number and shape of particles and aggregate particles in this study are reliable. The dark square regions which appear on the left hand side in Fig. 7.14 and Fig. 7.15 are one mesh out of 400 meshes of the TEM grid which was analyzed by SEM. By comparing the corresponding images in Fig. 7.14 with those in Fig. 7.15, it can be seen that the increase in engine load has an effect on increasing the size of the aggregate particles for all fueling modes. In addition, it can be observed that for the fumigation mode, there are many primary particles and many large aggregate particles at the low load of 57 Nm; and for the diesel mode, there are many primary particles and many large aggregate particles at the high engine load of 228 Nm; while for the blended mode, there are only a few primary particles and almost no large aggregate particles. These results are in line with the TNC and GMD results. In the F+B mode, both large particles (as fumigation mode) and small particles (as blended mode) can be found in the SEM and STEM images.

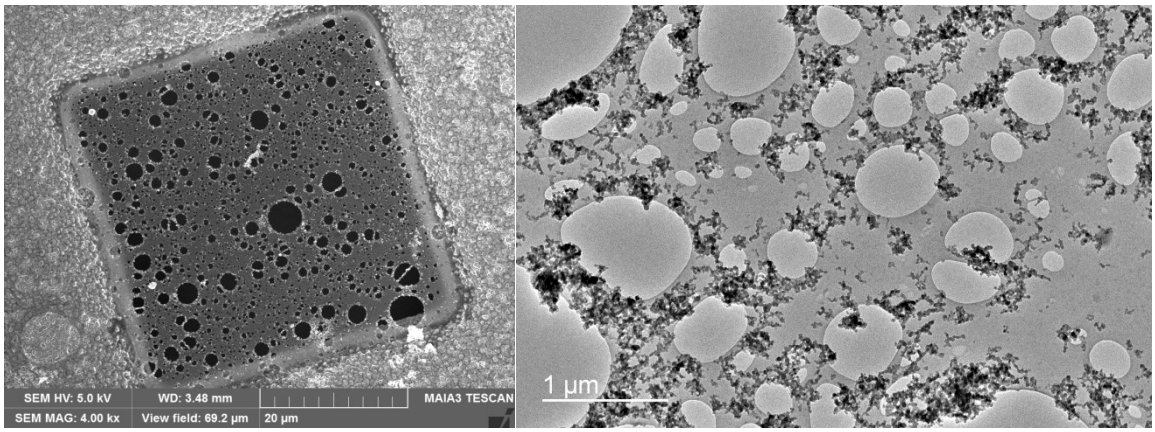

(Diesel mode)

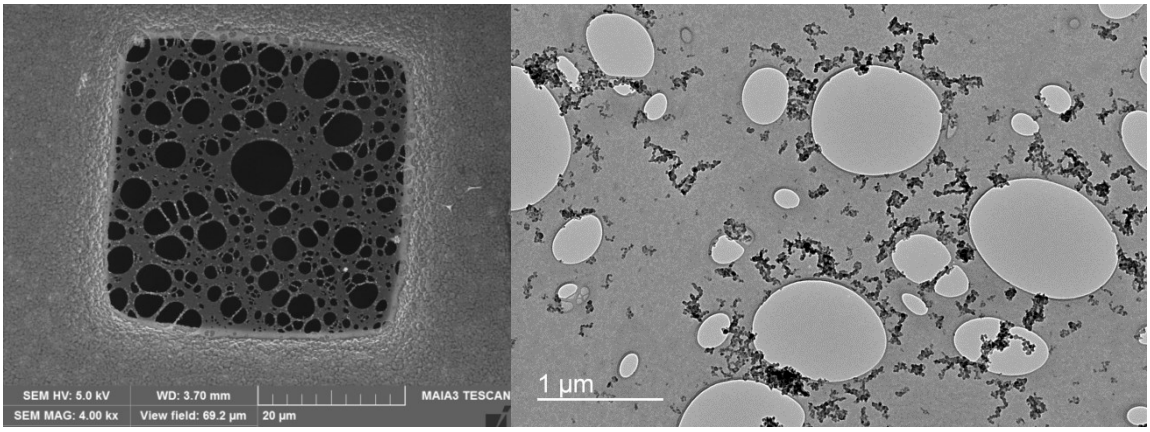

(Blended mode)

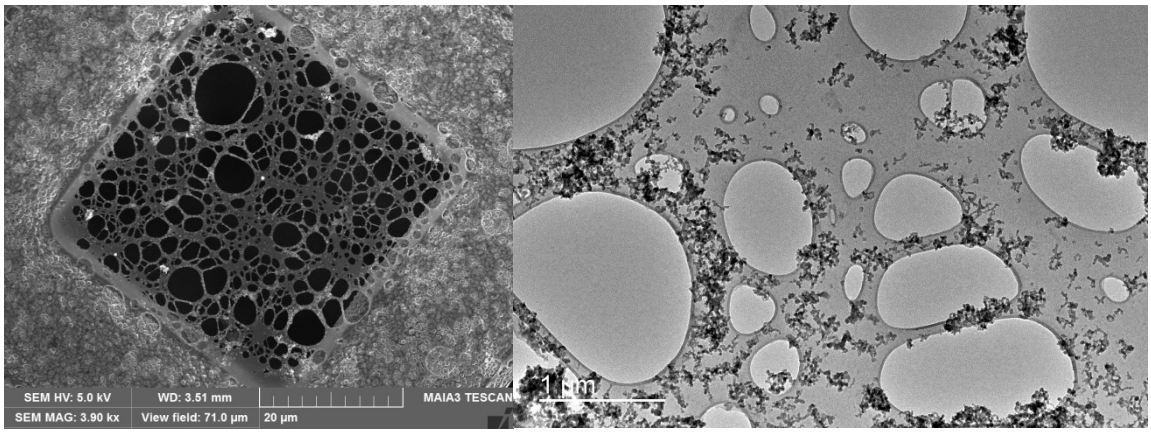

(F+B mode)

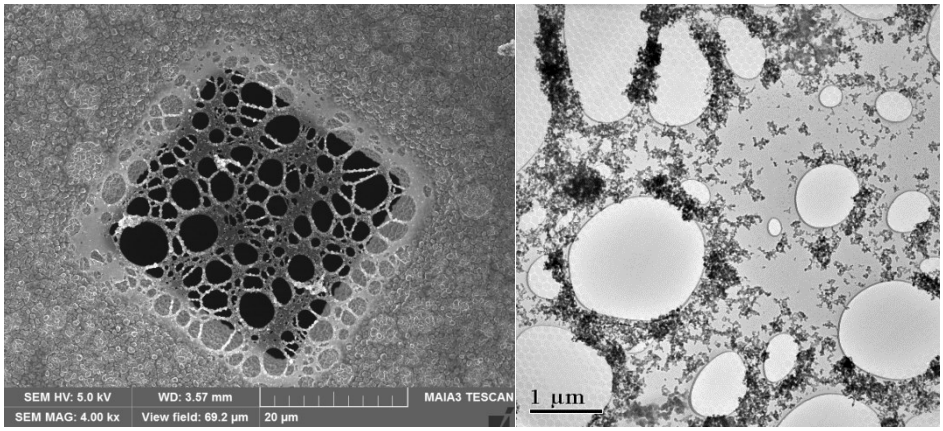

(Fumigation mode)

Fig. 7.14 Low magnification images of PM deposited on TEM grid, analyzed by SEM (left) and STEM (right) at 2200rpm-57Nm, for different fueling modes.

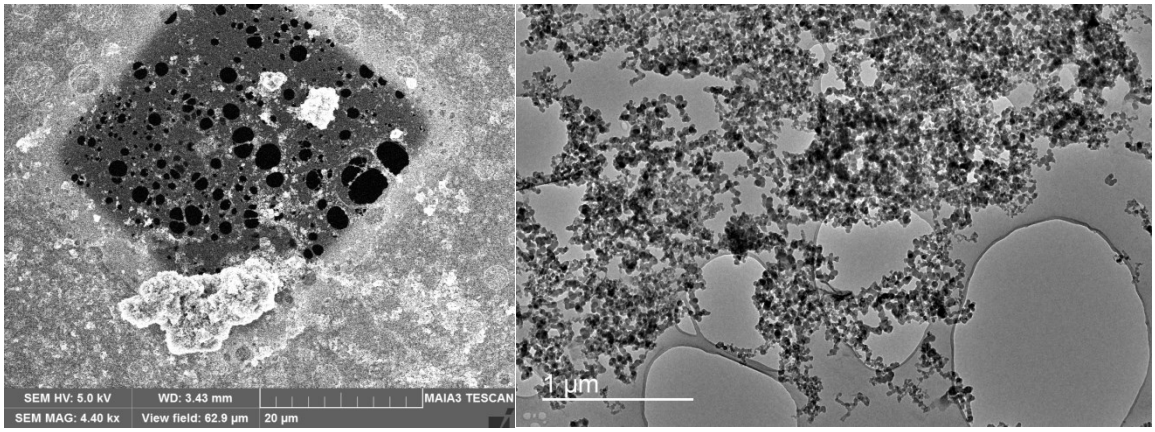

(Diesel mode)

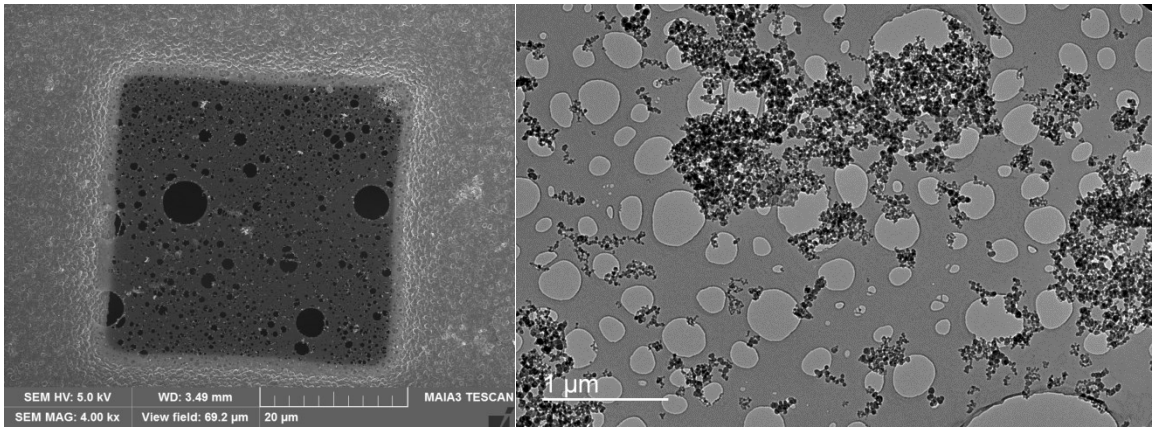

(Blended mode)

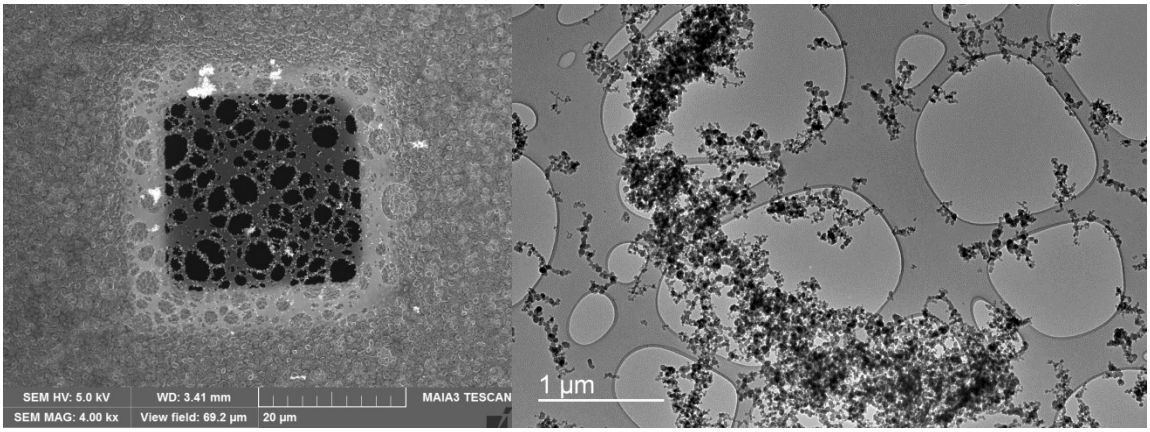

(F+B mode)

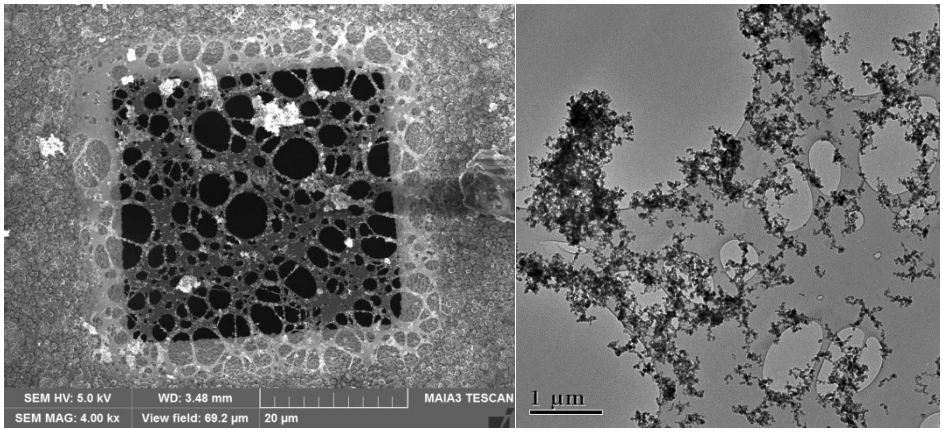

(Fumigation mode)

Fig. 7.15 Low magnification images of PM deposited on TEM grid, analyzed by SEM (left) and STEM (right) at 2200rpm-228Nm, for different fueling modes.

Fig. 7.16 shows the medium magnification images of PM deposited on TEM grid, analyzed by SEM and STEM at the operating condition of 2200rpm-57Nm; while Fig. 7.17 shows the corresponding results at the operating condition of 2200rpm-228Nm. According to the images, many quasi-spherical primary particles with different sizes can be seen for all the fueling modes. Yang et al. [214] also reported thet the primary particles from diesel and diesel/polyoxymethylene dimethyl ethers blends were in quasi-spherical shape with different sizes. The quasi-spherical primary particles in the diesel mode are connected to each other in different orientations and different particles layers are gathered (SEM images can show easily); while the connections between the particles and between the particle layers seem to be strong. However, the use of ethanol and biodiesel can change these behaviors. It is because the particles in the blended mode are connected to each other in almost one or two directions (chain like) and fewer particle layers can be found; while the connections between the particles and between the particle layers seem to be weaker than those in the diesel mode. Therefore, particles in the blended mode cannot be gathered to form large agglomrated particles, resulting in the lowest GMD in the blended mode. However, the use of ethanol and biodiesel in the fumigation mode has less significant effect compared to the blended mode due to the reasons mentioned in regard to BSPM, TNC and GMD. The F+B mode has the effect in between the blended and fumigation modes. Yang et al. [214] also found that the use of oxygenated fuel could decrease the particle number concentrations and large aggregate

particles (due to less collision between primary particles) and also the PM became looser compared to the particles obtained under the diesel mode.

In addition to the reasons mentioned in regard to the effects of BSPM, TNC and GMD, some other factors also have effects on the particle morphology for different fueling modes. These factors include the PM nano-structure parameters, PM oxidation reactivity, PAHs concentrations of PM associated with the fuel PAHs and PM chemical properties. According to the findings shown in the nano-structure section, the diesel mode contains more carbon layers than the other fueling modes; while these carbon layers are more compact and arranged in an organized orientation along with the largest primary particle diameter and fringe length and the lowest tortuosity and fringe separation distance. These parameters inhibit the accessibility of oxygen into the carbon layers for oxidation (diesel has the lowest oxidation reactivity as shown in Table 8-1) resulting in formation of the largest primary particle and particle agglomerates and clusters. In addition, the fringe lengths (Figs. 7.20 and 7.21) associated with the carbon atoms [214] and carbon layers at the edge-site positions of particles emitted from diesel mode are larger than that of the other fueling modes which weaken the oxidation process. The diesel mode also has the highest fuel which is the source of soot nuclei formation and enhance primary particles formation. Also, diesel PM consists of the highest EC (Fig. 8.1), non-volatile substance (Figs. 8.3 and 8.4) and inorganic ions (cause surrounding of the particles) (Figs. 8.12 to 8.14), and the lowest OC concentration (Fig. 8.1) and volatile substance (Figs. 8.3 and 8.4); therefore, these parameters cause formation of the largest primary particles with strong connection to form larger particle agglomerates and clusters. However, the use of ethanol and biodiesel in the blended, F+B and fumigation modes can change these behaviors to produce the smaller particles with looser connection than that in the diesel mode; while the blended and fumigation modes have the highest and the lowest effects, respectively due to their different impacts on the nano-structure parameters (as descriped in this Chapter), PM oxidation reactivity, PAHs and PM chemical properties (Chapter 8).

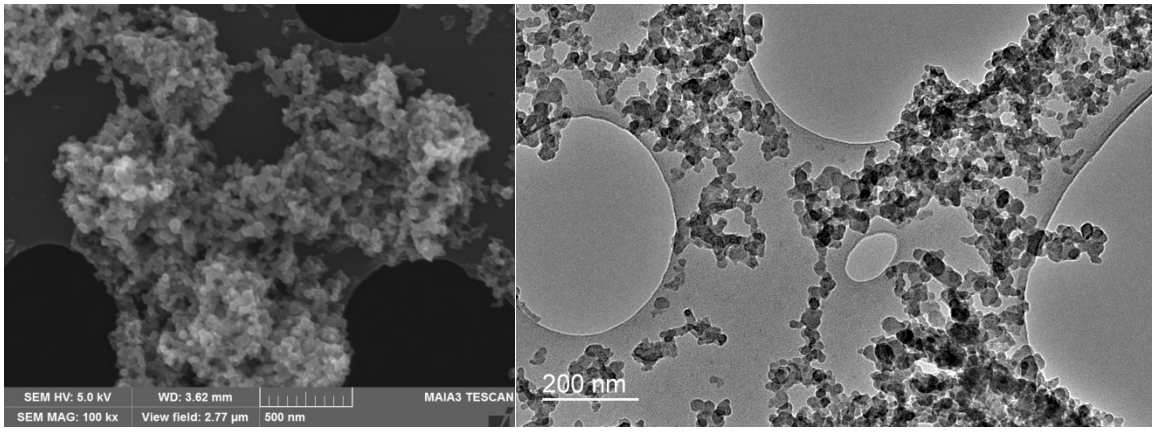

(Diesel mode)

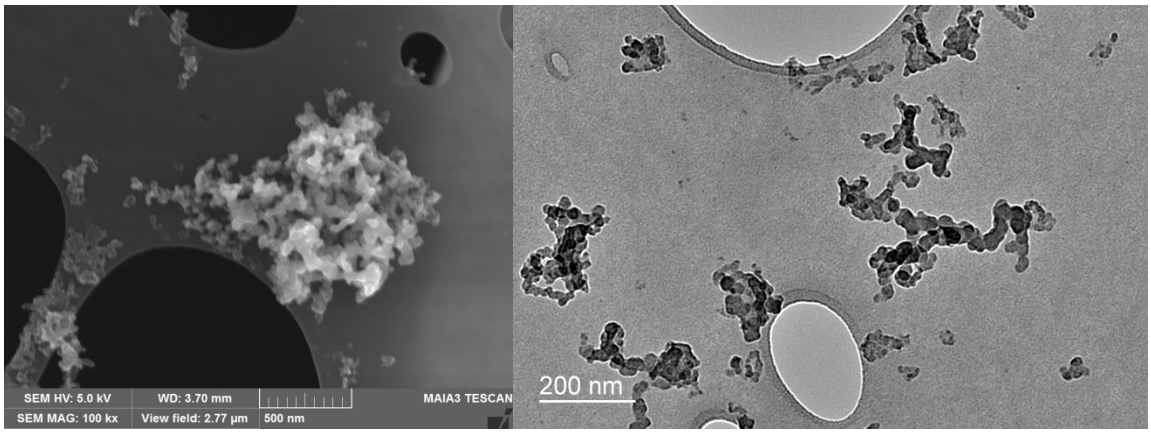

(Blended mode)

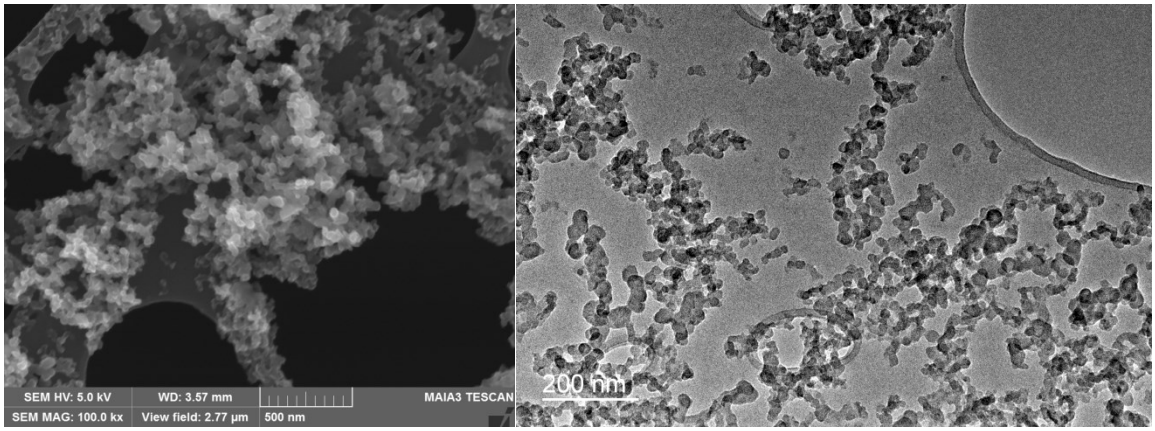

(F+B mode)

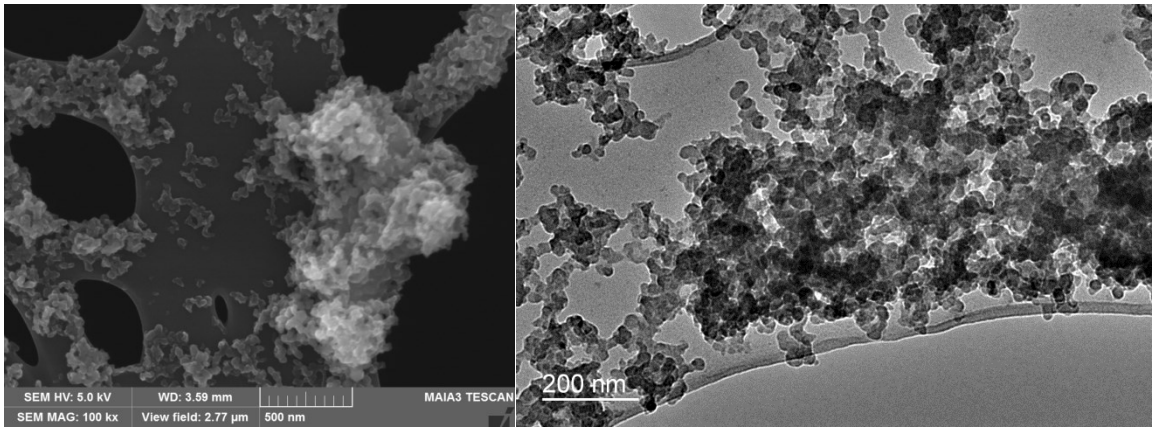

(Fumigation mode)

Fig. 7.16 Medium magnification images of PM deposited on TEM grid, analyzed by SEM (left) and STEM (right) at 2200rpm-57Nm, for different fueling modes.

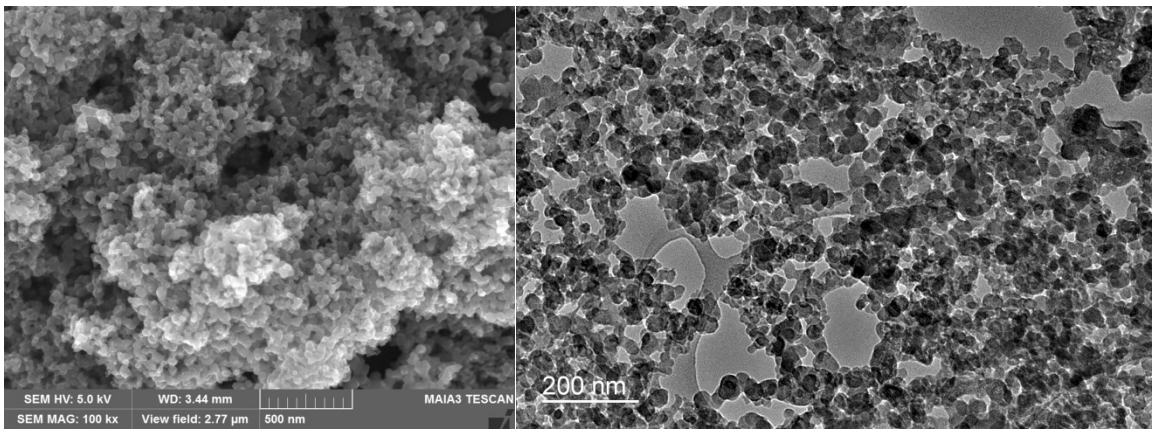

(Diesel mode)

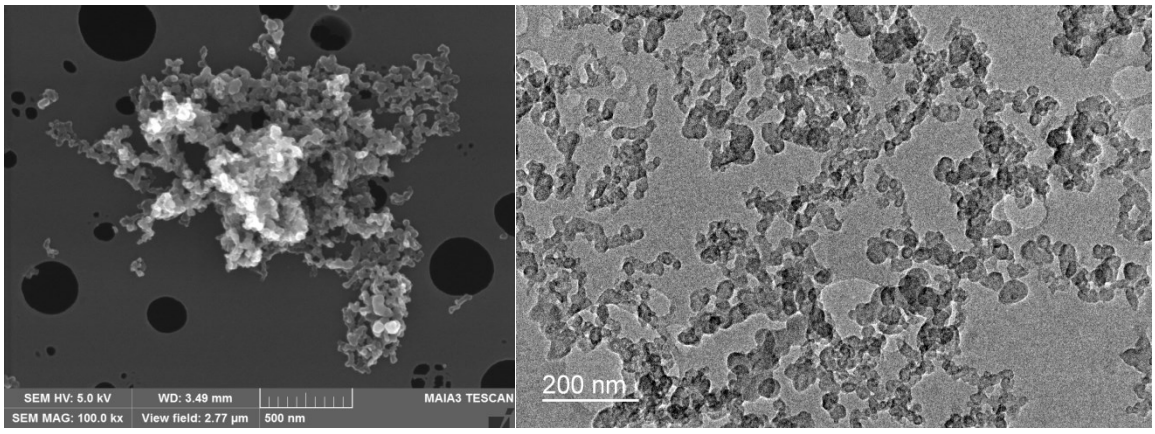

(Blended mode)

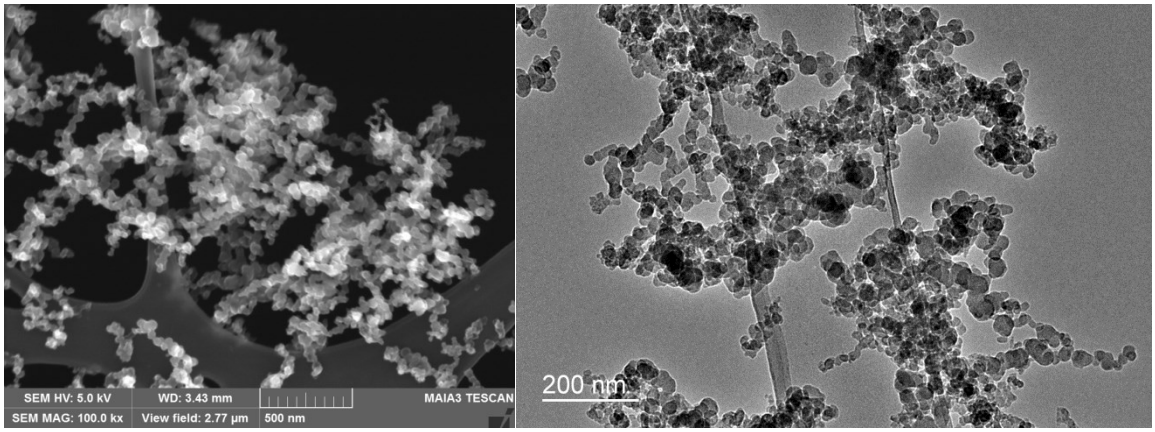

(F+B mode)

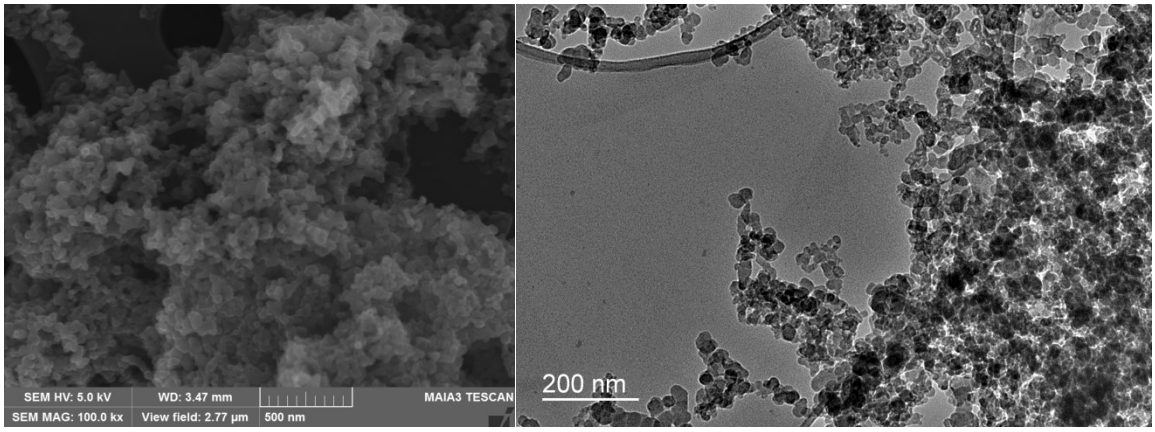

(Fumigation mode)

Fig. 7.17 Medium magnification images of PM deposited on TEM grid, analyzed by SEM (left) and STEM (right) at 2200rpm-228Nm, for different fueling modes.

7.2.2 Primary particle size

Primary particle diameters for different fueling modes and operating conditions are presented in Table 7-1. In addition, the distribution of primary particle diameter for different fueling modes at the operating conditions of 2200rpm-57Nm and 2200rpm-228Nm are shown in Fig. 7.18. According to Table 7-1 and Fig. 7.18, the increase in engine load has an impact on moving the primary particle diameter distribution towards the bigger size range, resulting in an increase in the mean primary particle diameter for all fueling modes; while almost no significant effect from engine speed is observed, which are in line with GMD results. The increase in primary particle diameter with

increase in engine load was also reported in the literature [128,214,335-337]. Table 7-1 also illustrates that the blended, F+B and fumigation modes cause decrease in the primary particle diameter in all four operating conditions (except at the engine load of 57 Nm for the fumigation mode); while the blended mode has the lowest value. These findings are also in line with the GMD results. On the average of four operating conditions, the blended mode (-15.0%) and F+B mode (-9.1%) have lower primary particle diameters, but the fumigation mode (-1.8%) has almost the same primary particle diameter compared to the diesel mode. These results are also in line with the GMD results. Ruiz et al. [191] and Gargiulo et al. [192] also found that ethanol or butanol in dual-fuel system had no effect on the average particle size compared to the diesel fuel. However, for the blended mode, the ethanol and biodiesel in DBE blend can reduce the carbon content and increase the oxygen content, resulting in the reduction of nuclei particles and hence smaller primary particles are formed compared to that of diesel fuel [128]. Smaller primary particle diameter using alternative fuels compared to the diesel fuel have also been reported in other studies [128,211,214,336,338].

Table 7-1 Mean primary particle diameter (nm (SD)) for different fueling modes and operating conditions

Condition (rpm-Nm)	Diesel	Blend	F+B	Fumigation
1400-57	25.6 (4.5)	21.5 (4.0)	22.9 (3.3)	25.8 (4.1)
1400-228	27.1 (6.0)	24.2 (3.9)	25.3 (3.6)	26.4 (3.7)
2200-57	23.7 (4.2)	19.5 (3.4)	22.0 (3.2)	24.5 (3.9)
2200-228	29.6 (7.2)	25.2 (3.9)	26.1 (4.0)	27.1 (4.8)

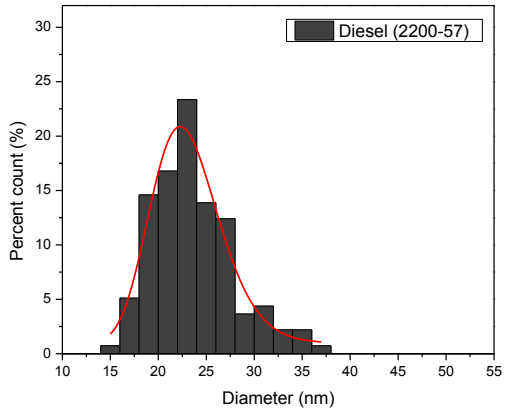

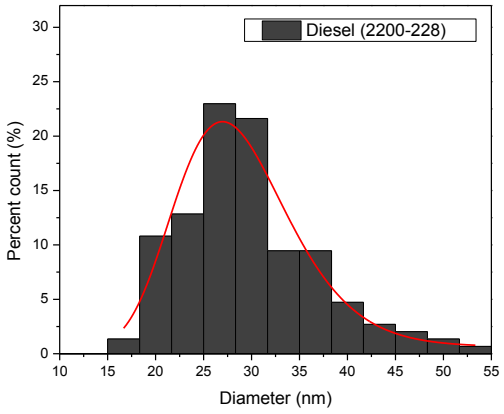

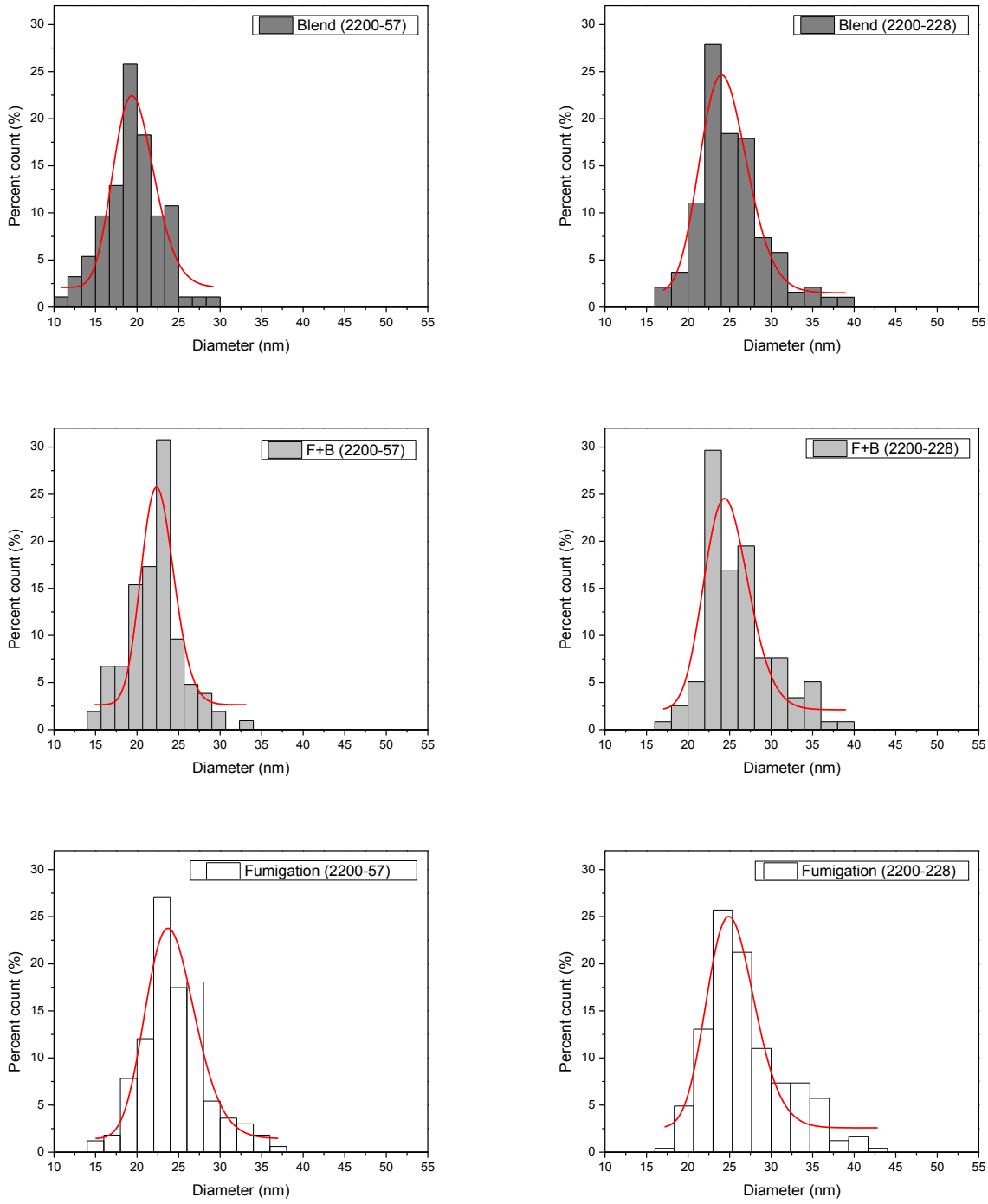

Fig. 7.18 Primary particle diameter distribution for different fueling mods at 2200rpm-57Nm (left) and 2200rpm-228Nm (right).

7.3 Nano-structure

7.3.1 Morphology of primary particle

Quantitative investigation of the nano-structure of primary particles is important parameter in PM investigation, because it provides information on the particle formation process and the particle oxidative reactivity [207]. According to the literature various types of structure for primary particle have been reported [212,335,337,339-341]. These structures include: (I) fullerenoid or onion-like morphology; (II) turbostratic structures produced from small plates of undefined orientation; (III) purely turbostratic layers and (IV) structures produced from multiple spherical nuclei surrounded by several graphitic layers as shell-amorphous or shell-core. Some common structures for primary particle are presented in Fig. 7.19.

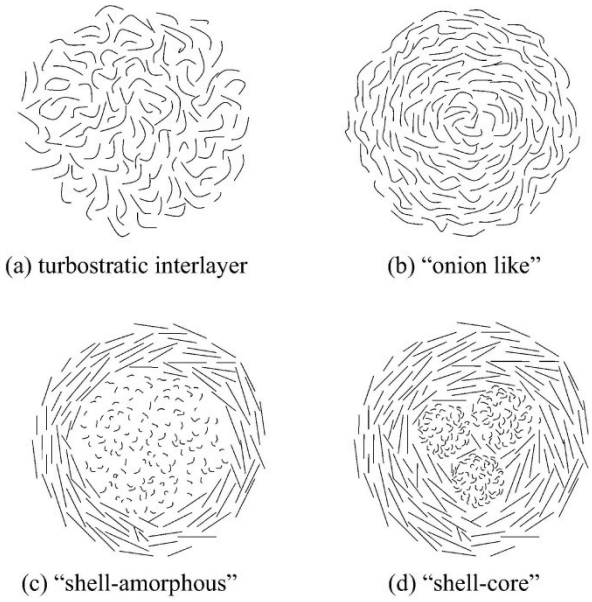

Fig. 7.19 Simplified sketch of nano-structure of primary particle [335].

For this study, it can be seen from Fig. 7.20 and Fig. 7.21 that at the low engine load of 57Nm, for both low and high speeds, the carbon lamellas are arranged in a disorganized orientation, and mostly having the "onion like" and ''turbostratic interlayer" structures due to high content of volatile organic carbons [128] and no clear core can be observed. At the high engine load of 228 Nm, for both low and high speeds, the carbon lamellas are more orderly and have clear cores which seem to be the "shell-amorphous" structure – which has amorphous interior, or so-called ''hollow center" and graphitized outer shell– for all fueling modes. Similar results were reported in the literature [335-337] which

found the carbon lamellas at high loads were more orderly than that at low loads. The length of outer carbon lamella is longer than the interior carbon lamella; while the interior amorphous structure is due to presence of the carbon sheets with higher reactivity towards the oxygen [335]. Also, the interior amorphous structure is related to the randomly orientated PAHs in PM [212]. However, no significant differences can be seen for the effect of engine speed on the nano-structure morphology for all the fueling modes compared to the huge effect of engine load on the nano-structure morphology. This is because the increase in engine speed has less effects on the combustion and performance parameters, e.g. peak HRR, DOC, diffusion combustion phase, exhaust gas temperature and equivalence ratio, and also has opposite effects on ID and BTE compared with the increase in engine load.

Fig. 7.20 and Fig. 7.21 also show that the blended, F+B and fumigation modes lead to a change in the nano-structure morphology, compared to the diesel mode. It can be seen that for the diesel mode, there are more carbon layers than the other fueling modes due to more carbon is available for soot formation and less oxygen is available for soot oxidation, especially at the high load for both speeds. The blended mode has almost the lowest number of carbon layers. In addition, the blended mode has smoother particles (shown in the pictures as brighter particles for blended mode compared to other modes) than the other modes which is in line with [202] using oxygenated fuel (butanol) compared to the diesel fuel. However, the fumigation mode has less effect compared with the blended mode on the nano-structure morphology due to the reasons mentioned in regard to BSPM, TNC, GMD and morphology of the aggregate particles.

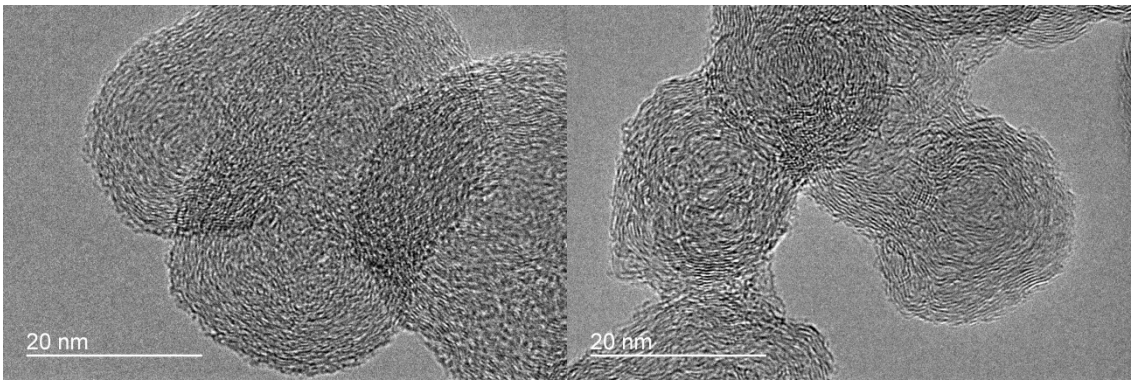

(Diesel mode)

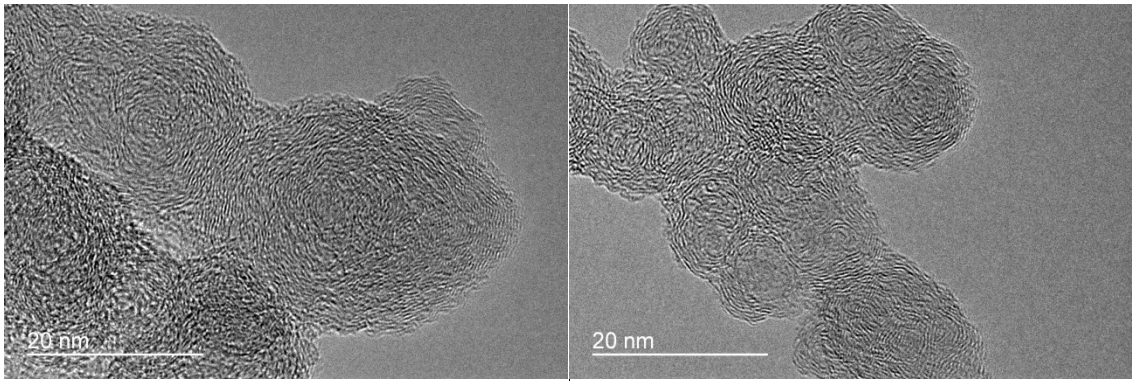

(Blended mode)

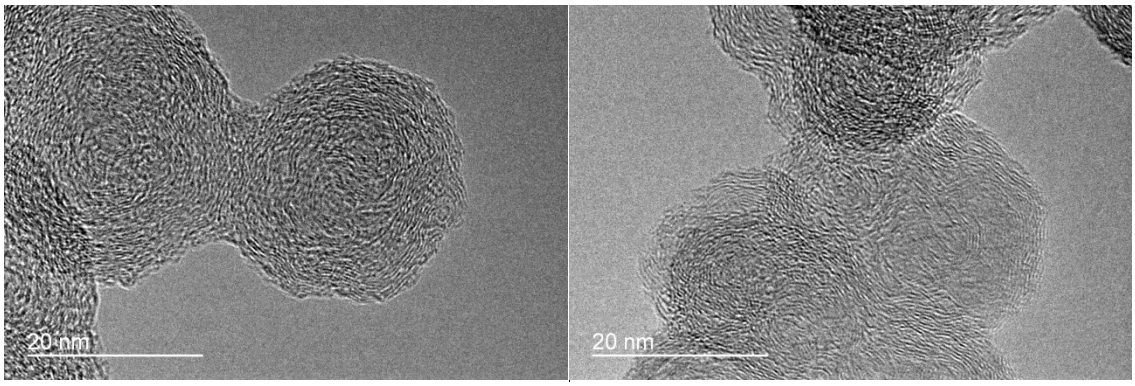

(F+B mode)

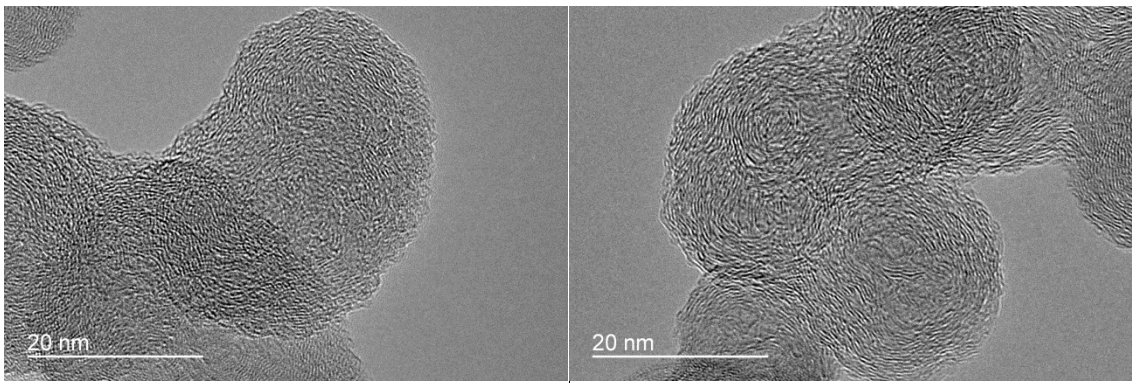

(Fumigation mode)

Fig. 7.20 Nano-structure of PM analyzed by STEM (high resolution image) for different fueling modes at 1400rpm-57Nm (left) and 1400rpm-228Nm (right).

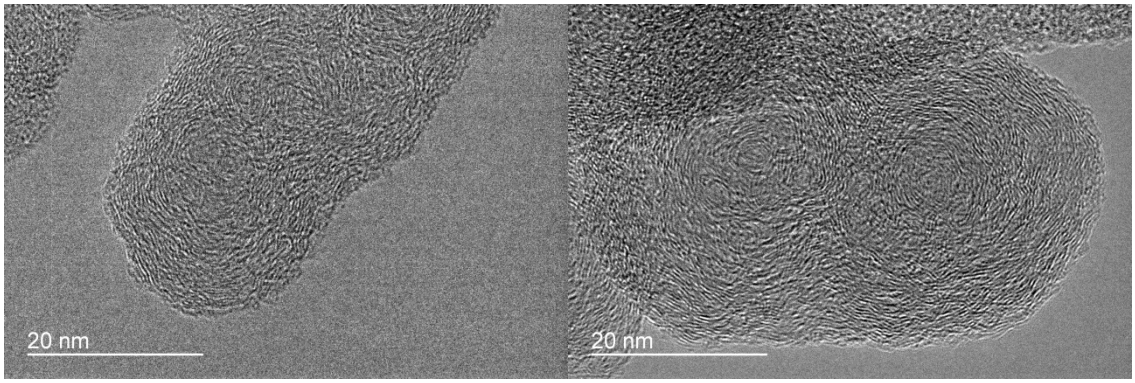

(Diesel mode)

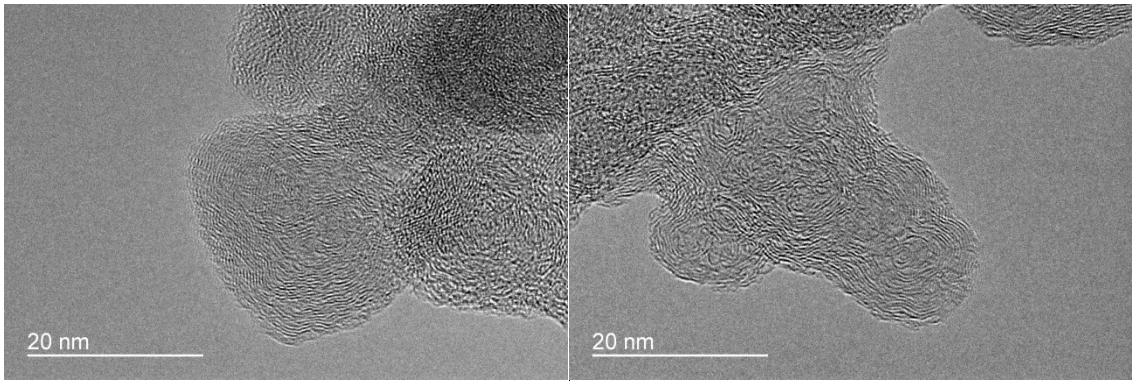

(Blended mode)

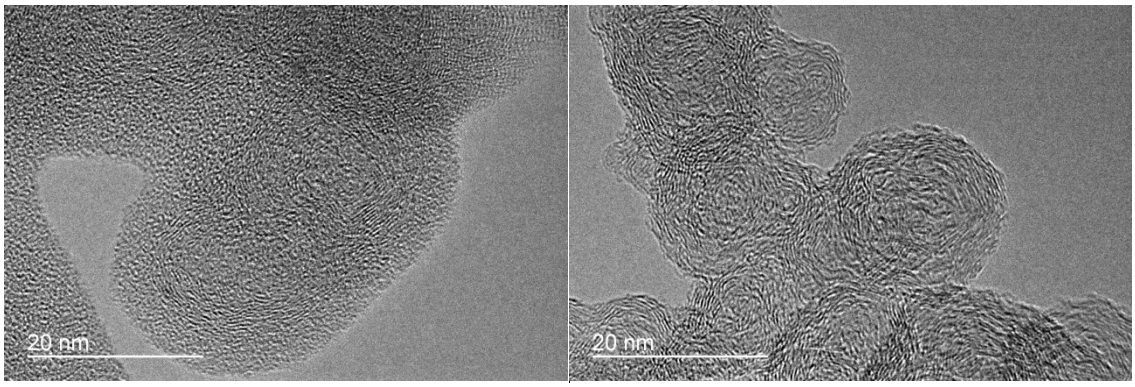

(F+B mode)

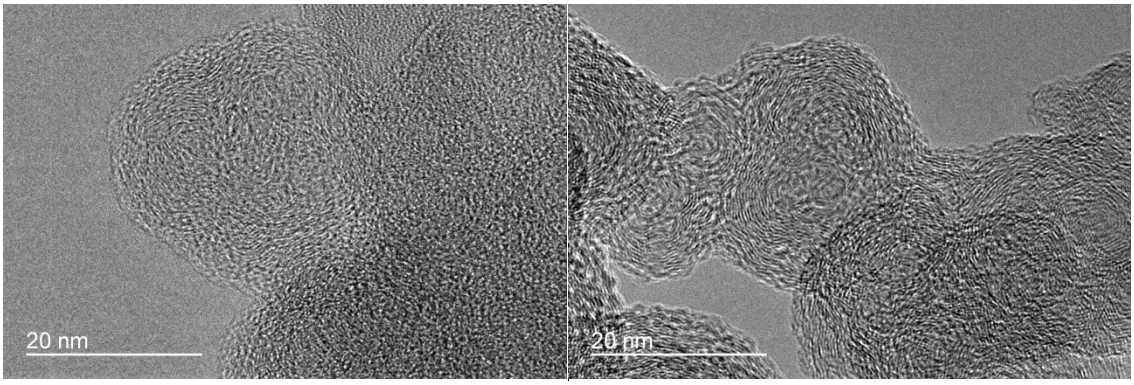

(Fumigation mode)

Fig. 7.21 Nano-structure of PM analyzed by STEM (high resolution image) for different fueling modes at 2200rpm-57Nm (left) and 2200rpm-228Nm (right).

7.3.2 Fringe length, tortuosity and fringe separation distance

The change in carbon lamellas due to change in engine speed, load or fueling mode affects the fringe length (L_a), tortuosity (T_f) and fringe separation distance (D_S) of the primary particles. According to Table 7-2, the increase in engine load or speed (except at the operating condition of 1400rpm-57Nm) causes increase in fringe length and decrease in tortuosity and fringe separation distance, which are in line with results in other studies [214,335-338] based on engine load. At the low engine speed and load case of 1400rpm-57Nm, the low combustion temperature and incomplete combustion cause formation of longer fringe length and lower tortuosity and fringe separation distance of the primary particles compared to the case of 2200rpm-57Nm.

In addition, Table 7-2 shows that the blended, F+B and fumigation modes cause decrease in fringe length and increase in fringe separation distance in all operating conditions (except for the fringe length at the fumigation mode under the operating conditions of 1400rpm-57Nm and 2200rpm-57Nm). It is because at low engine load (57Nm), the same reasons that lead to the higher GMD in the fumigation mode compared to the diesel mode also cause increase in fringe length as well. For tortuosity, Table 7-2 illustrates that only the fumigation mode has a small increase in tortuosity compared to the diesel mode. On the average of the four operating conditions, the blended and F+B modes have lower fringe length (-12.9%, -9.6%), equal tortuosity (0.4%, 0.9%) and higher fringe separation distance (4.4%, 5.5%) compared to the diesel mode. However, the fumigation mode has almost no effect on the fringe length (-2.2%, insignificant difference with T-test), but small increase in tortuosity (2.2%) and fringe separation distance (6.8%) compared to the

diesel mode. Since the fumigation mode particles have higher tortuosity than the blended mode particles; therefore, they have higher fringe separation distance. Ruiz et al. [191] also found that the use of ethanol or butanol in a dual-fuel system had no effect on the fringe length of primary particle compared to the diesel fuel. The decrease in fringe length and increase in tortuosity and fringe separation distance using alternative fuels have also been reported in the other studies [214,338]. The distribution of fringe length, tortuosity and fringe separation distance at the operating conditions of 2200rpm-57Nm and 2200rpm-228Nm for different fueling modes are also presented in Fig. 7.22, Fig. 7.23 and Fig. 7.24, respectively.

Table 7-2 Fringe length (L_a), tortuosity (T_f) and fringe separation distance (D_S) of primary particles for different fueling modes and conditions

Parameter	**Mode**	**1400rpm-57Nm**	**1400-228**	**2200-57**	**2200-228**
L_a (SD)	Diesel	0.648 (0.045)	0.761 (0.012)	0.626 (0.050)	0.814 (0.036)
(nm)	Blend	0.605 (0.027)	0.615 (0.048)	0.574 (0.022)	0.670 (0.032)
	F+B	0.638 (0.031)	0.640 (0.027)	0.588 (0.032)	0.692 (0.034)
	Fumigation	0.684 (0.033)	0.709 (0.050)	0.646 (0.030)	0.727 (0.025)
T_f (SD)	Diesel	1.159 (0.018)	1.146 (0.017)	1.156 (0.013)	1.154 (0.017)
	Blend	1.162 (0.028)	1.150 (0.018)	1.168 (0.016)	1.155 (0.015)
	F+B	1.165 (0.014)	1.157 (0.027)	1.177 (0.014)	1.159 (0.016)
	Fumigation	1.185 (0.018)	1.167 (0.014)	1.195 (0.018)	1.169 (0.016)
D_S (SD)	Diesel	0.397 (0.020)	0.385 (0.009)	0.401 (0.005)	0.365 (0.008)
(nm)	Blend	0.402 (0.005)	0.399 (0.007)	0.420 (0.016)	0.394 (0.011)
	F+B	0.412 (0.006)	0.399 (0.008)	0.428 (0.022)	0.394 (0.008)
	Fumigation	0.414 (0.007)	0.401 (0.012)	0.433 (0.013)	0.404 (0.020)

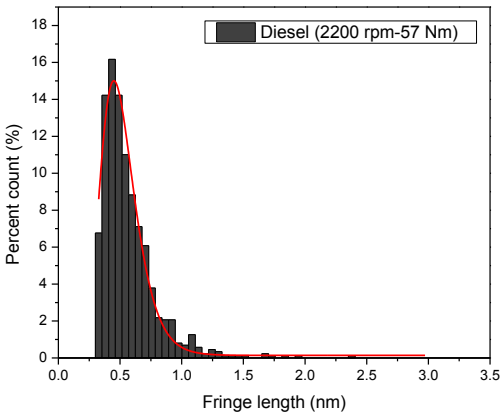
Diesel (2200 rpm-57 Nm)
Percent count (%)
Fringe length (nm)

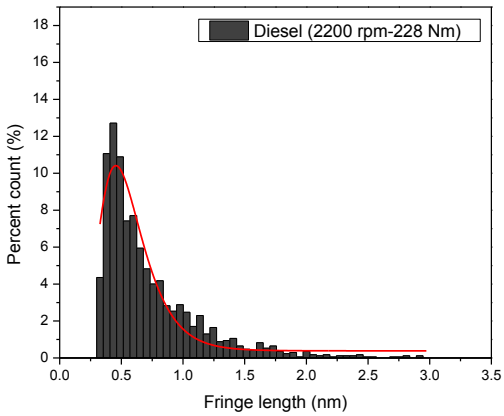
Diesel (2200 rpm-228 Nm)
Percent count (%)
Fringe length (nm)

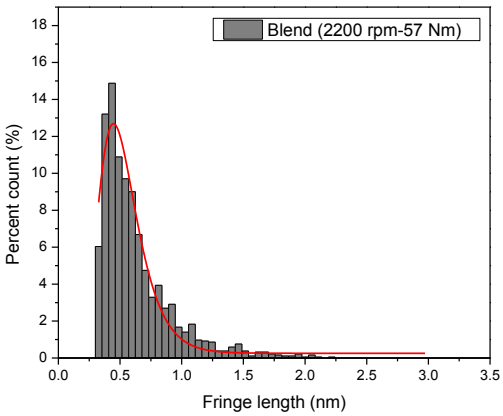
Blend (2200 rpm-57 Nm)
Percent count (%)
Fringe length (nm)

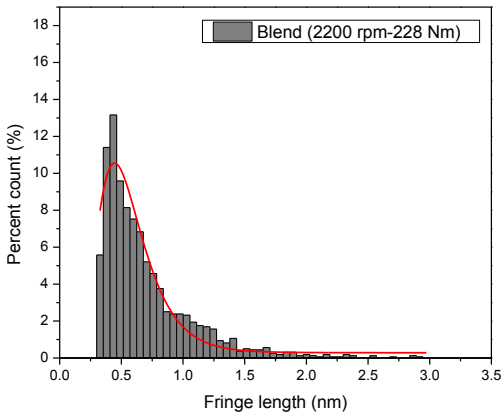
Blend (2200 rpm-228 Nm)
Percent count (%)
Fringe length (nm)

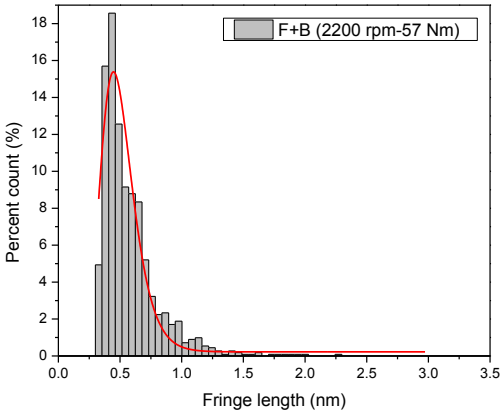
F+B (2200 rpm-57 Nm)
Percent count (%)
Fringe length (nm)

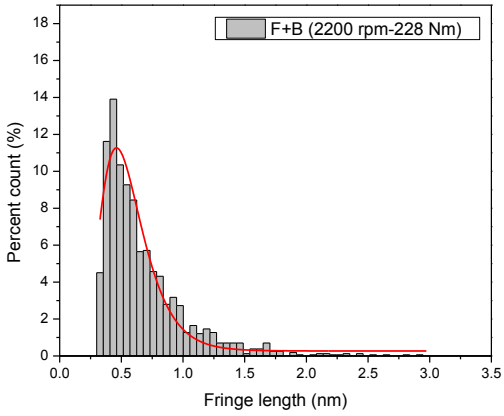
F+B (2200 rpm-228 Nm)
Percent count (%)
Fringe length (nm)

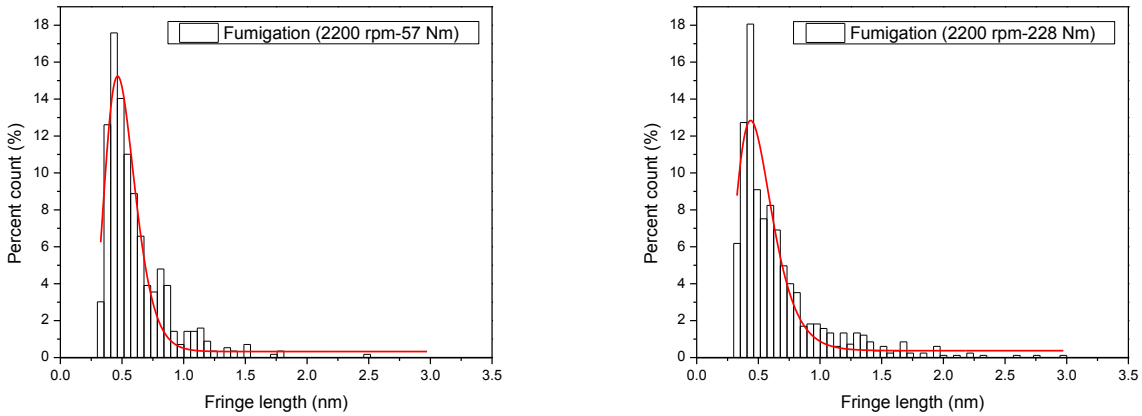

Fig. 7.22 Distribution of fringe length of primary particles for different fueling modes at 2200rpm-57Nm and 2200rpm-228Nm.

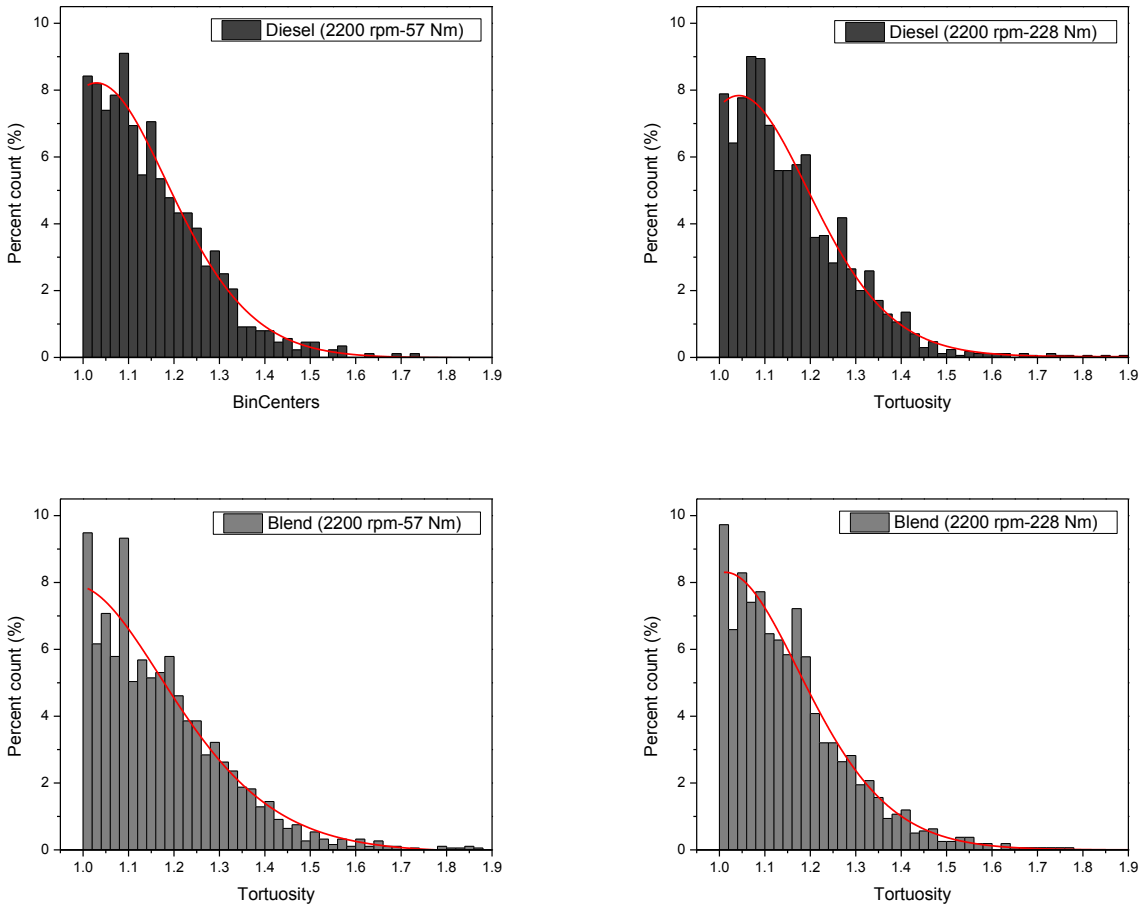

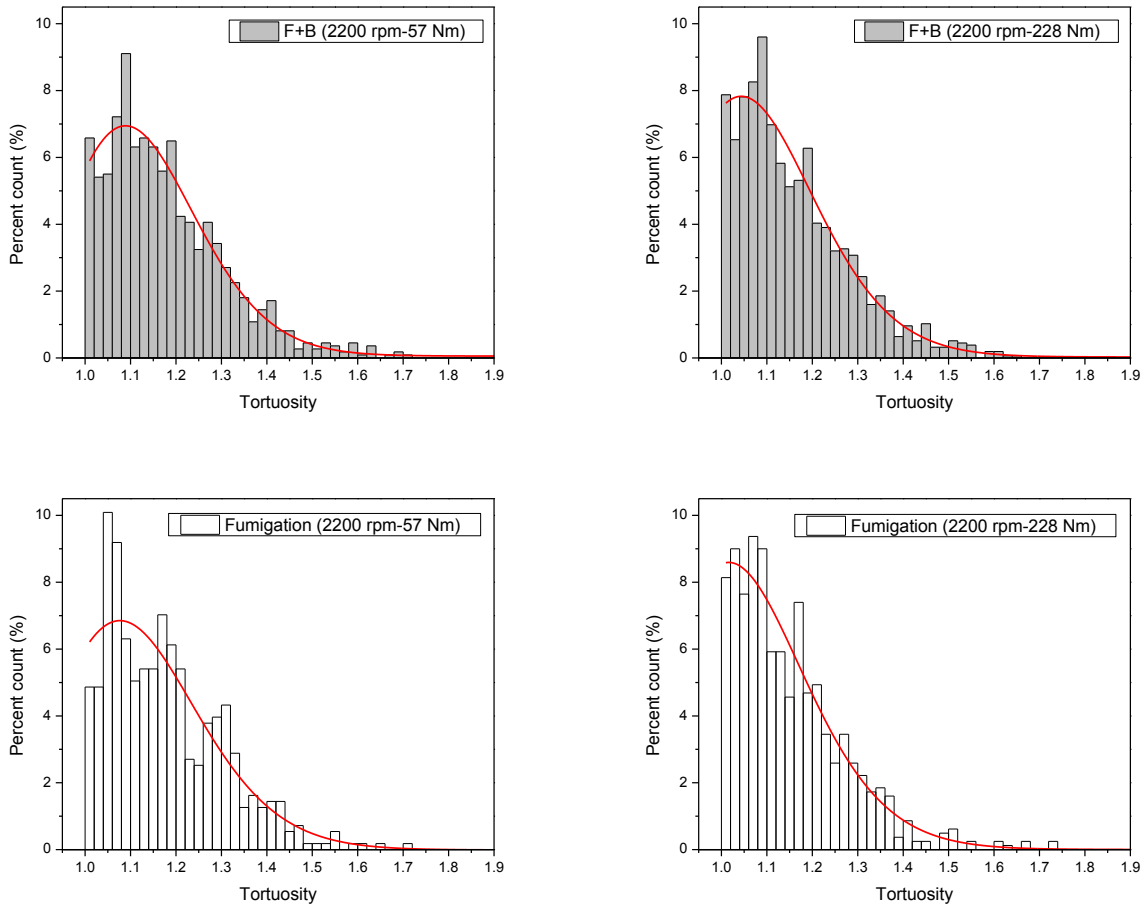

Fig. 7.23 Distribution of tortuosity of primary particles for different fueling modes at 2200rpm-57Nm and 2200rpm-228Nm.

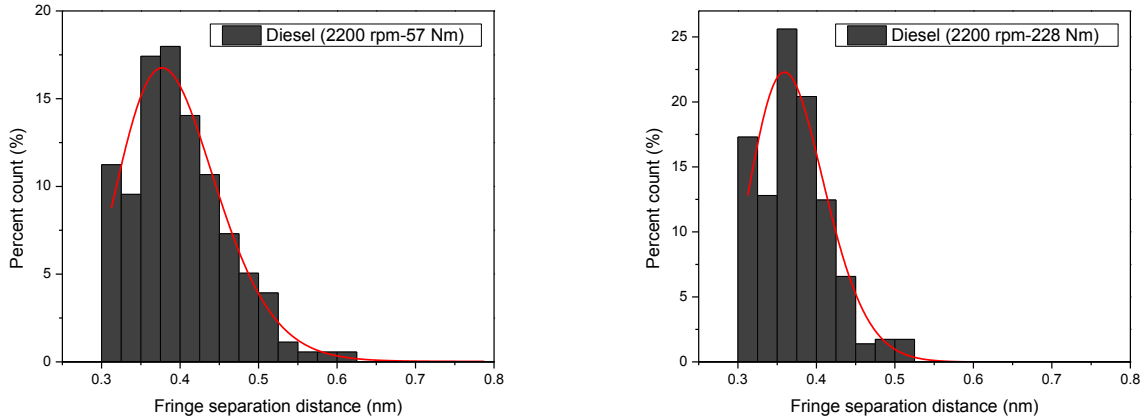

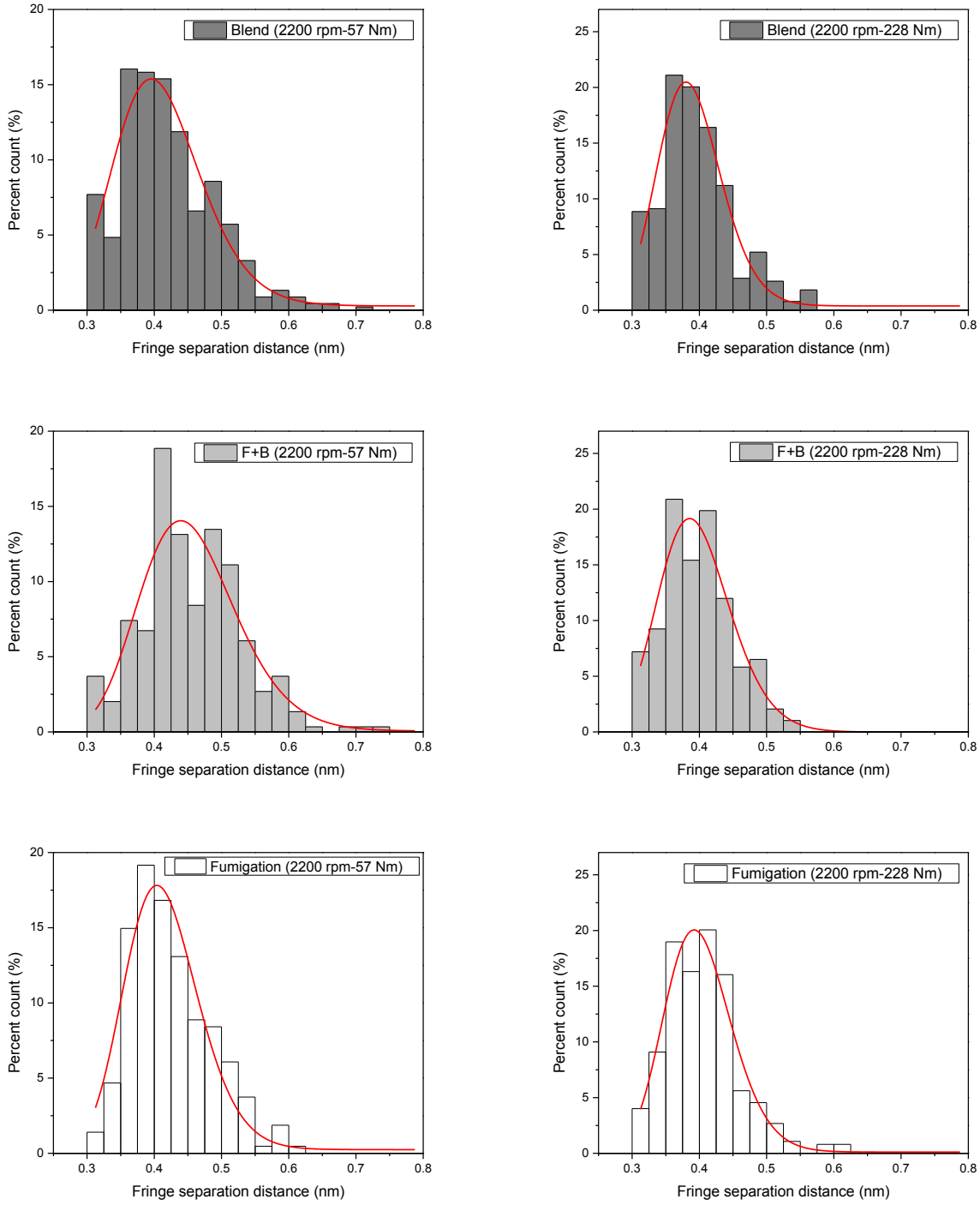

Fig. 7.24 Distribution of fringe separation distance of primary particles for different fueling modes at 2200rpm-57Nm and 2200rpm-228Nm.

7.4 Electron diffraction pattern

The TEM imaging function combined with selected-area electron diffraction (SAED) can be used to understand the crystallinity of a sample. In the SAED method, an aperture in the image plane of the objective lens is used for limiting the area that the diffracted electrons are collected [342]. A SAED pattern can determine the distinct intensity maxima form (also called as "reflections") in the case of crystalline materials (with bright spots appearing in the picture) and diffuse scattering from defective crystalline and amorphous substances (with diffuse rings appearing in the picture) [342-345].

In the present study, the SAED pattern images of PM deposited on TEM grid were analyzed by STEM for the operating condition of 2200rpm-228Nm. It can be seen from Fig. 7.25 that the SAED pattern image of each fueling modes has three bright rings which show that the sample contains amorphous substances (carbon is major substance) which is in line with the amorphous structures of particles for all fueling modes at the conditions of 2200rpm-228Nm as shown in Fig. 7.21. Each ring in the SAED pattern image corresponds to the atomic plane of different orientation and different interplanar d-spacing [344]. Sahu et al. [346] and Buseck et al. [343] also found that the soot and black carbon have three bright rings in SAED pattern images. In addition, Fig. 7.25 shows that there are almost no significant differences in the SAED pattern images among the different fueling modes in regard to the number of rings and the diameter of each ring (d-value and lattice spacing), because carbon is the main substance of PM for all the fueling modes.

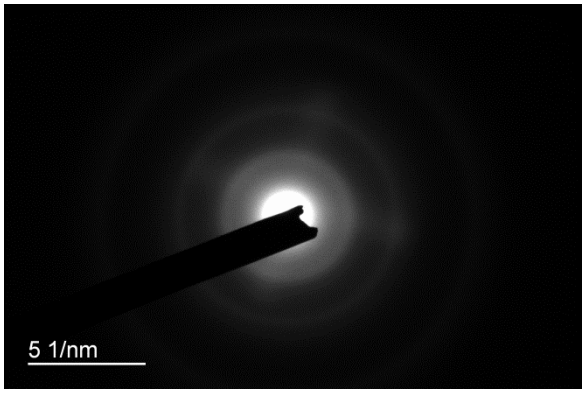

(Diesel mode)

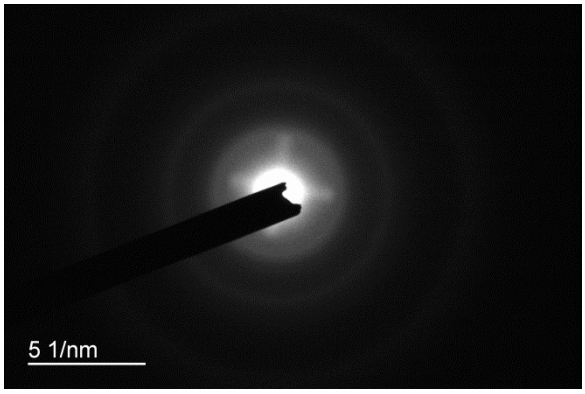

(Blended mode)

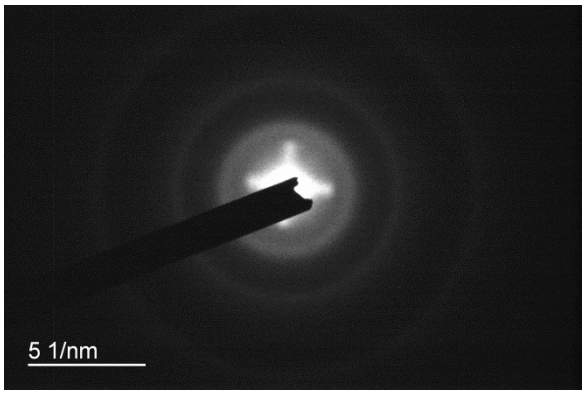

(F+B mode)

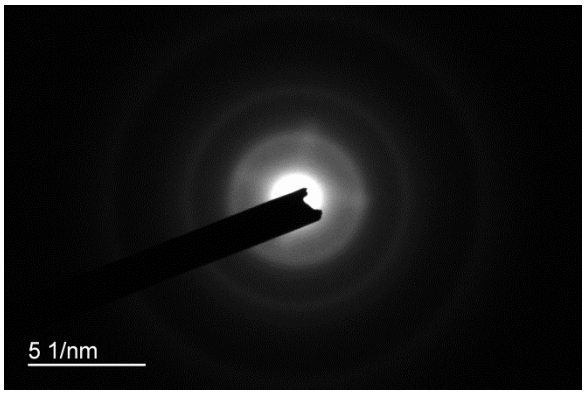

(Fumigation mode)

Fig. 7.25 SAED pattern images of PM deposited on TEM grid, analyzed by STEM at 2200rpm-228Nm, for different fueling modes.

7.5 Summary

The effects of blended, F+B and fumigation modes on PM emissions and the physical properties of PM, based on the average results of various operating conditions, compared to those of the diesel mode, are presented in Table 7-3. The impact of using different fueling modes on the BSPM, TNC and GMD is independent of the different engine loads or speeds, because the trends and percentages of increase or reduction in these parameters are almost similar to each other. This finding is similar to the finding in regard to the regulated emissions. It is also found the use of DBE in blended and fumigation modes affects the micro and nano-structures of the PM by changes in the primary particle diameter, fringe length, tortuosity and fringe separation distance, compared to the diesel mode. Also, the connections between the particles and between the particle layers using DBE in blended and fumigation modes seem to be weaker than the diesel mode; while the blended mode has the weakest connections.

Table 7-3 Effect of fueling modes on the PM emissions and physical properties of PM based on the average of various conditions

Parameter	Order (Highest to lowest)
Based on five loads	
PM mass	Fumigation (1.2%) ≈ **Diesel** > F+B (-28.4%) > Blend (-47.9%)
TNC	Fumigation (27.8%) > **Diesel** ≈ F+B (-1.2%) > Blend (-18.5%)
GMD	Fumigation (1.5%) ≈ **Diesel** > F+B (-4.8%) > Blend (-9.3%)
Nano-particle concentration	Fumigation (16.5%) > F+B (5.0%) > **Diesel** > Blend (-6.5%)
Ultra-fine particle concentration	Fumigation (34.5%) > F+B (0.5%) ≈ **Diesel** > Blend (-19.3%)
Fine particle concentration	Fumigation (31.7%) > **Diesel** > F+B (-15.3%) > Blend (-35.4%)
Based on five speeds	
PM mass	Fumigation (1.5%) ≈ **Diesel** > F+B (-20.6%) > Blend (-51%)
TNC	Fumigation (31.6%) > F+B (0.7%) ≈ **Diesel** > Blend (-12.1%)
GMD	Fumigation (0.6%) ≈ **Diesel** > F+B (-5.2%) > Blend (-9%)
Nano-particle concentration	Fumigation (19.8%) > F+B (5.1%) > **Diesel** > Blend (-3.4%)
Ultra-fine particle concentration	Fumigation (32.5%) > F+B (0.8%) ≈ **Diesel** > Blend (-12.1%)
Fine particle concentration	Fumigation (44.3%) > **Diesel** > F+B (-4.4%) > Blend (-21.8%)
Based on four conditions	
PM mass	Fumigation (1.9%) ≈ **Diesel** > F+B (-25.3%) > Blend (-42.5%)
TNC	Fumigation (36.2%) > **Diesel** ≈ F+B (-1.8%) > Blend (-22.3%)
GMD	Fumigation (1.4%) ≈ **Diesel** > F+B (-3.4%) > Blend (-8.8%)
Nano-particle concentration	Fumigation (19.2%) > F+B (3.1%) > **Diesel** > Blend (-9.1%)

Ultra-fine particle concentration	Fumigation (49.4%) > F+B (1.4%) ≈ **Diesel** > Blend (-23.2%)
Fine particle concentration	Fumigation (50.1%) > **Diesel** > F+B (-13.5%) > Blend (-38.5%)
Primary particle diameter	**Diesel** ≈ Fumigation (-1.8%) > F+B (-9.1%) > Blend (-15.0%)
Fringe length	**Diesel** ≈ Fumigation (-2.2%) > F+B (-9.6%) > Blend (-12.9%)
Tortuosity	Fumigation (2.2%) > F+B (0.9%) ≈ Blend (0.4%) ≈ **Diesel**
Fringe separation distance	Fumigation (6.8%) > F+B (5.5%) > Blend (4.4%) > **Diesel**

CHAPTER 8 CHEMICAL PROPERTIES OF PM FOR DIFFERENT FUELING MODES

The results and discussion in regard to the chemical properties of the PM of a diesel engine operated under the four fueling modes and various operating conditions are presented in this chapter. The chemical properties investigated include organic carbon (OC) and elemental carbon (EC), volatile and non-volatile substances (VS and non-VS), oxidation reactivity, water-soluble organic carbon (WSOC), inorganic ions, metals and elements, PAHs and n-alkanes.

8.1 Carbonaceous components analysis

The PM sample contains different components, such as soot, unburned hydrocarbon, inorganic ions, metals, elements and etc. The organic carbon (OC) and elemental carbon (EC), and hence the total carbon (TC) in the PM, can be evaluated as described in Chapter 3.

Fig. 8.1 (a) shows the variation of specific emissions of OC (OC1-OC4), EC (EC1-EC3), total carbon (TC) and PM at four operating conditions for the four fueling modes of operation; while the variation of mass fraction of OC and EC in the TC is shown in Fig. 8.1 (b). The TC is less than that of PM due to the presence of non-carbonaceous substances in the PM. It can be clearly observed from Fig. 8.1 (a) that the TC increases with increasing load or speed for all the four fueling modes. In addition, the EC at the high load of 228 Nm is more than that at the low load of 57 Nm at each tested speed. The increase in TC and EC with increasing engine load was also reported in the literature [223,347-352] using LSD, ULSD, biodiesel, pentanol and butanol. At the higher engine load, the higher combustion temperature, higher mass of fuel consumption and more local fuel-rich regions can promote the formation of EC components [348] and consequently increases the TC.

It can be seen from Fig. 8.1 (b) that the increase in load causes decrease in the mass fraction of OC and increase in mass fraction of EC for all fueling modes; while the engine speed has less influence on these parameters compared to the huge effect of engine load. Generally, EC can be produced via gas-to-particle conversion at high combustion temperature [221,353]. Therefore, at the high load of 228 Nm for each speed

(Fig. 8.1 (a and b)), the EC component of all fueling modes are higher than that at the low load of 57 Nm. At the high engine load, the increasing gas-to-particle transformation in the high temperature environment causes the formation of more EC; while the low oxygen concentration (lower air-fuel ratio) suppresses the oxidation of EC; therefore, there is an increase in EC [348].

In regard to the effect of DBE, Fig. 8.1 (a and b) show that the use of DBE in the blended, F+B or fumigations mode cause decrease in TC, EC and OC (except in the fumigation mode which has higher TC and OC than the diesel mode at low engine loads) at all tested operating conditions compared to the diesel mode. While the blended mode has more effect in reducing TC, EC and OC in comparison with the F+B and fumigation modes. It is because, the blended mode has lower BSFC (less availability of diesel which has sulfur and aromatic components) than fumigation mode. Also, the blended mode has the lowest TNC and the smallest GMD and hence the lowest BSPM, resulting in more effect on the decrease in the TC, EC and OC. However, since the fumigation mode at the low engine loads (57Nm) has the highest TNC, GMD and hence BSPM; therefore it has the highest amount of TC and OC and a small effect on the EC reduction. Thus, it can be found that the amounts of TC, EC and OC can be affected by the number, size and mass of PM (regardless to the effect of oxygen, sulfur and aromatic components of the fuel on the TC, EC and OC). When the particle is in a small size (for instance particle in the blended mode), it contains less carbon layers resulting in lesser formation of TC, EC and OC compared to the large particle size (in the diesel mode).

In addition, it can be seen from Fig. 8.1 (a and b) that OC1 is the major component of OC and EC2 is the major component of EC (except for the blended and F+B modes) and EC3 is almost zero in all the fueling modes at all the tested operating conditions. The amount of EC1 is higher than EC2 for the blended mode; while EC1 is almost equal to EC2 for the F+B mode.

According to the average of four conditions, the reductions in TC are in the order of blended mode (-46.3%) and F+B mode (-28.9%); while the fumigation mode has an equal TC (only -2.1%) compared to the diesel mode. Also, the reductions in EC are in the order of blended mode (-66.1%), F+B mode (-48.4%) and fumigation mode (-25.9%). In addition, the reductions in OC are in the order of blended mode (-19.8%) and F+B mode (-5.5%); while the fumigation mode has higher OC (18.3%) than diesel mode. Some

studies [347,350,354,355] also found that the use of oxygenated fuels like biodiesel and pentanol led to decrease in EC and increase in OC in comparison with those of diesel. Zhang and Balasubramanian [98,223,242,243,356] found that biodiesel, pentanol and butanol generated lower EC than diesel and the proportion of OC in the particles was higher than that of diesel. In addition, the dual-fuel engine using ethanol generated lower EC and higher OC than conventional diesel [357]. The lower aromatic and sulfur contents and the lower C/H mass ratio of the alcohol blend and the higher oxygen content of the fuels [105,350] that lead to the reduction in PM will also cause reduction in TC and EC. In addition, the oxygenate fuels cause increase in free radical concentrations (e.g. O, OH, etc.) resulting in the promotion of carbon oxidation to CO and CO_2 in the premixed flame zone; therefore, less carbon is available for the production of soot precursor species [358]. On the other hand, OC is mainly generated from the incomplete combustion of fuel and lubricating oil, while the lower combustion temperature of alcohol blend can inhibit the pyrolysis of the fuel and lubricating oil which causes the increase in OC compared to the diesel fuel [348]. However, in this study, increase in OC is recorded only in the fumigation mode. Because the fumigation mode has the lowest BTE, and the highest BSFC and BSHC, resulting in more availability of ethanol which has high vaporization enthalpy to form OC, compared to the other fueling modes which have no ethanol consumption (diesel mode) and lower ethanol consumption (blended mode). Since the amounts of PM and TC in the blended mode are very low compared to the diesel mode; therefore, the OC is also lower than that of the diesel mode. However, the ratio of OC/TC of the blended mode is higher than that of the diesel mode, and even the fumigation mode (Fig. 8.2 (a)).

It can be observed from Fig. 8.2 (a-d) that the use of biodiesel and ethanol in the blended, F+B or fumigation mode has an effect on reducing the ratios of EC/TC and TC/PM (insignificant reduction) and increasing the ratios of OC/TC and OC/EC at all the tested operating conditions compared to those of the diesel mode; while the blended mode has the highest impact. On the average of four operating conditions (Fig. 8.2 (a-d)), the ratios of OC/TC are 0.44 for diesel mode, 0.65 for blended mode, 0.58 for F+B mode and 0.54 for fumigation mode. The EC/TC ratios are 0.56 for diesel mode, 0.35 for blended mode, 0.42 for F+B mode and 0.46 for fumigation mode. Also, the ratios of OC/EC are 0.99 for diesel mode, 4.11 for blended mode, 2.10 for F+B mode and 1.80 for fumigation mode. In addition, for the TC/PM ratio, it can be found from Fig. 8.1 (a) and Fig. 8.2 (d) that on

the average of four conditions, the TC/PM ratios are about 0.858 for diesel mode, 0.804 for blended mode, 0.815 for F+B mode and 0.826 for fumigation mode. Guarieiro et al. [359] reported that 80% to 90% of particle emissions from diesel engine consist of organic and inorganic carbons. Similarly, Lu et al. [347] found the carbon emissions (OC+EC) were more than 80% of the $PM_{1.8}$ emission for LSD, ULSD and biodiesel. Miguel and Hansen [360] also found that the TC/PM mass ratio was 0.85 and the ratio of OC/TC was 0.51, the ratio of EC/TC was 0.49 and EC/PM mass was 0.41 in diesel engine fueled with diesel.

It can be inferred from the results that the blended mode is more effective on the reduction of TC and EC than the fumigation mode; while the F+B has the TC and EC values in between those of the blended and fumigation modes. The lowest amount of TC and EC and also higher EC1 than EC2 in the blended mode can be attributed to the lowest PM mass, TNC, GMD, primary particle diameter, fringe length and weak connection between the particles (regarding to the physical properties of PM) in the blended mode as discussed above. However, the fumigation mode, which use the same fuel of the blended mode, has less effect on the reduction in TC and EC, which shows that the effect of fueling mode is stronger than the type of fuel being used. This effect is more sensitive at low load (low combustion temperature). Because, it can be seen from Fig. 8.1 (a) that the differences between PM, TC, EC and OC of the blended and fumigation modes are high at low engine loads; while there are less differences in these parameters at high loads. However, the effect of engine speed is not observed. This is because the increase in engine speed has less effects on the combustion and performance parameters, e.g. peak HRR, DOC, diffusion combustion phase, exhaust gas temperature and equivalence ratio, and also has opposite effects on ID and BTE in comparison with the increase in engine load.

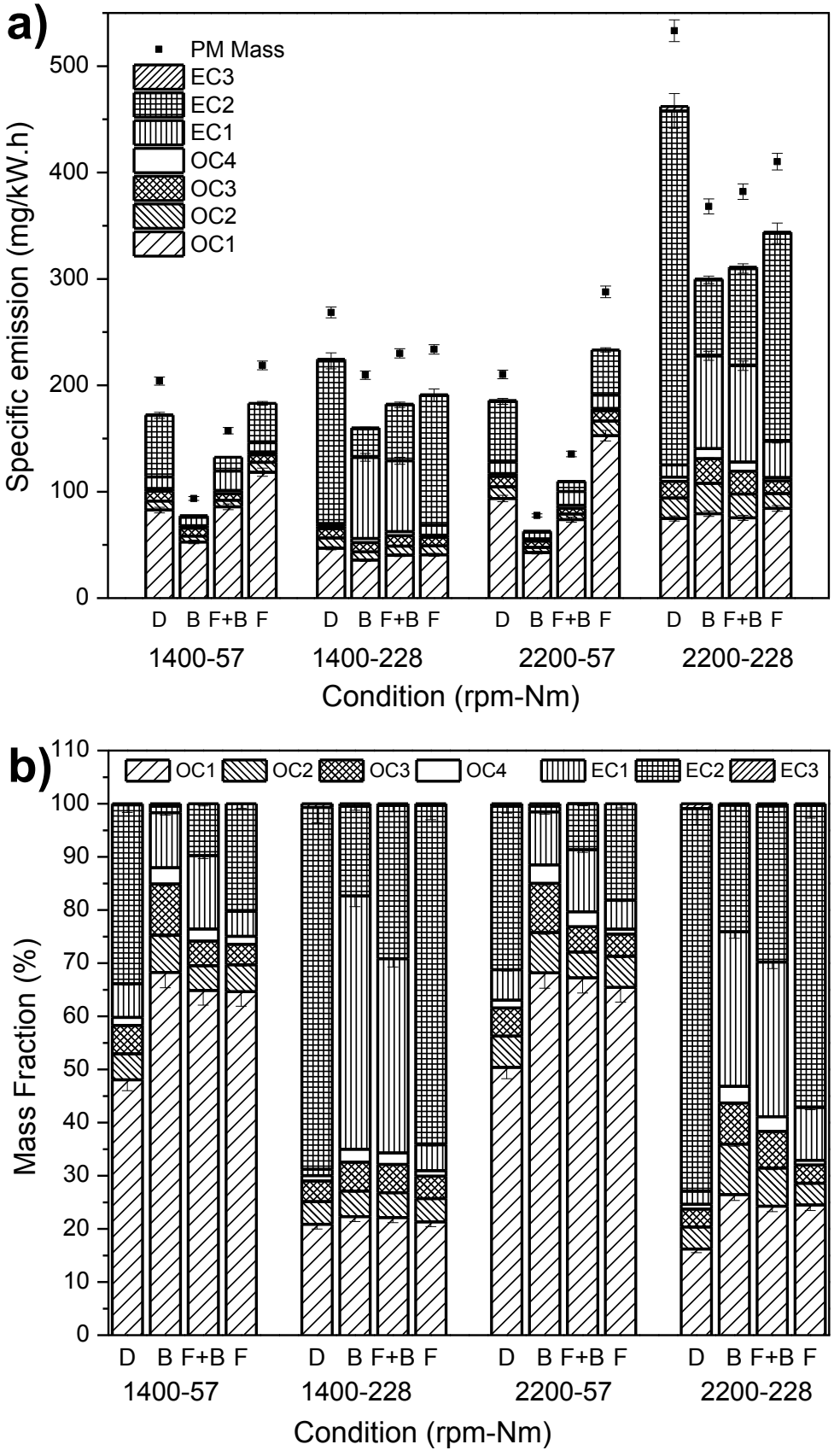

Fig. 8.1 Variations of (a) specific emission and (b) mass fraction of OC1-OC4 and EC1-EC3 in TC for diesel (D), blended (B), F+B and fumigation (F) modes with engine speed and load.

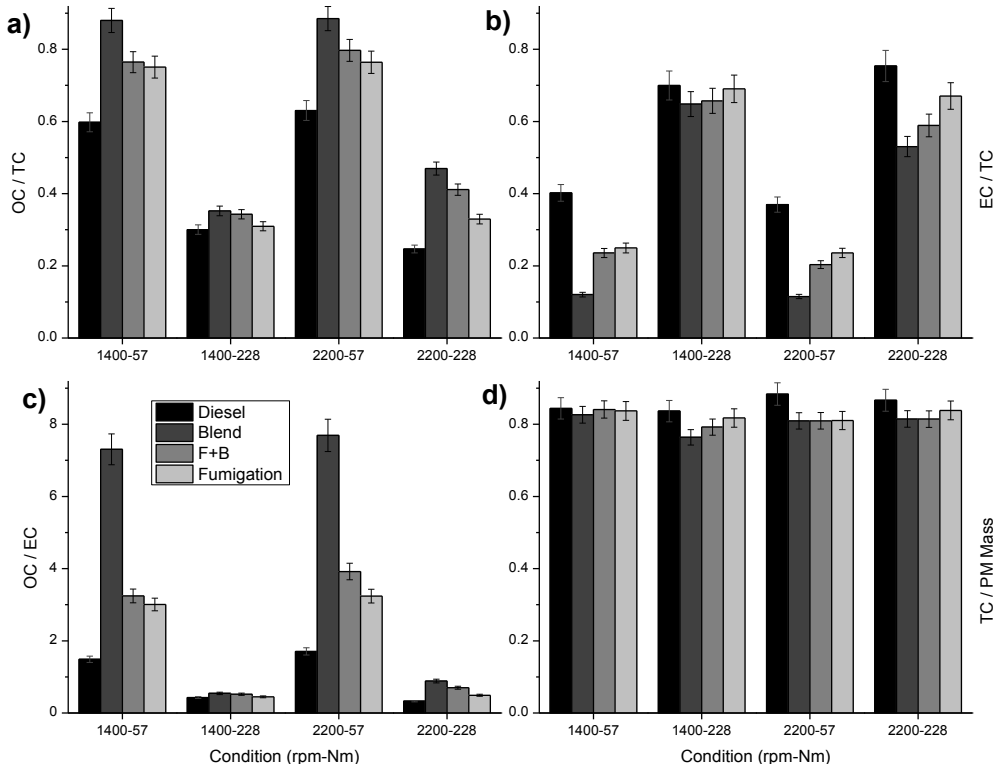

Fig. 8.2 Variations of (a) OC/TC, (b) EC/TC, (c) OC/EC and (d) TC/PM mass ratios with engine speed and load.

8.2 Particle volatility and oxidation reactivity

8.2.1 Volatile and non-volatile substances

Fig. 8.3 shows the particle mass reduction curve for different fueling modes and operating conditions. The substances, according to the temperature at which mass reduction occurs, can be categorized into volatile organic fractions (%VOF) and non-volatile organic fractions (% non-VOF). The VOF, which is mostly OC, can be divided into high-volatile substances (H-VS) with the TGA furnace temperature range of 50°C ≤ T ≤ 250°C and low-volatile substances (L-VS) with the TGA furnace temperature range of 250°C < T ≤ 400°C. The non-VOC or called non-volatile substances (non-VS), which are mostly EC, are the substances available at the TGA furnace temperature range of 400°C < T ≤ 850°C. The results of these three groups of substances are presented in Fig. 8.4. It can be seen from Fig. 8.3 and Fig. 8.4 that the increase in engine load causes reduction in mass fraction of H-VS and increase in mass fraction of non-VS for all fueling modes; while the engine speed has less influence on these parameters, which are consistent with the findings for OC and EC as shown in Fig. 8.1 (b). Similar trends

(reduction in H-VS and increase in non-VS due to increase in engine load) were found in the literature using diesel, biodiesel and DBE [128,146,336,361]. On the average of four operating conditions from Fig. 8.3 and Fig. 8.4, the increases in H-VS mass fractions are 12.8% for the blended mode, 9.4% for the F+B mode and 6.9% for the fumigation mode, compared to the diesel mode. Also the blended mode has a small effect on the increase in L-VS (4.5%); while the F+B (1.6%) and fumigation (-0.6%) modes have similar mass fraction of L-VS, compared to the diesel mode. In addition, the reductions in the mass fraction of non-VS are -25.1%, -16.9% and -11.1% for the blended, F+B and fumigation modes, respectively, in comparison with the diesel mode. According to the results, it can be revealed that the blended mode has the highest mass fraction of H-VS and the lowest mass fraction of non-VS at all the operating conditions among all the fueling modes, which are in line with OC-EC results. The mass fractions of L-VS under all the fueling modes are almost equal. Other studies also found that DBE and biodiesel led to higher VOF and lower non-VS than diesel fuel [128,146,336,338,362].

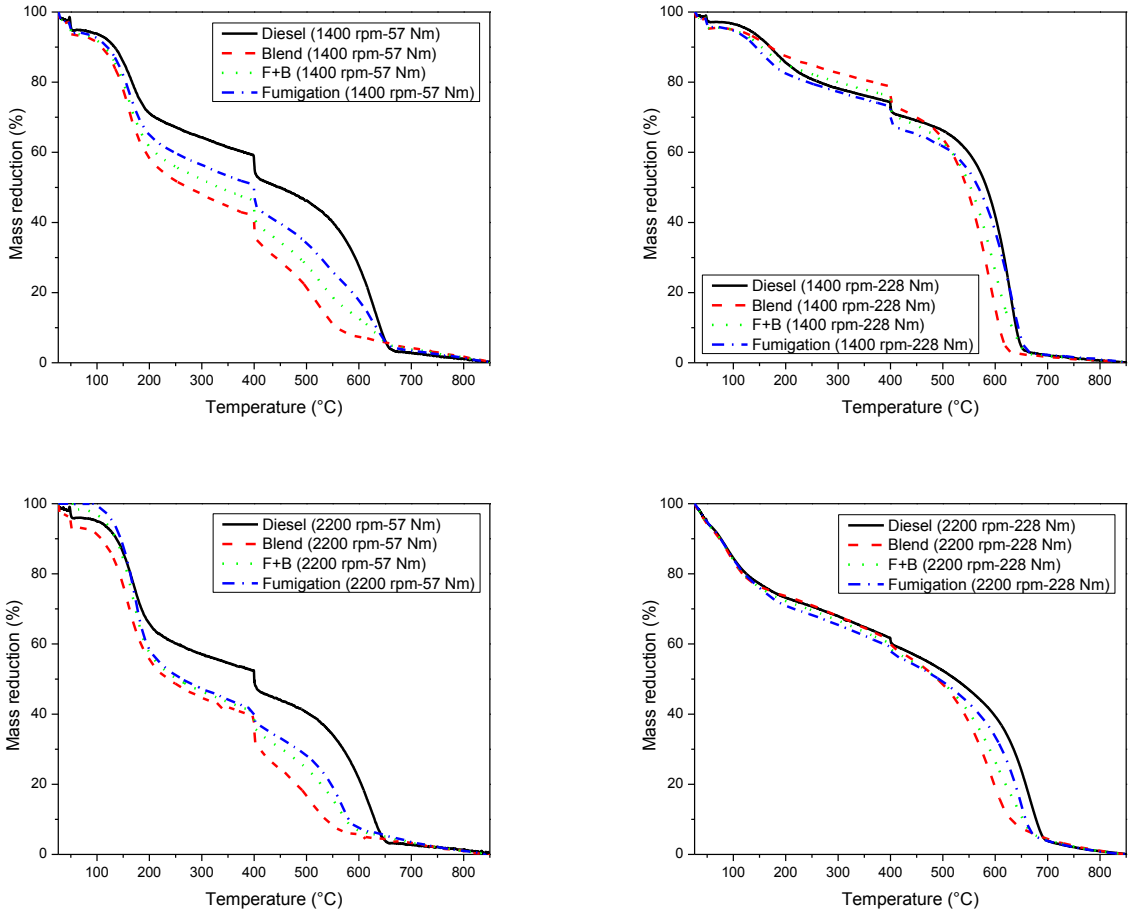

Fig. 8.3 Particle mass reduction curve for different fueling modes and operating conditions.

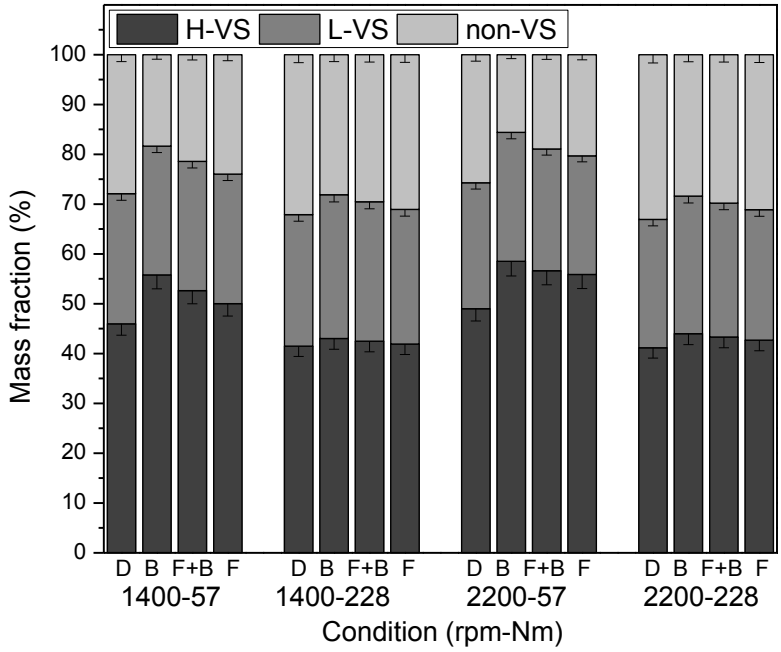

Fig. 8.4 H-VS, L-VS and non-VS compositions of particles for diesel (D), blended (B), F+B and fumigation (F) modes at different operating conditions.

8.2.2 Particle oxidation kinetic parameters

The particle oxidation kinetic parameters in this study include the activation energy (E) and frequency factor (A) which are calculated in the TGA furnace temperature range of 400°C to 850 °C. The activation energy and frequency factor for various fueling modes and operating conditions are presented in Table 8-1. The range of activation energy is from 126.9 kJ/mol to 209.9 kJ/mol for diesel mode as shown in Table 8-1 which is in line with results reported in the literature. According to the literature, the range of activation energy for soot particles with diesel fuel is from about 100 kJ/mol to about 200 kJ/mol, under different operating conditions [146,250,335,336,338,363-366]. In addition, the range of frequency factor for soot oxidation for the diesel mode in this study is also consistent with results reported in the literature [146,336,338,366]. It can be seen that the increase in engine load or speed (except at the operating condition of 1400rpm-57Nm) cause increase in both activation energy and frequency factor due to increase in amount of EC.

According to Table 8-1, the DBE used in the blended, F+B and fumigation modes has an effect on the reduction in activation energy and frequency factor at all the operating

conditions (except activation energy for fumigation mode at low loads) compared to the diesel mode. On the average of four operating conditions, the reductions in activation energy are -34.0% for blended mode, -10.6% for F+B mode and -4.9% for fumigation mode. Also, the reductions in frequency factor are -96.9% for blended mode, -84.7% for F+B mode and -53.0% for fumigation mode. Since the higher activation energy means that the PM has lower oxidation reactivity; therefore, it can be inferred that PM emitted from the blended mode has the highest oxidation reactivity, due to the lowest mass fraction of non-volatile and highest mass fraction of VOF, among all the fueling modes. Yehliu et al. [367] also found that the soot reactivity increases with increase in VOF. The reduction in activation energy (even up to 65.2 kJ/mol) and frequency factor was also reported in the literature using DBE and biodiesel [146,336,338,365,366,368].

Table 8-1 Particle oxidation kinetic parameters for different fueling modes and operating conditions

Parameter	**Mode**	**1400rpm-57Nm**	**1400-228**	**2200-57**	**2200-228**
E (SD) (kJ/mol)	Diesel	145.4 (1.4)	179.2 (1.9)	126.9 (1.7)	209.9 (2.3)
	Blend	79.9 (1.3)	139.3 (1.3)	61.2 (1.5)	174.3 (3.1)
	F+B	136.2 (1.7)	149.3 (3.9)	118.7 (4.3)	182.8 (3.3)
	Fumigation	148.4 (2.5)	156.0 (1.7)	126.7 (1.3)	191.7 (1.9)
A (SD) (s^{-1})	Diesel	4.9E+06 (1.3E+04)	2.2E+08 (1.7E+04)	3.3E+05 (8.1E+03)	3.1E+08 (4.8E+04)
	Blend	3.5E+04 (1.2E+02)	3.2E+06 (1.1E+04)	2.6E+04 (1.3E+02)	7.6E+06 (3.1E+04)
	F+B	8.0E+05 (1.5E+04)	4.0E+06 (3.5E+04)	1.3E+05 (3.9E+02)	1.6E+07 (3.4E+04)
	Fumigation	3.6E+06 (2.3E+04)	1.4E+07 (1.5E+04)	3.1E+05 (1.2E+04)	5.1E+07 (3.8E+04)

8.2.3 Particle oxidation reactivity versus particle structure parameters

Since diesel engines can produce reactive soot particles which are harmful for environmental chemistry, climate and public health; therefore, there are needs of increase in the knowledge and information about the relationship between the soot structure and soot reactivity [41]. Some studies have been conducted to investigate the relationship between the nano-structure of particle with soot reactivity [41,335,367] which found that

the increase in fringe length or decrease in tortuosity caused lower oxidation reactivity of the particles. In this study, the relationship between activation energy (representing oxidation reactivity) with primary particle diameter, fringe length, tortuosity and fringe separation distance for the four operating conditions (each point in the graph represents one operating condition) is presented in Fig. 8.5 (a-d), respectively. It can be seen that the increase in primary particle diameter and fringe length and decrease in tortuosity and fringe separation distance have effect on the increase in activation energy (lower oxidation reactivity) of PM for all the fueling modes. Since the diesel mode has the largest primary particle diameter and fringe length and lowest tortuosity and fringe separation distance; therefore, it has the highest activation energy (lower oxidation reactivity) of PM. Because, as mentioned in micro-structure and nano-structure sections, these parameters inhibit the accessibility of oxygen into the carbon layers for oxidation; therefore, the PM emitted from the diesel mode has the lowest oxidation reactivity. On the other hand, the ethanol and biodiesel in combustion and PM formation process have an effect to reduce the primary particle diameter and fringe length and increase the tortuosity and fringe separation distance resulting in more accessibility of oxygen into the carbon layers and hence higher oxidation reactivity. In addition, the use of ethanol and biodiesel can inhibit the stacking of primary particles together (graphite-like) for the formation of large agglomerates and clusters. Therefore, the agglomerates and clusters are in small size and the particles have a loose connection (as shown in Figs. 7.16 and 7.17). Thus, oxygen can pass easily through the single particles or small agglomerates with loose connection between the particles, resulting in increase in oxidation reactivity. Also, the higher oxygen concentration of ethanol and biodiesel promotes the oxidation reactivity compared to diesel fuel. However, these effects of ethanol and biodiesel are more obvious in the format of the blended mode. The fumigation mode has lower effect on oxidation reactivity compared with the blended mode due to the reasons mentioned in regard to BSPM, TNC, GMD and morphology of aggregate particles.

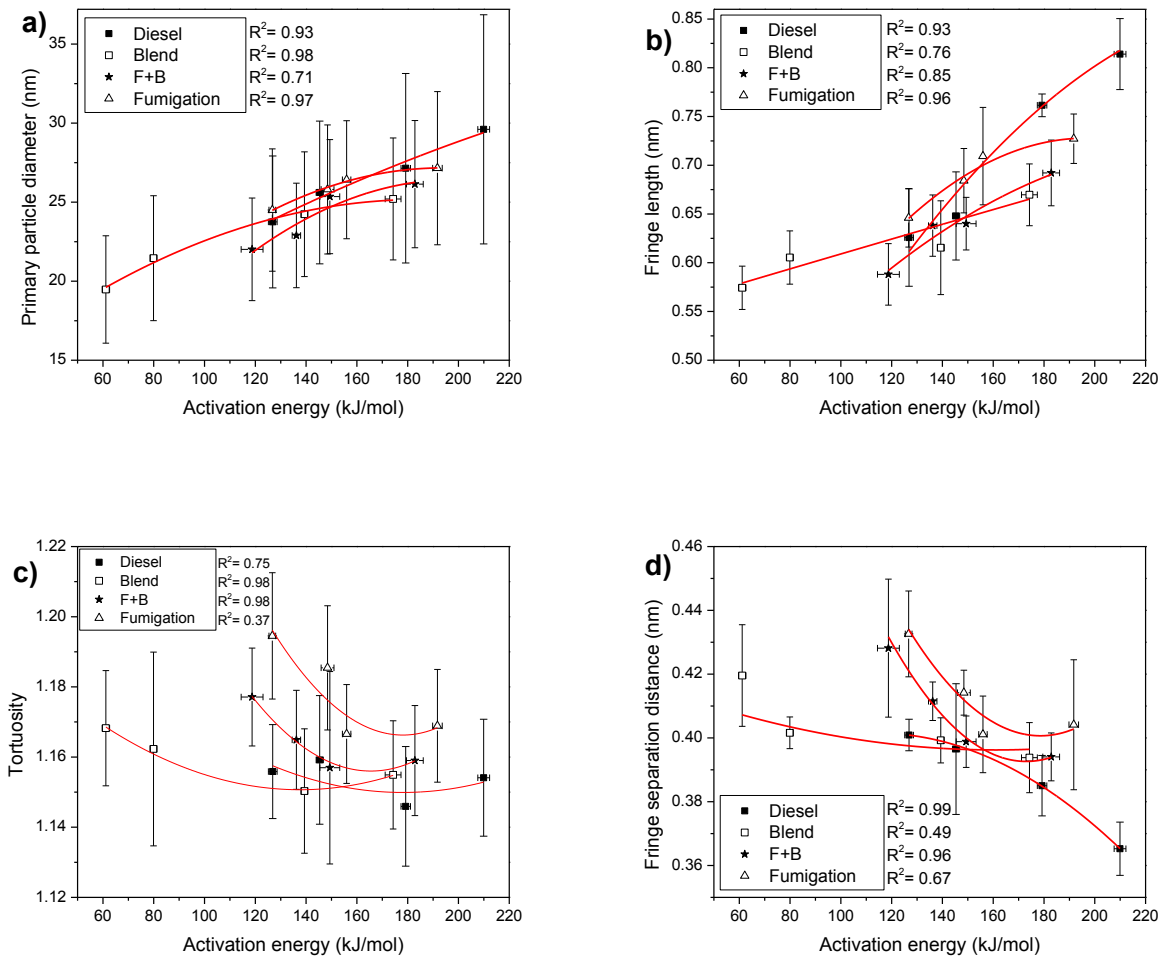

Fig. 8.5 Activation energy versus (a) primary particle diameter (b) fringe length, (c) tortuosity and (d) fringe separation distance for different fueling modes and conditions.

8.3 Water-soluble organic carbon

Fig. 8.6 (a-c) illustrate the variations of water-soluble total carbon (WSTC), water-soluble inorganic carbon (WSIC) and water-soluble organic carbon (WSOC) with engine speed and load. The WSTC decreases with engine load (except for the blended mode which increases with engine load), but increases with engine speed for the four fueling modes. The WSIC increases with both engine load and engine speed for the four fueling modes. The WSOC decreases with engine load (except for the blended mode which increases with engine load), but increases with engine speed for the four fueling modes. Some studies also found that the increase in engine load led to reduction in WSOC for diesel, biodiesel, butanol and pentanol [92,242] due to decrease in OC. Fig. 8.6 (a and c) also show that the trends of WSTC and WSOC are similar to the trends of TC and OC

shown in Fig. 8.1 (a and b). It can be seen from Fig. 8.6 that the blended, F+B and fumigation modes cause increase in WSTC and WSOC and reduction in WSIC compared to the diesel mode in the four operating conditions, except that the blended mode leads to opposite results for WSTC and WSOC at the low load. It is because at the low engine load, the amount of PM mass, TC and OC of the blended mode are very low, resulting in the formation of less WSTC and WSOC compared to the diesel mode. On the other hand, at the high engine load, the OC contents are almost equal for all the fueling modes; therefore, the effect of the amount of OC is neglected resulting in higher WSOC in the blended mode, compared to the diesel mode.

On the average of four conditions, the increases in the WSTC and WSOC are in the order of fumigation mode (39.4% and 44%), F+B mode (19.6 % and 23.6%) and blended mode (2.1 % (no significant difference with T-test) and 7%) compared to those of the diesel mode. And the reduction in WSIC is in the order of blended mode (-55.8%), F+B mode (-33.1%) and fumigation mode (-24.5%) in comparison with the diesel mode. Since the fumigation mode contains higher PM mass, TC and OC; therefore, more TC and OC can be dissolved in water resulting in higher WSTC and WSOC. The increase in WSOC using oxygenated fuels like biodiesel, butanol and pentanol compared to pure diesel is also reported in the literature [92,242,243]. Since the WSOC consists of almost oxygen-containing compounds [260]; therefore, the DBE (as an oxygenated fuel) has higher WSOC than pure diesel due to its higher oxygen concentration. In addition, the oxygen content of oxygenated fuels cause increase in the water solubility of OC, resulting in higher formation of polar organic compound and WSOC [242]. Since the fumigation mode has very high OC concentration; therefore, this mode has the highest effect on the increase in WSOC (44% increase compared to the diesel mode). On the other hand, the blended mode has very low OC concentration resulting in only 7% increase in WSOC compared to the diesel mode. While on the average of four operating conditions, the blended mode has the highest WSOC/OC ratio among all the fueling modes, as shown in Fig. 8.7 (b). Fig. 8.7 (a-d) show the variations of WSOC/WSTC, WSOC/OC, WSOC/TC and WSOC/PM mass ratios under the four operating conditions. It can be seen that the WSOC is a major component of WSTC, because the WSOC/WSTC ratio is more than 0.90 for all the fueling modes at all the tested operating conditions. According to Table 8-2, the blended, F+B and fumigation modes have higher WSOC/WSTC, WSOC/OC, WSOC/TC and WSOC/PM ratios than those of the diesel mode; while the blended mode

has the highest values. Popovicheva et al. [260] also observed an increase in WSOC/PM mass using biofuel compared to diesel. In addition, the rise in WSOC/OC was also reported in the literature [92,242,243] using biodiesel, butanol and pentanol. The results show that the WSOC/OC ratio is in the range of 0.13- 0.19 for the diesel mode and it is in the range of 0.14-0.31 for the other three modes, depending on the operating condition. The literature [92,242,243] also showed that the WSOC/OC ratio for diesel was up to 0.20, and the biofuel had higher WSOC/OC ratio of up to 0.30 at low, medium and high engine loads.

Table 8-2 Variations of WSOC/WSTC, WSOC/OC, WSOC/TC and WSOC/PM mass ratios based on average of four conditions

Ratio	Diesel mode	Blended mode	F+B mode	Fumigation mode
WSOC/WSTC	0.93 (±0.16)[a]	0.97 (±0.17)	0.96 (±0.16)	0.96 (±0.16)
WSOC/OC	0.16 (±0.02)	0.23 (±0.03)	0.22 (±0.03)	0.21 (±0.02)
WSOC/TC	0.07 (±0.01)	0.15 (±0.01)	0.13 (±0.01)	0.10 (±0.01)
WSOC/PM mass	0.06 (±0.01)	0.12 (±0.01)	0.10 (±0.01)	0.09 (±0.01)

a: ± standard error at 95% confidence level.

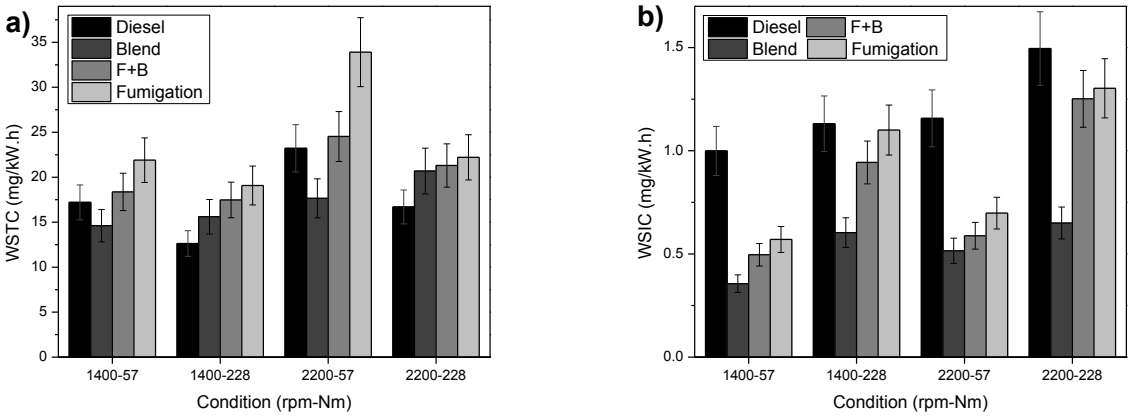

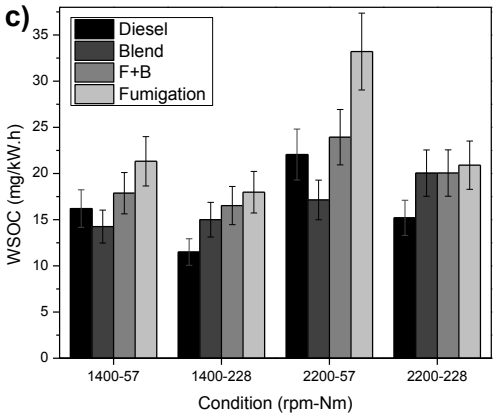

Fig. 8.6 Variations of (a) WSTC, (b) WSIC and (c) WSOC with engine speed and load.

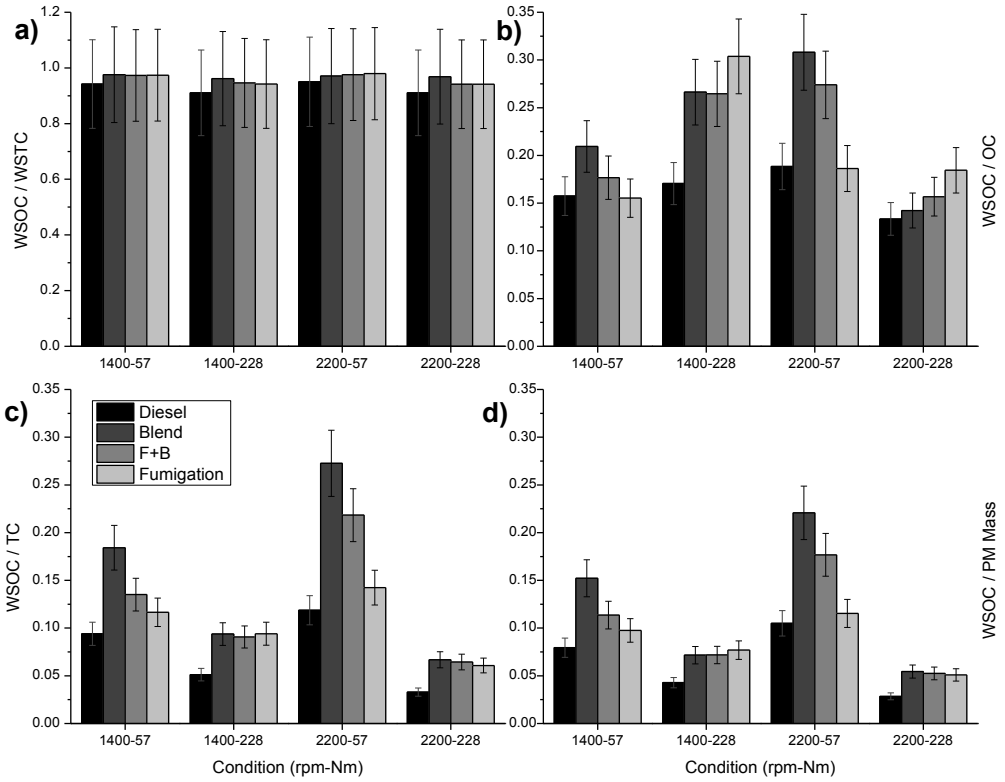

Fig. 8.7 Variations of (a) WSOC/WSTC, (b) WSOC/OC, (c) WSOC/TC and (d) WSOC/PM mass ratios with engine speed and load.

8.4 Particle-phase organic compounds

8.4.1 Particle-phase polycyclic aromatic hydrocarbons (PAHs)

Table 8-3 shows the variation of individual PAH for diesel, blended, F+B and fumigation modes under two engine loads (low and high) at a constant speed of 2200rpm. In addition, the variation of PAHs concentration based on low (MW $\leq$ 200), medium (200 < MW $\leq$ 250) and high (MW > 250) molecular weight (MW) for the four fueling modes is presented in Fig. 8.8. It can be seen that almost all the measured PAHs increase with increase in engine load for all the fueling modes. Because, the increase in engine load causes increase in F/A ratio and combustion temperature resulting in more decomposition of olefinic and olefins radicals and hence formation of more alkynes and alkadienes, which are the major precursors of the PAH components or resulting in more pyrosynthesis (synthesis resulting from or initiated by the action of heat) of the fuel fragments and hence more PAH formation [147,369]. Other studies also found increase in most of the PAHs due to increase in engine load using diesel, biodiesel, BPe and DBE [147,347,350]. In addition, it is observed that the blended, F+B and fumigation modes can reduce the PAHs at both loads (except for the fumigation mode at low load), compared to the diesel mode. According to the average of two engine loads, the blended mode has lower PAHs based on L-MW (-73.9%), M-MW (-64.4%), H-MW (-86.0%) and total PAHs (-78.4%), compared to the diesel mode. The F+B mode also has lower PAHs based on L-MW (-56.8%), M-MW (-41.3%), H-MW (-65.7%) and total PAHs (-57.6%). The fumigation mode causes lower PAHs based on L-MW (-42.4%), H-MW (-42.1%) and total PAHs (-31.3%); while there is no effect on M-MW PAHs (-1.3%) due to high concentration of M-MW PAHs at low load. It is because when operating at low engine load under the fumigation mode, the combustion temperature is very low, resulting in incomplete combustion and increase in the amount of unburned fuel, which are the factors for the formation of PAHs (Fig. 8.8). Since both ethanol and biodiesel do not contain PAHs and have oxygen in their molecules [147]; therefore, the blended, F+B and fumigation modes have lower PAHs compared to the diesel mode. However, the fumigation mode has the lowest effect on the reduction in PAHs due to the highest fuel consumption at both loads and incomplete combustion (more unburned fuel) at low load among the blended, F+B and fumigation modes. The reduction in PAHs using biodiesel, BPe and DBE was also reported in [147,347,350].

Also, it can be seen from Table 8-3 that the blended (-88.4%), F+B (-80.7%) and fumigation (-50.7%) modes can reduce the benzo[a]pyrene which is the most toxic species among the measured PAHs. It was observed from an investigation [370] that the surviving fuel from the combustion was the major source of benzo[a]pyrene in the diesel engine; while pyrosynthetic formation inside the combustion chamber and lubricating oil had effect of not more than 20% of total-PAHs formation. Therefore, in the present study the ethanol and biodiesel have effect on the reduction in benzo[a]pyrene mainly because they do not contain PAHs. It can be concluded from the above results that the blended mode has the lowest PAHs among all the fueling modes. However, the fumigation mode can reduce the PAHs only at high engine load which are similar to the reduction of PM mass, TNC and other chemical properties of PM.

Table 8-3 Individual PAH for different fueling modes and loads at 2200rpm, (mean±SD; µg/kwh)

Species name	MW[a]	Ring No.	Diesel (57 Nm)	Diesel (228 Nm)	Blend (57)	Blend (228)	F+B (57)	F+B (228)	F (57)	F (228)
1-Naphthaldehyde	156	2	25.1 ±1.0	162.8 ±5.1	5.8 ±0.2	45.4 ±1.7	8.7 ±0.3	73.6 ±3.0	9.3 ±0.3	104.8 ±3.6
Fluorene	166	3	118.8 ±3.9	161.3 ±6.0	-[b]	113.4 ±4.3	24.5 ±0.8	126.7 ±4.5	38.2 ±1.4	165.7 ±5.5
Phenanthrene	178	3	112.6 ±3.7	553.0 ±20.0	25.8 ±0.8	163.9 ±6.3	50.7 ±1.7	214.7 ±7.7	73.6 ±2.4	260.2 ±9.3
Anthracene	178	3	33.6 ±1.7	70.0 ±5.2	-	62.5 ±3.3	16.2 ±0.9	69.4 ±9.5	34.3 ±1.6	60.1 ±3.5
9-Fluorenone	180	3	48.9 ±1.6	272.3 ±7.4	13.4 ±0.4	89.4 ±3.0	33.2 ±1.0	90.2 ±2.8	43.6 ±1.7	99.2 ±3.2
Fluoranthene	202	3	242.8 ±8.1	990.1 ±34.7	115.7 ±3.9	304.0 ±10.7	140.8 ±4.4	421.7 ±13.8	172.2 ±5.8	576.6 ±20.2
Pyrene	202	4	772.9 ±24.7	4382.9 ±139.5	336.0 ±11.2	1017.2 ±38.3	746.5 ±23.3	1484.1 ±47.6	1574.6 ±52.5	1797.9 ±60.6
9,10-Anthraquinone	208	3	75.6 ±2.1	1030.6 ±31.1	45.2 ±1.3	61.6 ±1.5	43.5 ±1.3	67.8 ±2.0	49.1 ±1.7	79.3 ±2.4
Benzo[a]anthracene	228	4	67.4 ±2.1	208.9 ±6.6	56.6 ±1.9	71.1 ±2.7	61.1 ±1.9	81.5 ±2.6	63.0 ±2.2	88.6 ±3.2
Chrysene	228	4	28.0 ±1.0	104.2 ±3.5	27.2 ±0.9	41.4 ±1.4	31.9 ±1.0	40.1 ±1.4	26.2 ±0.9	44.1 ±1.6
Benzo[b]fluoranthene	252	5	60.4 ±2.4	246.0 ±8.4	23.3 ±0.8	79.7 ±2.5	34.8 ±1.1	84.3 ±2.8	35.5 ±1.3	103.5 ±3.5
Benzo[k]fluoranthene	252	5	94.6 ±4.3	329.4 ±11.7	33.8 ±1.2	73.2 ±2.3	46.2 ±1.5	87.2 ±3.4	61.7 ±2.5	147.3 ±4.1
Benzo[a]fluoranthene	252	5	27.8 ±1.4	56.5 ±2.2	4.2 ±0.2	15.5 ±0.5	13.2 ±0.4	19.4 ±1.0	13.2 ±0.5	21.4 ±0.6
Benzo[e]pyrene	252	5	0.3 ±0.0	1.6 ±0.1	0.1 ±0.0	0.5 ±0.0	0.4 ±0.0	0.3 ±0.0	0.2 ±0.0	0.6 ±0.0
Benzo[a]pyrene	252	5	99.7 ± 2.8	366.0 ±14.1	18.4 ±0.6	35.4 ±1.4	35.2 ±1.1	54.7 ±1.5	72.3 ±2.5	157.2 ±5.4
Perylene	252	5	103.4 ±3.9	297.5 ±11.2	15.6 ±0.5	58.0 ±2.2	31.3 ±1.4	64.4 ±2.4	50.7 ±1.8	124.6 ±3.8
6H-Benzo(c,d)pyrene-6-one	254	5	40.8 ±1.2	186.4 ±5.6	-	35.9 ±1.1	33.1 ±1.0	32.9 ±1.0	37.9 ±1.1	55.9 ±1.7
Benzo(a)anthracene-7,12-dione	258	4	88.9 ±2.7	2661.8 ±79.9	-	64.1 ±1.7	104.8 ±3.7	128.2 ±4.3	112.0 ±3.4	204.1 ±6.2
Indeno[1,2,3-cd]pyrene	276	6	1613.5 ±82.4	1577.4 ±60.0	321.3 ±10.5	293.5 ±11.4	866.7 ±38.8	674.1 ±34.5	1198.2 ±47.5	999.3 ±29.7

Benzo[ghi]perylene	276	6	-	-	-	-	-	-	-	-
Dibenzo[a,h]anthracene	278	5	-	-	-	-	-	-	-	-
Coronene	300	6	1129.1 ±33.5	159.4 ±4.9	117.1 ±3.9	32.9 ±1.3	384.0 ±11.8	47.7 ±1.5	1088.0 ±50.4	118.1 ±4.5
Dibenzo(a,e)pyrene	302	6	94.4 ±2.8	0.0 ±0.0	12.4 ±0.4	0.0 ±0.0	67.6 ±2.1	0.0 ±0.0	110.6 ±3.7	0.0 ±0.0

a: molecular weight [371-373]; b: below detection limit

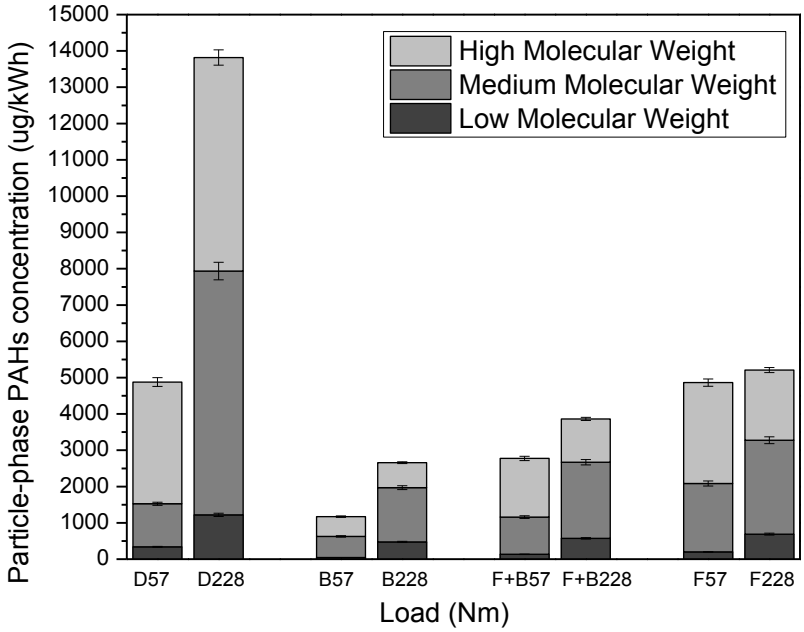

Fig. 8.8 Variation of total PAHs concentration based on low (MW ≤ 200), medium (200 < MW ≤ 250) and high (MW > 250) molecular weight for different fueling modes and loads (57Nm and 228Nm) at 2200rpm.

8.4.1.1 Toxicity consideration of PAHs based on benzo[a]pyrene (BaP)

Since BaP is the most toxic components among the 16 United States Environmental Protection Agency (U.S.EPA) priority PAHs; therefore, it is selected as a reference to obtain the overall toxicity of PAHs. Nisbet and LaGoy [255] proposed a specific toxic equivalent factor (TEF) using the BaP as a reference to calculate the overall toxicity of PAHs. The overall toxicity of PAHs based on BaP can be calculated from equation below.

$$BaP_{eq} = \sum C_i \times TEF_i \qquad 8.1$$

Where, BaP_{eq} is the benzo[a]pyrene equivalent (total toxicity of PAHs), C_i is the concentration of each PAH component and TEF_i is the specific toxic equivalent factor for

each PAH component.

It can be seen from Fig. 8.9 that the blended, F+B and fumigation modes can effectively reduce the BaP_{eq} at both engine loads compared to the diesel mode; while the blended mode has the highest reduction in BaP_{eq} due to its lowest PAHs concentration. On the average of two engine loads, the reductions in BaP_{eq} are -81.7% for blended mode, -63.5% for F+B and -38.9% for fumigation mode in comparison with the diesel mode.

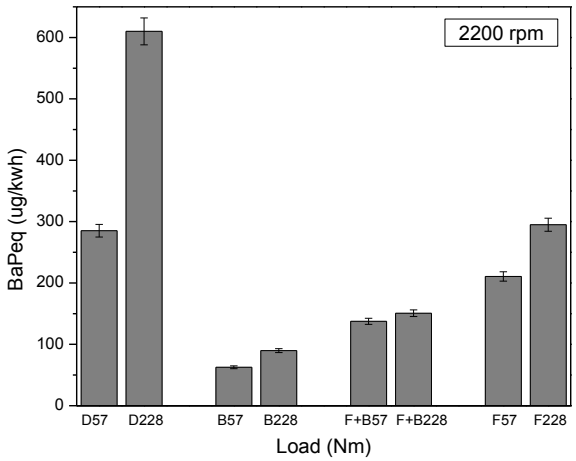

Fig. 8.9 Variation of BaP_{eq} for different fueling modes and loads (57Nm and 228Nm) at 2200rpm.

8.4.2 Particle-phase n-alkanes

Fig. 8.10 illustrates the distribution of particle-phase n-alkanes from C16-C30 for different fueling modes at low and high engine loads at a constant engine speed of 2200 rpm. Fig. 8.11 also shows the total n-alkanes concentrations classified into medium chain (C16-C22) and long chain (C23-C30). The n-alkanes classification based on number of carbon in the chain is followed by [147]; while the short chain is not considered in this study because most of n-alkanes in low chain are in gas-phase due to their vapor pressure. It can be seen from Fig. 8.10 and Fig. 8.11 that the concentrations of almost all the n-alkanes increase with increase in engine load which is due to the higher fuel equivalence ratio and hence the formation of more HC and PM. In addition, Fig. 8.10 and Fig. 8.11 also show that medium chain n-alkanes is the major component for all the fueling modes; while the distribution of particle-phase n-alkanes is like a bell shape (similar to [243] for C14-C26 with C21 as the most abundant component) and the C20 is the most abundant component at low load and C19 is the most abundant component at high engine load.

Other studies also reported that medium chain n-alkanes was the major component using diesel and oxygenated fuels [147,243].

It can be found from Fig. 8.10 and Fig. 8.11 that the DBE used in the blended, F+B and fumigation modes can reduce almost all the medium and long chain n-alkanes at both loads (except medium chain at low load for fumigation) compared to the diesel mode. On the average of two engine loads, the blended mode has lower medium chain (-45.1%), long chain (-55.9%) and total n-alkanes (-46.5%) in comparison with the diesel mode. The F+B mode also has lower medium chain (-32.8%), long chain (-40.9%) and total n-alkanes (-33.9%). The fumigation mode also causes reduction in medium chain (-18.9%), long chain (-39.9%) and total n-alkanes (-21.5%). The reduction in n-alkanes using DBE is due to the lower C and H contents and higher oxygen content of ethanol and biodiesel compared to the diesel fuel. Guan et al. [147] also found that the use of oxygenated fuel like DB and DBE reduced the n-alkanes compared to the diesel fuel. Since the fumigation mode has higher fuel consumption at both engine loads and more incomplete combustion due to lower combustion temperature at low engine load; therefore, it has less effect on the reduction in n-alkanes compared to the blended mode.

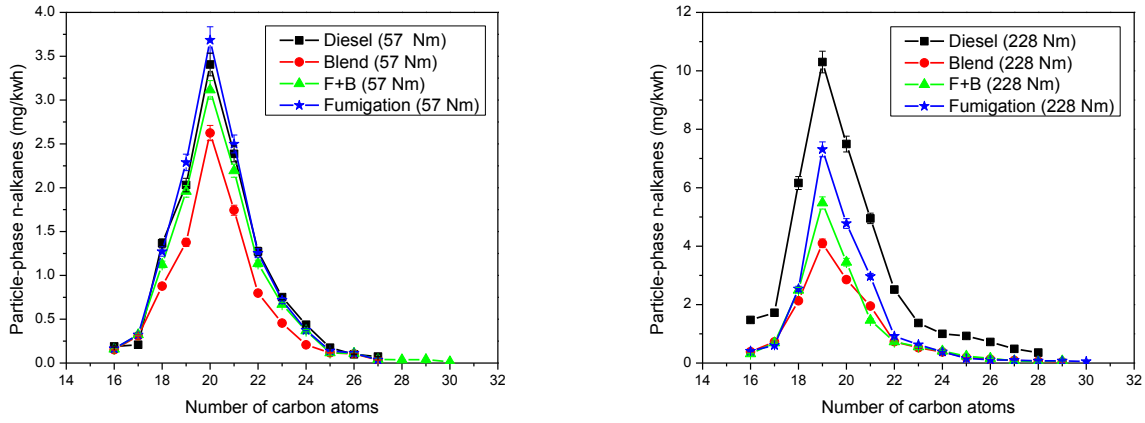

Fig. 8.10 Variation of n-alkanes concentration for different fueling modes and loads (57Nm and 228Nm) at 2200rpm.

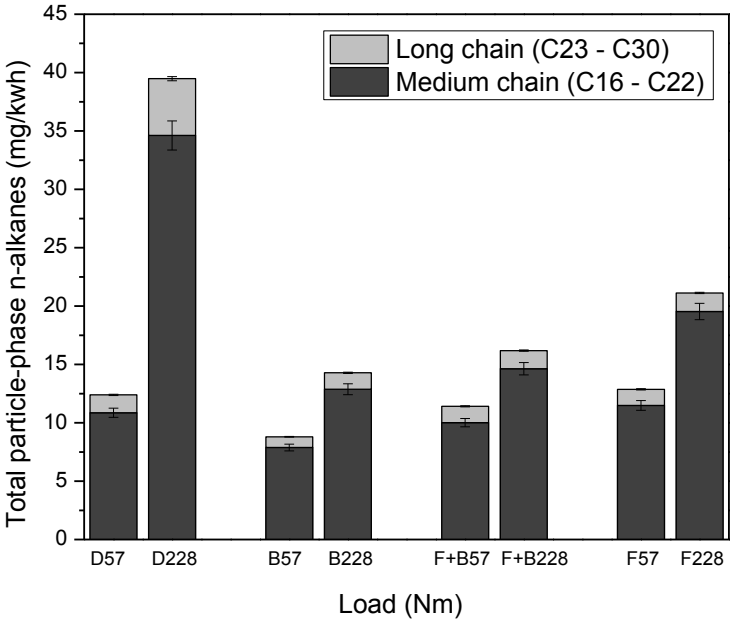

Fig. 8.11 Variation of total n-alkanes concentration based on medium chain and long chain for different fueling modes and loads (57Nm and 228Nm) at 2200rpm.

8.5 Inorganic ions

In this study, four inorganic ions including sodium (Na^+), potassium (K^+), ammonium (NH_4^+) and nitrate (NO_3^-) are analyzed; while the concentrations of potassium for all the fueling modes were lower than the detection limit of the Ion chromatograph. Therefore, only the results of sodium, ammonium and nitrate are presented. Fig. 8.12 to Fig. 8.14 show the variation of sodium, ammonium and nitrate, respectively, with engine speed and load. It can be seen that the increase in engine speed or load causes increase in all the analyzed ions (except for ammonium at 2200rpm-57Nm) for all the fueling modes which is similar to the increase in PM masses with engine speed and load. More PM mass available leads to increase in the amount of the inorganic ions. The concentrations of nitrate for all the fueling modes are higher than those of sodium and ammonium which are in line with other studies [261-264] using diesel and biodiesel.

Also, Fig. 8.12 to Fig. 8.14 illustrate that the blended, F+B and fumigation modes can reduce the sodium, ammonium and nitrate compared to those of the diesel mode. On the average of four operating conditions, the reductions in sodium are -79.7% for blended mode, -71.4% for F+B mode and -55.5% for fumigation mode compared to the diesel mode. Also, the reductions in ammonium are -55.4% for blended mode, -42.9% for F+B

mode and -17.9% for fumigation mode. While the reductions in nitrate are -46.6% for blended mode, -30.6% for F+B mode and -8.1% for fumigation mode. It is well known that the earth is a source of ions and mineral impurities and since the diesel fuel (as a fossil fuel) is directly extracted from the earth, resulting in higher concentration of sodium, ammonium and nitrate in the diesel mode. On the other hand ethanol is pure and it contains almost no ions, resulting in lower concentrations of sodium, ammonium and nitrate by DBE. The fumigation mode has higher ions concentration than the blended mode due to its lowest BTE and highest BSFC (more availability of diesel). According to the average of four operating conditions, the blended mode has a similar BTE (1.0%) and only a slight increase in BSFC (4.5%) compared to diesel mode. However, the fumigation mode has lower BTE (-6.2%) and hence a huge increase in BSFC (11.6%) compared to diesel mode. Therefore, the fumigation mode has lesser effect than blended mode on the reduction of inorganic ions.

Popovicheva et al. [260] also reported that the biofuel had lower inorganic impurities in comparison with the conventional diesel fuel which has an effect on the concentrations of soot, PM mass, metals and ions. Popovicheva et al. [354] also reported that the use of biofuel like pure biodiesel in transient cycle had lower sodium, ammonium and nitrate compared to those of pure diesel. The reduction in ammonium by pure biodiesel compared to the diesel was also reported in another study [262]. In addition, Timonen et al. [374] found that the use of pure ethanol (E100) reduced the ammonium and nitrate compared to the gasoline-ethanol (E10).

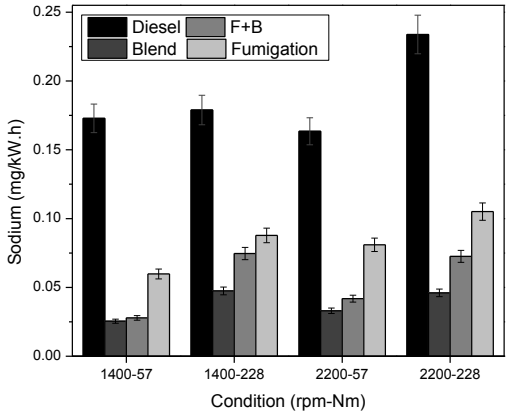

Fig. 8.12 Variation of sodium with engine speed and load.

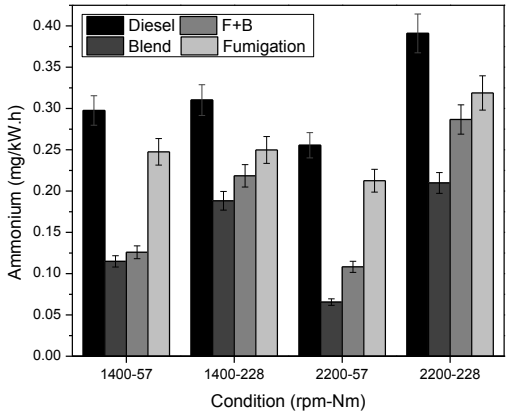

Fig. 8.13 Variation of ammonium with engine speed and load.

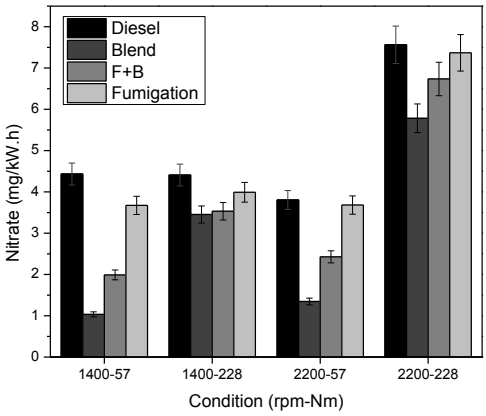

Fig. 8.14 Variation of nitrate with engine speed and load.

8.6 Metals and elements analysis

Metals and elements can be found in the engine exhaust from three sources: (1) trace metals and elements available in the fuel; (2) addition of organo-metallic into the lubricating oil; and (3) wear metals and elements available at the metallic engine components (e.g. cylinder wall, pistons, rings, valve seats or etc.) [278,375]. Fig. 8.15 shows the variations of metals and elements with engine speed and load. It can be seen that almost all the analyzed metals and elements increase with increase in engine speed (irrespective of reduction at 2200rpm-57Nm for a few metals and elements) or engine load; while the effect of engine load on the increase in metals and elements is higher than that of engine speed. The increase in engine load or speed (especially load) cause increase in PM emissions and hence more metal and elements are available. Also, increase in

engine load or speed causes increase in combustion temperature resulting in more vaporization and oxidation of lubricating oil [277] and wear down of some metallic components of engine (e.g. cylinder wall, pistons, rings, valve seats or etc.) which are the sources of emitted metals and elements in the engine exhaust. Ashraful et al. [277] also found that the increase in engine speed caused rise in metals and elements such as Ca, Ci, Cr, Fe, Na, S and Zn using diesel and diesel-biodiesel fuels. According to Fig. 8.15 for all the tested fueling modes, Ca (about 52% of total metals and elements) is the majority component of the total metals and elements. Shukla et al. [278], Sharma et al. [279] and Agarwal et al. [280] also reported that Ca was the major component of total metal for diesel and diesel-biodiesel blend. After Ca, Zn (about 20% of total metals and elements), Al (about 9%), S (about 8%) and Fe (about 4%) have higher percentages than the other metals and elements. The remaining components have only a portion of about 7% of total metals and elements.

In regard to the effect of DBE on the metals and elements, Fig. 8.15 illustrates that the blended, F+B and fumigation modes have higher metal and elements (except S) at almost all the tested conditions compared to those of diesel mode. According to the average of four operating conditions, the increases in total metals and elements are 180.4% for fumigation mode, 134.3% for F+B mode and 85.7% for blended mode in comparison with the diesel mode. Other studies [143,277,278] also found that the use of biodiesel and ethanol causes increase in almost all the metals and elements compared to the pure diesel. The reduction in S by using the blended, F+B and fumigation modes is due to higher concentration of sulfur in diesel than ethanol. While the fumigation mode has the lowest effect on the reduction of S than the blended mode due to its higher fuel consumption (more diesel and biodiesel are available which have sulfur contents). More details in the effect of the fueling modes on the individual metals and elements are presented in Table 8-4. The higher metals and elements in the PM of the blended, F+B and fumigation modes compared to the diesel mode is due to the following reasons. Firstly, biodiesel is a polar compound and has higher metals and elements compositions than diesel fuel due to their resources, production process (refining, distillation), transportation, and storage [144]. Secondly, since ethanol is a corrosive liquid, it can wash the lubricating oil from the cylinder wall. Shukla et al. [278] also reported that the washing of lubricating oil from the cylinder wall during the combustion process by biofuels (biodiesel was used in that study) led to increase in metallic species compared to the diesel fuel. Thirdly, the higher

oxygen concentration of biodiesel and ethanol causes increase in the oxidation of lubricating oil during the combustion process, especially at high combustion temperature [277]. In this study, the effect of fumigation mode is higher than blended mode on the increase in metals and elements. Because the fumigation mode has the highest BSFC (increase of 11.6% compared to the diesel mode) resulting in more availability of biodiesel and ethanol in combustion process and hence increases the metal and elements contents in the PM; while the blended mode has only a slight increase in BSFC (4.5%). Also, the use of fumigated BE in the cylinder has more corrosivity effect to wash the lubricating oil and metallic equipment compared (e.g. cylinder wall, pistons, rings, valve seats or etc.) with the blended mode which the ethanol was mixed with diesel and biodiesel before injection. In addition the fumigated BE has more time wash the lubricating oil and metallic equipment before ignition than the blended mode.

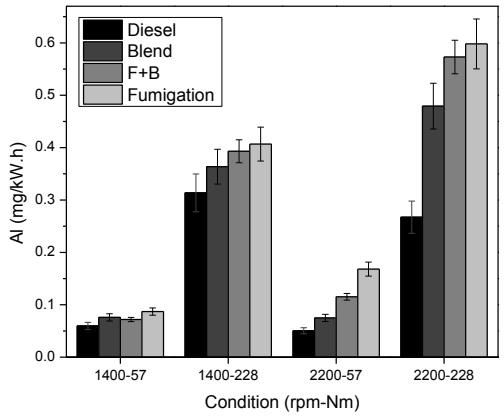

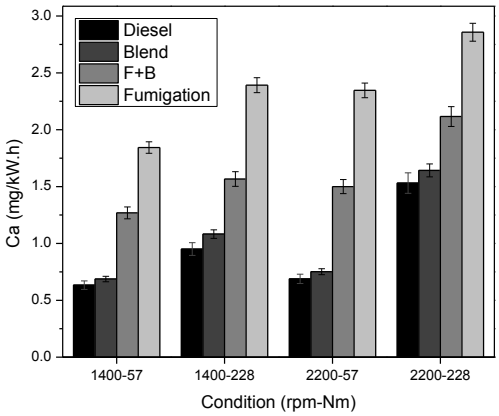

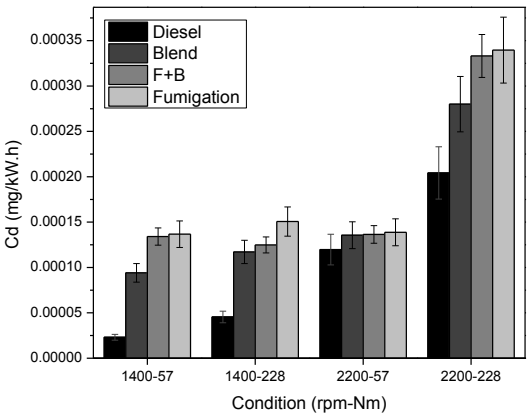

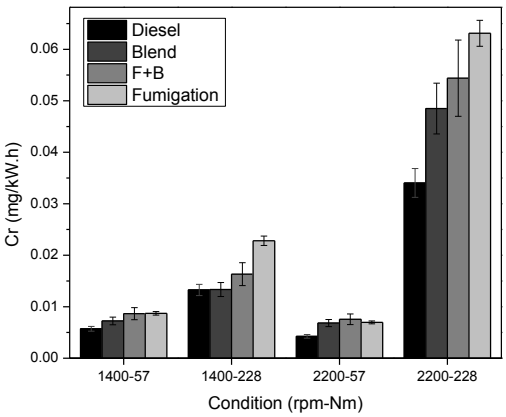

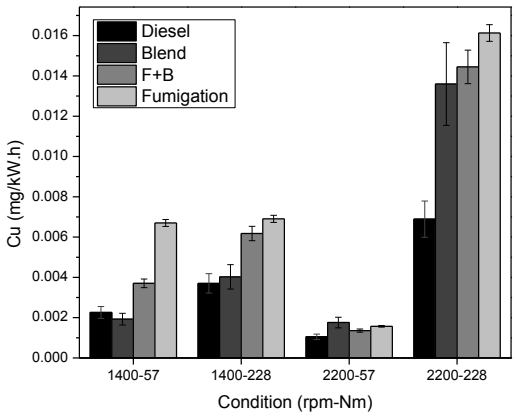
Diesel
Blend
F+B
Fumigation
Cu (mg/kW.h)
0.000
0.002
0.004
0.006
0.008
0.010
0.012
0.014
0.016
1400-57
1400-228
2200-57
2200-228
Condition (rpm-Nm)

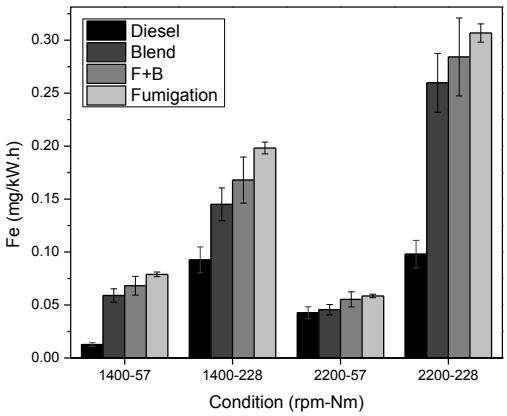
Diesel
Blend
F+B
Fumigation
Fe (mg/kW.h)
0.00
0.05
0.10
0.15
0.20
0.25
0.30
1400-57
1400-228
2200-57
2200-228
Condition (rpm-Nm)

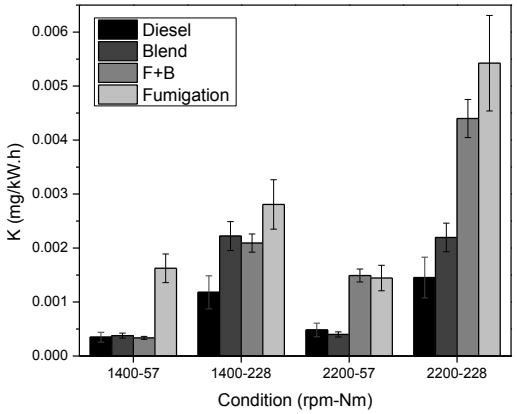
Diesel
Blend
F+B
Fumigation
K (mg/kW.h)
0.000
0.001
0.002
0.003
0.004
0.005
0.006
1400-57
1400-228
2200-57
2200-228
Condition (rpm-Nm)

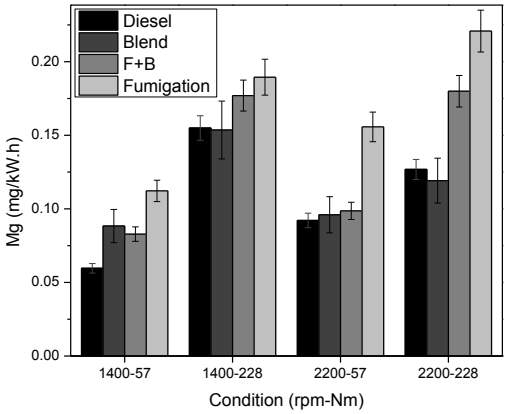
Diesel
Blend
F+B
Fumigation
Mg (mg/kW.h)
0.00
0.05
0.10
0.15
0.20
1400-57
1400-228
2200-57
2200-228
Condition (rpm-Nm)

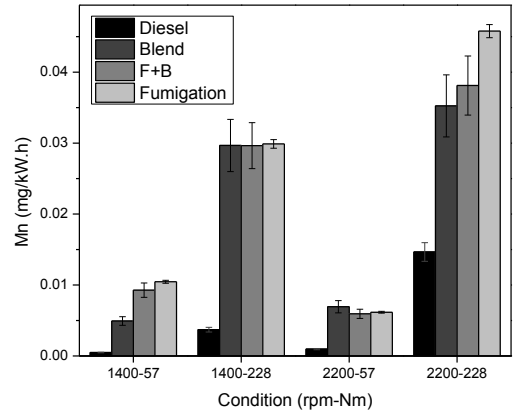
Diesel
Blend
F+B
Fumigation
Mn (mg/kW.h)
0.00
0.01
0.02
0.03
0.04
1400-57
1400-228
2200-57
2200-228
Condition (rpm-Nm)

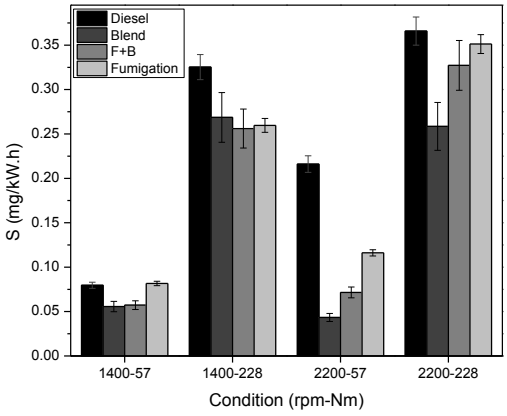
Diesel
Blend
F+B
Fumigation
S (mg/kW.h)
0.00
0.05
0.10
0.15
0.20
0.25
0.30
0.35
1400-57
1400-228
2200-57
2200-228
Condition (rpm-Nm)

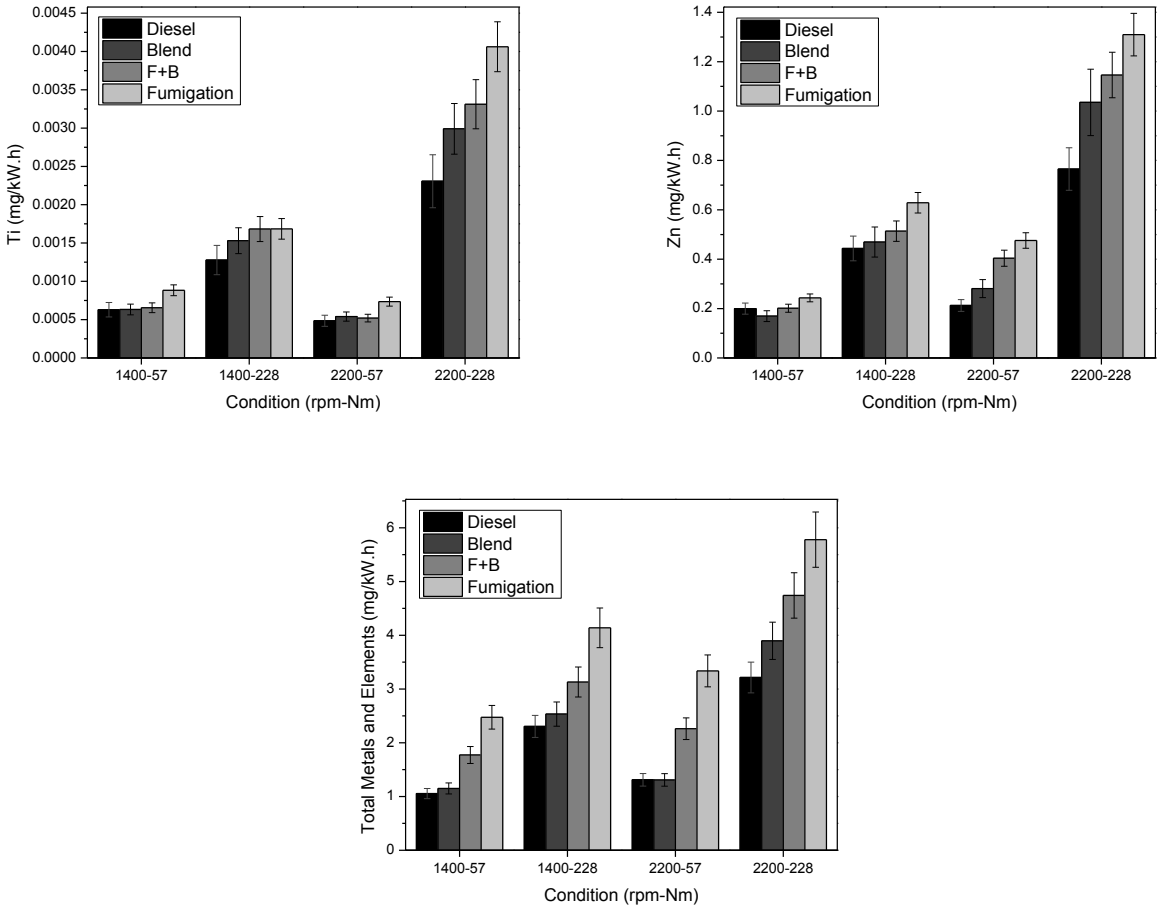

Fig. 8.15 Variations of metals and elements with engine speed and load.

Table 8-4 Effect of the fueling modes on the individual metals and elements compared to the diesel mode in percentage (%)

Metals and elements	Blended mode (%)	F+B mode (%)	Fumigation mode (%)
Al	42.8	72.3	108.4
Ca	9.7	80.3	167.5
Cd	128.9	183.1	201.5
Co	-[a]	-	-
Cr	32.7	53.1	68.5
Cu	39.7	67.4	116.7
Fe	148.5	184.8	221.7
K	32.6	121.4	244.2
Mg	11.4	25.5	63.4

Mn	592.1	794.1	875.6
Na	-	-	-
Ni	-	-	-
Pb	-	-	-
S	-39.2	-31.7	-17.0
Ti	15.3	21.7	50.0
Zn	14.5	39.1	64.6

a: the results were not available because the amount of components were very low and below detection limit.

8.7 Composition of PM mass

The composition of PM mass for diesel, blended, F+B and fumigation modes at different engine speeds and loads is presented in Fig. 8.16. The TC, within the range of 76.4% to 88.4% (depending on the fueling modes and operating conditions), is the most abundant component for all the fueling modes at all the tested conditions. On the other hand, metal and elements, within the range of 0.5% to 1.8% and inorganic ions (sodium, ammonium and nitrate), within the range of 1.3% to 2.4%, have very low contributions to the PM mass. The amount of other species (e.g. water, other types of ions, metals and elements or etc.) in this study varies from 9.0% to 20.6% depending on the fueling modes and operating conditions. According to the average of four operating conditions from Fig. 8.17, the PM mass emitted from the diesel mode has the highest percentages of TC (85.8%), EC (47.6%) and inorganic ions (1.9%) and the lowest percentages of OC (38.2%), metals and elements (0.7%) and unknown species (11.6%). In contrast, the blended mode has the lowest percentages of TC (80.4%), EC (28.0%) and inorganic ions (1.6%) and the highest percentages of OC (52.4%) and other species (16.7%). In addition, the highest percentage of metals and elements (1.4%) is found in the fumigation mode.

Wu et al. [376] also observed that the $PM_{2.5}$ had the composition of OC (32%), EC (55%), inorganic ions (3.2%), metals and elements (0.57%) and unknown species (9.23%) for the average results from eighteen diesel trucks. In addition, Chiang et al. [263] found that the $PM_{2.5}$ consisted of OC (24.5%), EC (47.7%), inorganic ions (1.6%), metals and elements (3.8%) and unknown species (22.5%) for the average results from six light-duty diesel vehicles; while the PM_{10} had the composition of OC (24.6%), EC

(47.3%), inorganic ions (2.1%), metals and elements (5.1%) and unknown species (21.0%). Oanh et al. [264] also reported that based on the average results from 93 diesel vehicles (39 light duty and 54 heavy duty), the $PM_{2.5}$ consisted of approximately 19% of OC, 47% of EC and 6% of inorganic ions and metals and elements. Sharma et al. [279] also found that OC (25%), EC (48%), metals (1.27%) and unknown species (25.73%) were the compositions of PM mass emitted from a diesel engine at 70% load. Guarieiro et al. [359] reported that 80% to 90% of particle emissions from a diesel engine consisted of organic and inorganic carbons. Similarly, Lu et al. [347] found the carbon emissions (OC+EC) were more than 80% of the $PM_{1.8}$ emission for LSD, ULSD and biodiesel. Miguel and Hansen [360] also found that the TC/PM mass ratio was 0.85 in a diesel engine fueled with diesel. Popovicheva et al. [262] found that the nitrate had the composition of about 1% of PM mass for diesel and biodiesel. In addition, Popovicheva et al. [260] reported that the ammonium had the composition range of 0.02% to 0.28% of PM mass; while the total ions accounted for about 1.5% of PM mass for diesel and biodiesel.

In this study, the differences between the diesel mode with the blended, F+B and fumigation modes on the composition of PM mass are mostly due to the use of different fuels (biodiesel and ethanol) and the type of fueling mode (simple mode like the diesel and blended modes compare with the fumigation mode). However, the effect of type of fueling mode is stronger than type of fuels used, because, the same overall fuel composition of D80B5E15 was used for both the blended and fumigation modes, but different results in the composition of PM mass are obtained.

The use of biodiesel and ethanol for mixing with diesel to form DBE fuels causes reduction in the TC and EC due to the lower aromatic and sulfur contents and the lower C/H mass ratio and the higher oxygen content of the DBE fuels compared to pure diesel fuel. However, the effect of using biodiesel and ethanol in fumigation mode is lesser than that in the blended mode due to difference in type of fueling mode. Since the fumigation mode has higher BSFC, equivalence ratio, DOC and diffusion combustion phase (due to short ID) than the blended mode; therefore, it has less effect on the reduction of TC and EC compared with the huge effect of the blended mode. In regard to the concentration of metals and elements in the composition of PM mass, the use of ethanol has a significant effect on the increase in metals and elements due to its corrosivity compared to diesel fuel. The ethanol used in this study had a high purity of 99.9% which contained almost no

metals and elements; however it can wash the lubricating oil inside the cylinder and remove some metals from the metallic equipment (e.g. cylinder wall, pistons, rings, valve seats or etc.). The effect of fumigation mode is higher than that of the blended mode on the increase in metals and elements, because the use of fumigated BE in the cylinder has more corrosivity to wash the lubricating oil and metallic equipment compared with the blended mode which the ethanol was mixed with diesel and biodiesel before injection. Also, the fumigated BE has more time for washing the lubricating oil and metallic equipment before ignition compared to the blended mode. In addition, the fumigation mode has the highest BSFC which causes more availability of biodiesel and ethanol in combustion process and hence increases the metal and elements contents in the PM. For inorganic ions, diesel fuel is the source of ions; therefore, the use of alternative fuels like biodiesel and ethanol in both blended and fumigation modes causes reduction in the concentration of inorganic ions in the composition of PM mass. While fumigation mode has lesser effect compared with the blended mode due to its higher fuel consumption and equivalence ratio which contains more diesel fuel for the formation of inorganic ions.

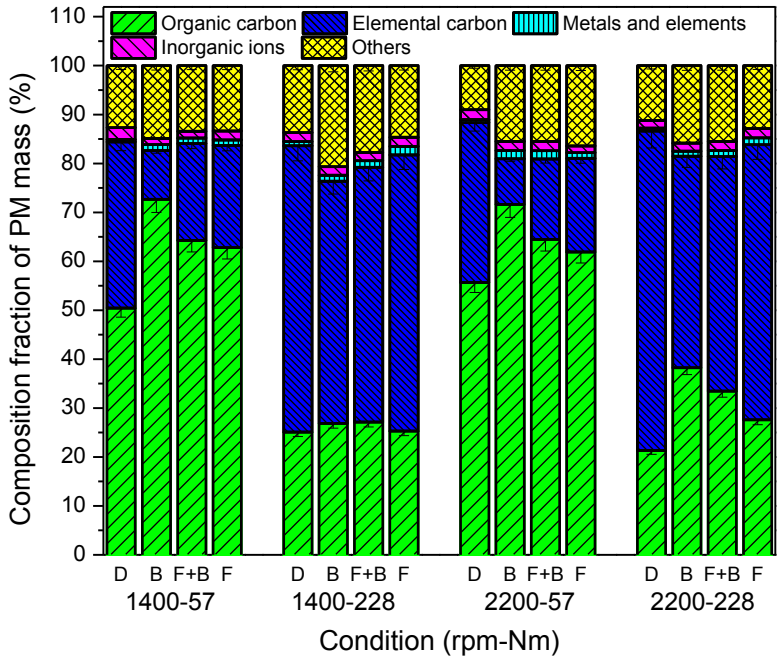

Fig. 8.16 Composition of PM mass for diesel, blended, F+B and fumigation modes at different engine speeds and loads.

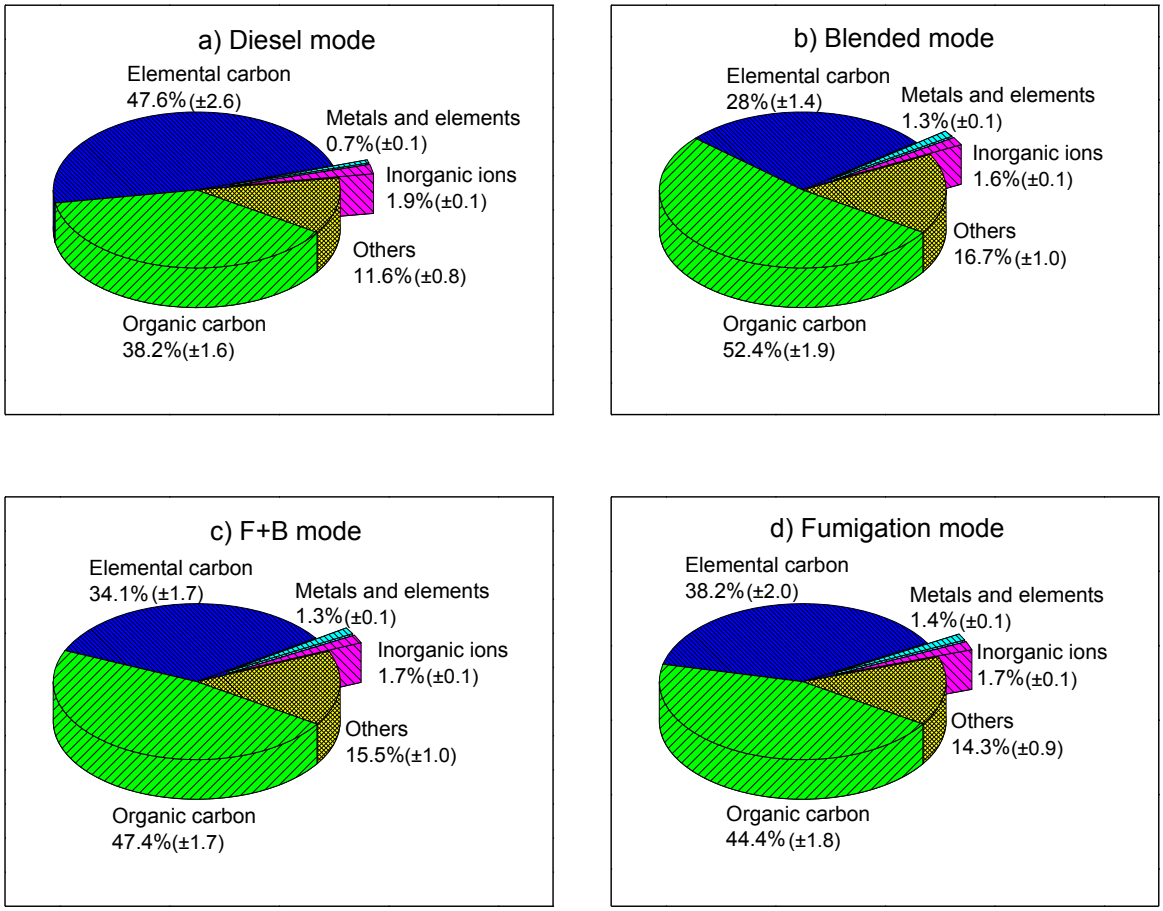

Fig. 8.17 Composition of PM mass (± standard error at 95% confidence level) for (a) diesel mode, (b) blended mode, (c) F+B mode and (d) fumigation mode based on the average of four conditions.

8.8 Summary

The results for chemical properties of PM are presented in Table 8-5. It can be seen from Table 8-5 that the blended mode has almost the lowest values in all the parameters or chemical properties investigated. However, the fumigation mode has the reduction effect compared to the diesel only on some of these parameters or chemical properties. While the F+B mode has the impact in between those of the fumigation and blended modes.

In regard to the composition of the PM, it is found that PM from the diesel mode has the highest percentage of TC (85.8%), EC (47.6%) and inorganic ions (1.9%) and the lowest percentage of OC (38.2%), metals and elements (0.7%) and unknown species (11.6%). In contrast, PM from the blended more has the lowest percentage of TC (80.4%), EC (28.0%) and inorganic ions (1.6%) and the highest ratios of OC (52.4%) and unknown

species (16.7%). The highest percentage of metals and elements (1.4%) is found in the fumigation mode. It is also found that the blended, F+B and fumigation modes can reduce almost all the PAHs compared the diesel mode; while the blended mode has the lowest PAHs. In addition, it is observed that the particles from the diesel mode and the blended mode have the lowest and highest oxidation reactivity, respectively.

Table 8-5 Effect of fueling modes on the chemical properties of PM based on the average of four conditions

Parameter	Order (Highest to lowest)
TC	**Diesel** ≈ Fumigation (-2.1%) > F+B (-28.9%) > Blend (-46.3%)
EC	**Diesel** > Fumigation (-25.9%) > F+B (-48.4%) > Blend (-66.1%)
OC	Fumigation (18.3%) > **Diesel** > F+B (-5.5%) > Blend (-19.8%)
H-VS/total-VS ratio	Blend (12.8%) > F+B (9.4%) > Fumigation (6.9%) > **Diesel**
L-VS/total-VS ratio	Blend (4.5%) > F+B (1.6%) ≈ **Diesel** ≈ Fumigation (-0.6%)
non-VS/total-VS ratio	**Diesel** > Fumigation (-11.1%) > F+B (-16.9%) > Blend (-25.1%)
Activation energy	**Diesel** > Fumigation (-4.9%) > F+B (-10.6%) > Blend (-34.0%)
Frequency factor	**Diesel** > Fumigation (-53.0%) > F+B (-84.7%) > Blend (-96.9%)
WSTC	Fumigation (39.4%) > F+B (19.6 %) > Blend (2.1 %) ≈ **Diesel**
WSOC	Fumigation (44%) > F+B (23.6%) > Blend (7%) > **Diesel**
WSIC	**Diesel** > Fumigation (-24.5%) > F+B (-33.1%) > Blend (-55.8%)
PAHs	**Diesel** > Fumigation (-31.3%) > F+B (-57.6%) > Blend (-78.4%)
BaP_{eq}	**Diesel** > Fumigation (-38.9%) > F+B (-63.5%) > Blend (-81.7%)
n-Alkanes	**Diesel** > Fumigation (-21.5%) > F+B (-33.9%) > Blend (-46.5%)
Sodium	**Diesel** > Fumigation (-55.5%) > F+B (-71.4%) > Blend (-79.7%)
Ammonium	**Diesel** > Fumigation (-17.9%) > F+B (-42.9%) > Blend (-55.4%)
Nitrate	**Diesel** > Fumigation (-8.1%) > F+B (-30.6%) > Blend (-46.6%)
Metals and elements	Fumigation (180.4%) > F+B (134.3%) > Blend (85.7%) > **Diesel**

CHAPTER 9 CONCLUSIONS AND SUGGESTIONS

This study aims to investigate the effects of different fueling modes of operation, including diesel, blended, F+B and fumigation modes, on the engine combustion, performance and emissions of a diesel engine fueled with a ternary fuel (DBE) under various engine speeds and loads. Ethanol is selected among various alcohols including methanol, ethanol, propanol, butanol and pentanol to mix with diesel and biodiesel to form the ternary fuels. The results indicate that the DBE is the most suitable ternary fuel for further investigation. The tests were conducted at a constant fuel volume ratio of 80% diesel, 5% biodiesel and 15% ethanol (D80B5E15) in the blended, F+B and fumigation modes to provide the same fuel composition for comparing the effects of the three fueling modes with the effects of the diesel mode. The experiments were divided into three groups. The first group was conducted to investigate the effects of using different fueling modes on the engine combustion, performance and emissions at different engine loads. In this case, the experiments were conducted at a constant engine speed of 1800 rpm with five engine loads of 57, 99.8, 142.5, 185.3 and 228 Nm. The second group was conducted to investigate the effects of using different fueling modes on the engine combustion, performance and emissions at different engine speeds. In this group, the experiments were performed at a constant engine torque of 142.5 Nm (50% of the full engine torque) with five engine speeds of 1400, 1600, 1800, 2000 and 2200 rpm. The third group was conducted to study the physicochemical properties of PM sampled in the different fueling modes. In this case, four operating conditions were selected as: 1400 rpm at 20% and 80% loads, and 2200 rpm at 20% and 80% loads, corresponding to low and high engine speeds, and low and high engine loads, respectively. The major conclusions drawn according to the average results are the following points.

9.1 Concluding remarks

9.1.1 Effect of different fueling modes on the engine combustion, performance and regulated gaseous emissions

The blended mode causes increase in peak HRR, ID, COV_{IMEP}, $COV_{Max(dP/d\theta)}$, BSFC, CO, HC and NO_2, and decrease in duration of combustion (slight drop in DOC based on five loads, but similar DOC based on five speeds), CO_2, NO_X and NO, and equal peak in-cylinder pressure, BTE and exhaust gas temperature in comparison with those of the pure

diesel mode. Also, the fumigation mode has higher peak HRR (slight rise in peak HRR based on five loads, but similar peak HRR based on five speeds), DOC, COV_{IMEP}, BSFC, CO, HC and NO_2, lower ID, $COV_{Max(dP/d\theta)}$, BTE, NO_X and NO, and similar peak in-cylinder pressure, exhaust gas temperature and CO_2 compared to those of the diesel mode.

It is found that, compared to the diesel mode, the effects of using different fueling modes (blended, F+B and fumigation modes) on almost all the combustion, performance and emissions parameters based on the average of five loads, are similar to those parameters on the average of five speeds. Therefore, this finding suggests that conducting of the experiments on only one type of operating condition (load or speed) is sufficient to understand the effect of different fueling modes on the combustion, performance and emissions parameters. This can reduce the time and facilities required for conducting the experiments.

9.1.2 Effect of different fueling modes on the PM emissions and physical properties of PM

According to the average of five speeds, five loads or four engine operating conditions, the blended mode has lower PM mass, GMD and TNC (in all nano-particle, ultra-fine particle and fine particle concentrations) compared to the diesel mode. However, the fumigation mode has equal PM mass and GMD, and higher TNC (in all nano-particle, ultra-fine particle and fine particle concentrations) in comparison with the diesel mode. For micro and nano-structures analyses, it is found that the blended or fumigation mode causes changes (but different trends) in the both micro and nano-structures. The average results from four operating conditions shows that blended mode has smaller primary particle diameter and fringe length, similar fringe tortuosity, and higher fringe separation distance than those of the diesel mode. While the fumigation mode has no effect on the primary particle diameter and fringe length, but higher tortuosity and fringe separation distance compared to the diesel mode. Similar to the finding for the engine combustion, performance and emissions, it is observed that the impacts of using different fueling modes (blended, F+B and fumigation modes) on the PM mass, TNC and GMD based on the average of five loads compared to the diesel mode, are similar to those based on the average of five speeds.

9.1.3 Effect of different fueling modes on the chemical properties of PM

According to the average of four operating conditions, the blended mode has an effect on the reduction in TC, EC, OC, activation energy, frequency factor, WSIC, inorganic ions, PAHs, BaP_{eq} and n-alkanes, similar WSTC, but increase in WSOC, metals and elements and oxidation reactivity compared to the diesel mode. On the other hand, the fumigation mode has lower EC, activation energy, frequency factor, WSIC, inorganic ions, PAHs, BaP_{eq} and n-alkanes, equal TC, and higher OC, WSTC, WSOC, metals and elements and oxidation reactivity in comparison with the diesel mode.

In regard to the mass composition of PM, both blended and fumigation mode have higher ratios of H-VS/total-VS and OC/TC and lower ratios of non-VS/total-VS, EC/TC and TC/PM compared to the diesel mode. It is observed that PM from the diesel mode has the highest ratios of TC (85.8%), EC (47.6%) and inorganic ions (1.9%) and the lowest ratios of OC (38.2%), metals and elements (0.7%) and unknown species (11.6%). In contrast, the lowest ratios of TC (80.4%), EC (28.0%) and inorganic ions (1.6%) and the highest ratios of OC (52.4%) and unknown species (16.7%) are found in the PM emitted from the blended mode. The highest ratio of metals and elements (1.4%) is found in the fumigation mode.

The results show that the increase in primary particle diameter and fringe length and decrease in tortuosity and fringe separation distance have effect on increasing the activation energy (lower oxidation reactivity) of PM for all the fueling modes. Since the diesel mode has the largest primary particle diameter and fringe length and the lowest tortuosity and fringe separation distance; therefore, it has the highest activation energy (lower oxidation reactivity) of PM.

9.1.4 Effect of engine speed and load on the engine combustion, performance and emissions

In regard to the effects of engine speed and load, the results reveal that the increase in engine speed causes reduction in peak in-cylinder pressure, BTE, HC, NO_X, NO and NO_2, but increase in peak HRR, ID, DOC, BSFC, CO_2, PM mass and TNC and similar CO and GMD for almost all the tested fueling modes. Also, the increase in engine load causes reduction in ID, BSFC, CO_2, CO, HC, NO_X, NO, NO_2, but increase in peak in-cylinder pressure, HRR, DOC, BTE, PM mass, TNC and GMD.

In regard to the effects of engine speed and load on the physicochemical of PM, since the experiments were conducted only on two engine speeds and loads; therefore, no trustable conclusion can be obtained. However, it is noticeable that the effect of engine load on the physicochemical of PM is higher than engine speed.

9.1.5 Comparison effects of blended mode with fumigation mode on the engine combustion, performance and emissions

According to the average results, the blended mode has higher peak HRR, ID, BTE, NO, NO_X, COV $_{Max(dP/d\theta)}$, but lower DOC, COV_{IMEP}, BSFC, CO_2, CO, HC, NO_2, PM mass, TNC and GMD, and similar peak in-cylinder pressure and EGT in comparison with those of the fumigation mode. In regard to the physicochemical properties of the PM, the blended mode has higher H-VS/total-VS, L-VS/total-VS and OC/TC ratios and faster oxidization reactivity, but lower non-VS/total-VS ratio, TC, OC, EC, EC/TC ratio, activation energy, frequency factor, metals and elements, WSOC, primary particle size, fringe length, tortuosity, fringe separation distance, inorganic ions, PAHs, BaP_{eq} and n-alkanes compared to those of the fumigation mode. In addition, it is observed that the values of all the parameters in the F+B mode are in between those of the fumigation mode and the blended mode, showing that the F+B mode has the effects in between those of the other two modes.

It is further observed that that the blended mode has almost the same trend on the combustion, performance and emissions of the diesel engine from low engine load or speed to high load or speed. However, in the fumigation mode, there are different effects at low engine load or speed with high load or speed. In the fumigation mode, there is reduction in emissions only at high engine load or speed compared to the diesel mode. For instance, the PM emissions in the blended mode are lower than the diesel mode at all the engine loads and speeds. However, the fumigation mode has lower PM emissions than the diesel mode only at high engine loads and speeds which shows that the mode of operation has significant effects on the engine combustion, performance and emissions.

It can be found from the HRR results that the combustion processes of pure diesel, blended and fumigation modes in a diesel engine are similar to each other, which consist of a premixed combustion phase followed by a diffusion combustion phase. However, the magnitudes of these combustion phases and also the other combustion parameters (e.g. peak-HRR, peak-in-cylinder pressure, ID, DOC or etc.) varied for each mode due to

different modes of fueling and different modes of initiation of combustion (heterogeneous combustion versus homogeneous+heterogeneous combustion).

In the diesel mode, pure diesel fuel is directly injected into the engine cylinder and the ignition is initiated by hot compressed air which is a type of heterogeneous combustion. In the blended mode, DBE is directly injected into the engine cylinder (similar to the diesel mode). Thus, the difference effects between the diesel mode and the blended mode is due to the difference in the properties of the fuels in use: diesel compared to the DBE. However, in the fumigation mode, which is dual-fuel combustion mode, a mixture of biodiesel and ethanol (BE) is injected into the engine cylinder through the intake port (manifold) and the main fuel (pure diesel) is directly injected into the engine cylinder. During the intake and compression strokes, the BE is mixed with air to form a homogeneous mixture and then the main fuel is injected into the cylinder, resulting initiation of combustion by the hot compressed air/BE mixture (homogeneous+ heterogeneous combustion), which is different from that of the diesel or blended mode (heterogeneous combustion). In the F+B mode, the main fuel is again DBE, rather than pure diesel. In this case, the DBE is injected into the engine cylinder and ignited by the hot compressed air/BE mixture. In comparison, in the blended mode, all the DBE is burned heterogeneously in air; while in the fumigated mode, diesel fuel is burned heterogeneously in a BE/air mixture; while the BE/air mixture is also ignited by the diesel fuel and burned homogeneously.

Since initiation and quality of combustion are dependent on the fuel, oxidizer (air) and temperature, thus the combustion, performance and emissions parameters are almost different for diesel, blended and fumigation modes of operation. In the blended mode, the lower cetane number (causes longer ID) and higher heat of evaporation of ethanol (causes lower combustion temperature) cause late combustion and affect other combustion, performance and emission parameters compared to the pure diesel mode. In the fumigation mode, the combustion temperature is also low due to using fumigated ethanol; however, the homogeneous mixture (also higher equivalence ratio) and using diesel as the main fuel which has higher cetane number show different effects in combustion, performance and emissions. In other words, since the blended mode has the same combustion mode (heterogeneous combustion) with diesel mode; therefore, the differences in the combustion, performance and emissions parameters are only due to differences in fuel properties (DBE versus diesel). However, in fumigation mode, the

differences in the parameters are due to differences in both fuel properties and combustion mode (heterogeneous combustion versus homogeneous+heterogeneous combustion).

In this study, the same overall fuel composition of D80B5E15 was used for both the blended and fumigation modes, but different results in the combustion, performance and emissions, as well as the physicochemical properties of the PM, were obtained. Therefore, it can be found that the engine combustion, performance and emissions are mostly dependent on the fueling mode (combustion mode) rather than the type of fuel used. The results of the F+B mode also confirm this finding because the values of all the parameters in the F+B mode are in between those of the blended and fumigation modes.

In regard to the human health and environment, the blended mode can reduce CO_2 as a greenhouse emission (about 3%, based on average of five engine loads and speeds) and also NO_X (about 3.5%) compared to the diesel mode. However, the fumigation mode has a reduction effect only in NO_X (about 8%). On the other hand, both fueling modes have a penalty of HC and CO emissions; while the fumigation mode has the highest values. The amount of HC (about 6.5% higher than the diesel mode) and CO (about 18.5%) emissions of the blended mode can be lower than that of the diesel mode with use of different concentration of biodiesel and ethanol (like findings in Chapter 4). However, reduction in these emissions under the fumigation mode to obtain lower values than the diesel mode will be a difficult task. Because fumigation mode has a huge increase in both HC (about 160%) and CO (about 170%) emissions compared to those of the diesel mode.

The differences in the particulate emission and physical properties of PM arising from different fueling modes might have different effects on the human health and environment. For instance, the blended mode has the lowest PM mass, TNC, GMD and primary particle size which has a positive effect on the air quality, environment and global climate by reducing absorption of the solar radiation (resulting lesser effect on melting the snow and ice) and reducing reaction with other types of atmospheric constituents (e.g. formation of black rain). In contrast, the lowest GMD and primary particle size obtained from the blended mode have a negative effect on the human and even animal health, because the smaller particles can penetrate deeply into the lung tissue through the respiratory passageways which cause more damage to lung tissue compared to the larger particles [199]. However, the negative effect of lowest GMD and primary

particle size from the blended mode on both human health and environment can be compensated by its huge positive effects of the lowest PM mass and TNC. On the other hand, the fumigation mode will have different effects on the human health and environment due to its different results in PM emissions compared with the blended mode.

Effect of the chemical substances of PM emitted from different fueling modes on the human health and environment is another important aspect which should be concern. Fortunately, the blended mode can reduce most of the harmful chemical substance of PM for the human health and environment including the EC, PAHs, and n-alkanes compared to the diesel mode. However, the fumigation mode has less effect on the reduction of these substances compared to the huge effect of the blended mode.

According to the results obtained from this study, it can be concluded that the blended mode is a better method than the fumigation mode for the diesel engine operation due to its higher performance and lower emissions and also lesser negative effects on the human health and environment. While these findings may be different with use of different type of engines, fuels, operating conditions, injection pressures or etc.

9.2 Suggestions for future research

In the present study, some experiments were conducted to investigate the effects of different fueling modes of operation, including diesel, blended, F+B and fumigation modes, on the engine combustion, performance and emissions (regulated emissions and physicochemical of PM) of a diesel engine fueled with a ternary fuel (DBE) under various engine speeds and loads. However, still there are some related investigations which can be tackled with further studies.

- The experiments were conducted only with one fuel mixture (D80B5E20), the use of different ethanol and biodiesel contents is suggested.
- Methanol as a fumigated fuel has been investigated in many studies and it has a good potential to reduce the emissions as found in this study; therefore, a comprehensive study for comparison of using methanol in fumigated and blended modes on the engine combustion, performance and emissions is recommended.
- This study is experimental in nature; while numerical simulation is recommended for future investigation.

- In this study, only the regulated gaseous emissions including CO_2, CO, HC, NO_X, NO and NO_2 were analyzed. The measurement of unregulated emissions is recommended for further study.
- Only four inorganic ions have been measured in this study and there are various types of organic and inorganic ions (cation and anion) in the PM which need to be investigated in the future studies.
- In this study, the effects of engine speed and load, with five operating conditions in each case, on the combustion, performance and regulated emissions have been fully investigated. However, for the physicochemical properties of PM, the experiments were conducted only at four operating conditions; therefore, more conditions are needed to understand the influence of engine speed and load on the physicochemical of PM.
- The results of this study are based on the same engine configuration and setting without any changes. Different results may be obtained if the engine can be adjusted to their optimum operating condition, for example, the optimum fuel injection timing, for specific type of fuel. This can be considered as a part of the future research.

APPENDICES

Appendix A

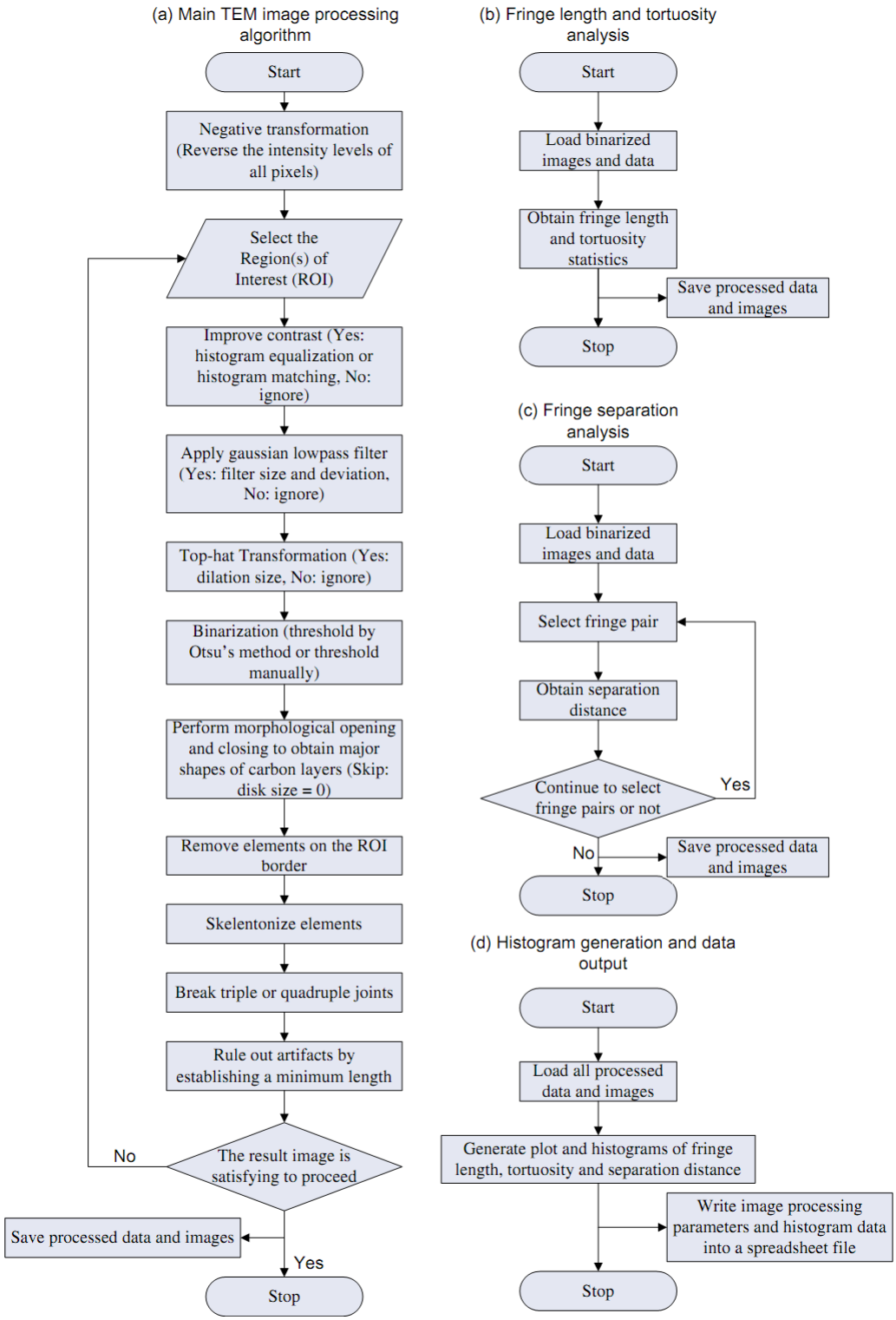

Fig. A.1 Flow chart of the image processing program for STEM images [217].

Appendix B

Table B-1 Specifications of the total organic carbon analyzer

Analyzer	**Total Organic Carbon Analyzer (TOC-L_{CSN})**
Analyte	TC, IC, TOC (TOC=TC-IC), NPOC
Measurement principle	680°C catalytically-aided combustion oxidation/non-dispersive infrared detection (NDIR)
Measuring range	TC: 0 - 30000 mg/L IC: : 0 - 3000 mg/L
Detection limits	TC: 50 µg/L IC: 4 µg/L
Measurement time	TC: Approx. 3 min IC: Approx. 4 min
Repeatability	TC, NPOC: Coefficient of Variation (COV) 1.5 % or ±50 µg/L max. IC: COV 1.5 % or ±4 µg/L max.
Sample introduction	Auto injection using syringe pump/slider
Sample injection volume	TC: 10 to 150 µL (variable) IC: 10 to 4500 µL (variable)
Sample dilution function	Dilution within syringe, dilution factor 2 - 50 times
Pretreatment for IC	Automatic acid addition and sparging
Carrier gas	High purity air (from cylinder); High purity nitrogen (with addition of the N_2 carrier gas kit); Pressurized air (with addition of the carrier gas purification kit)
Carrier gas pressure	Approx. 200 ± 10 kPa (300 to 600 kPa when using the carrier gas regulator option)
Carrier gas flow rate	230 mL/min (150 mL/min for present study)
Sparge gas flow	80 mL/min
NDIR temperature	65 °C
Ambient temperature	5-35 °C

TC: Total Carbon; IC: Inorganic Carbon; TOC: Total Organic Carbon; NPOC: Non-Purgeable Organic Carbon.

Appendix C

Table C-1 Specifications of the scanning spectrophotometer

Analyzer	**scanning spectrophotometer (UV-2101PC)**
Wavelength Range	190 nanometers (nm) ~ 900nm
Spectral band width (slit width)	10 steps in 0.1, 0.2, 0.3, 0.5, 0.8, 1, 2, 5, (02), (05) nm. 02, 05 mean that its slit width is 2nm, 5nm respectively, but the height is half so as to reduce the stray light.
Resolution	0.1nm
Display of wavelength	0.1nm increments
Wavelength accuracy	± 0.3nm (at slit width of 0.2nm)
Wavelength repeatability	0.1nm
Ambient temperature	15° ~ 35° C
Ambient Humidity	46% ~ 80%
Photometric range	Absorbance: -4 ~ 5 Abs Transmittance: 0 ~ 999.9%T

Appendix D

Table D-1 Operation conditions for ICP-OES

Parameters	**Value**
Power	1.10 (kW)
Plasma flow	15.0 (L/min)
Auxiliary flow	1.50 (L/min)
Nebulizer pressure	200 (kPa)
Replicate time	5.000 (s)
Stabilization time	15 (s)
Multi frame	On
Replicates	3
Sample uptake	30 (s)
Rinse time	10 (s)
Pump rate	15 (rpm)
Fast pump	On

Appendix E

Since the errors and uncertainties are the most important factors in regard to the accuracy and reliability of the results; therefore, some information about the errors and uncertainties are summarized. Then, the uncertainties calculation for this study is presented.

The term “error” in a measurement is usually defined as the difference between the measured value and the true value; or the deviation of an instrument reading from a known value [281]. The errors cause uncertainty in an experimental measurement. The valuable and appropriate concept of the "uncertainty" is "a possible value that an error may have." [377-379]. The term of uncertainty was appeared in the early 1950s for the experiments that could not be repeated enough times (due to time or economy limitations) to collect the enough statistical data [281]. And, nowadays, uncertainty analysis is an important statistical interpretation of the errors in the measurements.

E1 Sources of errors

There are almost three types of errors which cause to formation of uncertainties in the measurements [379]. The classification of types of error depends on how the source behaves with time and the sampling frequency of the observations.

1) The error of the observations which causes invalidate data due to gross blunders in the apparatus or instrument construction. However, this error can be eliminated by the careful experimenters.

2) The error from the apparatus or instrument (e.g. accuracy, linearity or offset of equipment [380]) which is fixed and they cannot be changed by careful experimenters or repeating of the experiments. This error is called “fixed error” (sometimes called bias error or systematic error).

3) Personal fluctuations, influences of friction, random electronic fluctuations in the equipment or so forth, cause to initiate an error with certain statistical distribution (not always) in the measurements. This error is called “random error” which can be reduced by repeating of the experiments to get higher number of samples. There is also another type of error for most engineering experiments that can be changed during an experiment, but not randomly which is called “variable but deterministic”. The variable error includes

both the random and deterministic components of unsteady error; however, variable error is eliminated at steady state conditions which only normally distributed random error is formed [281].

The total (overall) uncertainty can be calculated by the root-sum-square combination of fixed and random errors contributions in both single-sample and multiple-sample analyses. For more information, Kline and McClintock [377] and Moffat [381,382] described the calculation of single-sample uncertainty. On the other hand, Abernethy and Thompson [383] explained the multiple-sample analysis; while Abernethy et al. [384] summarized the multiple-sample analysis in their works.

E2 Total uncertainty calculation for measuring parameters

Total (overall) uncertainty can be calculated as:

$$X_i = \overline{X_i} \pm U \quad \text{E1}$$

$$U = \sqrt{(\omega_s)^2 + (\omega_r)^2} \quad \text{E2}$$

Where $\overline{X_i}$ is the observation in a single-sample experiment or the mean of a set of N observations in a multiple-sample experiment. And U is the total uncertainty, ω_s is systematic error and ω_r is random error.

E2.1 Systematic error:

Systematic error consists various parameters such as accuracy (ω_{s1}), linearity (ω_{s2}) or offset (ω_{s3}) of instruments based on the manufacturers' specifications [380].

$$\omega_s = \sqrt{(\omega_{s1})^2 + (\omega_{s2})^2 + (\omega_{s3})^2 + \ldots + (\omega_{sN})^2} \quad \text{E3}$$

E2.2 Random error:

The random error can be calculated as:

$$\omega_r = \frac{t \times SD}{\sqrt{N}} \quad \text{E4}$$

Where t represents the Student's t statistic appropriate for the number of samples (N) and the confidence level desired (t= 1.96 for 95% confidence level), and SD is the standard deviation of the set of N observations used to calculate the mean value $\overline{X_i}$.

The standard deviation or root-mean-square deviation (*SD*) can be determined for two groups of samples [378]. The standard deviation of the large observations which is also called population or biased standard deviation, is defined by:

$$SD=\left[\frac{1}{N}\sum_{i=1}^{N}(\overline{X_i}-X_m)^2\right]^{1/2} \quad \text{E5}$$

And the standard deviation of the limited observations (20 measurements) which is sometimes called unbiased or sample standard deviation, is defined by:

$$SD=\left[\frac{1}{N-1}\sum_{i=1}^{N}(\overline{X_i}-X_m)^2\right]^{1/2} \quad \text{E6}$$

Where N is the number of measurements, $\overline{X_i}$ is the observation of each sample and X_m is the arithmetic mean of measurements calculating by:

$$X_m=\frac{1}{N}\sum_{i=1}^{N}\overline{X_i} \quad \text{E7}$$

E3 Uncertainty of calculated parameters

The above equations are suitable for the uncertainties of single or multiple samples (non-calculated measurements) taken from the instruments and analyzers. However, some engine performance metrics cannot be measured directly (e.g. torque, power, BSFC and BTE). Therefore, the uncertainties for the calculated-parameters can be estimated basis of the uncertainties in the primary measurements from the following equations.

The result R is a given function of the independent variables of $X_1, X_2, X_3, \ldots, X_N$. Therefore:

$$R=R(X_1,X_2,X_3,\ldots,X_N) \quad \text{E8}$$

And ω_R is an uncertainty of the result and $\omega_1,\omega_2,\omega_3,\ldots,\omega_N$ are the uncertainties of the independent variables. If the odds (e.g. 20:1) of uncertainties in the independent variables be same; therefore, the uncertainty in the result having these odds according to:

$$\omega_R=\left[\left(\frac{\partial R}{\partial X_1}\omega_1\right)^2+\left(\frac{\partial R}{\partial X_2}\omega_2\right)^2+\left(\frac{\partial R}{\partial X_3}\omega_3\right)^2+\ldots+\left(\frac{\partial R}{\partial X_N}\omega_N\right)^2\right]^{1/2} \quad \text{E9}$$

E4 Uncertainty calculation for the present work

In this study, recording of 5 min (1HZ) of direct measurement parameters (like gaseous emissions or PM mass) made 300 samples for calculation of uncertainties based on

random errors. All the uncertainties were computed with 95% confidence level and 300 samples (N=300) except for combustion analysis (500 cycles); therefor, degrees of freedom (v=N-1) lead to obtain the Student's t statistic of 1.96 (t=1.96).

Accuracy and linearity (Table 3-8) of equipment according to manufacturer's specifications were applied for calculation of uncertainties based on systematic errors. The total uncertainty at 95% confidence level was calculated as:

$$U_{0.95}=\sqrt{(Systematic\ errors)^2+\left(\frac{1.96\times SD}{\sqrt{300}}\right)^2}$$

For calculated-parameters like torque, power, BSFC and BTE, equation E9 was employed. For example, the uncertainty of BSFC was computed as:

$$BSFC=\frac{\dot{m}}{P_b}$$

$$U_{BSFC}=\sqrt{\left(\frac{\partial BSFC}{\partial \dot{m}}\times U_{\dot{m}}\right)^2+\left(\frac{\partial BSFC}{\partial P_b}\times U_{P_b}\right)^2}$$

$$\frac{\partial BSFC}{\partial \dot{m}}=\frac{P_b\text{-}0}{{P_b}^2}=\frac{1}{P_b}$$

$$\frac{\partial BSFC}{\partial P_b}=\frac{0\text{-}\dot{m}}{{P_b}^2}=\frac{\text{-}\dot{m}}{{P_b}^2}$$

Where $\dot{m}$ is fuel consumption and P_b is power.

$$U_{\dot{m}}=\sqrt{\left(\frac{\partial \dot{m}}{\partial Mass}\times U_{Mass}\right)^2+\left(\frac{\partial \dot{m}}{\partial Time}\times U_{Time}\right)^2}$$

$$U_{P_b}=\sqrt{\left(\frac{\partial P_b}{\partial Torque}\times U_{Torque}\right)^2+\left(\frac{\partial P_b}{\partial Speed}\times U_{Speed}\right)^2}$$

$$\dot{m}=\frac{Mass}{Time}$$

$$\frac{\partial \dot{m}}{\partial Mass}=\frac{Time\text{-}0}{Time^2}=\frac{1}{Time}$$

$$\frac{\partial \dot{m}}{\partial Time}=\frac{0\text{-}Mass}{Time^2}=\frac{\text{-}Mass}{Time^2}$$

Where U_{Time} is the error (accuracy) of time recorder (stopwatch, Table 3-8) and U_{Mass} is the error (accuracy) of digital balance as shown in Table 3-8.

$$P_b = 2\pi \times Speed \times Torque$$

$$\frac{\partial P_b}{\partial Torque} = 2\pi \times Speed$$

$$\frac{\partial P_b}{\partial Speed} = 2\pi \times Torque$$

Where U_{Torque} and U_{Speed} are the errors (accuracy and control) of the torque and speed from engine control system, respectively (Table 3-8).

In regard to the uncertainties of parameters extracted from the charge amplifier (e.g. pressure, heat release rate, COV of pressure or IMEP and etc.), the errors of charge amplifier, crank angle encoder and pressure sensor were calculated as the systematic errors. For example the uncertainty of IMEP (for 500 cycles) was computed [78,385] as:

$$U_{IMEP} = \sqrt{(U_{Pr})^2 + (U_V)^2 + \left(\frac{1.96 \times SD_{IMEP}}{\sqrt{500}}\right)^2}$$

Where U_{Pr} is the uncertainty of in-cylinder pressure and U_V is the uncertainty of instantaneous cylinder displacement.

$$U_{Pr} = \sqrt{(U_{pt})^2 + (U_a)^2 + (U_{A/D})^2}$$

Where U_{pt} is the error (accuracy) of piezoelectric pressure sensor (Table 3-8), U_a is the error of charge amplifier (Table 3-8) and $U_{A/D}$ is the error from analog/digital *(A/D)* converter for ±10 Volt and resolution of 12 bit (from manufacturer's specifications of charge amplifier).

$$U_{A/D} = \frac{\theta}{FSR} \times 100\%$$

$$\theta = \frac{FSR}{2^r}$$

$$U_{A/D} = \frac{1}{2^r} \times 100\% = \frac{1}{2^{12}} \times 100 = 0.024\%$$

Where θ represents the quantization interval, *FSR* is the *A/D* convertor range and *r* is the resolution of *A/D* convertor.

$$U_V = \sqrt{(U_{CA})^2 + (U_{A/D})^2}$$

Where U_{CA} is the crank angle error (from manufacturer's specifications Table 3-8).

The uncertainty calculation of COV_{IMEP} is another example as an uncertainty of non-repeatability factor of *IMEP* ($U_{COV_{IMEP}}$). It was assumed that, the uncertainty was normally distributed (Gaussian distribution), thus [385]:

$$COV_{IMEP}=\frac{SD_{IMEP}}{IMEP}\times 100\%$$

$$U_{COV_{IMEP}}=t\times\frac{SD_{COV_{IMEP}}}{\sqrt{N}}$$

t is equal to 1.96 for 95% confidence level.

$$SD_{COV_{IMEP}}=\sqrt{\left(\frac{\partial COV_{IMEP}}{\partial SD_{IMEP}}\times SD_{SD_{IMEP}}\right)^2+\left(\frac{\partial COV_{IMEP}}{\partial IMEP}\times SD_{IMEP}\right)^2}$$

$$SD_{COV_{IMEP}}=100\%\times\sqrt{\left(\frac{1}{IMEP}\times SD_{SD_{IMEP}}\right)^2+\left(\frac{-SD_{IMEP}}{IMEP^2}\times SD_{IMEP}\right)^2}$$

SD_{IMEP} is the standard deviation of *IMEP* and $SD_{SD_{IMEP}}$ represents the standard deviation of the *IMEP* standard deviation (fractional standard deviation of SD_{IMEP}) which can be calculated [385] as:

$$SD_{IMEP}=\left[\frac{1}{N-1}\sum_{i=1}^{N}(\overline{IMEP}-IMEP_m)^2\right]^{1/2}$$

$$SD_{SD_{IMEP}}=SD_{IMEP}\frac{1}{\sqrt{2(N-1)}}$$

Where *N* in the number of measurements (500 for the present study), $\overline{IMEP}$ is the observation of *IMEP* at each cycle and $IMEP_m$ is the mean of *IMEP* observations.

REFERENCES

[1] 2018 Outlook for Energy: A View to 2040 - ExxonMobil. 2018 [cited 2018 Apr 10]. Available from: http://cdn.exxonmobil.com/~/media/global/files/outlook-for-energy/2018/2018-outlook-for-energy.pdf.

[2] 2018 BP Energy Outlook: 2018 edition. 2018 [cited 2018 Apr 10]. Available from: https://www.bp.com/content/dam/bp/en/corporate/pdf/energy-economics/energy-outlook/bp-energy-outlook-2018.pdf.

[3] 2017 Outlook for Energy: A View to 2040 - ExxonMobil. 2017 [cited 2018 Apr 10]. Available from: https://cdn.exxonmobil.com/~/media/global/files/outlook-for-energy/2017/2017-outlook-for-energy.pdf.

[4] Ghorani-Azam A, Riahi-Zanjani B, Balali-Mood M. Effects of air pollution on human health and practical measures for prevention in Iran. Journal of Research in Medical Sciences 2016;21.doi:10.4103/1735-1995.189646.

[5] Rumana HS, Sharma RC, Beniwa V, Sharma AK. A retrospective approach to assess human health risks associated with growing air pollution in urbanized area of Thar Desert, western Rajasthan, India. Journal of Environmental Health Science and Engineering 2014;12.doi:10.1186/2052-336X-12-23.

[6] Yamamoto SS, Phalkey R, Malik AA. A systematic review of air pollution as a risk factor for cardiovascular disease in South Asia: Limited evidence from India and Pakistan. International Journal of Hygiene and Environmental Health 2014;217(2-3):133-144.

[7] Zhang W, Qian CN, Zeng YX. Air pollution: a smoking gun for cancer. Chinese Journal of Cancer 2014;33(4):173-175.

[8] Brucker N, Charão MF, Moro AM, Ferrari P, Bubols G, Sauer E, Fracasso R, Durgante J, Thiesen FV, Duarte MM, Gioda A, Castro I, Saldiva PH, Garcia SC. Atherosclerotic process in taxi drivers occupationally exposed to air pollution and co-morbidities. Environmental Research 2014;131:31-38.

[9] Vermaelen K, Brusselle G. Exposing a deadly alliance: Novel insights into the biological links between COPD and lung cancer. Pulmonary Pharmacology and Therapeutics 2013;26(5):544-554.

[10] Kan H, Chen B, Zhao N, London SJ, Song G, Chen G, Zhang Y, Jiang L. Part 1. A time-series study of ambient air pollution and daily mortality in Shanghai, China. Research report (Health Effects Institute) 2010;154:17-78.

[11] Habre R, Coull B, Moshier E, Godbold J, Grunin A, Nath A, Castro W, Schachter N, Rohr A, Kattan M, Spengler J, Koutrakis P. Sources of indoor air pollution in New York City residences of asthmatic children. Journal of Exposure Science and Environmental Epidemiology 2014;24:269-278.

[12] Robinson DL. Air pollution in Australia: review of costs, sources and potential solutions. Health Promotion Journal of Australia 2005;16(3):213-220.

[13] Khalili NR, Duecker S, Ashton W, Chavez F. From cleaner production to sustainable development: the role of academia. Journal of Cleaner Production 2015;96:30-43.

[14] Algayyim MS, Wandel A, Yusaf T, Hamawand I. Production and application of ABE as a biofuel. Renewable and Sustainable Energy Reviews 2018;82(1):1195-1214.

[15] Mofijur M, Rasul MG, Hyde J, Azad AK, Mamat R, Bhuiya MMK. Role of biofuel and their binary (diesel-biodiesel) and ternary (ethanol-biodiesel-diesel) blends on internal combustion engines emission reduction. Renewable and Sustainable Energy Reviews 2016;53:265-278.

[16] Shahir SA, Masjuki HH, Kalam MA, Imran A, Fattah IMR, Sanjid A. Feasibility of diesel-biodiesel-ethanol/bioethanol blend as existing CI engine fuel: An assessment of properties, material compatibility, safety and combustion. Renewable and Sustainable Energy Reviews 2014;32:379-395.

[17] Dharma S, Ong HC, Masjuki HH, Sebayang AH, Silitonga AS. An overview of engine durability and compatibility using biodiesel-bioethanol-diesel blends in compression-ignition engines. Energy Conversion and Management 2016;128:66-81.

[18] Suresh M, Jawahar CP, Richard A. A review on biodiesel production, combustion, performance, and emission characteristics of non-edible oils in variable compression ratio diesel engine using biodiesel and its blends. Renewable and Sustainable Energy Reviews 2018;92:38-49.
[19] Ramalingam S, Rajendran S, Ganesan P. Performance improvement and exhaust emissions reduction in biodiesel operated diesel engine through the use of operating parameters and catalytic converter: A review. Renewable and Sustainable Energy Reviews 2018;81(2):3215-3222.
[20] Barabas I, Todoruj A. Key fuel properties of biodiesel-diesel fuel-ethanol blends. SAE Technical Paper 2009;2009-01-1810.
[21] Imran A, Varman M, Masjuki HH, Kalam MA. Review on alcohol fumigation on diesel engine: A viable alternative dual fuel technology for satisfactory engine performance and reduction of environment concerning emission. Renewable and Sustainable Energy Reviews 2013;26:739-751.
[22] Gomasta S, Mahla S. An experimental investigation of ethanol blended diesel fuel on engine performance and emission of a diesel engine. International Journal on Emerging Technologies 2012;3(1):74-79.
[23] Jamuwa D, Sharma D, Soni S. Experimental investigation of performance, exhaust emission and combustion parameters of compression ignition engine with varying ethanol energy fractions. Energy 2017;127:544-557.
[24] Surawski NC, Miljevic B, Roberts BA, Modini RL, Situ R, Brown RJ, Bottle SE, Ristovski ZD. Particle emissions, volatility, and toxicity from an ethanol fumigated compression ignition engine. Environmental Science and Technology 2010;44(1):229-235.
[25] Zöldy M. Ethanol-biodiesel-diesel blends as a diesel extender option compression ignition engines. Transport 2011;26(3):303-309.
[26] Barabás I, Todoruţ IA. Utilization of biodiesel-diesel-ethanol blends in CI engine. In: Montero G, editor. Biodiesel-quality, emissions and by-products. InTech; 2011. pp. 215-234.
[27] Shahir SA, Masjuki HH, Kalam MA, Imran A, Ashraful AM. Performance and emission assessment of diesel-biodiesel-ethanol/bioethanol blend as a fuel in diesel engines: A review. Renewable and Sustainable Energy Reviews 2015;48:62-78.
[28] Ghadikolaei MA. Effect of alcohol blend and fumigation on regulated and unregulated emissions of IC engines- A review. Renewable and Sustainable Energy Reviews 2016;57:1440-1495.
[29] Çelebi Y, Aydın H. An overview on the light alcohol fuels in diesel engines. Fuel 2019;236:890-911.
[30] Abu-Qudais M, Haddad O, Qudaisat M. The effect of alcohol fumigation on diesel engine performance and emissions. Energy Conversion and Management 2000;41(4):389-399.
[31] Cheng CH, Cheung CS, Chan TL, Lee SC, Yao CD, Tsang KS. Comparison of emissions of a direct injection diesel engine operating on biodiesel with emulsified and fumigated methanol. Fuel 2008;87(10-11):1870-1879.
[32] Şahin Z, Durgun O, Aksu ON. Experimental investigation of n-butanol/diesel fuel blends and n-butanol fumigation - Evaluation of engine performance, exhaust emissions, heat release and flammability analysis. Energy Conversion and Management 2015;103:778-789.
[33] Mariasiu F, Burnete N, Moldovanu D, Varga B, Iclodean C, Kocsis L. Effects of bioethanol ultrasonic generated aerosols application on diesel engine performances. Thermal Science 2015;19(6):1931-1941.
[34] Lee S, Kim TY. Feasibility study of using wood pyrolysis oil-ethanol blended fuel with diesel pilot injection in a diesel engine. Fuel 2015;162:65-73.
[35] Lee S, Jang Y, Kim TY, Kang KY, Kim H, Lim J. Performance and emission characteristics of a diesel engine fueled with pyrolysis oil-ethanol blend with diesel and biodiesel pilot injection. SAE International Journal of Fuels and Lubricants 2013;6(3):785-793.
[36] Akhtar US, Rastogi N, McWhinney RD, Urch B, Chow CW, Evans GJ, Scott JA. The combined effects of physicochemical properties of size-fractionated ambient particulate

matter on in vitro toxicity in human A549 lung epithelial cells. Toxicology Reports 2014;1:145-156.
[37] Shin SW, Song IH, Um SH. Role of physicochemical properties in nanoparticle toxicity. Nanomaterials 2015;5(3):1351-1365.
[38] Dockery DW, Pope CA, Xu X, Spengler JD, Ware JH, Fay ME, Ferris BG, Speizer FE. An association between air pollution and mortality in six U.S. Cities. The New England Journal of Medicine 1993;329:1753-1759.
[39] Gauderman WJ, Avol E, Gilliland F, Vora H, Thomas D, Berhane K, McConnell R, Kuenzli N, Lurmann F, Rappaport E, Margolis H, Bates D, Peters J. The effect of air pollution on lung development from 10 to 18 years of age. The New England Journal of Medicine 2004;351 :1057-1067.
[40] Katsouyanni K, Touloumi G, Samoli E, Gryparis A, Le Tertre A, Monopolis Y, Rossi G, Zmirou D, Ballester F, Boumghar A, Anderson HR, Wojtyniak B, Paldy A, Braunstein R, Pekkanen J, Schindler C, Schwartz J. Confounding and effect modification in the short-term effects of ambient particles on total mortality: results from 29 European cities within the APHEA2 project. Epidemiology 2001;12(5):521-531.
[41] Knauer M, Schuster ME, Su D, Schlögl R, Niessner R, Ivleva NP. Soot structure and reactivity analysis by Raman microspectroscopy, temperature-programmed oxidation, and high-resolution transmission electron microscopy. The Journal of Physical Chemistry A 2009;113(50):13871-13880.
[42] Agarwal AK. Biofuels (alcohols and biodiesel) applications as fuels for internal combustion engines. Progress in Energy and Combustion Science 2007;33(3):233-271.
[43] Lapuerta M, Armas O, Rodríguez-Fernández J. Effect of biodiesel fuels on diesel engine emissions. Progress in Energy and Combustion Science 2008;34(2):198-223.
[44] Lapuerta M, Fernández JR, Rodríguez DF, Camino RP. Cold flow and filterability properties of n-butanol and ethanol blends with diesel and biodiesel fuels. Fuel 2018;224:552-559.
[45] Madiwale S, Karthikeyan A, Bhojwani V. Properties investigation and performance analysis of a diesel engine Properties investigation and performance analysis of a diesel engine using Ethanol as an additive. Materials Today: Proceedings 2018;5:657-664.
[46] Low MH, Mukhtar MNA, Hagos FY, Noor MM. Tri-fuel (diesel-biodiesel-ethanol) emulsion characterization, stability and the corrosion effect. IOP Conference Series: Materials Science and Engineering 2017;257.doi:10.1088/1757-899X/257/1/012082.
[47] Kwanchareon P, Luengnaruemitchai A, Jai-In S. Solubility of a diesel-biodiesel-ethanol blend, its fuel properties, and its emission characteristics from diesel engine. Fuel 2007;86:1053-1061.
[48] Thangavelu SK, Ahmed AS, Ani FN. Impact of metals on corrosive behavior of biodiesel-diesel-ethanol (BDE) alternative fuel. Renewable Energy 2016;94:1-9.
[49] Lapuerta M, García-Contreras R, Campos-Fernández J, Dorado MP. Stability, lubricity, viscosity, and cold-flow properties of alcohol-diesel blends. Energy and Fuels 2010;24(8):4497-4502.
[50] Reyes Y, Aranda DAG, Santander LAM, Cavado A, Belchior CRP. Action principles of cosolvent additives in ethanol-diesel blends: stability studies. Energy and Fuels 2009;23(5):2731-2735.
[51] Torres-Jimenez E, Svoljsak-Jerman M, Gregorc A, Lisec I, Dorado M, Kegl B. Physical and chemical properties of ethanol-biodiesel blends for diesel engines. Energy and Fuels 2010;24(3):2002-2009.
[52] McCormick RL, Parish R. Advanced petroleum based fuels program and renewable diesel program. Colorado: National Renewable Energy Laboratory NREL/MP-540-32674; 2001 Milestone Report.
[53] Fernando S, Flanna M. Development of a novel biofuel blend using ethanol- biodiesel-diesel microemulsions: EB-diesel. Energy and Fuels 2004;18(6):1695-1703.
[54] Lapuerta M, Armas O, Garria-Contreras R. Effect of ethanol on blending stability and diesel engine emissions. Energy and Fuels 2009;23(9):4343-4354.
[55] Bhale PV, Deshpande NV, Thombre SB. Improving the low temperature properties of

biodiesel fuel. Renewable Energy 2009;34(3):794-800.
[56] Shi X, Yu Y, He H, Shuai S, Wang J, Li R. Emission characteristics using methyl soyate-ethanoldiesel diesel fuel blends on a diesel engine. Fuel 2005;84:1543-1549.
[57] Hulwan DB, Joshi SV. Performance, emission and combustion characteristic of a multicylinder DI diesel engine running on diesel-ethanol-biodiesel blends of high ethanol content. Applied Energy 2011;88(12):5042-5055.
[58] Yesilyurt MK. The effects of the fuel injection pressure on the performance and emission characteristics of a diesel engine fuelled with waste cooking oil biodiesel-diesel blends. Renewable Energy 2019;132:649-666.
[59] Sathiyamoorthi R, Sankaranarayanan G, Adhith kumaar SB, Chiranjeevi T, Kumar DD. Experimental investigation on performance, combustion and emission characteristics of a single cylinder diesel engine fuelled by biodiesel derived from Cymbopogon Martinii. Renewable Energy 2019;132:394-415.
[60] How HG, Masjuki HH, Kalam MA, Teoh YH. Influence of injection timing and split injection strategies on performance, emissions, and combustion characteristics of diesel engine fueled with biodiesel blended fuels. Fuel 2018;213:106-114.
[61] Musthafa MM, Kumar TA, Mohanraj T, Chandramouli R. A comparative study on performance, combustion and emission characteristics of diesel engine fuelled by biodiesel blends with and without an additive. Fuel 2018;225:343-348.
[62] Wei L, Cheng R, Mao H, Geng P, Zhang Y, You K. Combustion process and NO_X emissions of a marine auxiliary diesel engine fuelled with waste cooking oil biodiesel blends. Energy 2018;144:73-80.
[63] Yilmaz N, Atmanli A. Experimental assessment of a diesel engine fueled with diesel-biodiesel-1-pentanol blends. Fuel 2017;191:190-197.
[64] Ramesh DK, Kumar JLD, Kumar SGH, Namith V, Jambagi PB, Sharath S. Study on effects of alumina nanoparticles as additive with poultry litter biodiesel on performance, combustion and emission characteristic of diesel engine. Materials Today: Proceedings 2018;5(1):1114-1120.
[65] Žaglinskis J, Lukács K, Bereczky Á. Comparison of properties of a compression ignition engine operating on diesel–biodiesel blend with methanol additive. Fuel 2016;170:245-253.
[66] Akar MA. Performance and emission characteristics of compression ignition engine operating with false flax biodiesel and butanol blends. Advances in Mechanical Engineering 2016;8(2):1-7.
[67] Ghanbari M, Najafi G, Ghobadian B, Yusaf T, Carlucci AP, Kiani MKD. Performance and emission characteristics of a CI engine using nano particles additives in biodiesel-diesel blends and modeling with GP approach. Fuel 2017;202:699-716.
[68] Imdadul HK, Masjuki HH, Kalam MA, Zulkifli NWM, Alabdulkarem A, Rashed MM, Teoh YH, How HG. Higher alcohol-biodiesel-diesel blends: An approach for improving the performance, emission, and combustion of a light-duty diesel engine. Energy Conversion and Management 2016;111:174-185.
[69] Tüccar G, Özgür T, Aydın K. Effect of diesel-microalgae biodiesel-butanol blends on performance and emissions of diesel engine. Fuel 2014;132:47-52.
[70] Song H, Quinton KS, Peng Z, Zhao H, Ladommatos N. Effects of oxygen content of fuels on combustion and emissions of diesel engines. Energies 2016;9(28). doi:10.3390/en9010028.
[71] Yasin MHM, Aziz A, Mamat R, Yusop AF, Najafi G. Comparative study on biodiesel-methanol-diesel low proportion blends operating with a diesel engine. Energy Procedia 2015;75:10-16.
[72] Balakrishnan A, Parthasarathy RN, Gollahalli SR. A Review on the effects of biodiesel blends on compression ignition engine NOx emissions. Journal of Energy and Environmental Sustainability 2016;1:67-76.
[73] Atmanli A. Comparative analyses of diesel-waste oil biodiesel and propanol, n-butanol or 1-pentanol blends in a diesel engine. Fuel 2016;176:209-215.
[74] Hirkude J, Belokar V, Randhir J. Effect of compression ratio, injection pressure and injection timing on performance and smoke emissions of CI engine fuelled with waste fried

oil methyl esters - diesel blend. Materials Today: Proceedings 2018;5(1):1563-1570.
[75] Yilmaz N, Atmanli A, Vigil FM. Quaternary blends of diesel, biodiesel, higher alcohols and vegetable oil in a compression ignition engine. Fuel 2018;212:462-469.
[76] Tutak W, Jamrozik A, Pyrc M, Sobiepański M. A comparative study of co-combustion process of diesel-ethanol and biodiesel-ethanol blends in the direct injection diesel engine. Applied Thermal Engineering 2017;117:155-163.
[77] Emiroğlu AO, Şen M. Combustion, performance and emission characteristics of various alcohol blends in a single cylinder diesel engine. Fuel 2018;212:34-40.
[78] Jamrozik A. The effect of the alcohol content in the fuel mixture on the performance and emissions of a direct injection diesel engine fueled with diesel-methanol and diesel-ethanol blends. Energy Conversion and Management 2017;148:461-476.
[79] Wei L, Cheung CS, Ning Z. Effects of biodiesel-ethanol and biodiesel-butanol blends on the combustion, performance and emissions of a diesel engine. Energy 2018;155:957-970.
[80] Datta A, Mandal BK. Engine performance, combustion and emission characteristics of a compression ignition engine operating on different biodiesel-alcohol blends. Energy 2017;125:470-483.
[81] Sayin C. Engine performance and exhaust gas emissions of methanol and ethanol-diesel blends. Fuel 2010;89(11):3410-3415.
[82] Sayin C, Ozsezen AN, Canakci M. The influence of operating parameters on the performance and emissions of a DI diesel engine using methanol-blended-diesel fuel. Fuel 2010;89(7):1407-1414.
[83] Zhu L, Cheung CS, Zhang WG, Huang Z. Emissions characteristics of a diesel engine operating on biodiesel and biodiesel blended with ethanol and methanol. Science of The Total Environment 2010;408(4):914-921.
[84] Anand K, Sharma RP, Mehta PS. Experimental investigations on combustion, performance and emissions characteristics of neat karanji biodiesel and its methanol blend in a diesel engine. Biomass and Bioenergy 2011;35(1):533-541.
[85] Yilmaz N. Comparative analysis of biodiesel-ethanol-diesel and biodiesel-methanol-diesel blends in a diesel engine. Energy 2012;40 (1):210-213.
[86] Venu H, Madhavan V. Influence of diethyl ether (DEE) addition in ethanol-biodiesel-diesel (EBD) and methanol-biodiesel-diesel (MBD) blends in a diesel engine. Fuel 2017;189:377-390.
[87] Qi DH, Chen H, Geng LM, Bian YZH, Ren XCH. Performance and combustion characteristics of biodiesel-diesel-methanol blend fuelled engine. Applied Energy 2010;87(5):1679-1686.
[88] Çelebi Y, Aydın H. Investigation of the effects of butanol addition on safflower biodiesel usage as fuel in a generator diesel engine. Fuel 2018;222:385-393.
[89] Zheng Z, Xia M, Liu H, Shang R, Ma G, Yao M. Experimental study on combustion and emissions of n-butanol/biodiesel under both blended fuel mode and dual fuel RCCI mode. Fuel 2018;226:240-251.
[90] Nanthagopal K, Ashok B, Saravanan B, Patel D, Sudarshan B, Ramasamy RA. An assessment on the effects of 1-pentanol and 1-butanol as additives with Calophyllum Inophyllum biodiesel. Energy Conversion and Management 2018;158:70-80.
[91] Ashok B, Nanthagopal K, Saravanan B, Azad K, Patel D, Sudarshan B, Ramasamy RA. Study on isobutanol and Calophyllum inophyllum biodiesel as a partial replacement in CI engine applications. Fuel 2019;235:984-994.
[92] Zhang ZH, Chua SM, Balasubramanian R. Comparative evaluation of the effect of butanol-diesel and pentanol-diesel blends on carbonaceous particulate composition and particle number emissions from a diesel engine. Fuel 2016;176:40-47.
[93] Kumar BR, Saravanan S. Effects of iso-butanol/diesel and n-pentanol/diesel blends on performance and emissions of a DI diesel engine under premixed LTC (low temperature combustion) mode. Fuel 2016;170:49-59.
[94] Campos-Fernández J, Arnal JM, Gómez J, Dorado MP. A comparison of performance of higher alcohols/diesel fuel blends in a diesel engine. Applied Energy 2012;95:267-275.
[95] Satsangi DP, Tiwari N. Experimental investigation on combustion, noise, vibrations,

performance and emissions characteristics of diesel/n-butanol blends driven genset engine. Fuel 2018;221:44-60.
[96] Atmanli A, Yilmaz N. A comparative analysis of n-butanol/diesel and 1-pentanol/diesel blends in a compression ignition engine. Fuel 2018;234:161-169.
[97] Atmanli A, Ileri E, Yuksel B, Yilmaz N. Extensive analyses of diesel-vegetable oil-n-butanol ternary blends in a diesel engine. Applied Energy 2015;145:155-162.
[98] Zhang ZH, Balasubramanian R. Influence of butanol addition to diesel-biodiesel blend on engine performance and particulate emissions of a stationary diesel engine. Applied Energy 2014;119:530-536.
[99] Atmanli A, Ileri E, Yilmaz N. Optimization of diesel-butanol-vegetable oil blend ratios based on engine operating parameters. Energy 2016;96:569-580.
[100] Atmanli A, Yüksel B, İleri E, Karaoglan AD. Response surface methodology based optimization of diesel-n-butanol-cotton oil ternary blend ratios to improve engine performance and exhaust emission characteristics. Energy Conversion and Management 2015;90:383-394.
[101] Atmanli A, Yüksel B, İleri E. Experimental investigation of the effect of diesel-cotton oil-n-butanol ternary blends on phase stability, engine performance and exhaust emission parameters in a diesel engine. Fuel 2013;109:503-511.
[102] Atmanli A, İleri E, Yüksel B. Effects of higher ratios of n-butanol addition to diesel-vegetable oil blends on performance and exhaust emissions of a diesel engine. Journal of the Energy Institute 2015;88(3):209-220.
[103] Atmanli A, İleri E, Yüksel B. Experimental investigation of engine performance and exhaust emissions of a diesel engine fueled with diesel-n-butanol-vegetable oil blends. Energy Conversion and Management 2014;81:312-321.
[104] Ibrahim A. Performance and combustion characteristics of a diesel engine fuelled by butanol-biodiesel-diesel blends. Applied Thermal Engineering 2016;103:651-659.
[105] Wei L, Cheung CS, Huang Z. Effect of n-pentanol addition on the combustion, performance and emission characteristics of a direct-injection diesel engine. Energy 2014;70:172-180.
[106] Nanthagopal K, Ashok B, Saravanan B, Korah SM, Chandra S. Effect of next generation higher alcohols and Calophyllum inophyllum methyl ester blends in diesel engine. Journal of Cleaner Production 2018;180:50-63.
[107] Imdadul HK, Masjuki HH, Kalam MA, Zulkifli NWM, Alabdulkarem A, Rashed MM, Ashraful AM. Influences of ignition improver additive on ternary (diesel-biodiesel-higher alcohol) blends thermal stability and diesel engine performance. Energy Conversion and Management 2016;123:252-264.
[108] Babu D, Anand R. Effect of biodiesel-diesel-n-pentanol and biodiesel-diesel-n-hexanol blends on diesel engine emission and combustion characteristics. Energy 2017;133:761-776.
[109] Balamurugan T, Nalini R. Effect of blending alcohol with diesel on performance, combustion and emission characteristics of four stroke diesel engine- An experimental study. International Journal of ChemTech Research 2014;6 (1):750-762.
[110] Muthaiyan P, Gomathinayagam S. Combustion characteristics of a diesel engine using propanol diesel fuel blends. Journal of The Institution of Engineers (India): Series C 2016;97(3):323-329.
[111] Singh A, Mishra C, Vibhanshu V, Kumar N. Performance evaluation and emission studies of a single cylinder diesel engine fuelled with isopropyl alcohol and diesel. SAE Technical Paper 2013;2013-01-1132.doi:10.4271/2013-01-1132.
[112] Balamurugan T, Nalini R. Experimental investigation on performance, combustion and emission characteristics of four stroke diesel engine using diesel blended with alcohol as fuel. Energy 2014;78:356-363.
[113] Yoshimoto Y, Onodera M, Tamaki H. Performance and emission characteristics of diesel engines fueled by vegetable oils. SAE Technical Paper 2001;2001-01-1807. doi:10.4271/2001-01-1807.
[114] Dhanasekaran R, Ganesan S, Kumar BR, Saravanan S. Utilization of waste cooking oil in a

light-duty DI diesel engine for cleaner emissions using bio-derived propanol. Fuel 2019;235:832-837.
[115] Yogesh P, Sakthi SD, Aravinth C, Sathiyakeerthy K, Susenther M. Performance test on diesel-biodiesel-propanol blended fuels in CI engine. International Journal of Innovative Science and Research Technology 2018;3(2):294-299.
[116] Krishnamoorthy V, Dhanasekaran R, Rana D, Saravanan S, Kumar BR. A comparative assessment of ternary blends of three bio-alcohols with waste cooking oil and diesel for optimum emissions and performance in a CI engine using response surface methodology. Energy Conversion and Management 2018;156:337-357.
[117] Gopal K, Sathiyagnanam AP, Kumar BR, Saravanan S, Rana D, Sethuramasamyraja B. Prediction of emissions and performance of a diesel engine fueled with n-octanol/diesel blends using response surface methodology. Journal of Cleaner Production 2018;184:423-439.
[118] Deep A, Kumar N, Karnwal A, Gupta D, Vibhanshu V, Sharma A, Patel JS. Assessment of the performance and emission characteristics of 1-octanol/diesel fuel blends in a water cooled compression ignition engine. SAE Technical Paper 2014.doi.org/10.4271/2014-01-2830:2014-01-2830.
[119] Koul R. Performance characteristics of a single cylinder diesel engine fuelled with 1-octanol diesel blends. International Journal of Latest Trends in Engineering and Technology 2015;5(1):302-306.
[120] Ashok B, Nanthagopal K, Anand V, Aravind KM, Jeevanantham AK, Balusamy S. Effects of n-octanol as a fuel blend with biodiesel on diesel engine characteristics. Fuel 2019;235:363-373.
[121] Suhaimi H, Adam A, Mrwan AG, Abdullah Z, Othman MF, Kamaruzzaman MK, Hagos FY. Analysis of combustion characteristics, engine performances and emissions of long-chain alcohol-diesel fuel blends. Fuel 2018;220:682-691.
[122] Vijayakumar M, kumar PCM. Performance enhancement and emissions analysis of diesel engine with biodiesel, n-propanol and 1-butanol blend. Journal of Applied Fluid Mechanics 2017;10:79-84.
[123] Luo J, Zhang Y, Wang J, Zhang Q. Effect of acetone-butanol-ethanol addition to diesel on the soot reactivity. Fuel 2018;226:555-563.
[124] Ali Y, Hanna MA, Borg JE. Optimization of diesel, methyl tallowate and ethanol blend for reducing emissions from diesel engine. Bioresource Technology 1995;52(3):237-243.
[125] Shi X, Pang X, Mu Y, He H, Shuai S, Wang J, Chen H, Li R. Emission reduction potential of using ethanol-biodiesel-diesel fuel blend on a heavy-duty diesel engine. Atmospheric Environment 2006;40:2567-2574.
[126] Barabás I, Todoruţ A, Băldean D. Performance and emission characteristics of an CI engine fueled with diesel-biodiesel-bioethanol blends. Fuel 2010;89(12):3827-3832.
[127] de Oliveira A, de Morais AM, Valente OS, Sodré JR. Combustion characteristics, performance and emissions from a diesel power generator fuelled by B7-ethanol blends. Fuel Processing Technology 2015;139:67-72.
[128] Tse H, Leung CW, Cheung CS. Performances, emissions and soot properties from a diesel-biodiesel ethanol blend fuelled engine. Advances in Automobile Engineering 2016;S1:005. doi:10.4172/2167-7670.S1-005.
[129] Tse H, Leung CW, Cheung CS. Investigation on the combustion characteristics and particulate emissions from a diesel engine fueled with diesel-biodiesel-ethanol blends. Energy 2015;83:343-350.
[130] Shinde SV, Sonawane RR, Palande DD. Performance and emission analysis of diesel-ethanol-biodiesel blend on CI engine. International Journal of Advance Research and Innovative Ideas in Education 2016;2(4):792-801.
[131] Paul A, Panua R, Debroy D. An experimental study of combustion, performance, exergy and emission characteristics of a CI engine fueled by diesel-ethanol-biodiesel blends. Energy 2017;141:839-852.
[132] Aydın F, Öğüt H. Effects of using ethanol-biodiesel-diesel fuel in single cylinder diesel engine to engine performance and emissions. Renewable Energy 2017;103:688-694.

[133] Jamrozik A, Tutak W, Pyrc M, Sobiepanski M. Effect of diesel-biodiesel-ethanol blend on combustion, performance, and emissions characteristics on a direct injection diesel engine. Thermal Science 2017;21(1B):591-604.
[134] Tan YH, Abdullah MO, Nolasco-Hipolito C, Zauzi NSA, Abdullah GW. Engine performance and emissions characteristics of a diesel engine fueled with diesel-biodiesel-bioethanol emulsions. Energy Conversion and Management 2017;132:54-64.
[135] Hu N, Tan J, Wang X, Zhang X, Yu P. Volatile organic compound emissions from an engine fueled with an ethanol-biodiesel-diesel blend. Journal of the Energy Institute 2017;90:101-109.
[136] Emiroğlu AO, Şen M. Combustion, performance and exhaust emission characterizations of a diesel engine operating with a ternary blend (alcohol-biodiesel-diesel fuel). Applied Thermal Engineering 2018;133:371-380.
[137] Noorollahi Y, Azadbakht M, Ghobadian B. The effect of different diesterol (diesele-biodiesele-ethanol) blends on small air-cooled diesel engine performance and its exhaust gases. Energy 2018;142:196-200.
[138] Guedes ADM, Braga SL, Pradelle F. Performance and combustion characteristics of a compression ignition engine running on diesel-biodiesel-ethanol (DBE) blends - Part 2: Optimization of injection timing. Fuel 2018;225:174-183.
[139] Prakash T, Geo VE, Martin LJ, Nagalingam B. Effect of ternary blends of bio-ethanol, diesel and castor oil on performance, emission and combustion in a CI engine. Renewable Energy 2018;122:301-309.
[140] Turkcan A. Effects of high bioethanol proportion in the biodiesel-diesel blends in a CRDI engine. Fuel 2018;223:53-62.
[141] Mahmudul HM, Hagos FY, Mukhtar MNA, Mamat R, Abdullah A. Effect of alcohol on diesel engine combustion operating with biodiesel-diesel blend at idling conditions. IOP Conf. Series: Materials Science and Engineering 2018;318.doi:10.1088/1757-899X/318/1/012071.
[142] Di Y, Cheung CS, Huang Z. Comparison of the effect of biodiesel-diesel and ethanol-diesel on the particulate emissions of a direct injection diesel engine. Aerosol Science and Technology 2009;43(5):455-465.
[143] Gioda A, Rodríguez-Cotto RI, Amaral BS, Encarnación-Medina J, Ortiz-Martínez MG, Jiménez-Vélez BD. Biodiesel from soybean promotes cell proliferation in vitro. Toxicology In Vitro 2016;34:283-288.
[144] Amaral BS, Ventura LMB, Amaral AS, Neto FRA, Gioda A. Concentration profiles of regulated and unregulated pollutants emitted from the combustion of soybean biodiesel and diesel/biodiesel blend originating of a diesel cycle engine. Journal of the Brazilian Chemical Society 2017;28(4):659-668.
[145] Chen H, Shuai SJ, Wang JX. Study on combustion characteristics and PM emission of diesel engines using ester-ethanol-diesel blended fuels. Proceedings of the Combustion Institute 2007;31:2981-2989.
[146] Tse H. Combustion and emissions of a diesel engine fueled with diesel-biodiesel-ethanol blends and supplemented with intake CO_2 charge dilution. In: Kyprianidis K, editor. Developments in Combustion Technology. London: Intech Open; 2016. pp. 187-232.
[147] Guan C, Cheung CS, Li X, Huang Z. Effects of oxygenated fuels on the particle-phase compounds emitted from a diesel engine. Atmospheric Pollution Research 2017;8:209-220.
[148] Jamrozik A, Tutak W, Pyrc M, Gruca M, Kočiško M. Study on co-combustion of diesel fuel with oxygenated alcohols in a compression ignition dual-fuel engine. Fuel 2018;221:329-345.
[149] Jia Z, Denbratt I. Experimental investigation into the combustion characteristics of a methanol-Diesel heavy duty engine operated in RCCI mode. Fuel 2018;226:745-753.
[150] Yao C, Pan W, Yao A. Methanol fumigation in compression-ignition engines: A critical review of recent academic and technological developments. Fuel 2017;209:713-732.
[151] Dou Z, Yao C, Wei H, Wang B, Liu M, Chen C, Gao J, Shi J. Experimental study of the effect of engine parameters on ultrafine particle in diesel/methanol dual fuel engine. Fuel 2017;192:45-52.

[152] Chen Z, Yao C, Yao A, Dou Z, Wang B, Wei H, Liu M, Chen C, Shi J. The impact of methanol injecting position on cylinder-to-cylinder variation in a diesel methanol dual fuel engine. Fuel 2017;191:150-163.
[153] Park S, Cho J, Park J, Song S. Numerical study of the performance and NO_X emission of a diesel-methanol dual-fuel engine using multi-objective Pareto optimization. Energy 2017;124:272-283.
[154] Lu H, Yao A, Yao C, Chen C, Wang B. An investigation on the characteristics of and influence factors for NO_2 formation in diesel/methanol dual fuel engine. Fuel 2019;235:617-626.
[155] Iorio SD, Magno A, Mancaruso E, Vaglieco BM. Analysis of the effects of diesel/methane dual fuel combustion on nitrogen oxides and particle formation through optical investigation in a real engine. Fuel Processing Technology 2017;159:200-210.
[156] Saxena MR, Maurya RK. Effect of premixing ratio, injection timing and compression ratio on nano particle emissions from dual fuel non-road compression ignition engine fueled with gasoline/methanol (port injection) and diesel (direct injection). Fuel 2017;203:894-914.
[157] Wei H, Yao C, Pan W, Han G, Dou Z, Wu T, Liu M, Wang B, Gao J, Chen C, Shi J. Experimental investigations of the effects of pilot injection on combustion and gaseous emission characteristics of diesel/methanol dual fuel engine. Fuel 2017;188:427-441.
[158] Li Y, Zhang C, Yu W, Wu H. Effects of rapid burning characteristics on the vibration of a common-rail diesel engine fueled with diesel-methanol dual-fuel. Fuel 2016;170:176-184.
[159] Wang Q, Wang B, Yao C, Liu M, Wu T, Wei H, Dou Z. Study on cyclic variability of dual fuel combustion in a methanol fumigated diesel engine. Fuel 2016;164:99-109.
[160] Li G, Zhang C, Li Y. Effects of diesel injection parameters on the rapid combustion and emissions of an HD common-rail diesel engine fueled with diesel-methanol dual-fuel. Applied Thermal Engineering 2016;108:1214-1225.
[161] Chen Z, Yao C, Wang Q, Han G, Dou Z, Wei H, Wang B, Liu M, Wu T. Study of cylinder-to-cylinder variation in a diesel engine fueled with diesel/methanol dual fuel. Fuel 2016;170:67-76.
[162] Iorio SD, Magno A, Mancaruso E, Vaglieco BM. Characterization of particle number and mass size distributions from a small compression ignition engine operating in diesel/methane dual fuel mode. Fuel 2016;180:613-623.
[163] Wang Q, Wei L, Pan W, Yao C. Investigation of operating range in a methanol fumigated diesel engine. Fuel 2015;140:164-170.
[164] Pan W, Yao C, Han G, Wei H, Wang Q. The impact of intake air temperature on performance and exhaust emissions of a diesel methanol dual fuel engine. Fuel 2015;162:101-110.
[165] Liu J, Yao A, Yao C. Effects of diesel injection pressure on the performance and emissions of a HD common-rail diesel engine fueled with diesel/methanol dual fuel. Fuel 2015;140:192-200.
[166] Wang Q, Yao C, Dou Z, Wang B, Wu T. Effect of intake pre-heating and injection timing on combustion and emission characteristics of a methanol fumigated diesel engine at part load. Fuel 2015;159:796-802.
[167] Zhang ZH, Cheung CS, Yao CD. Influence of fumigation methanol on the combustion and particulate emissions of a diesel engine. Fuel 2013;111:442-448.
[168] Zhang ZH, Tsang KS, Cheung CS, Chan TL, Yao CD. Effect of fumigation methanol and ethanol on the gaseous and particulate emissions of a direct-injection diesel engine. Atmospheric Environment 2011;45(11):2001-2008.
[169] Zhang ZH, Cheung CS, Chan TL, Yao CD. Experimental study on particulate emissions of a methanol fumigated diesel engine equipped with diesel oxidation catalyst. Aerosol Science and Technology 2011;45(2):262-271.
[170] Zheng Z, Xia M, Liu H, Wang X, Yao M. Experimental study on combustion and emissions of dual fuel RCCI mode fueled with biodiesel/n-butanol, biodiesel/2,5-dimethylfuran and biodiesel/ethanol. Energy 2018;148:824-838.
[171] Xiao J, Jia M, Chang Y, Li Y, Xu Z, Xu G, Liu H, Wang T. Numerical optimization and comparative study of n-butanol concentration stratification combustion and n-butanol/diesel

reactivity stratification combustion for advanced compression ignition (CI) engine. Fuel 2018;213:83-97.
[172] Yadav J, Ramesh A. Injection strategies for reducing smoke and improving the performance of a butanol-diesel common rail dual fuel engine. Applied Energy 2018;212:1-12.
[173] Pan S, Li X, Han W, Huang Y. An experimental investigation on multi-cylinder RCCI engine fueled with 2-butanol/diesel. Energy Conversion and Management 2017;154:92-101.
[174] Zhang C, Zhang C, Xue L, Li Y. Combustion characteristics and operation range of a RCCI combustion engine fueled with direct injection n-heptane and pipe injection n-butanol. Energy 2017;125:439-448.
[175] Qian Y, Ouyang L, Wang X, Zhu L, Lu X. Experimental studies on combustion and emissions of RCCI fueled with n-heptane/alcohols fuels. Fuel 2015;162:239-250.
[176] Liu H, Wang X, Zheng Z, Gu J, Wang H, Yao M. Experimental and simulation investigation of the combustion characteristics and emissions using n-butanol/biodiesel dual-fuel injection on a diesel engine. Energy 2014;74:741-752.
[177] Vallinayagam R, Vedharaj S, Yang WM, Raghavan V, Saravanan CG, Lee PS, Chua KJE, Chou SK. Investigation of evaporation and engine characteristics of pine oil biofuel fumigated in the inlet manifold of a diesel engine. Applied Energy 2014;115:514-524.
[178] Vallinayagam R, Vedharaj S, Yang WM, Saravanan CG, Lee PS, Chua KJE, Chou SK. Impact of pine oil biofuel fumigation on gaseous emissions from a diesel engine. Fuel Processing Technology 2014;124:44-53.
[179] Tsang KS, Zhang ZH, Cheung CS, Chan TL. Reducing emissions of a diesel engine using fumigation ethanol and a diesel oxidation catalyst. Energy and Fuels 2010;24:6156-6165.
[180] Broukhiyan EMH, Lestz SS. Ethanol fumigation of a light duty automotive diesel engine. SAE Technical Paper 1981;811209.https://doi.org/10.4271/811209.
[181] Heisey JB, Lestz SS. Aqueous alcohol fumigation of a single-cylinder DI diesel engine. SAE Technical Paper 1981;811208.https://doi.org/10.4271/811208.
[182] Hayes TK, Savage LD, White RA, Sorenson SC. The effect of fumigation of different ethanol proofs on a turbocharged diesel engine. SAE Technical Paper 1988;880497.https://doi.org/10.4271/880497.
[183] Chauhan BS, Kumar N, Pal SS, Jun YD. Experimental studies on fumigation of ethanol in a small capacity diesel engine. Energy 2011;36(2):1030-1038.
[184] Pannirselvam A, Ramajayam M, Gurumani V, Arulselvan S, Karthikeyan G. Experimental studies on the performance and emission characteristics of an ethanol fumigated diesel engine. International Journal of Engineering Research and Applications 2012;2(2):1519-1527.
[185] Morsy MH. Assessment of a direct injection diesel engine fumigated with ethanol/water mixtures. Energy Conversion and Management 2015;94:406-414.
[186] Bharathiraja M, Venkatachalam R, Murugesan A, Tiruvenkadam N. Experimental investigation of a novel alcohol fumigation in a single-cylinder constant speed diesel engine. International Journal of Ambient Energy 2017;38(8):794-802.
[187] Kumar MS, Nataraj G, Arulselvan S. A comprehensive assessment on the effect of high octane fuels induction on engine's combustion behaviour of a Mahua oil based dual fuel engine. Fuel 2017;199:176-184.
[188] Geo VE, Sonthalia A, Nagarajan G, Nagalingam B. Studies on performance, combustion and emission of a single cylinder diesel engine fuelled with rubber seed oil and its biodiesel along with ethanol as injected fuel. Fuel 2017;209:733-741.
[189] Lee J, Lee S, Lee S. Experimental investigation on the performance and emissions characteristics of ethanol/diesel dual-fuel combustion. Fuel 2018;220:72-79.
[190] Pedrozo VB, Zhao H. Improvement in high load ethanol-diesel dual-fuel combustion by Miller cycle and charge air cooling. Applied Energy 2018;210:138-151.
[191] Ruiz FA, Cadrazco M, López AF, Sanchez-Valdepeñas J, Agudelo JR. Impact of dual-fuel combustion with n-butanol or hydrous ethanol on the oxidation reactivity and nanostructure of diesel particulate matter. Fuel 2015;161:18-25.

[192] Gargiulo V, Alfè M, Blasio GD, Beatrice C. Chemico-physical features of soot emitted from a dual-fuel ethanol-diesel system. Fuel 2015;150:154-161.
[193] Bresenham D, Reisel J, Neusen K. Spindt air-fuel ratio method generalization for oxygenated fuels. SAE Technical Paper 1998; Paper No:982054. doi:https://doi.org/10.4271/982054.
[194] SAE J1088. Test procedure for the measurement of gaseous exhaust emissions from small utility engines. SAE International 1993.
[195] Moore K, Polidori A, Sioutas C. Toxicological assessment of particulate emissions from the exhaust of old and new model heavy-and light-duty vehicles. METRANS Project 09-07. Los Angeles: METRANS; 2011. Available from: https://www.metrans.org/sites/default/files/research-project/09-07_Moore_METRANS_final_report_0_0.pdf.
[196] Jimenez S, Ballester J. A comparative study of different methods for the sampling of high temperature combustion aerosols. Aerosol Science and Technology 2005;39:811-821.
[197] Rmili B, Bihan OLCL, Dutouquet C, Charriol OA, Frejafon E. Particle sampling by TEM grid filtration. Aerosol Science and Technology 2013;47:767-775.
[198] Vargas AM, Gülder ÖL. A multi-probe thermophoretic soot sampling system for high-pressure diffusion flames. Review of Scientific Instruments 2016;87(5). doi.org/10.1063/1.4947509.
[199] Neer A, Koylu UO. Effect of operating conditions on the size, morphology, and concentration of submicrometer particulates emitted from a diesel engine. Combustion and Flame 2006;146: 142-154.
[200] Ogura I, Hashimoto N, Kotake M, Sakurai H, Kishimoto A, Honda K. Aerosol particle collection efficiency of holey carbon. Aerosol Science and Technology 2014;48:758-767.
[201] Li Z, Qiu L, Cheng X, Li Y, Wu H. The evolution of soot morphology and nanostructure in laminar diffusion flame of surrogate fuels for diesel. Fuel 2018;211:517-528.
[202] Yan F, Cheng X, Qiu L, Huang R, Huang S, Liu B. Spray flame soot sampling and morphology analysis of butanol-diesel blends. Journal of the Energy Institute 2017;90(6):855-863.
[203] Zhang R, Kook S. Influence of fuel injection timing and pressure on in-flame soot particles in an automotive-size diesel engine. Environmental Science and Technology 2014;48:8243-8250.
[204] Zhang R, Zhang Y, Kook S. Morphological variations of in-flame and exhaust soot particles associated with jet-to-jet variations and jet-jet interactions in a light-duty diesel engine. Combustion and Flame 2017;176:377-390.
[205] Wang C, Chan QN, Kook S, Hawkes ER, Lee J, Medwell PR. External irradiation effect on the growth and evolution of in-flame soot species. Carbon 2016;102:161-171.
[206] Su DS, Müller JO, Jentoft RE, Rothe D, Jacob E, Schlögl R. Fullerene-like soot from EURO-IV diesel engine: consequences for catalytic automotive pollution control. Topics in Catalysis 2004;30(1-4):241-245.
[207] Rohani B, Bae C. Morphology and nano-structure of soot in diesel spray and in engine exhaust. Fuel 2017;203:47-56.
[208] Kirchner U, Scheer V, Vog R, Kagi R. TEM study on volatility and potential presence of solid cores in nucleation mode particles from diesel powered passenger cars. Journal of Aerosol Science 2009;40:55-64.
[209] Mathis U, Kaegi R, Mohr M, Zenobi R. TEM analysis of volatile nanoparticles from particle trap equipped diesel and direct-injection spark-ignition vehicles. Atmospheric Environment 2004;38:4347-4355.
[210] Salamanca M, Mondragón F, Agudelo JR, Santamaría A. Influence of palm oil biodiesel on the chemical and morphological characteristics of particulate matter emitted by a diesel engine. Atmospheric Environment 2012;62:220-227.
[211] Qu L, Wang Z, Zhang J. Influence of waste cooking oil biodiesel on oxidation reactivity and nanostructure of particulate matter from diesel engine. Fuel 2016;181:389-395.
[212] Wal RLV, Yezerets A, Currier NW, Kim DH, Wang CM. HRTEM Study of diesel soot collected from diesel particulate filters. Carbon 2007;45:70-77.

[213] Soriano JA, Agudelo JR, López AF, Armas O. Oxidation reactivity and nanostructural characterization of the soot coming from farnesane - A novel diesel fuel derived from sugar cane. Carbon 2017;125:516-529.
[214] Yang H, Li X, Wang Y, Mu M, Li X, Kou G. Experimental investigation into the oxidation reactivity and nanostructure of particulate matter from diesel engine fuelled with diesel/polyoxymethylene dimethyl ethers blends. Scientific Reports 2016;6.doi: 10.1038/srep37611.
[215] Bérubé KA, Jones TP, Williamson BJ, Winters C, Morgan AJ, Richards RJ. Physicochemical characterisation of diesel exhaust particles: Factors for assessing biological activity. Atmospheric Environment 1999;33(10):1599-1614.
[216] Fierz M, Kaegi R, Burtscher H. Theoretical and experimental evaluation of a portable electrostatic TEM sampler. Aerosol Science and Technology 2007;41(5):520-528.
[217] Yehliu K, Wal RLV, Boehman AL. Development of an HRTEM image analysis method to quantify carbon nanostructure. Combustion and Flame 2011;158(9):1837-1851.
[218] Wal RLV, Tomasek AJ, Pamphlet MI, Taylor CD, Thompson WK. Analysis of HRTEM images for carbon nanostructure quantification. Journal of Nanoparticle Research 2004;6(6):555-568.
[219] Wal RLV. Soot nanostructure: Definition, quantification and implications. SAE Technical Paper 2005;2005-01-0964.doi.org/10.4271/2005-01-0964.
[220] Wichmann HE. Diesel exhaust particles. Inhalation Toxicology 2007;19(1):241-244.
[221] Han Y, Cao J, Chow JC, Watson JG, An Z, Jin Z, Fung K, Liu S. Evaluation of the thermal/optical reflectance method for discrimination between char- and soot-EC. Chemosphere 2007;69(4):569-574.
[222] Bond TC, Doherty SJ, Fahey DW, Forster PM, Berntsen T, DeAngelo BJ, Flanner MG, Ghan S. Bounding the role of black carbon in the climate system: A scientific assessment. Journal of Geophysical Research: Atmospheres 2013;118:5380-5552.
[223] Zhang ZH, Balasubramanian R. Effects of oxygenated fuel blends on carbonaceous particulate composition and particle size distributions from a stationary diesel engine. Fuel 2015;141:1-8.
[224] Watson JG, Chow JC, Chen LWA. Summary of organic and elemental carbon/black carbon analysis methods and intercomparisons. Aerosol and Air Quality Research 2005;5(1):65-102.
[225] Han YM, Han ZW, Cao JJ, Chow JC, Watson JG, An ZS, Liu SX, Zhang RJ. Distribution and origin of carbonaceous aerosol over a rural high-mountain lake area, Northern China and its transport significance. Atmospheric Environment 2008;42(10):2405-2414.
[226] Chow JC, Watson JG, Crow D, Lowenthal DH, Merrifield T. Comparison of IMPROVE and NIOSH carbon measurements. Aerosol Science and Technology 2001;34(1):23-34.
[227] Chow JC, Watson JG, Chen LWA, Chang MCO, Robinson NF, Trimble D, Kohl S. The IMPROVE_A temperature protocol for thermal/optical carbon analysis: Maintaining consistency with a long-term database. Journal of the Air and Waste Management Association 2007;57(9):1014-1023.
[228] Chow JC, Watson JG, Pritchett LC, Pierson WR, Frazier CA, Purcell RG. The dri thermal/optical reflectance carbon analysis system: description, evaluation and applications in U.S. Air quality studies. Atmospheric Environment. Part A. General Topics 1993;27(8):1185-1201.
[229] Han Y, Cao J, An Z, Chow JC, Watson JG, Jin Z, Fung K, Liu S. Evaluation of the thermal/optical reflectance method for quantification of elemental carbon in sediments. Chemosphere 2007;69(4):526-533.
[230] Birch ME. Analysis of carbonaceous aerosols: interlaboratory comparison. Analyst 1998;123(5):851-857.
[231] Cavalli F, Viana M, Yttri KE, Genberg J, Putaud JP. Toward a standardised thermal-optical protocol for measuring atmospheric organic and elemental carbon: the EUSAAR protocol. Atmospheric Measurement Techniques 2010;3:79-89.
[232] Peterson MR, Richards MH. Thermal-optical-transmittance analysis for organic, elemental, carbonate, total carbon, and OCX2 in $PM_{2.5}$ by the EPA/NIOSH method. In: Symposium on

Air Quality Measurement Methods and Technology; 2002; Pittsburgh.
[233] Han Y, Chen A, Cao J, Fung K, Ho F, Yan B, Zhan C, Liu S, Wei C, An Z. Thermal/optical methods for elemental carbon quantification in soils and urban dusts: Equivalence of different analysis protocols. Plos One 2013;8(12).doi.org/10.1371/journal.pone.0083462.
[234] Daher N, Ruprecht A, Invernizzi G, Marco CD, Miller-Schulze J, Heo JB, Shafer MM, Schauer JJ, Sioutas C. Chemical characterization and source apportionment of fine and coarse particulate matter inside the refectory of Santa Maria Delle Grazie Church, Home of Leonardo Da Vinci's "Last Supper". Environmental Science and Technology 2011;45(24):10344-10353.
[235] Short D, Vu D, Durbin TD, Karavalakis G, Asa-Awuku A. Particle speciation of emissions from iso-butanol and ethanol blended gasoline in light-duty vehicles. Journal of Aerosol Science 2015;84:39-52.
[236] Ramgolam K, Favez O, Cachier H, Gaudichet A, Marano F, Martinon L, Baeza-Squiban A. Size-partitioning of an urban aerosol to identify particle determinants involved in the proinflammatory response induced in airway epithelial cells. Particle and Fibre Toxicology 2009;6(10).https://doi.org/10.1186/1743-8977-6-10.
[237] Gutiérrez-Castillo ME, Roubicek DA, Cebrián-García ME, De Vizcaya-Ruíz A, Sordo-Cedeño M, Ostrosky-Wegman P. Effect of chemical composition on the induction of DNA damage by urban airborne particulate matter. Environmental and Molecular Mutagenesis 2006;47(3):199-211.
[238] Valavanidis A, Fiotakis K, Vlachogianni T. Airborne particulate matter and human health: toxicological assessment and importance of size and composition of particles for oxidative damage and carcinogenic mechanisms. Journal of environmental science and health. Part C, Environmental carcinogenesis and ecotoxicology reviews 2008;26(4):339-362.
[239] Ervens B, Feingold G, Kreidenweis SM. Influence of water-soluble organic carbon on cloud drop number concentration. Journal of Geophysical Research:Atmospheres 2005;110.https://doi.org/10.1029/2004JD005634.
[240] Biswas S, Verma V, Schauer JJ, Sioutas C. Chemical speciation of PM emissions from heavy-duty diesel vehicles equipped with diesel particulate filter (DPF) and selective catalytic reduction (SCR) retrofits. Atmospheric Environment 2009;43(11):1917-1925.
[241] Cheung KL, Polidori A, Ntziachristos L, Tzamkiozis T, Samaras Z, Cassee FR, Gerlofs M, Sioutas C. Chemical characteristics and oxidative potential of particulate matter emissions from gasoline, diesel, and biodiesel cars. Environmental Science and Technology 2009;43(16):6334-6340.
[242] Zhang ZH, Balasubramanian R. Investigation of particulate emission characteristics of a diesel engine fueled with higher alcohols/biodiesel blends. Applied Energy 2016;163:71-80.
[243] Zhang ZH, Balasubramanian R. Effect of oxygenated fuels on physicochemical and toxicological characteristics of diesel particulate emissions. Environmental Science and Technology 2014;48:14805-14813.
[244] Wen J, Shi G, Tian Y, Chen G, Liu J, Huang-Fu Y, Ivey CE, Feng Y. Source contributions to water-soluble organic carbon and water-insoluble organic carbon in $PM_{2.5}$ during Spring Festival, heating and non-heating seasons. Ecotoxicology and Environmental Safety 2018;164:172-180.
[245] Psichoudaki M, Pandis SN. Atmospheric aerosol water-soluble organic carbon measurement: a theoretical analysis. Environmental Science and Technology 2013;47(17):9791-9798.
[246] Khare P, Baruah BP, Rao PG. Water-soluble organic compounds (WSOCs) in $PM_{2.5}$ and PM_{10} at a subtropical site of India. Tellus 2011;63(5):990-1000.
[247] Turpin BJ, Lim HJ. Species contributions to $PM_{2.5}$ mass concentrations: revisiting common assumptions for estimating organic mass. Aerosol Science and Technology 2001;35(1):602-610.
[248] Gioda A, Amaral BS, Monteiro ILG, Pierre TDS. Chemical composition, sources, solubility, and transport of aerosol trace elements in a tropical region. Journal of Environmental Monitoring 2011;13:2134-2142.

[249] Neeft JPA, Nijhuis TX, Smakman E, Makkee M, Moulijn JA. Kinetics of the oxidation of diesel soot. Fuel 1997;76(12):1129-1136.
[250] Stratakis GA, Stamatelos AM. Thermogravimetric analysis of soot emitted by a modern diesel engine run on catalyst-doped fuel. Combustion and Flame 2003;132(1-2):157-169.
[251] Moussout H, Ahlafi H, Aazza M, Amechrouq A. Bentonite/chitosan nanocomposite: Preparation, characterization and kinetic study of its thermal degradation. Thermochimica Acta 2018;659:191-202.
[252] Winberry WT, Jungclaus G. Compendium of methods for the determination of toxic organic compounds in ambient air; Compendium Method TO-13A; Determination of polycyclic aromatic hydrocarbons (PAHs) in ambient air using gas chromatography/mass spectrometry (GC/MS). Cincinnati: U.S. Environmental Protection Agency; 1999. EPA/625/R-96/010b.
[253] Ravindra K, Sokhi R, Grieken RV. Atmospheric polycyclic aromatic hydrocarbons: Source attribution, emission factors and regulation. Atmospheric Environment 2008;42:2895-2921.
[254] Lin YC, Lee WJ, Chen CB. Characterization of polycyclic aromatic hydrocarbons from the diesel engine by adding light cycle oil to premium diesel fuel. Journal of the Air and Waste Management Association 2006;56(6):752-758.
[255] Nisbet ICT, LaGoy PK. Toxic equivalency factors (TEFs) for polycyclic aromatic hydrocarbons (PAHs). Regulatory Toxicology and Pharmacology 1992;16(3):290-300.
[256] Lung SCC, Liu CH. Fast analysis of 29 polycyclic aromatic hydrocarbons (PAHs) and nitro-PAHs with ultra-high performance liquid chromatography-atmospheric pressure photoionization-tandem mass spectrometry. Scientific Reports 2015;5:10.1038/srep12992.
[257] Ho SSH, Chow JC, Watson JG, Ng LPT, Kwok Y, Ho KF, Cao J. Precautions for in-injection port thermal desorption-gas chromatography/mass spectrometry (TD-GC/MS) as applied to aerosol filter samples. Atmospheric Environment 2011;45(7):1491-1496.
[258] Ho SSH, Yu JZ. In-injection port thermal desorption and subsequent gas chromatography-mass spectrometric analysis of polycyclic aromatic hydrocarbons and n-alkanes in atmospheric aerosol samples. Journal of Chromatography A 2004;1059(1-2):121-129.
[259] Ho SSH, Yu JZ, Chow JC, Zielinska B, Watson JG, Sit EHL, Schauer JJ. Evaluation of an in-injection port thermal desorption-gas chromatography/mass spectrometry method for analysis of non-polar organic compounds in ambient aerosol samples. Journal of Chromatography A 2008;1200(2):217-227.
[260] Popovicheva O, Engling G, Lin KT, Persiantseva N, Timofeev M, Kireeva E, Völk P, Hubert A, Wachtmeister G. Diesel/biofuel exhaust particles from modern internal combustion engines: Microstructure, composition, and hygroscopicity. Fuel 2015;157:232-239.
[261] Tan PQ, Zhong YM, Hu ZY, Lou DM. Size distributions, PAHs and inorganic ions of exhaust particles from a heavy duty diesel engine using B20 biodiesel with different exhaust aftertreatments. Energy 2017;141:898-906.
[262] Popovicheva OB, Kireeva ED, Steiner S, Rutishauser BR, Persiantseva NM, Timofeev MA, Shonija NK, Comte P, Czerwinski J. Microstructure and chemical composition of diesel and biodiesel particle exhaust. Aerosol and Air Quality Research 2014;14:1392-1401.
[263] Chiang HL, Lai YM, Chang SY. Pollutant constituents of exhaust emitted from light-duty diesel vehicles. Atmospheric Environment 2012;47:399-406.
[264] Oanh NTK, Thiansathit W, Bond TC, Subramanian R, Winijkul E, Armart IP. Compositional characterization of $PM_{2.5}$ emitted from in-use diesel vehicles. Atmospheric Environment 2010;44(1):15-22.
[265] Chmielewski M, Heimburger O, Stenvinkel P, Lindholm B. Uremic Toxicity. In: Kopple JD, Massry SG, Kalantar-Zadeh K, editors. Nutritional management of renal disease. 3rd ed. Elsevier; 2013. pp. 49-77.
[266] Tsai HH, Yuan CS, Hung CH, Lin C. Physicochemical Properties of $PM_{2.5}$ and $PM_{2.5-10}$ at inland and offshore sites over Southeastern Coastal Region of Taiwan Strait. Aerosol and Air Quality Research 2011;11:664-678.
[267] Zhao R, Han B, Lu B, Zhang N, Zhu L, Bai Z. Element composition and source apportionment of atmospheric aerosols over the China Sea. Atmospheric Pollution

Research 2015;6:191-201.
[268] Heal MR, Hibbs LR, Agius RM, Beverland IJ. Total and water-soluble trace metal content of urban background PM_{10}, $PM_{2.5}$ and black smoke in Edinburgh, UK. Atmospheric Environment 2005;39:1417-1430.
[269] Lawrence S, Sokhi R, Ravindra K, Mao H, Prain HD, Bull ID. Source apportionment of traffic emissions of particulate matter using tunnel measurements. Atmospheric Environment 2013;77:548-557.
[270] Ho KF, Lee SC, Cao JJ, Chow JC, Watson JG, Chan CK. Seasonal variations and mass closure analysis of particulate matter in Hong Kong. Science of the Total Environment 2006;355 :276-287.
[271] Islam MF, Majumder SS, Mamun AA, Khan MB, Rahman MA, Salam A. Trace metals concentrations at the atmosphere particulate matters in the southeast asian mega city (Dhaka, Bangladesh). Open Journal of Air Pollution 2015;4:86-98.
[272] Lin YC, Tsai CJ, Wu YC, Zhang R, Chi KH, Huang YT, Lin SH, Hsu SC. Characteristics of trace metals in traffic-derived particles in Hsuehshan Tunnel, Taiwan: size distribution, potential source, and fingerprinting metal ratio. Atmospheric Chemistry and Physics 2015;15:4117-4130.
[273] Sarti E, Pasti L, Rossi M, Ascanelli M, Pagnoni A, Trombini M, Remelli M. The composition of PM_1 and $PM_{2.5}$ samples, metals and their water soluble fractions in the Bologna area (Italy). Atmospheric Pollution Research 2015;6(4):708-718.
[274] Lough GC, Schauer JJ, Park JS, Shafer MM, DeMinter JT, Weinstein JP. Emissions of metals associated with motor vehicle roadways. Environmental Science and Technology 2005;39(3):826-836.
[275] Zhang R, Jing J, Tao J, Hsu SC, Wang G, Cao J, Lee CSL, Zhu L, Chen Z, Zhao Y, Shen Z. Chemical characterization and source apportionment of $PM_{2.5}$ in Beijing: seasonal perspective. Atmospheric Chemistry and Physics 2013;13:7053-7074.
[276] Becker S, Dailey LA, Soukup JM, Grambow SC, Devlin RB, Huang YC. Seasonal variations in air pollution particle-induced inflammatory mediator release and oxidative stress. Environmental Health Perspectives 2005;113:1032-1038.
[277] Ashraful AM, Masjuki HH, Kalam MA. Particulate matter, carbon emissions and elemental compositions from a diesel engine exhaust fuelled with diesel-biodiesel blends. Atmospheric Environment 2015;120:463-474.
[278] Shukla PC, Gupta T, Labhsetwar NK, Agarwal AK. Trace metals and ions in particulates emitted by biodiesel fuelled engine. Fuel 2017;188:603-609.
[279] Sharma M, Agarwal AK, Bharathi KVL. Characterization of exhaust particulates from diesel engine. Atmospheric Environment 2005;39 :3023-3028.
[280] Agarwal AK, Kumar A, Lukose J, Singh AP. Particulate characterization and size distribution in the exhaust of a gasoline homogeneous charge compression ignition engine. Aerosol and Air Quality Research 2015;15:504-516.
[281] Moffat RJ. Describing the uncertainties in experimental results. Experimental Thermal and Fluid Science 1988;1(1):3-17.
[282] Ghadikolaei MA, Cheung CS, Yung KF. Study of combustion, performance and emissions of diesel engine fueled with diesel/biodiesel/alcohol blends having the same oxygen concentration. Energy 2018;157:258-269.
[283] Ghadikolaei MA, Cheung CS, Yung KF. Study of performance and emissions of diesel engine fueled with blends of diesel, biodiesel and alcohols (ethanol, methanol and n-butanol), based on a constant fuel oxygen content. In: The 13th International Conference on Combustion and Energy Utilization (ICCEU); 2016; Taipei, Taiwan.
[284] Kumar BR, Saravanan S. Use of higher alcohol biofuels in diesel engines: A review. Renewable and Sustainable Energy Reviews 2016;60:84-115.
[285] Wei L, Cheung CS, Ning Z. Influence of waste cooking oil biodiesel on combustion, unregulated gaseous emissions and particulate emissions of a direct-injection diesel engine. Energy 2017;127:175-185.
[286] Zhu L, Cheung CS, Zhang WG, Huang Z. Combustion, performance and emission characteristics of a DI diesel engine fueled with ethanol-biodiesel blends. Fuel

2011;90:1743-1750.
[287] Kumar BR, Saravanan S, Rana D, Nagendran A. A comparative analysis on combustion and emissions of some next generation higher-alcohol/diesel blends in a direct-injection diesel engine. Energy Conversion and Management 2016;119:246-256.
[288] Park SH, Youn IM, Lee CS. Influence of ethanol blends on the combustion performance and exhaust emission characteristics of a four-cylinder diesel engine at various engine loads and injection timings. Fuel 2011;90:1748-1755.
[289] Hansdah D, Murugan S. Bioethanol fumigation in a DI diesel engine. Fuel 2014;130:324-333.
[290] Zheng Z, Li C, Liu H, Zhang Y, Zhong X, Yao M. Experimental study on diesel conventional and low temperature combustion by fueling four isomers of butanol. Fuel 2015;141:109-119.
[291] Karavalakis G, Stamoulis S, Bakeas E. Light vehicle regulated and unregulated emissions from different biodiesels. Science of The Total Environment 2009;407:3338-3346.
[292] Tat M, Van GJ. Measurement of biodiesel speed of sound and its impact on injection timing: Final Report; Report 4 in a Series of 6. Final report. Colorado : National Renewable Energy Laboratory; 2003. doi: 10.2172/15003584. Available from: https://www.nrel.gov/docs/fy03osti/31462.pdf.
[293] Monyem A, Van GJH. The effect of biodiesel oxidation on engine performance and emissions. Biomass and Bioenergy 2001;20(4):317-325.
[294] Gnanamoorthi V, Devaradjane G. Effect of compression ratio on the performance, combustion and emission of DI diesel engine fueled with ethanol - diesel blend. Journal of the Energy Institute 2015;88:19-26.
[295] Donahue R, Foster DE. Effects of oxygen enhancement on the emissions from a DI diesel via. Manipulation of fuels and combustion chamber gas composition. SAE Technical Paper 2000;2000-01-0512.doi.org/10.4271/2000-01-0512.
[296] Koivisto E, Ladommatos N, Gold M. Systematic study of the effect of the hydroxyl functional group in alcohol molecules on compression ignition and exhaust gas emissions. Fuel 2015;153:650-663.
[297] Heywood JB. Internal combustion engine fundamentals. 2nd ed. New York: McGraw-Hill; 2003.
[298] Pidol L, Lecointe B, Starck L, Jeuland N. Ethanol-biodiesel-diesel fuel blends: Performances and emissions in conventional diesel and advanced low temperature combustions. Fuel 2012;93:329-338.
[299] Ajav EA, Singh B, Bhattacharya TK. Experimental study of some performance parameters of a constant speed stationary diesel engine using ethanol-diesel blends as fuel. Biomass and Bioenergy 1999;17(4):357-365.
[300] He BQ, Shuai SJ, Wang JX, He H. The effect of ethanol blended diesel fuels on emissions from a diesel engine. Atmospheric Environment 2003;37:4965-4971.
[301] Ozener O, Yuksek L, Ergenc AT, Ozkan M. Effects of soybean biodiesel on a DI diesel engine performance, emission and combustion characteristics. Fuel 2014;115:875-883.
[302] Ying W, Longbao Z, Hewu W. Diesel emission improvements by the use of oxygenated DMW/diesel blend fuels. Atmospheric Environment 2006;40:2313-2320.
[303] Paul G, Datta A, Mandal B. Numerical investigation of the performance and emission characteristics of a CI engine using diesel and its blends with ethanol and Jatropha biodiesel. International Journal of Current Engineering and Technology 2014;3:5-9.
[304] Yilmaz N, Vigil FM, Donaldson AB, Darabseh T. Investigation of CI engine emissions in biodiesel-ethanol-diesel blends as a function of ethanol concentration. Fuel 2014;115:790-793.
[305] Yilmaz N, Ileri E, Atmanli A. Performance of biodiesel/higher alcohols blends in a diesel engine. International Journal of Energy Research 2016;40:1134-1143.
[306] Huang J, Wang Y, Li S, Rosilly AP, Yu H, Li H. Experimental investigation on the performance and emissions of a diesel engine fuelled with ethanol–diesel blends. Applied Thermal Engineering 2009;29:2484-2490.
[307] Sayin C, Uslu K, Canakci M. Influence of injection timing on the exhaust emissions of a

dual-fuel CI engine. Renewable Energy 2008;33:1314-1323.
[308] Muralidharan M, Subramanian M, Kanal PC, Malhotra RK. Evaluation of a novel biofuel blend using diesel-biodiesel-ethanol on light commercial vehicle. SAE Technical Paper 2011;2011-28-0015.doi:10.4271/2011-28-0015.
[309] Westbrook CK, Pitz WJ, Curran HJ. Chemical kinetic modeling study of the effects of oxygenated hydrocarbons on soot emissions from diesel engines. The Journal of Physical Chemistry A 2006;110:6912-6922.
[310] Buchholz BA, Mueller CJ, Upatnieks A, Martin GC, Pitz WJ, Westbrook CK. Using carbon-14 isotope tracing to investigate molecular structure effects of the oxygenate dibutyl maleate on soot emissions from a DI diesel engine. SAE Technical Paper 2004;2004-01-1849.doi:10.4271/2004-01-1849.
[311] Farooq A, Ren W, Lam KY, Davidson DF, Hanson RK, Westbrook CK. Shock tube studies of methyl butanoate pyrolysis with relevance to biodiesel. Combustion and Flame 2012;159:3235-3241.
[312] McCunn LR, Lau KC, Krisch MJ, Butler LJ, Tsung JW, Lin JJ. Unimolecular dissociation of the CH_3OCO radical: An intermediate in the CH_3O + CO reaction. The Journal of Physical Chemistry A 2006;110:1625-1634.
[313] Westbrook CK. Biofuels combustion. Annual Review of Physical Chemistry 2013;64:201-219.
[314] Di Y, Cheung CS, Huang Z. Experimental investigation on regulated and unregulated emissions of a diesel engine fueled with ultra-low sulfur diesel fuel blended with biodiesel from waste cooking oil. Science of the Total Environment 2009;407:835-846.
[315] Ghadikolaei MA, Cheung CS, Yung KF. Study of combustion, performance and emissions of a diesel engine fueled with ternary fuel in blended and fumigation modes. Fuel 2019;235:288-300.
[316] Wang LJ, Song RZ, Zou HB, Liu SH, Zhou LB. Study on combustion characteristics of a methanol-diesel dual-fuel compression ignition engine. Proceedings of the Institution of Mechanical Engineers, Part D: Journal of Automobile Engineering 2008;222:619-627.
[317] Labeckas G, Slavinskas S, Mažeika M. The effect of ethanol-diesel-biodiesel blends on combustion, performance and emissions of a direct injection diesel engine. Energy Conversion and Management 2014;79:698-720.
[318] Wei L, Yao C, Wang Q, Pan W, Han G. Combustion and emission characteristics of a turbocharged diesel engine using high premixed ratio of methanol and diesel fuel. Fuel 2015;140:156-163.
[319] Song R, Liu J, Wang L, Liu S. Performance and emissions of a diesel engine fuelled with methanol. Energy and Fuels 2008;22(6):3883-3888.
[320] Britto RF, Martins CA. Experimental analysis of a diesel engine operating in diesel-ethanol dual-fuel mode. Fuel 2014;134:140-150.
[321] Pedrozo VB, May I, Guan W, Zhao H. High efficiency ethanol-diesel dual-fuel combustion: A comparison against conventional diesel combustion from low to full engine load. Fuel 2018;230:440-451.
[322] López AF, Cadrazco M, Agudelo AF, Corredor LA, Vélez JA, Agudelo JR. Impact of n-butanol and hydrous ethanol fumigation on the performance and pollutant emissions of an automotive diesel engine. Fuel 2015;153:483-491.
[323] Surawski NC, Ristovski ZD, Brown RJ, Situ R. Gaseous and particle emissions from an ethanol fumigated compression ignition engine. Energy Conversion and Management 2012;54 (1):145-151.
[324] Ileri E, Atmanli A, Yilmaz N. Comparative analyses of n-butanol-rapeseed oil-diesel blend with biodiesel, diesel and biodiesel-diesel fuels in a turbocharged direct injection diesel engine. Journal of the Energy Institute 2016;89 (4):586-593.
[325] Imdadul HK, Masjuki HH, Kalam MA, Zulkifli NWM, Alabdulkarem A, Kamruzzaman M, Rashed MM. A comparative study of C_4 and C_5 alcohol treated diesel-biodiesel blends in terms of diesel engine performance and exhaust emission. Fuel 2016;179:281-288.
[326] Chu PK, Lu XP. Low temperature plasma technology: Methods and applications. Florida: CRC Press; 2013.

[327] Zhang ZH, Cheung CS, Chan TL, Yao CD. Emission reduction from diesel engine using fumigation methanol and diesel oxidation catalyst. Science of the Total Environment 2009;407:4497-4505.
[328] Cheng CH, Cheung CS, Chan TL, Lee SC, Yao CD. Experimental investigation on the performance, gaseous and particulate emissions of a methanol fumigated diesel engine. Science of the Total Environment 2008;389:115-124.
[329] Cheung CS, Cheng C, Chan TL, Lee SC, Yao C, Tsang KS. Emissions characteristics of a diesel engine fueled with biodiesel and fumigation methanol. Energy and Fuels 2008;22:906-914.
[330] Man XJ, Cheung CS, Ning Z, Wei L, Huang ZH. Influence of engine load and speed on regulated and unregulated emissions of a diesel engine fueled with diesel fuel blended with waste cooking oil biodiesel. Fuel 2016;180:41-49.
[331] Tsolakis A. Effects on particle size distribution from the diesel engine operating on RME-biodiesel with EGR. Energy and Fuel 2006;20:1418-1424.
[332] Di Y, Cheung CS, Huang Z. Experimental investigation of particulate emissions from a diesel engine fueled with ultralow-sulfur diesel fuel blended with diglyme. Atmospheric Environment 2010;44(1):55-63.
[333] Kittelson DB. Engines and nanoparticles: a review. Journal of Aerosol Science 1998;29(5-6):575-588.
[334] Kittelson DB, Watts WF, Johnson JP. Nanoparticle emissions on Minnesota highways. Atmospheric Environment 2004;38(1):9-19.
[335] Zhou JH, Cheung CS, Zhao WZ, Ning Z, Leung CW. Impact of intake hydrogen enrichment on morphology, structure and oxidation reactivity of diesel particulate. Applied Energy 2015;160:442-455.
[336] Lu T, Cheung CS, Huang Z. Investigation on particulate oxidation from a DI diesel engine fueled with three fuels. Aerosol Science and Technology 2012;46(12):1349-1358.
[337] Lu T, Cheung CS, Huang Z. Effects of engine operating conditions on the size and nanostructure of diesel particles. Journal of Aerosol Science 2012;47:27-38.
[338] Wei L, Cheung CS, Ning Z. Influence of waste cooking oil biodiesel on the nanostructure and volatility of particles emitted by a direct-injection diesel engine. Aerosol Science and Technology 2016;50(9):893-905.
[339] Ishiguro T, Takatori Y, Akihama K. Microstructure of diesel soot particles probed by electron microscopy: First observation of inner core and outer shell. Combustion and Flame 1997;108(1-2):231-234.
[340] Wentzel M, Gorzawski H, Naumann KH, Saathoff H, Weinbruch S. Transmission electron microscopical and aerosol dynamical characterization of soot aerosols. Journal of Aerosol Science 2003;34(10):1347-1370.
[341] Chen Y, Shah N, Braun A, Huggins FE, Huffman GP. Electron microscopy investigation of carbonaceous particulate matter generated by combustion of fossil fuels. Energy and Fuels 2005;19(4):1644-1651.
[342] Williams DB, Carter CB. Transmission electron microscopy:A textbook for materials science. 2nd ed. New York: Springer; 2009.
[343] Buseck PR, Adachi K, Gelencsér A, Tompa É, Pósfai M. Ns-soot: A material-based term for strongly light-absorbing carbonaceous particles. Aerosol Science and Technology 2014;48(7):777-788.
[344] Egerton RF. Physical principles of electron microscopy. New York: Springer; 2005.
[345] Someya T. Advanced Combustion Science. 1st ed. Tokyo: Springer-Verlag; 1993.
[346] Sahu V, Shekhar S, Ahuja P, Gupta G, Singh SK, Sharma RK, Singh G. Synthesis of hydrophilic carbon black; role of hydrophilicity in maintaining the hydration level and protonic conduction. RSC Advances 2013;3:3917-3924.
[347] Lu T, Huang Z, Cheung CS, Ma J. Size distribution of EC, OC and particle-phase PAHs emissions from a diesel engine fueled with three fuels. Science of The Total Environment 2012;438:33-41.
[348] Li X, Xu Z, Guan C, Huang Z. Particle size distributions and OC, EC emissions from a diesel engine with the application of in-cylinder emission control strategies. Fuel

2014;121:20-26.
[349] Zhang J, He K, Shi X, Zhao Y. Comparison of particle emissions from an engine operating on biodiesel and petroleum diesel. Fuel 2011;90(6):2089-2097.
[350] Yang K, Wei L, Cheung CS, Tang C, Huang Z. The effect of pentanol addition on the particulate emission characteristics of a biodiesel operated diesel engine. Fuel 2017;209:132-140.
[351] Song WW, He KB, Wang JX, Wang XT, Shi XY, Yu C, Chen WM, Zheng L. Emissions of EC, OC, and PAHs from cottonseed oil biodiesel in a heavy-duty diesel engine. Environmental Science and Technology 2011;45:6683-6689.
[352] Shukla PC, Gupta T, Agarwal AK. A comparative morphological study of primary and aged particles emitted from a biodiesel (B20) vis-à-vis diesel fuelled CRDI engine. Aerosol and Air Quality Research 2014;14:934-942.
[353] Watson JG, Chow JC, Lowenthal DH, Pritchett LC, Frazier CA, Neuroth GR, Robbins R. Differences in the carbon composition of source profiles for diesel- and gasoline-powered vehicles. Atmospheric Environment 1994;28(15):2493-2505.
[354] Popovicheva OB, Irimiea C, Carpentier Y, Ortega IK, Kireeva ED, Shonija NK, Schwarz J, Vojtíšek-Lom M, Focsa C. Chemical composition of diesel/biodiesel particulate exhaust by FTIR spectroscopy and mass spectrometry: Impact of fuel and driving cycle. Aerosol and Air Quality Research 2017;17(7):1717-1734.
[355] Cheung KL, Ntziachristos L, Tzamkiozis T, Schauer JJ, Samaras Z, Moore KF, Sioutas C. Emissions of particulate trace elements, metals and organic species from gasoline, diesel, and biodiesel passenger vehicles and their relation to oxidative potential. Aerosol Science and Technology 2010;44(7):500-513.
[356] Zhang ZH, Balasubramanian R. Influence of butanol-diesel blends on particulate emissions of a non-road diesel engine. Fuel 2014;118:130-136.
[357] Storey JM, Curran SJ, Lewis SA, Barone TL, Dempsey AB, Moses-DeBusk M, Hanson RM, Prikhodko VY, Northrop WF. Evolution and current understanding of physicochemical characterization of particulate matter from reactivity controlled compression ignition combustion on a multicylinder light-duty engine. International Journal of Engine Research 2017;18(5-6):505-519.
[358] Cheng AS, Dibble RW, Buchholz BA. The effect of oxygenates on diesel engine particulate matter. SAE Technical Paper 2002;2002-01-1705.https://doi.org/10.4271/2002-01-1705.
[359] Guarieiro LLN, Guarieiro ALN. Impact of the biofuels burning on particle emissions from the vehicular exhaust. In: Biernat K, editor. Biofuels. IntechOpen; 2015.
[360] Miguel AH, Hansen ADA. High-time resolution measurements of black carbon particles in the exhaust emissions of a diesel engine during acceleration, deceleration and cruise conditions. Journal of the Brazilian Chemical Society 2012;23:1140-1145.
[361] Mustafi NN, Raine RR, James B. Characterization of exhaust particulates from a dual fuel engine by TGA, XPS, and Raman techniques. Aerosol Science and Technology 2010;44:954-963.
[362] Ballesteros R, Hernández JJ, Lyons LL, Cabañas B, Tapia A. Speciation of the semivolatile hydrocarbon engine emissions from sunflower biodiesel. Fuel 2008;87(10-11):1835-1843.
[363] Sharma HN, Pahalagedara L, Joshi A, Suib SL, Mhadeshwar AB. Experimental study of carbon black and diesel engine soot oxidation kinetics using thermogravimetric analysis. Energy and Fuels 2012;26(9):5613-5625.
[364] Rodríguez-Fern J, Oliva F, Vázquez RA. Characterization of the diesel soot oxidation process through an optimized thermogravimetric method. Energy and Fuels 2011;25(5):2039-2048.
[365] Song J, Alam M, Boehman AL. Impact of alternative fuels on soot properties and DPF regeneration. Combustion Science and Technology 2007;179(9):1991-2037.
[366] Man XJ, Cheung CS, Ning Z, Yung KF. Effect of waste cooking oil biodiesel on the properties of particulate from a DI diesel engine. Aerosol Science and Technology 2015;49(4):199-209.
[367] Yehliu K, Vander Wal RL, Armas O, Boehman AL. Impact of fuel formulation on the nanostructure and reactivity of diesel soot. Combustion and Flame 2012;159(12):3597-

3606.
[368] Chien YC, Lu M, Chai M, Boreo FJ. Characterization of biodiesel and biodiesel particulate matter by TG, TG-MS, and FTIR. Energy and Fuels 2009;23(1):202-206.
[369] Babushok VI, Tsang W. Kinetic modeling of heptane combustion and PAH formation. Journal of Propulsion and Power 2004;20:403-414.
[370] Tancell PJ, Rhead MM, Trier CJ, Bell MA, Fussey DE. The sources of benzo[a]pyrene in diesel exhaust emissions. Science of The Total Environment 1995;162(2-3):179-186.
[371] National Research Council (US) Committee on Pyrene and Selected Analogues. Polycyclic aromatic hydrocarbons: evaluation of sources and effects. Washington: National Academies Press; 1983.
[372] Bjorseth A, Becher G. Polycyclic aromatic hydrocarbons in work atmospheres: Occurrence and determination. Florida: CRC Press; 2018.
[373] Pampanin DM, Sydnes MO. Petrogenic polycyclic aromatic hydrocarbons in the aquatic environment: Analysis, synthesis, toxicity and environmental impact. Sharjah: Bentham Science Publishers; 2017.
[374] Timonen H, Karjalainen P, Saukko E, Saarikoski S, Saksa PA, Simonen P, Murtonen T, Maso MD, Kuuluvainen H, Bloss M, Ahlberg E, Svenningsson B, Pagels J, Brune WH, Keskinen J, Worsnop DR, Hillamo R, Rönkkö T. Influence of fuel ethanol content on primary emissions and secondary aerosol formation potential for a modern flex-fuel gasoline vehicle. Atmospheric Chemistry and Physics 2017;17:5311-5329.
[375] Winther M, Slentø E. Heavy metal emissions for Danish road transport. National Environmental Research Institute; 2010. 780. Available from: http://www.dmu.dk/Pub/FR780.pdf.
[376] Wu B, Shen X, Cao X, Yao Z, Wu Y. Characterization of the chemical composition of $PM_{2.5}$ emitted from on-road China III and China IV diesel trucks in Beijing, China. Science of the Total Environment 2016;551-552:579-589.
[377] Kline SJ, McClintock FA. Describing uncertainties in single sample experiments. Mechanical Engineering 1953;75:3-8.
[378] Airy SGB. Theory of errors of observation. London: Macmillan; 1879.
[379] Holman JP. Experimental methods for engineers. 8th ed. New York: McGraw-Hill; 2012.
[380] Taylor JL. Computer-based data acquisition systems: Design techniques. North Carolina: Instrument Society of America; 1986.
[381] Moffat RJ. Contributions to the theory of single sample. Journal of Fluids Engineering 1982;104(2):250-258.
[382] Moffat RJ. Using uncertainty analysis in the planning of an experimen. Journal of Fluids Engineering 1985;107(2):173-178.
[383] Abernethy RB. Measurement uncertainty handbook. Pennsylvania: Instrument Society of America; 1980.
[384] Abernethy RB, Benedict RP, Dowdell RB. ASME measurement uncertainty. Journal of Fluids Engineering 1985;107(2):161-164.
[385] Taylor JR. Introduction to error analysis: The study of uncertainties in physical measurements. 2nd ed. California: University Science Books;1997.